Defining Mechanisms and Pathways of Enhanced Bioremediation During Pump and Treat Intervention.

Michael John Cook

Submitted in accordance with the requirements for the degree of Doctor of Philosophy.

University of Leeds

School of Earth and Environment

February 2019

Intellectual Property and Publication Statements

The candidate confirms that the work submitted is his own and that appropriate credit has been given where reference has been made to the work of others.

This copy has been supplied on the understanding that it is copyright material and that no quotation from the thesis may be published without proper acknowledgement.

The right of Michael John Cook to be identified as author of this work has been asserted by Michael John Cook in accordance with the Copyright, Designs and Patents Act 1988.

Acknowledgements

This research has been carried out by a team which is included Professor Simon Bottrell and Doctor Robert Newton (University of Leeds, School of Earth and Environment) and Professor Steven Thornton, Doctor Steven Rolfe, Doctor Juan Mujica and Andrew Fairburn (University of Sheffield, Groundwater Protection and Restoration Group). My own contributions, fully and explicitly stated in this thesis, have been undertaking fieldworks (in-situ isotopes, sulphide and TDIC), laboratory analysis (in-situ isotopes, sulphide and TDIC; microcosm chemistry), data analysis and interpretation. The other members of this group and their contributions have been as follows:

Professor Simon Bottrell – Training, technical guidance, supervision.
Doctor Robert Newton – Technical guidance, secondary supervision.
Professor Steven Thornton – Technical guidance, collaboration.
Doctor Steven Rolfe – Fieldwork assistance (in-situ hydrochemistry).
Doctor Juan Mujica – Fieldwork assistance (in-situ hydrochemistry).
Andrew Fairburn – Laboratory assistance (in-situ hydrochemistry).

I would like to thank my supervisors, Professor Simon Bottrell and Doctor Robert Newton, for their time and dedication throughout my doctorate. I would also like the thank Professor Steven Thornton and his associates at the Groundwater Protection and Restoration Group for their collaborative efforts throughout my studies.

In addition, I would like to thank Andy Connelly in his role as laboratory manager, and his associates within the Cohen Geochemistry Laboratories, for their continued patience in enabling the processing of the large number of samples analysed as part of this thesis.

Furthermore, I would like to thank my family and friends for supporting me through this period during which I suffered the sad losses of father and mother.

This project was funded by Leeds and York Natural Environment Research Council (NERC) through their Doctoral Training Partnership (DTP).

Abstract

It is estimated that around 30,000 sites requiring active remediation are present across the UK. Amongst active remediation technologies, pump and treat (PAT) is one of the most widely used, however, its value in stimulating in-situ bioremediation is often overlooked.

Using multi-level samplers this thesis provides further hydro-chemical and stable isotopic data for a plume of phenolic compounds within a sandstone aquifer which is under the effect of PAT. Analysis of this data indicates that near to the areas of PAT operation, a consistent 50 % - 70 % decrease in contaminant concentrations is enacted. In addition, contaminant turnover is raised from <200 mg L^{-1} to ~400 mg L^{-1}, indicating enhanced bioremediation. Enrichment of $\delta^{34}S\text{-}SO_4$, by up to 15 ‰, is indicative that bacterial sulphate reduction (BSR) is stimulated by the PAT system within regions of reduced contamination.

In contrast, further data shows that in regions where the PAT does not operate, contaminant concentrations remain high and contaminant turnover low. Furthermore, in regions where PAT ceases operation, in-situ hydrochemistry returns to pre-pumping values in less than 2 years, with contaminant turnover returning to <200 mg/L.

Data gathered from microcosm studies indicate $\delta^{34}S\text{-}SO_4$ enrichment factors during BSR range from -6 ‰ and -10 ‰, with slightly stronger enrichment found at lower contaminant concentrations. Utilising the calculated enrichment values, an enhanced carbon balance model is created defining the proportions of BSR, methanogenesis and other respiration within separate regions of the plume. This model indicates that ~75 % of the increased contamination turnover is attributable to BSR. However, methanogenesis remains dominant in areas of high contamination due to toxic inhibition of BSR. Furthermore, an oxic/nitrate reducing fringe persists.

A plume model based upon the parameters above may have applicability to contaminant plumes in the wider environment, particularly in circumstances where there is the potential for BSR and/or toxic inhibition.

Contents

Table of Contents

1. Introduction 1
1.1. Rationale 1
1.2. Study Focus 2
1.3. A History of Land Contamination 2
1.4. Methods of Remediation 3
1.4.1. Dig and Dump 5
1.4.2. Natural Attenuation (NA) 5
1.4.3. Pump and Treat (PAT) 6
1.4.4. Other Methods 8
1.5. Organic Contaminants Within Aquifers 8
1.5.1. Migration of Contaminants Above the Water Table 8
1.5.2. Migration of Contaminants Below the Water Table 9
1.6. Advection, Dispersion and Diffusion 11
1.7. Sorption and Retardation 13
1.8. Persistence 14
1.9. Biodegradation Processes for Organic Contamination 14
1.10. Biodegradation Sequencing Within Contaminant Plumes 15
1.11. Groundwater Sampling 17
1.11.1. Boreholes 17
1.11.2. Purging Pumps 18
1.11.3. Sampling Pumps 19
1.11.4. Chemical Tools for Groundwater Analysis 19
1.11.5. Stable Isotope Tools for Groundwater Analysis 20
1.12. Study Site 22
1.12.1. Site Geology 23
1.12.2. Borehole Locations 24
1.12.3. Contaminant Chemistry 25
1.12.4. DNAPL Migration 28

1.13. Pre-treatment Site Data 28
1.13.1. Contaminant Concentrations and Natural Attenuation 28
1.13.2. Mass Flux Calculations 31
1.13.3. Oxic Plume Fringe 35
1.13.4. Anaerobic Plume Core 36
1.13.5. Total Dissolved Inorganic Carbon 38
1.14. Isotopic Evidence for Pre-pumping Plume Processes 40
1.14.1. Isotopic Effects Associated with TDIC Creation 40
1.14.2. Isotopic Effects Associated with Methanogenesis 41
1.14.3. Isotopic Effects Associated with Anaerobic Methane Oxidation (AMO) 42
1.14.4. Isotopic Effects Associated with Bacterial Sulphate Reduction 43
1.15. Pre-pumping Plume Models 44
1.15.1. The Cirpka et al. Model 44
1.15.2. Study Site Pre-pumping Model 46
1.16. Pilot Study Site Data 46
1.16.1. Changes in TPC Concentrations 46
1.16.2. Increases in Biodegradation Rate 48
1.16.3. Enhanced Remediation Processes 50
2. Methodologies 52
2.1. Field Methodologies 52
2.1.1. Well Purging 52
2.1.2. Groundwater Hydro-chemistry 53
2.1.3. Gas Chemistry 54
2.1.4. Groundwater Isotopes 55
2.1.5. Methane Isotopes 56
2.1.6. Sampling of Surrogate Microbes for Microcosms 57
2.2. Laboratory Methodologies 59
2.2.1. δ^{13}C-CH_4 Analysis 60
2.2.2. Recovery of TDIC Data and δ^{13}C-TDIC Analysis 60

2.2.3. Recovery of Sulphide 61
2.2.4. Recovery of $BaSO_4$ and $\delta^{34}S$-SO_4 Analysis 61
2.2.1. Hydrochemistry Analysis 62
3. New Field Data from the Four Ashes Site 63
3.1. Contaminant Concentrations 63
3.1.1. Contaminants (TPC) at MLS59 64
3.1.2. Contaminants (TPC) at MLS60 66
3.2. Nitrate Concentrations 68
3.2.1. Nitrate at MLS59 (2014 and 2015) 68
3.2.2. Nitrate at MLS60 72
3.3. TDIC Concentrations 74
3.3.1. TDIC at MLS59 74
3.3.2. TDIC at MLS60 78
3.4. $\delta^{13}C$-TDIC Values 81
3.4.1. $\delta^{13}C$ -TDIC at MLS59 81
3.4.2. $\delta^{13}C$-TDIC at MLS60 86
3.5. $\delta^{34}S$-SO_4 Values 88
3.5.1. $\delta^{34}S$ -SO_4 at MLS59 88
3.5.2. $\delta^{34}S$-SO_4 at MLS60 90
3.6. $\delta^{13}C$-CH_4 Values 93
3.6.1. $\delta^{13}C$-CH_4 at MLS59 93
3.6.2. $\delta^{13}C$-CH_4 at MLS60 98
3.7. Sulphide Data 100
3.7.1. Sulphide Data for MLS59 100
3.7.2. Sulphide Data for MLS60 101
4. fMicrocosm Studies of Phenol Oxidation by BSR 103
4.1. Experimental Background 104
4.2. Experimental Methodology 106
4.2.1. Microcosm Setup 106
4.2.2. Sampling Regime 107
4.2.3. Analysis Parameters 108

4.3. Limitations 110
4.4. Modelling with the Rayleigh Equation 111
4.5. Microcosm Results 112
4.5.1. Sterile Microcosms (Set X) 112
4.5.2. Active Microcosms (Sets A to F) 113
4.5.3. Sulphate Concentrations 118
4.5.4. Nitrate Concentrations 121
4.5.5. $\delta^{34}SO_4$ Values (Sets A-C, Without Acetate) 121
4.5.6. $\delta^{34}SO_4$ Values (Sets D-F, Without Acetate) 124
4.6. Calculation of the Enrichment Factor (ε) 127
4.6.1. Similarities and Significant Differences Between Microcosm Sets 128
4.6.2. Similarities Between Acetate and Non-acetate Microcosm Sets 129
4.6.3. Comparison of TPC and ε Values 129
4.6.4. Suitability of Range of ε Values 131
5. Enhanced Carbon Balance 132
5.1. Spatial Distribution of Dominant Pathways 132
5.2. A Carbon Balance for Semi-quantitative Analysis 132
5.2.1. Apportioning Carbon Turnover Between Respiration and Methanogenesis 133
5.3. Creating the Enhanced Carbon Balance 134
5.3.1. Utilising Fractionation Factors 134
5.3.2. Apportioning Respiration TDIC between BSR and Non-BSR Processes 135
5.3.1. Advantages of the Enhanced Carbon Balance 135
5.4. Assumptions and Limitations 136
5.5. Grouping of Carbon Balance Data 137
5.6. Carbon Balance Results – Process Proportions 137
5.6.1. MLS59 Results – Pre-pumping 137
5.6.2. MLS59 Results – During Pumping 139
5.6.3. MLS59 Results – Post-pumping 142

5.6.4. MLS60 Results – Pre-pumping 144
5.6.5. MLS60 Results – During Pumping 146
5.7. Carbon Balance Results – Changes in Turnover 149
5.7.1. MLS59 – TDIC Turnover by Process 150
5.7.2. MLS60 – TDIC Turnover by Process 151
5.8. Carbon Balance Results – Implications..... 153
6. Discussion and Conclusions 159
6.1. Discussion 159
6.1.1. Historical Plume Condition..... 159
6.1.2. Plume Condition During the Pilot Study (Thornton et al, 2014) 161
6.1.3. Plume Conditions 2014 to 2016..... 161
6.1.4. Shifting Biodegradation Mechanisms During PAT..... 167
6.1.5. Optimal Positioning of the PAT System 169
6.2. Revised Plume Model..... 170
6.3. Conclusions 173
6.4. Recommendations for Further Work 174
References 176

Table of Figures

Figure 1. Overview of contaminants affecting soil and groundwater in Europe as reported by 27 countries in 2011 (Huber & Prokop, 2012). 4
Figure 2. Illustration of horizontal and vertical capture zones for a partially penetrating extraction well (US EPA, 2008). This is similar to the pumped well on site (section 1.12.2). 7
Figure 3. (a) Typical LNAPL spill migration pathways (b) Typical DNAPL migration pathways. Adapted from National Research Council (2005)..... 10
Figure 4. A typical contaminant plume created by aqueous phase contamination. Adapted from National Research Council., (2005). 10
Figure 5. Dispersion due to mechanical spreading (Adapted from Bear and Cheng, 2010). 12
Figure 6. Molecular diffusion (Bear and Cheng, 2010). 12
Figure 7. The effect of retardation on groundwater clean-up time (Mercer et al, 1990). 13
Figure 8. The plume fringe concept, showing the spatial distribution of dominant respiration processes in a hydrocarbon contaminant plume (Adapted from Meckenstock et al, 2015). 16
Figure 9. Depth integrated and depth specific groundwater sampling. Arrow length shows flow rate (Adapted from Appelo and Postma, 2005 and Cherry, 1984).....17
Figure 10. Layout of a multi-level sampler with tubes going to different depths (CL:AIRE, 2002). 18
Figure 11. Section view of the plume conceptual model, not to scale. Adapted from Baker et al (2012). 24
Figure 12. Plan view of the plume, not to scale. Adapted from Baker et al (2012). 25
Figure 13. Total Dissolved Solids (TDS) at MLS59 (Left) and MLS60 (Right), pre-pumping (Pre-pumping range shown as error bars). 27
Figure 13. Contaminant concentrations (2000-2009) at MLS59 before implementation of PAT (Data with permission from Thornton et al, 2001 and Spence et al, 2001b).....30
Figure 14. Contaminant concentrations (2000-2009) at MLS60 before implementation of PAT (Data with permission from Thornton et al, 2001 and Spence et al, 2001b).....31
Figure 15. Mass flux (2000-2009) at MLS59 before implementation of PAT. Error bars indicate uncertainty based on approximated regional hydraulic head values (Right). In comparison to contaminant concentrations from the same periods (Left. 33
Figure 16. Mass flux (2000-2009) at MLS60 before implementation of PAT. Error bars indicate uncertainty based on approximated regional hydraulic head values (Right). In comparison to contaminant concentrations from the same periods (Left). 34
Figure 17. Plot of contaminant concentrations (total phenolics) against δ^{34}S-SO_4 (Spence et al, 2001b). 38
Figure 18. Cirpka et al., (1999) model showing typical organic plume development in a heterogeneous aquifer (birds eye view). High

concentrations of electron acceptors (oxygen, kg^{-1}) are present outside of the plume (a), high substrate (organic contaminants, kg^{-1}) values are present inside the plume (b), with microbial biomass (kg-1, indicative of contaminant turnover) present at the at the plume fringe (c). 45
Figure 19. Plot of TPC (contamination) concentrations through time at MLS60. Including 2009, before PAT implementation and 2011/2012, after PAT implementation (Thornton et al, 2014).....47
Figure 20. Plot of TDIC (mg/L) against depth (MGBL) for 2009 and 2012 for MLS60 (Thornton et al, 2014). 49
Figure 21. Groundwater hydrochemistry sampling line, showing (1) HDPE tubing coming from well, (2) Peristaltic pump and (3) In-line monitoring equipment.....53
Figure 22. The setup for the gas chemistry sample collection, showing (1) Microseeps™ Vial, (2) N_2 Cylinder.....55
Figure 23. The setup for the $\delta^{34}S$-SO_4 field sample collection, showing (1) Peristaltic Pump, (2) Sampling Bottles, (3) HDPE Tubing, (4) Generator. Sampling bottles were then exchanged for the correct vessels during TDIC collection. 56
Figure 24. a) Blister trap set-up in the field and b) An inverted 'blister trap bubble' with (1) Inflow/outflow tubes (2) Valves. (Currently filled with a gas sample).....57
Figure 25. Attachment of the anaerobic gas bag.....59
Figure 26. Contaminant concentrations at MLS59 in 2014 and 2015 in comparison to the pre-PAT average (Pre-pumping range shown as error bars). 65
Figure 27.Contaminant concentrations at MLS59 in 2014. 2015 and 2016 in comparison to the pre-PAT average (Pre-pumping range shown as error bars). 66
Figure 28. Contaminant concentrations at MLS60 in 2014, 2015 and 2016 in comparison to the pre-PAT average (Pre-pumping range shown as error bars). 67
Figure 29. Nitrate concentrations at MLS59 in 2014 (left). Related to TPC 2014 and 2015 (right). 69
Figure 30. Nitrate concentrations at MLS59 in 2014 and 2016 (left). Related to TPC 2014, 2015 and 2016 (right).....71
Figure 31. Nitrate concentrations at MLS60 in 2014 and 2016 (left). Related to TPC 2014, 2015 and 2016 (right).....73
Figure 32.TDIC concentrations at MLS59 in 2014, 2015 and historical (left), in relation to TPC in2014 and 2015 (right).....75
Figure 33. TDIC concentrations at MLS59 in 2014, 2015 and 2016 (left), in relation to TPC 2014, 2015 and 2016 (right). 77
Figure 34. TDIC concentrations at MLS60 in 2014, 2015 and 2016. Related to TPC 2014, 2015 and 2016.....80
Figure 35. $\delta^{13}C$-TDIC (left) and TPC (right) at MLS59 for 2014, 2015 and 2016. 83
Figure 36. δ13C-TDIC (left) and TPC (right) at MLS59 for 2014, 2015 and 2016. 85

Figure 37. δ^{13}C-TDIC (left) and TPC (right) at MLS60 for 2014, 2015 and 2016. 87
Figure 38. δ^{34}S-SO_4 TDIC concentrations at MLS59 in 2014, 2015 and 2016, in comparison to source δ^{34}S-SO_4 (left). TPC in 2014, 2015 and 2016 (right). 89
Figure 39. δ^{34}S-SO_4 concentrations at MLS60 in 2014, 2015 and 2016, in comparison to source δ^{34}S-SO_4 (left). TPC in 2014, 2015 and 2016 (right). 92
Figure 40. δ13C-CH4 values at MLS59 in 2016, in comparison to the typical range of δ13C-CH4 values (left). Methane concentrations at MLS59 in in 2014, 2015 and 2016 (right). 97
Figure 41. δ13C-CH4 values at MLS59 in 2016, in comparison to the typical range of δ13C-CH4 values (left). Methane concentrations at MLS59 in in 2014, 2015 and 2016 (right). 99
Figure 42. P-cresol concentrations for the sterile microcosms; showing Percentage (%) of P-cresol remaining against time. 113
Figure 43. P-cresol concentrations for the active microcosms; showing percentage (%) of p-cresol remaining against time. 115
Figure 44. TPC concentrations for the active microcosms; showing percentage (%) of TPC remaining against time. 116
Figure 45. Acetate concentrations for the active microcosms; showing percentage (%) of acetate remaining against time. 118
Figure 46. SO_4 Concentrations against time. 120
Figure 47. $\delta^{34}SO_4$ isotope values for sets A and B. 122
Figure 48. $\delta^{34}SO^4$ isotope values. Set C and Set A-C Averages. 123
Figure 49. $\delta^{34}SO_4$ isotope values for sets D and E. 125
Figure 50. $\delta^{34}SO_4$ isotope values. Set F and Set D-F Averages 126
Figure 51. An example of a $\delta^{34}SO_4$ vs Ln(SO_4) plot, displaying trend lines with the gradient ε. 127
Figure 52. A plot of enrichment factor (ε) against TPC concentrations, between 0 mg/L and 6000 mg/L. Statistical extrapolation (linear extrapolation of averages – solid line), likely upper and lower bounds (polynomial extrapolation of max/min values – dashed lines). 130
Figure 53. Average carbon balance for MLS59 before 2011 when pumping started. 138
Figure 54. Average carbon balance for MLS59 for 2011 and 2012. 140
Figure 55. Carbon balance for the lower plume core at MLS59. 141
Figure 56. Carbon Balance for MLS59 in 2014 and 2015. 143
Figure 57. Carbon Balance for MLS59 in 2016. 144
Figure 58. Average carbon balance for MLS60 before 2011 when pumping started. 145
Figure 59. Average carbon balance for MLS60 for 2011 and 2012. 147
Figure 60. Average carbon balance for MLS60 between 2014 and 2016. 149
Figure 61. TDIC Created by process for MLS59, depth integrated (Yearly range indicated as error bars. 150
Figure 62. TDIC Created by process for MLS59, in relation to pre-pumping values (zero). Yearly range indicated as error bars. 151

Figure 63. TDIC Created by process for MLS60, depth integrated. Yearly range indicated as error bars. 152
Figure 64. TDIC Created by process for MLS60, in relation to pre-pumping values (zero). Yearly range indicated as error bars. 152
Figure 65. Front view of the plume at MLS59, showing an exaggerated conceptual model of an 'upconing' effect (not to scale). 165
Figure 66. Front view of the plume at MLS59, showing an exaggerated conceptual model of the 'fingering' effect (not to scale). 166
Figure 68. Revised conceptual plume model exhibiting data for 2014 to 2016 (Excluding nitrate breakthrough, see Section 6.1.3.3. 172

Table of Tables

Table 1. Natural attenuation processes. 5
Table 2. Relative energy yields of the major processes controlling organic matter biodegradation in the subsurface (Adapted from Canfield, 1993). .. 14
Table 3. Concentrations of organic compounds in the source area (data from Lerner et al, 2000). 26
Table 4. Carbon balance produced by the pilot study, apportioning the increased TDIC during the 2012 sampling round (relative to 2009), between methanogenesis and respiration end members (Thornton et al., 2014). 51
Table 5. Sulphide concentrations at MLS59, average for 2014, 2015 and 2016. 101
Table 6. Sulphide concentrations at MLS60, average for 2014, 2015 and 2016. 102
Table 7. Microcosm conditions after spiking. 107
Table 8. P-Cresol and Phenol loss statistics for active microcosms (Sets A to F). 114
Table 9. Enrichment factors and correlation strengths for all active microcosm sets (A-F). 128
Table 10. Similarity matrix for enrichment factors within all active microcosm sets (t-test only). 129

List of Symbols and Abbreviations

AMO	Anaerobic methane oxidation
Aq	Aqueous phase
BSR	Bacterial sulphate reduction
bgl	Below ground level
BH	Borehole
CL:AIRE	Contaminated Land: Applications In Real Environments
DNAPL	Dense non-aqueous phase liquid
DIC	Dissolved inorganic carbon
EA	Environment Agency
EPA	Environmental Protection Agency
EU	European Union
HDPE	High-density polyethene
V-CDT	IAEA Vienna-Cañon Diablo Troilite standard
LNAPL	Light non-aqueous phase liquid
mbgl	Metres below ground level
MNA	Monitored natural attenuation
MLS	Multi-level sampler
NHBC	National house-building council
NA	Natural attenuation
NAPL	Non-aqueous phase liquid
POC	Particulate organic carbon
PAT	Pump and Treat
SEPA	Scottish Environmental Protection Agency
TDIC	Total dissolved inorganic carbon
TDS	Total dissolved solids
TOC	Total organic carbon
TPC	Total phenolic compounds
UK	United Kingdom
US	United States of America
V-PDB	Vienna-Peedee Belemnite Standard

Chemical symbology

BaCl	Barium Chloride
$BaSO_4$	Barium Sulphate

$\delta^{13}C$	Carbon 13 Isotopes
CO_2	Carbon Dioxide
$CuCl_2$	Copper Chloride
CuS	Copper Sulphide
H_2S	Hydrogen Sulphide
Fe	Iron
Mn	Manganese
CH_4	Methane
$\delta^{13}C\text{-}CH_4$	Methane ^{13}C Isotopic Signature
NO_3	Nitrate
N_2	Nitrogen
O_2	Oxygen
H_3PO_4	Phosphoric Acid
Na	Sodium
$SrCO_3$	Strontium Carbonate
SO_4	Sulphate
$\delta^{34}S$	Sulphur 34 Isotopes
$\delta^{34}S\text{-}SO_4$	Sulphate ^{34}S Isotopic Signature
H_2SO_4	Sulphuric Acid
$\delta^{13}C\text{-}TDIC$	Total Dissolved Inorganic Carbon ^{13}C Isotopic Signature

Symbols		**Units**	
%	percent	M	Metres
‰	per mill	G	Grams
°	Degrees	L	litres
E	Enrichment Factor	°C	Degrees Centigrade
		pH	$-\log_{10}H^+$
Prefix		Eh	E° (volts)
N	Nano	m/d	metres per day
M	Micro	m/yr	metres per year
M	Milli	m^3h^{-1}	meters cubed per hour
C	Centi	Ml	millilitres
K	Kilo	v/v	Concentration (%)

CHAPTER 1

1. Introduction

1.1. Rationale

Groundwater resources around the world are often impacted by pollution from historical sources. The United Kingdom's (UKs) diverse industrial heritage is no exception from this, with groundwater at numerous sites across the UK being contaminated with organic and/or inorganic pollutants. In many locations, this contamination can be severe and requires treatment; this is often at great cost and on many occasions, remediation can be technically difficult to achieve the required standards.

Only through using well defined scientific measurements and analysis can we hope to improve knowledge of how to treat these sites effectively in a short timescale, and efficiently with low monetary and carbon footprint costs.

This study will be focused around one such site which has historically been contaminated by waste from a former coal-tar distillation plant. The choice of study site for this thesis is based upon the following considerations

(1) The good site characterisation achieved through previous studies between 1998 and 2014 (Spence et al, 2001a; Spence et al, 2001b; Baker, 2012; Thornton el al, 2001; Thornton et al, 2014) – see section 1.12;
(2) The site being a good real-world analogue for the Cirpka et al model (1999) – see section 1.15; and,
(3) The recent implementation of Pump and Treat (PAT) remediation on the site has created new biogeochemical conditions within the plume previously unexamined before the Thornton et al. (2014) pilot study (section 1.16).

1.2. Study Focus

This thesis will explore further the recent changes in in-situ biodegradation, as outlined by Thornton et al. (2014) in a study shortly after the implementation of Pump and Treat (PAT) remediation. New datasets will be compared to historical groundwater analyses (Spence et al, 2001b; Baker, 2012; Thornton et al, 2014) at the site before the implementation of PAT remediation.

The Thornton et al. (2014) pilot study has shown that a 'significant enhancement of in-situ biodegradation is possible by engineered intervention using Pump and Treat', with initial estimations putting the factor of increase around 2. This thesis will look to further define the mechanisms and pathways responsible for this increase in biodegradation by extending the Thornton et al. (2014) carbon balance model.

Previous studies on the site have also outlined the significance of Bacterial Sulphate Reduction (BSR), which can be a key in-situ biodegradation process in the plume (Spence et al, 2001b; Thornton et al, 2014). This thesis aims to create a more accurate assessment of the rate of BSR within the plume, both pre and post treatment. This increase in accuracy will allow better analysis of BSR's potential to significantly shorten the time-span (and therefore energy costs) of the engineered PAT intervention.

Finally, this thesis will present a new conceptual model of the plume based upon new findings. This model will aid in identifying approaches via which enhanced biodegradation can be optimised within the PAT system. The mechanisms outlined by this model may be more widely applicable to a wider range of sites which have conditions similar to that of the study site or hold largely to the Cirpka et al model (1999).

1.3. A History of Land Contamination

Various parts of the UK have a legacy of contaminated land as a product of over 200 years of diverse industrial heritage (EA, 2016). Historically, poor management of industrial sites and inadequate waste disposal practices have resulted in the intentional or accidental release or disposal of harmful

substances onto the land (European Commission, 2013). Consequently, many groundwater resources across developed nations have been impacted by this pollution, much of which is still harmful today. Remediation of this contaminated land (and associated groundwater) is a significant environmental issue across the UK as well as worldwide (Rivett et al, 2002).

UK statutory bodies define contaminated land as “any land which by reason of substances in, on or under the land that – (a) significant harm is being caused or there is a significant possibility of such harm being caused; or (b) significant pollution of controlled waters is being caused, or there is a significant possibility of such pollution being caused” (Environmental Protection Act, 1990).

Estimates of 50,000-100,000 contaminated sites across the UK (Parliamentary Office of Science and Technology, 1993) are often quoted. However, more recent figures from the Environment Agency (EA, 2005) say this estimate could rise to 325,000 sites.

Of these 325,000 sites, the EA (2005) consider >30,000 as requiring further active remediation, which is usually extremely expensive and carbon intensive. Finding the most appropriate and cost-effective for each site based upon its own hydrogeology, chemistry and proximity to receptors is necessary.

1.4. Methods of Remediation

Generally, soil pollutants can be classified into two main groups: ‘(1) organic pollutants, such as petroleum wastes and nutrients and (2) inorganic pollutants, such as heavy metals and radionuclides’ (EU, 2013). Huber & Prokop (2012) compiled a large dataset of the common types of contaminants across the EU (Figure 1).

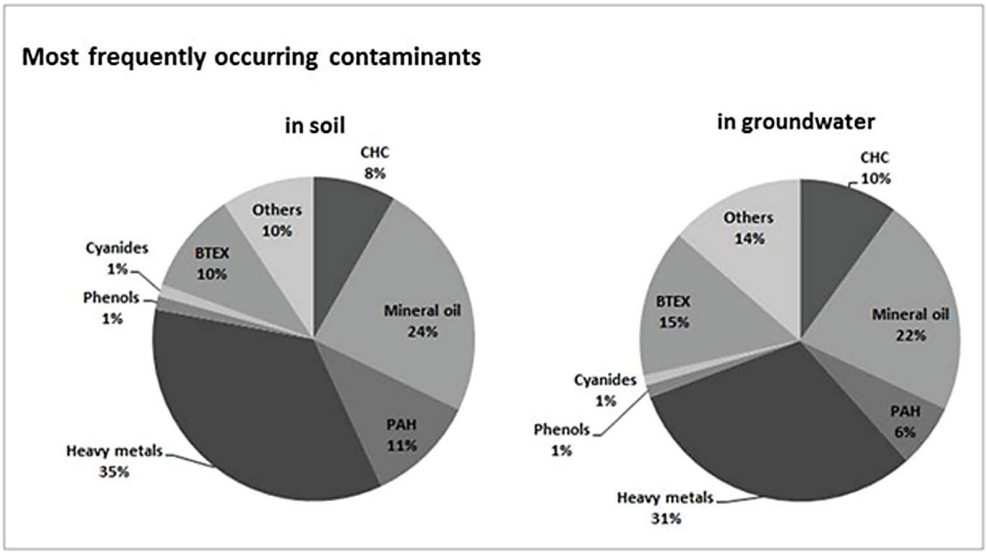

Figure 1. Overview of contaminants affecting soil and groundwater in Europe as reported by 27 countries in 2011 (Huber & Prokop, 2012).

A wide range of remediation methods are available for soils and water. Mechanisms for reducing the environmental impact of an environmental contaminant include '(1) removing/treating the pollutant, (2) breaking/removing the pathway from source to receptor and/or (3) protecting/removing the receptor' (Environmental Protection Act, 1990), although many modern techniques utilise more than one of these methods.

The exact choice of remediation technique depends on multiple factors, which are linked to both plume characteristics (contaminant(s) present, soil/rock properties) and socio-economic considerations (costs, risk management effectiveness and social impacts).

In practice, remediation methods can be generally divided into two categories (1) engineered methods (ex-situ) such as excavation and off-site disposal, and (2) process-based methods (in-situ) such as bioremediation that acts to remove, stabilise or degrade the contaminant in-situ (Rivett et al, 2002; EA, 2016). Standard use of these practices has varied through time due to changing legislation. Engineered methods have traditionally been common within the UK, however there is some evidence that process-based methods are becoming increasingly favoured (Rivett et al, 2002),

1.4.1. Dig and Dump

Historically, the physical removal of contaminated soil, followed by disposal in a suitable waste facility, or “dig and dump", has often taken precedence in the UK due to low costs and timescales (NHBC and EA, 2008). However, new legislation has begun to be introduced, such as the EU Landfill Directive (1999/31/EC), which is designed to discourage overuse of landfill in this way and encourage the usage and creation of other forms of technologies (Rivett et al. 2002; Syms, 2010).

1.4.2. Natural Attenuation (NA)

Many sites can be costly to remediate and often, where remediation costs are strictly prohibitive and receptors are not at risk, contaminants are left to reduce by natural attenuation (NA). NA is a combination of the naturally occurring physical, chemical and biological processes that serve to reduce contamination over a period of time (Table 1; Carey et al, 2000).

Physical	Dispersion Diffusion Dilution Volatilisation
Chemical	Sorption Abiotic reaction
Biological	Aerobic biodegradation Anaerobic biodegradation Bioaccumulation

Table 1. Natural attenuation processes.

NA can often take a long period of time and hence attenuation is normally closely monitored to evaluate its effectiveness and that conditions have not changed to increase the risk; this is simply termed Monitored Natural Attenuation (MNA).

1.4.3. Pump and Treat (PAT)

Pump ant Treat (PAT) remediation systems operate by the removal of contaminated water from an aquifer for subsequent treatment at the surface (ex-situ).

PAT systems work in two primary ways:

(1) clean-up and removal of contaminants (as described above); and,
(2) implementing hydraulic containment, whereby groundwater movement in the local area is controlled by preventing down-gradient movement of contaminants (Figure 2) (US EPA, 2008).

Conventional PAT systems typically pump water out of a (or multiple) borehole(s) which penetrate the full thickness of the aquifer in order to remove contaminants from all depths. Conventional PAT remediation has historically been one of the most widely used groundwater remediation technologies within the United States of America (US EPA, 1996), however use with the UK has been fairly limited.

More recently conventional PAT techniques have come under criticism for being too expensive, too time-consuming and for frequently failing to deliver the expected remediation due to issues such as lengthy tailing (Rivett et al., 2006). As an alternative, newer smart PAT techniques have been developed.

Smart PAT systems are designed for a more efficient delivery of remediation objectives. This is typically achieved by undertaking a more detailed initial plume characterisation and using this data to support decision making and to aid the design of the remediation. Detailed monitoring of the remediation is typically undertaken throughout with the results allowing re-evaluation and, if necessary, the redesign of the operating well field (Hoffman, 1993). In some cases, smart PAT can also include the removal of source terms.

There are many variations on PAT including chemical and biological enhancements technologies (US EPA, 1996).

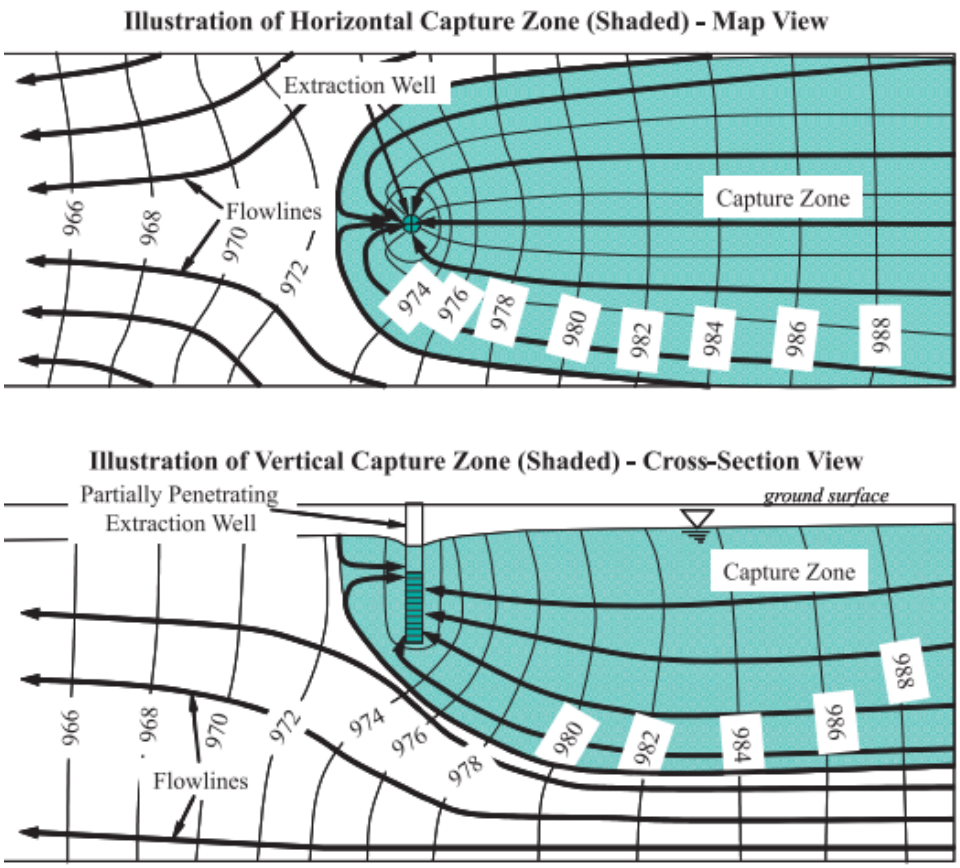

Figure 2. Illustration of horizontal and vertical capture zones for a partially penetrating extraction well (US EPA, 2008). This is similar to the pumped well on site (section 1.12.2).

1.4.4. Other Methods

The number of other methods for groundwater remediation are too numerous to describe, however, they can be broadly broken down into 4 categories (DEFRA, 2010; Appelo and Postma, 2005):

(1) Physical In-situ treatment. This involves physically extracting or sparging contaminants to remove them from groundwater that is in-situ and then dispose of them;
(2) Chemical/biological in-situ treatment. This involves chemically oxidising or biodegrading contaminants in-situ to change the contaminants into an inert form;
(3) Chemical/biological ex-situ treatment. This involves using method (1) to remove the contaminants from the groundwater, followed by method (2); and,
(4) Containment. This involves creating a barrier, either physical or hydrogeological to stop the contaminants migrating towards an endangered receptor.

1.5. Organic Contaminants Within Aquifers

1.5.1. Migration of Contaminants Above the Water Table

Organic contaminants left at or near ground surface level are invariably left above the water table in the unsaturated zone. Nevertheless, these contaminants can move downwards through the unsaturated zone in several ways, entering the saturated zone below (Lerner et al, 2003).

The method of this migration depends on the properties of the pollutants and the characteristics of the unsaturated zone, with more soluble compounds generally being more mobile in the subsurface. In unfractured bedrock the permeability of the unsaturated zone determines how rapidly contaminants migrate through it; however, in systems where fractures are prevalent, these fractures can often deliver large quantities of contaminants to the saturated zone in short spaces of time.

Organic contaminants left at or near ground surface level are generally in the form of solids, non-aqueous phase liquids (NAPL, e.g. oil) or are

already dissolved in an aqueous phase. Commonly however, NAPLs can contain a mixture of different organic compounds, and initial contact with rainwater moving through the unsaturated zone can cause dissolution of the more soluble components within this mixture. Thus, this creates additional aqueous phase contamination (National Research Council, 2005).

Mobile contaminants in the unsaturated zone are generally classified into three phases:

(1) As a Light Non-Aqueous Phase Liquid – LNAPL (low solubility, density lesser than water);
(2) As a Dense Non-Aqueous Phase Liquid – DNAPL (low solubility, density greater than water); or,
(3) As an Aqueous Phase Contaminant (high solubility).

Each of these phases will migrate downwards through the unsaturated zone due to gravity and the flushing effect from rainwater which lands above the spill (Figure 3).

1.5.2. Migration of Contaminants Below the Water Table

1.5.2.1. LNAPL and DNAPL

Each of the three phases listed above interacts differently with the saturated zone when it reaches it (Lerner et al, 2003; Rivett et al, 2014). LNAPLs, when acting as a separate free phase component are lighter than water, thus they will generally float on the upper surface of the aquifer when they reach it (Figure 3(a)). This contrasts with DNAPLs which will continue to sink until they reach an impervious boundary (Figure 3(b)).

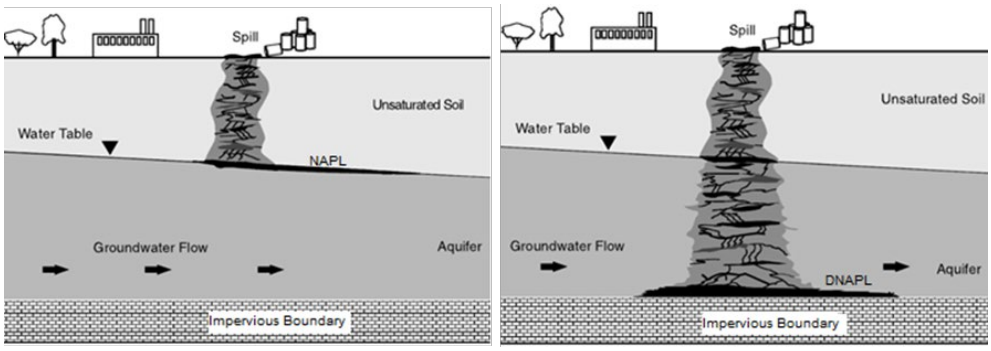

Figure 3. (a) Typical LNAPL spill migration pathways (b) Typical DNAPL migration pathways. Adapted from National Research Council (2005)

1.5.2.2. Aqueous Phase Contaminants

On reaching groundwater, aqueous phase contaminants that have already been dissolved will neither float nor sink, but will move with the flow of groundwater, forming a plume which moves away from the original point of contamination (Figure 4).

The movement of these aqueous organic contaminants is determined by the physical laws of advection, dispersion and diffusion as well as aquifer matrix characteristics that control effects such as sorption and retardation.

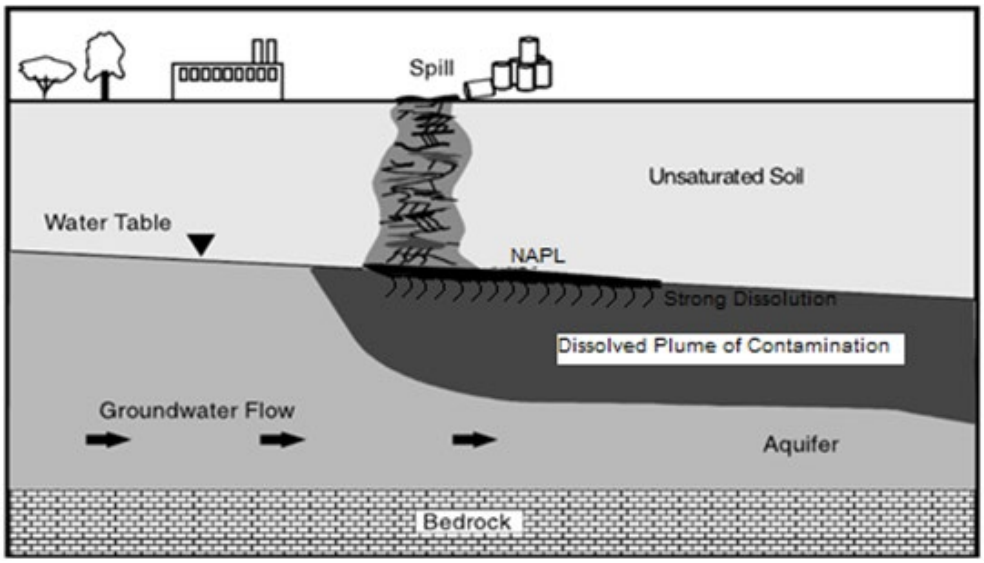

Figure 4. A typical contaminant plume created by aqueous phase contamination. Adapted from National Research Council., (2005).

These laws are discussed further in the next two sub-sections.

1.6. Advection, Dispersion and Diffusion

The main process controlling the size and shape of a contaminant plume is advection. Advection is the process of solute transport by the bulk movement of groundwater through the aquifer, and by the differential movement speeds of particles within this flowing groundwater (Schulze-Makuch, 2009).

The average bulk groundwater movement (average linear velocity) is called the advective velocity when referring to the transport of solutes.

Darcy's Law (Equation 1) can be used to describe flow rate of water, across a given cross sectional area, within an aquifer. If the water flow rate and the effective porosity are known, the average linear velocity can be ascertained (Equation 2).

Equation 1

$$Q = -K\,A\,\frac{dh}{dl}$$

Where:

Q = water flow rate (volumetric discharge);

K = hydraulic conductivity;

A = cross sectional area of flow; and,

dh/dl = hydraulic gradient, that is, the change in head over the length of interest.

Equation 2

$$V_l = \frac{Q}{An}$$

Where:

V_l = linear water flow velocity;

Q = water flow rate (volumetric discharge);

A = cross sectional area of flow; and,

n = effective porosity.

The law states that larger hydraulic conductivity and hydraulic head gradients lead to faster flow rates within any aquifer of a given cross-section.

Dispersion causes the spreading out the volume of contaminants they move through the subsurface (Figure 5). Particles (of contamination) will experience different flow paths, i.e. some particles move through larger pores and experience less friction, whilst others flow through smaller pores and are slowed down (Figure 5a). Some particles take a more direct route through larger pores, which are in a more linear orientation whilst others experience the opposite (Figure 5b). As a consequence of this, contaminant plumes spread over a larger area of aquifer by dispersion than that which would be predicted by advection alone.

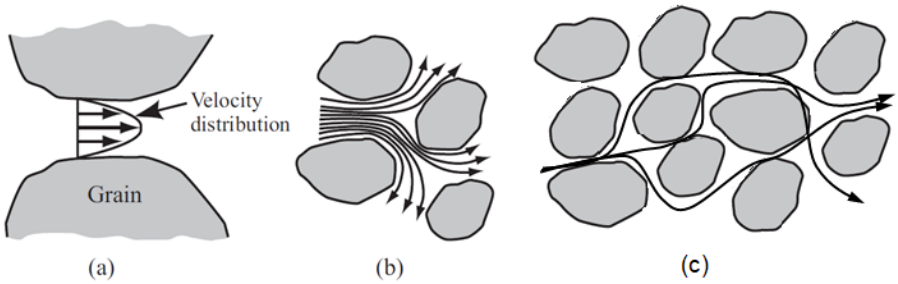

Figure 5. Dispersion due to mechanical spreading (Adapted from Bear and Cheng, 2010).

Diffusion causes contaminant migration across concentration gradients, with contaminants generally migrating down a concentration gradient from zones of high concentration to those of low concentration. However, it is worth noting that diffusion can also occur up a concentration gradient if there is a phase change present within the contaminants (i.e. a shift between aqueous and non-aqueous phases).

This has a similar effect to that of dispersion (described above), causing the spreading out of contaminants (Figure 6). This effect, however, is normally an order of magnitude weaker than that of dispersion.

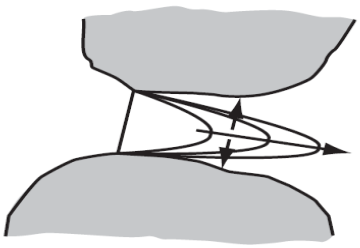

Figure 6. Molecular diffusion (Bear and Cheng, 2010).

1.7. Sorption and Retardation

The properties of the aquifer matrix also play a large part in the movement of organic contaminants through the saturated zone, as organics are often sorped to and desorbed from the aquifer matrix during their transport.

For organics, sorption can occur by partitioning to particulate organic matter or adsorption onto clay minerals, with sorption to particulate organic matter being considered the more important process at high levels of particulate organic carbon, POC (Guo et al, 1995). Generally, compounds that have low solubility, high polarity and high complexity are more strongly sorped to aquifer solids (Nyer, 2000). Soluble organic compounds with limited complexity (e.g. phenol) interact only weakly with the aquifer (Spence, 2001b).

Sorption, and then later desorption, of contaminants has the effect of the aquifer matrix temporarily holding the contaminants back, causing the water to move through the aquifer matrix faster than the contaminant. 'This process is known as retardation and causes a 'tailing' of contaminant concentrations whereby contaminants remain detectable, sometimes for a considerable timespan, after the main bulk of the contaminant plume has been removed or passed by' (Mercer et al, 1990; Figure 7).

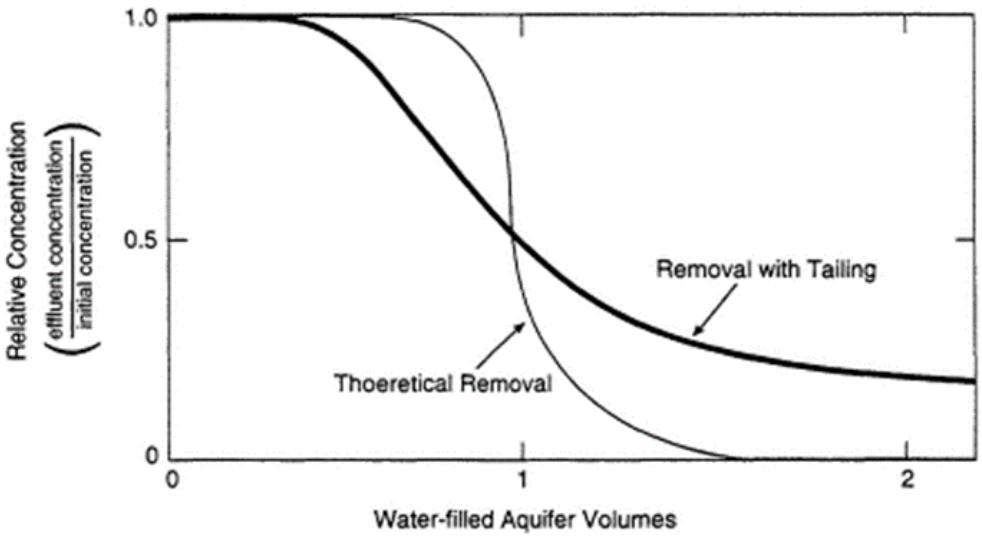

Figure 7. The effect of retardation on groundwater clean-up time (Mercer et al, 1990).

1.8. Persistence

The length of time that organic compounds of anthropogenic nature remain present in the subsurface (persistence), varies greatly from compound to compound. The persistence of any specific organic substrate often depends on the ability of microorganisms to use this substrate for energy.

Microorganisms are able to use substrates when (1) they possess the necessary tools (e.g. enzymes) to degrade them, (2) if required, electron acceptors are present (e.g. oxygen), and (3) the substrate is not toxic to the microorganisms.

1.9. Biodegradation Processes for Organic Contamination

The degradation of organic compounds in the subsurface is determined by the activity of microorganisms. Microorganisms can utilise a number of different reactions in order to gain energy from these substrates; these reactions can be categorised by energy yield (Table 2).

Energy Yield	Process	General Equation
Highest	Aerobic Respiration	$O_2 + 4H^+ + 4e^- \rightarrow 2H_2O$
	Denitrification	$NO_3^- + 6H^+ + 6e^- \rightarrow 0.5N_2 + 3H_2O$
	Manganese (IV) Reduction	$Mn0_2 + 4H^+ + 2e^- \rightarrow Mn^{2+} + 2H_2O$
	Iron (III) Reduction	$Fe(OH)_3 + 3H^+ + e^- \rightarrow Fe^{2+} + 3H_2O$
	Sulphate (IV) Reduction	$SO_4^{2-} + 10H^+ + 8e^- \rightarrow H_2S + 4H_2O$
Lowest	Methane Formation	$CO_2 + 8H^+ + 8e^- \rightarrow CH_4 + 2H_2O$

Table 2. Relative energy yields of the major processes controlling organic matter biodegradation in the subsurface (Adapted from Canfield, 1993).

Microorganisms that can use processes with a higher energy yield will gain a competitive advantage. Microorganisms will of course adapt a culture to best suit their environment; this coupled with competitive advantage means that microbes in a given system will normally use the most energetic process for which it has the electron acceptors (Christensen et al, 2000; Logue et al, 2015). There is one notable exception to this rule, which may

not always apply in systems with rapidly changing conditions (Logue et al, 2015).

Where no electron acceptors are available for respiration processes, fermentation (e.g. methanogenesis) becomes the most energetically favourable process. In additon, there is growing evidence that methanogenesis regularly co-occurs in conjunction with other more energetically favourable processes. As such methanogenesis is understood to be a dominant attenuation process under a wide range of conditions (Garg et al, 2017).

1.10. Biodegradation Sequencing Within Contaminant Plumes

Classically, within groundwater, depletion of electron acceptors occurs over time as electron acceptors are sequentially utilised. This leads to a profile where older, deeper water within aquifers tends to have lower amounts of available electron acceptors than newer water closer to the surface.

However, in a plume of contaminated groundwater this profile differs from the norm. Typically, in this scenario, oxygen and nitrate reduction only takes place at the fringe of the plume, where these electron acceptors are constantly present due to the action of diffusion and dispersion, which constantly mixes new oxidants into the fringe (Cirpka et al, 1999; Chu, 2005; Annesar, 2008).

Other electron acceptors such as Manganese (IV), Iron (III) and Sulphate (IV) are also often used within the plume fringe, however, these acceptors can usually be found slightly deeper within the plume core due to these reactions being less energetically favourable than oxygen and nitrate reduction (Cribbin et al, 2014; Meckenstock et al, 2015).

Where electron acceptors are significantly depleted, methanogenesis is likely to become a dominant process due to other processes being largely excluded. However, in some cases, Iron (III) and/or Manganese (IV) reduction may still be concurrently occurring with this methanogenesis due to bioavailable iron and/or manganese in the aquifer matrix (Foght, 2008).

This sequence of redox zones has led to the development of the plume fringe ‘model’ as shown in Figure 8 (Cirpka et al, 1999). Studies such as Thornton et al (2014) and Van Breukelen et al (2004) have further demonstrated that this model is fundamentally accurate by ‘using high frequency sampling to resolve gradients of electron acceptors through plumes in contaminated aquifers’ (Meckenstock et al, 2015). However, the applicability of such models is dependent on factors such as (1) aquifer homogeneity, (2) steady-state flow and (3) a steady contaminant source term (Cirpka et al, 1999)

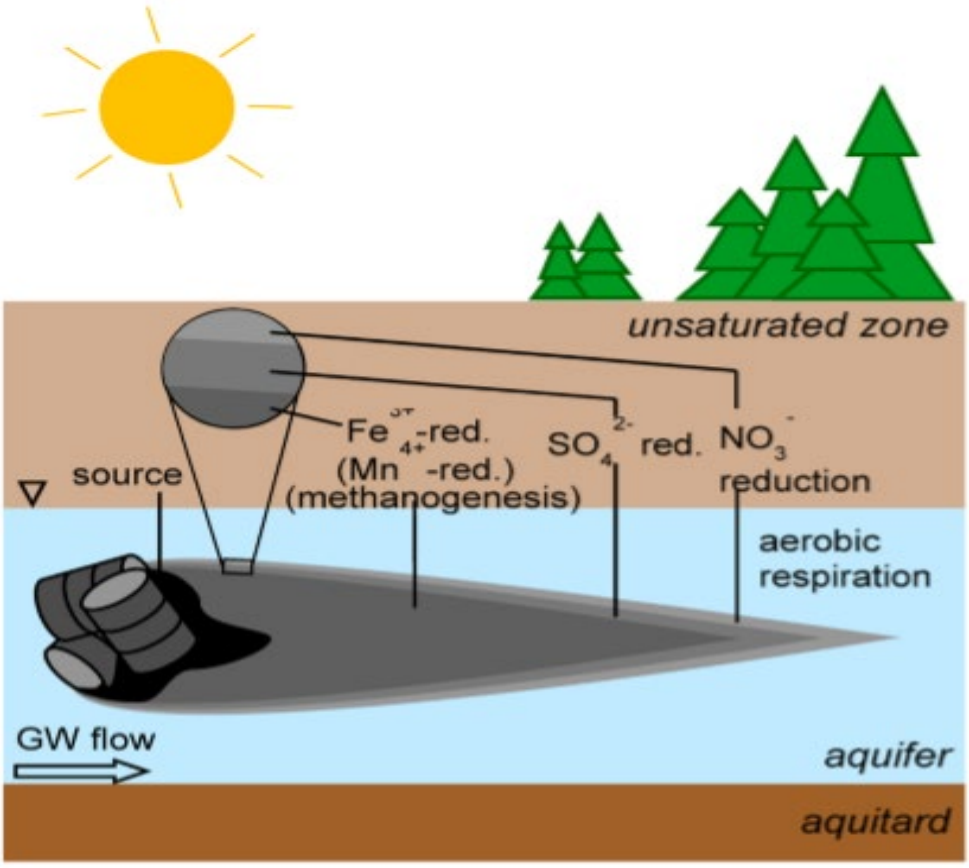

Figure 8. The plume fringe concept, showing the spatial distribution of dominant respiration processes in a hydrocarbon contaminant plume (Adapted from Meckenstock et al, 2015).

1.11. Groundwater Sampling

For information on specific tools and equipment used for this study, please see methodologies in section 2.

1.11.1. Boreholes

Borehole wells can be created by a variety of methods, primarily though they are created by augering or drilling. Wells can be either temporary or permanent and have a variety of designs, with design choices being linked to the short and long-term objectives of the well and the types of contaminants likely to be monitored (EA, 2006).

In general, boreholes are targeted to be either (1) depth integrated with a long well screen, or (2) depth specific with a short well screen (Appelo and Postma, 2005). Specific depth sampling is usually required for scientific studies, as depth integrated sampling gives mixed data from across the width of the sample screen, which limits data analysis significantly (Figure 9).

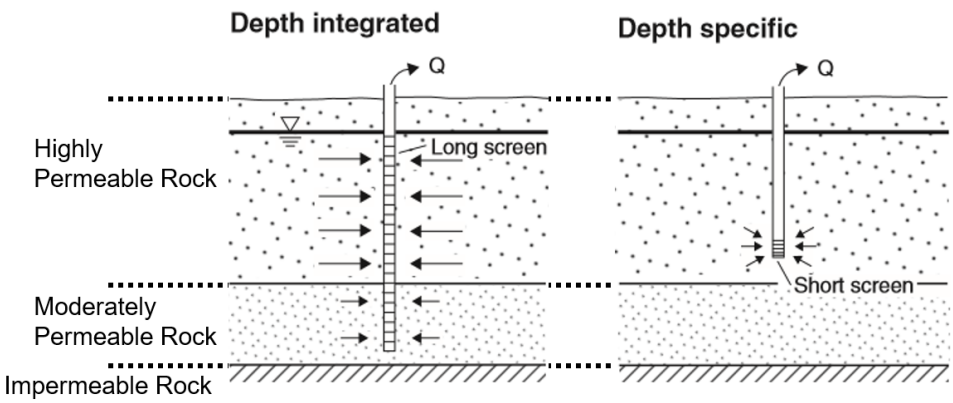

Figure 9. Depth integrated and depth specific groundwater sampling. Arrow length shows flow rate (Adapted from Appelo and Postma, 2005 and Cherry, 1984)

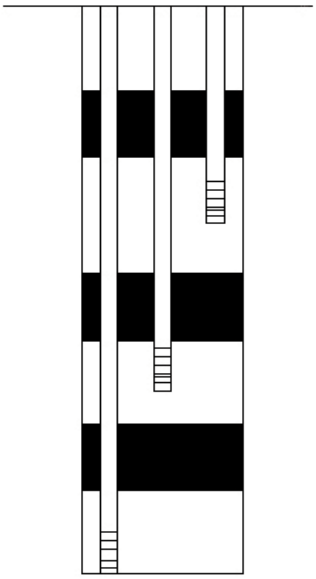

Figure 10. Layout of a multi-level sampler with tubes going to different depths (CL:AIRE, 2002).

One type of depth specific sampling system is called a multilevel sampler. A multi-level sampler includes multiple channels of tubing within one sampling well (Figure 10). These tubes reach down to different levels effectively allowing samples to be taken from multiple short screens at different depths (CL:AIRE, 2002).

Multi-level samplers are particularly useful for scientific analyses, as sampling from multiple depths allows a vertical profile of plume chemistry to be built up.

1.11.2. Purging Pumps

Prior to conducting sampling, the depth of the water table should be determined, and the well should be purged. Any pump can be used for this purpose as the water purged will not be used for any chemical analysis.

Purging is necessary as groundwater can remain in a monitoring point for long periods of time between samples, and during this time it can undergo significant chemical and biological changes such that it may no longer be representative of the water surrounding the well (EA, 2001; Nielsen and Nielsen, 2007).

‘In the absence of any technical evidence to support a specific purging, purging should be undertaken until the behaviour of field determinants (e.g. conductivity, pH), stabilises’ (EA, 2001). At least three borehole volumes should be pumped to demonstrate that the stabilisation is genuine. The results of the trial may then be used to determine a standard purge volume for the borehole.

In addition, all purging should typically be undertaken at a low flow rate, removing as limited an amount of water as possible based on the above. Low flow purging helps to reduce turbidity caused by purging, reducing the chances of mobilising excess unwanted sediment which can then end up in the sample (Puls et al, 1996).

1.11.3. Sampling Pumps

A variety of different pumps can be used to sample groundwater systems, including peristaltic, inertial and bladder pumps. Pumps can be divided into two main categories: submersible and non-submersible.

In general, pumps are chosen so that they generate an adequate flow rate, have acceptable power demands and do not affect sample chemistry.

1.11.4. Chemical Tools for Groundwater Analysis

Chemical analysis of groundwater can normally identify the groundwater’s potential to cause damage to properties, health or ecology (Dohare et al, 2014). Water samples can be tested for a suspected pollutant directly, or for other chemical parameters (e.g. pH, Eh, alkalinity, or electron acceptor concentrations) which may indicate the presence of an unknown type of contamination (Gorde and Jadhav, 2013; Baker, 2012; UKTAG 2012).

However, in real world scenarios, parameters such as Eh, alkalinity and electron acceptor concentrations are subject to a variety of complex processes, both chemical and biological. This can create large uncertainties when using these parameters to analyse redox conditions and/or to outline biogeochemical processes (Christensen et al, 2000).

Hence, under real world conditions it is normally impossible to estimate rates of biodegradation using these parameters.

Combining chemical analysis with other current techniques can often lead to enhanced results. These results can then be used better assess in-situ conditions (Christensen et al, 2000).

1.11.5. Stable Isotope Tools for Groundwater Analysis

Stable isotopes within element compounds can be fractionated during various chemical and biogeochemical processes, as such the isotope ratio of these compounds can act as a tracer for the historical presence, or lack of, these biogeochemical processes (Kaplan, 1975).

Kinetic isotope fractionation is a process that separates stable isotopes based upon their different masses. This can occur where either (1) molecules enriched in lighter isotopes diffuse faster across cell membranes, creating an isotopic shift, or (2) in compounds where a difference in bond energies is apparent between light heavy isotopes leading to the preferential consumption of the more energetically favourable compound fraction by microbes (Hoefs, 2018). Isotopic shifts are usually measured in the per mil measurement due to their small size.

There are numerous advantages to using stable isotope techniques for groundwater analyses and they are generally seen as one of the ‘most useful tracers in terms of providing new insights into hydrological and hydrogeological processes’ (Kendall and Caldwell, 1998). This is because of the scale upon which isotopic effects acts gives an effective tool for the analysis of both micro and macro scale processes (McDonnell and Kendall, 1992; Buttle, 1994). These tools, however, do require a ‘good understanding of the factors controlling isotopic fractionation, within the studied system as well as an understanding of the initial state of the system’ (Spence, 2001b).

In particular, stable isotopes of carbon and sulphur have been shown to be particularly useful with regards to carbon cycling and BSR respectively (Newton and Bottrell, 2007). Combining these isotope analyses with

concentration data for sulphate and dissolved inorganic carbon (DIC) can also lead to enhanced conclusions being drawn, with respect to analysing the two data sets individually.

1.11.5.1. The Rayleigh Model

In a closed system, where a reaction occurs that preferentially removes light or heavy isotopes, the subsequent enrichment of remaining reactant can be described by the Rayleigh function, Equation 3 (Rayleigh, 1896).

Equation 3

$$R = R_0 (X|X_0)^{\alpha-1}$$

Where:

R = ratio of given isotopes;

R_0 = initial ratio of given isotopes;

X = amount of more abundant isotope;

X_0 = initial amount of more abundant isotope; and,

α = Fractionation factor.

Where X_h is the concentration of the heavier isotope, then normally X >> X_h. Where this is the case, X/X_0 = fraction of material remaining (*f*). Hence the equation can be re-written as Equation 4 below:

Equation 4

$$R = R_0 f^{\alpha-1}$$

An isotope enrichment factor, ε, can be defined from the fractionation factor: ε(‰) = (α - 1)*1000.

1.11.5.2. Delta (δ) Notation

Isotope ratios are normally expressed in the delta standard (δ) measured on the per mill scale (‰), with positive (+ve) δ values showing a greater abundance of a heavy isotope relative to a standard. Two examples are given below (Equation 5 and Equation 6), however, by maintaining the placements of heavy and light isotopes in the equation, the formula can be rewritten for any given isotopic fractionation.

Equation 5

$$\delta^{13}C = \left(\frac{\left({}^{13}C\middle|{}^{12}C\right)_{sample}}{\left({}^{13}C\middle|{}^{12}C\right)_{standard}} - 1\right) * 1000\ ‰$$

$^{13}C/^{12}C_{\text{sample}}$ = the carbon isotope ratio of the sample.
$^{13}C/^{12}C_{\text{standard}}$ = the carbon isotope ratio of a standard, usually an international standard.

Equation 6

$$\delta^{34}S = \left(\frac{\left({}^{34}S\middle|{}^{32}S\right)_{sample}}{\left({}^{34}S\middle|{}^{32}S\right)_{standard}} - 1\right) * 1000\ ‰$$

$^{34}S/^{32}S_{\text{sample}}$ = the sulphur isotope ratio of the sample.
$^{34}S/^{32}S_{\text{standard}}$ = the sulphur isotope ratio of a standard, usually an international standard.

1.12. Study Site

The study site that this research is based on is located near Wolverhampton, UK. The site was historically a coal tar distillery but now no longer processes coal tar, with the site now used for various other chemical processes (Lerner et al, 2000).

The closest receptor at risk is a public supply borehole. This borehole is ~1.5 km downgradient of the plume's front, which equates to nearly 100 years travel time (Lerner et al, 2000).

1.12.1. Site Geology

The site is predominantly flat and overlies the Sherwood Sandstone aquifer. The region has shallow ground water levels, ~4 m below ground level (bgl), with a typical flow velocities of between ~4 m/yr to 10 m/yr (Lerner et al, 2000; Morris, 2005).

Aquifer porosity is ~26 % and bulk hydraulic conductivity is ~0.3 m/d to 0.7 m/d (Aspinwall and Co. 1992), but has further been defined locally for the different stratigraphic layers through which the plume passes (Thornton et al, 2014). The regional hydraulic gradient has been approximated to 0.003–0.007 towards a public water supply borehole approximately 2 km west of the site (Williams et al, 2001).

Limited superficial deposits, comprising drift, are known to be overlie the Sherwood Sandstone to depths typically less than 4m. This drift consists of mixed clays, silts, sands and gravels which are typically present within the unsaturated zone (Williams et al, 2001).

Plume hydraulic conductivity values (K) are typically within the range of 1.5m day^{-}1 and 2.5 m day^{-1} in the region of the plume (Thornton et al., 2014). Hydraulic conductivities in the wider site area have been found to range between 0.7 m day^{-1} and 3.2 m day^{-1} (Thornton et al, 2001), with the aquifer exhibiting a ‘limited variance in average hydraulic conductivity values in comparison to other aquifers’ (Thornton et al, 2014).

These hydraulic conductivity values are generally in line with background geological information (Morris, 2005) and are considered within the range suitable for enhanced bioremediation (Bedient and Rifai, 1992, Cohen et al., 1997). However, permeability within the aquifer generally decreases at greater depths with low permeability strata were encountered below the source at approximately 40m bgl (Aspinwall and Co, 1992). The depth of these low permeability strata deepens away from the source to the northwest, in line with a dip of approximately 2° within the local strata (Spence et al, 2001a).

In addition to the above, the Sherwood Sandstone aquifer is known to have a relatively low mean anisotropy ratio of 1.1 in this area, indicating that the horizontal hydraulic conductivity and vertical hydraulic conductivity are broadly similar (Allen et al., 1997).

1.12.2. Borehole Locations

Over 20 observation boreholes are currently located on site and these boreholes have been used for several historical studies, which have helped to define the location and gross morphology of the contaminant plume (Lerner et al, 2000; Spence et al, 2001b). More recently, however, investigations have focused on the two multi-level samplers (MLS) on site, MLS59 and MLS60, which yield good depth resolution (Thornton et al, 2001).

Both MLS59 and MLS60 transect the core of the plume, with MLS59 being closer to the source and 30 m in depth and MLS60 being further away from the source and 45 m in depth (Figure 11). Both of these positions penetrate the limited superficial deposits terminating in the layers of the Sherwood Sandstone with good hydraulic conductivity (Section 1.12.1).

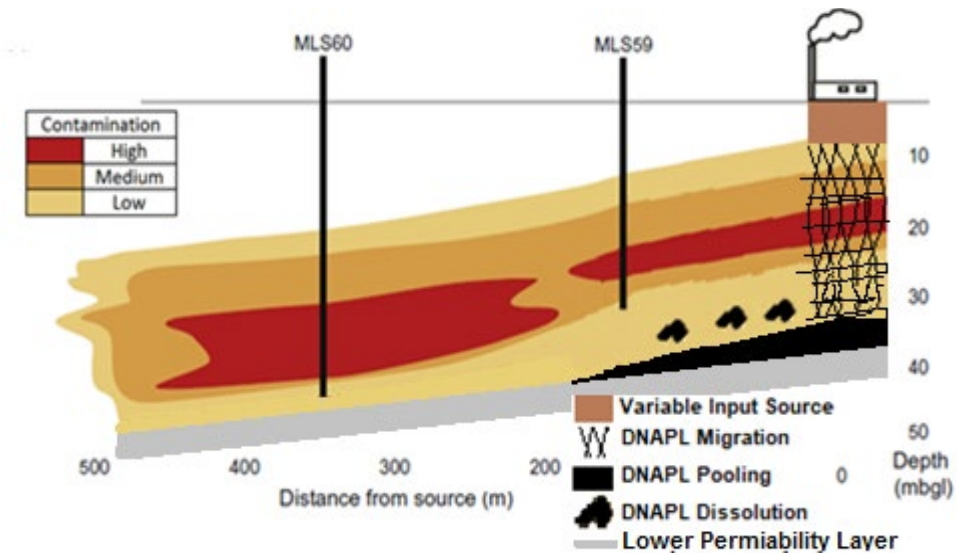

Figure 11. Section view of the plume conceptual model, not to scale. Adapted from Baker et al (2012).

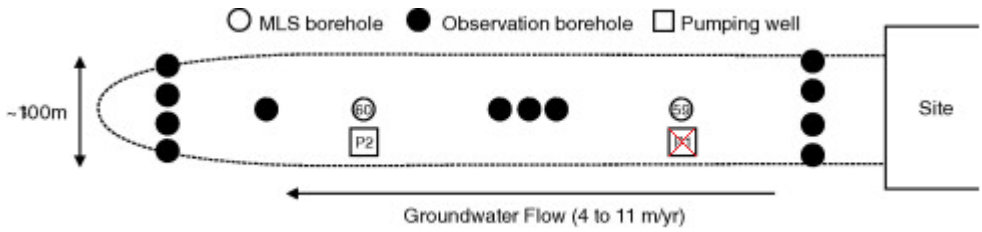

Figure 12. Plan view of the plume, not to scale. Adapted from Baker et al (2012).

The MLSs have a 'polypropylene well casing, with lengths of high-density polyethene (HDPE) tubing leading up to the surface from respective depths, water is pulled in through the HDPE tubing through a 5 cm long stainless-steel filter at the end of the tube' (Thornton et al, 2001).

Pumping is currently being undertaken on site, from a point in close proximity (approximately 5 m offset) to MLS60 and has been running since September 2009. Pumping rates are not known for the current period but have historically been within the range of 0.3 m^3h^{-1} to 2.6 m^3h^{-1}. The pumping well does not fully penetrate the aquifer and is preferentially targeted at the zone of highest contamination, 39 mbgl (Figure 2; Thornton et al, 2014).

It should be appreciated that the Sherwood Sandstone aquifer is high storage (Morris, 2005). Hence, in the absence of significant fracture flow, the effects of pumping are unlikely to take place instantaneously but rather over a considerable length of time.

Whilst pumping operated from November 2009 to June 2011, from a point in close proximity (approximately 5 m offset) to MLS59, this pumping is currently inactive.

1.12.3. Contaminant Chemistry

The plume being studied is a large plume predominantly comprising phenols, tar acids and neutral aromatic compounds. This plume occurs as a result of the historical coal tar distillation at this site. The plume is around 500 m in length and 50 m in depth, when defined by a 1 mg/L phenol contour (Aspinwall and Co. 1992).

The plume has been well characterised over a prolonged period (Lerner et al, 2000; Spence et al, 2001b; Baker et al, 2012; Thornton et al. 2014), using multi-level samplers. This profiling has created a strong dataset of plume hydrochemistry and stable isotopic compositions. Previous profiling occurred between 1998 through to 2012, however, sampling did not take place every year. Only one, limited, sampling round has taken place since the implementation of the PAT in 2011.

The plume is anchored by a strong source; where free phase contaminants are still believed to be actively dissolving into groundwater within the aquifer. Concentrations of organic compounds at the source are around 24,800 mg/L (Lerner et al, 2000) (Table 3).

Of these organic compounds phenols, cresols and xylenols, together known as total phenolic compounds (TPC), are amongst the most readily dissolvable and are found in large quantities within the plume.

Total Organic Compounds, mg/L	Phenol, mg/L	Cresol (methylphenols), mg/L	Xylenols (dimethylphenols), mg/L	Monoaromatics and Others, mg/L
24,800	12,500	8,900	2,400	1,000

Table 3. Concentrations of organic compounds in the source area (data from Lerner et al, 2000).

Na and SO_4 are also present in the profile due to alkali and mineral acid spillages respectively (Lerner et al, 2000).

It is worthy of note that the concentrations of total dissolved solids (TDS) are generally in excess of 25 g/L at the source and in some cases are above 10 g/L within the plume core (Figure 13). Due to this contaminant loading the plume is substantially denser than the surrounding uncontaminated groundwater, such that the plume will tend to sink in relation to the surrounding water (McMahon et al, 2001) and may account for the greater plume depth observed at MLS60, which is further from the source than MLS59.

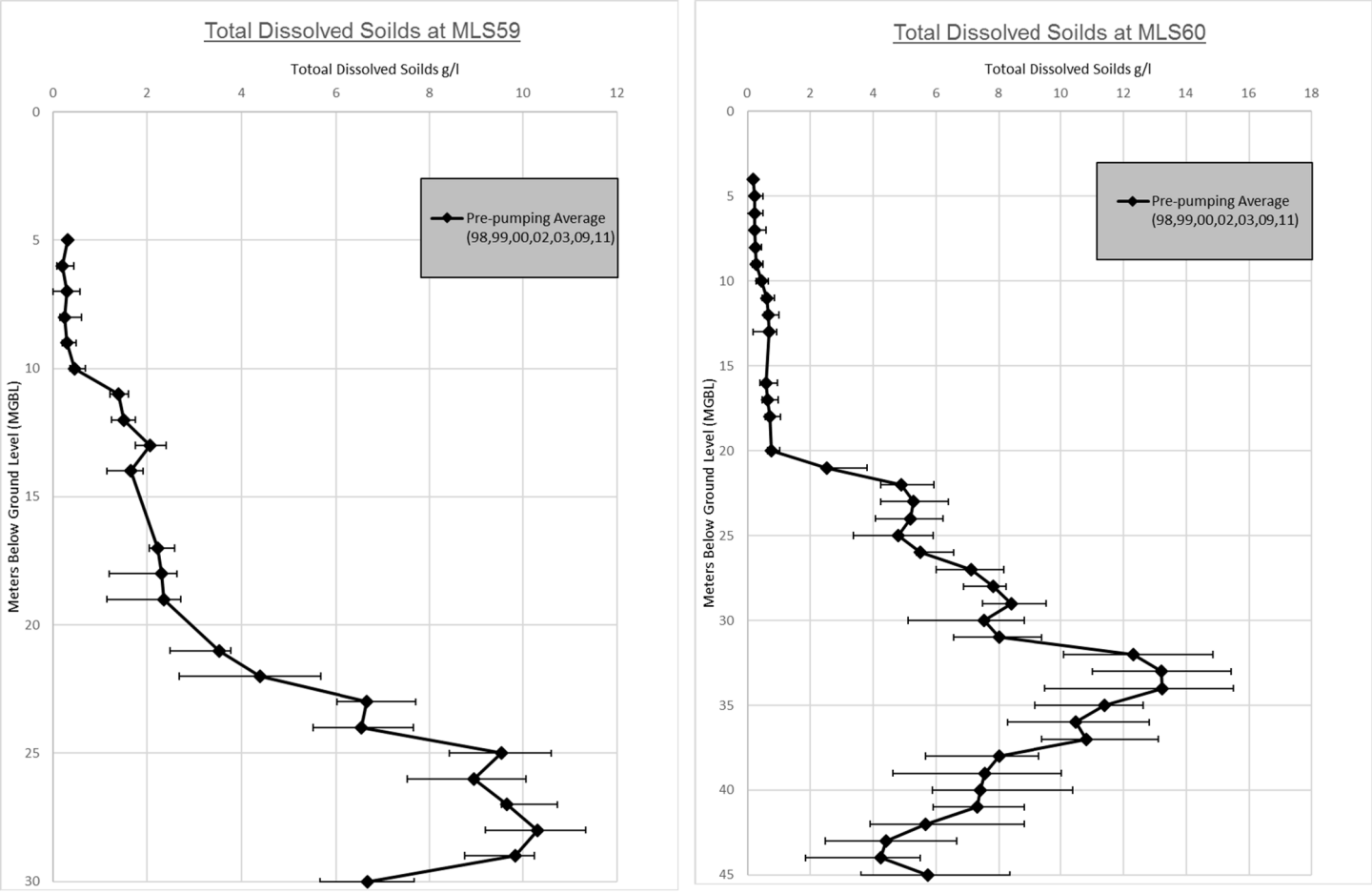

Figure 13. Total Dissolved Solids (TDS) at MLS59 (Left) and MLS60 (Right), pre-pumping (Pre-pumping range shown as error bars).

1.12.4. DNAPL Migration

Whilst the majority of the plumes volume is comprised by the highly soluble phenolic components, fractions of the coal tar source at the site are known to be viscous, some of which are present DNAPL in the subsurface (Thornton et al, 2001). This DNAPL tends to migrate downwards within the aquifer until an reaching an impervious boundary (Section 1.5.2).

At the study site layers with low hydraulic conductivity (K) are thought to be present at depths just beyond 45 mbgl (Aspinwall and Co, 1992). It is considered that DNAPL may migrate downwards from the source until It reaches layers with low K values, at which point lateral spreading of the DNAPL begins to occur extremely slowly, potentially over decades (Figure 11).

It is worthy of note the DNAPL components more recalcitrant to dissolution may dissolve slowly during the downward and lateral migration of the DNAPL. This may continue to increase contaminant loading deeper within the plume (Figure 11) and may be partially responsible for the high TPC concentrations observed at depth pre-pumping (Figure 14, Figure 15)..

1.13. Pre-treatment Site Data

1.13.1. Contaminant Concentrations and Natural Attenuation

Before the implementation of PAT at the site, contaminant concentrations at both MLS59 (Figure 14) and MLS60 (Figure 15) were extremely high.

However, some variation in TPC has been observed to occur between sampling rounds. There are a number of reasons for which this could occur including changes in source characteristics through time (Lerner et al, 2000), seasonal or annual variations in groundwater flow, or plume heterogeneity. Amongst these reasons, plume heterogeneity is considered to be low (Section 1.12.1) and hence of limited significance.

Previous cell counts within the plume have indicated that the plume is not sterile (Lerner et al, 2000). The pH within the aquifer was monitored during

all sampling rounds and was observed to fall between 5.6 to 7.4 at the location of MLS59 and between 5.0 to 7.1 at the location of MLS60. These values fall within the range of pH values for which common neutrophilic microorganisms can grow, which is typically considered as between pH 5 and pH 8 (Ajoku et al, 2010). Groundwater temperatures were also found to fall well within 15 to 45 degrees centigrade considered optimal for most microbial activity (Vidali, 2001).

However, further data implies that bacterial population is stressed at, due to contaminant toxicity from high TPC in the inner plume core (Spence et al, 2001b).

Data also indicated that NA (via the processes of biodegradation and dispersion) was occurring at the site, albeit very slowly (Lerner et al, 2000; Williams et al, 2001). An estimated half-life for the plume, based solely upon NA processes, is in the region of 50 years (Lerner et al, 2000; Thornton et al, 2001).

Under these natural conditions, the plume was predicated to grow despite the ongoing NA processes, as the input of contaminants from the source would overwhelm the effect of the NA processes (Lerner et al, 2000).

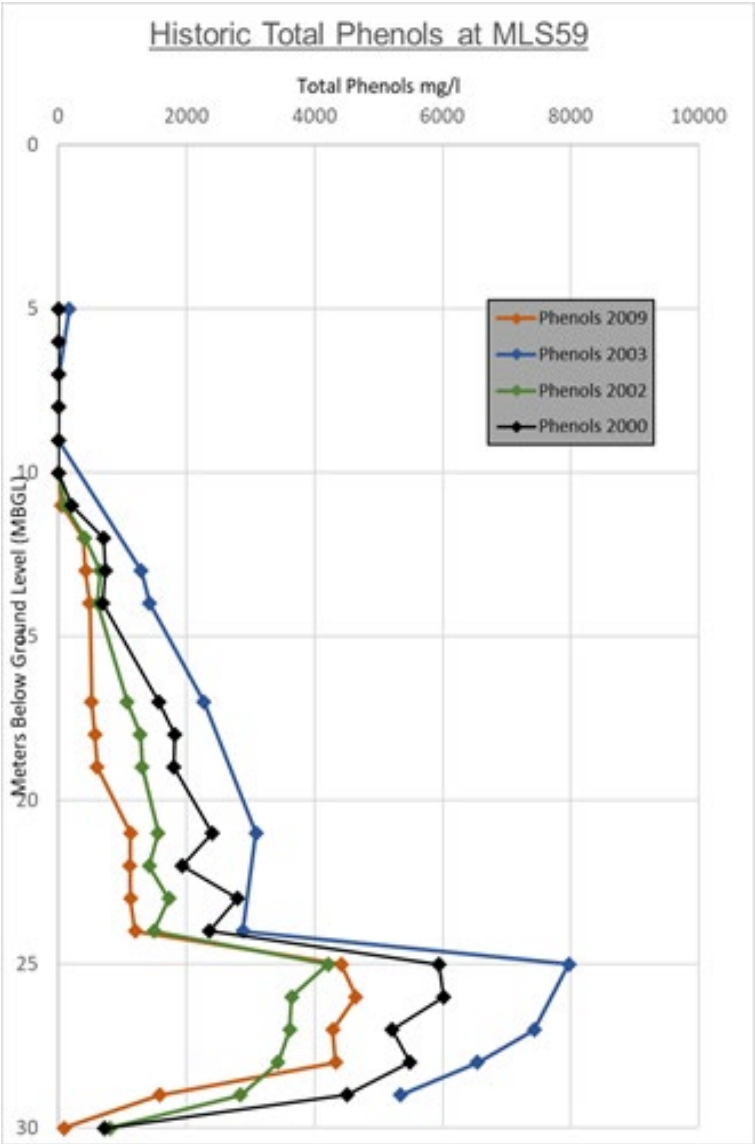

Figure 14. Contaminant concentrations (2000-2009) at MLS59 before implementation of PAT (Data with permission from Thornton et al, 2001 and Spence et al, 2001b).

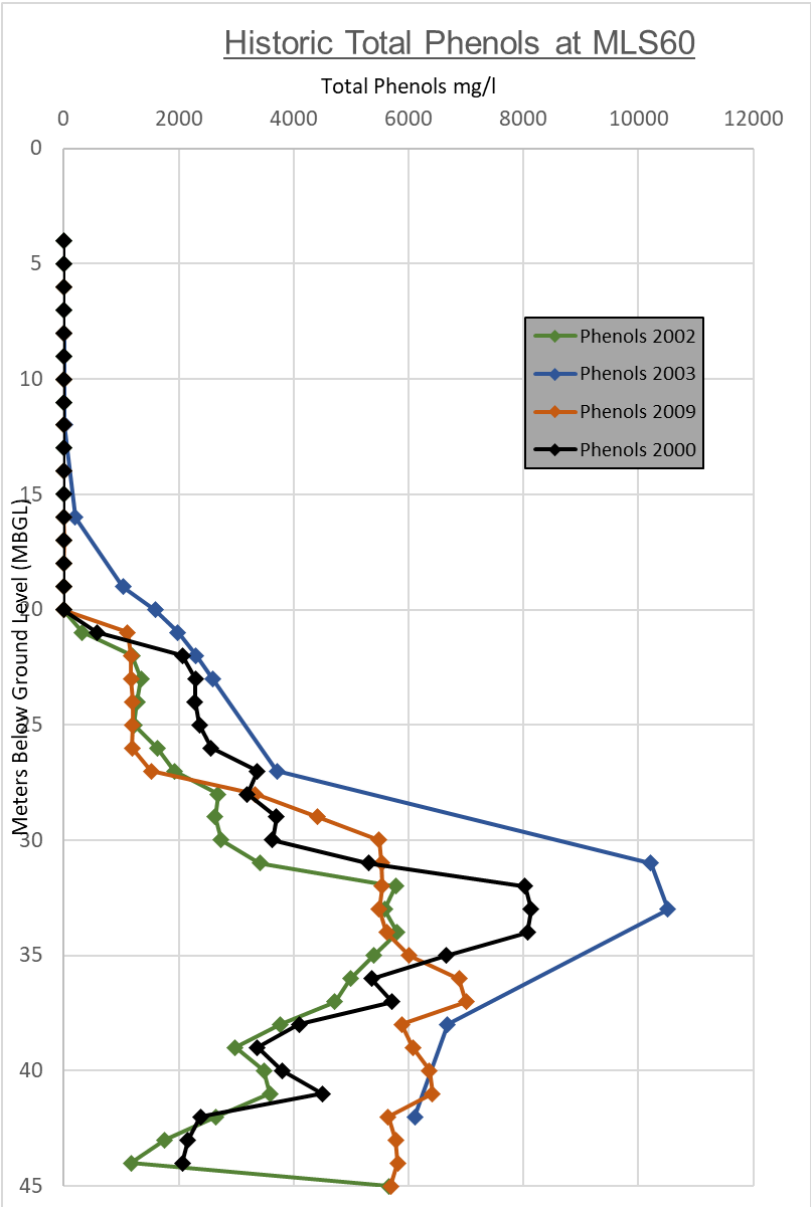

Figure 15. Contaminant concentrations (2000-2009) at MLS60 before implementation of PAT (Data with permission from Thornton et al, 2001 and Spence et al, 2001b).

1.13.2. Mass Flux Calculations

Mass flux (*J*) can be used to describe the mass of contamination, or other relevant substrate, moving across a unit area of an aquifer perpendicular to flow direction. Mass flux is calculated by combining concentration data and groundwater velocity information (Equation 7; McMillan et al, 2018).

Equation 7

$$J = K\frac{dh}{dl}C$$

Where:

J = Mass flux (volumetric discharge);

dh/dl = hydraulic gradient, that is, the change in head over the length of interest;

K = hydraulic conductivity. and,

C = contaminant concentration.

Quantifying the flux of a given substrate (contaminants, electron acceptors or other) can be particularly important for heterogeneous aquifers in which a variety of flow rates, either between depths or laterally across the site, can have a significant consequence on observed substrate concentrations. By calculating mass flux these concentrations can be weighted in light of the flow rates which helps to obtain a clearer picture of the overall plume.

Hydraulic conductivities (K) have been tested at the Wolverhampton site, within a number of studies (Spence et al, 2001b; Thornton et al, 2001; Thornton et al, 2014). These studies have observed hydraulic conductivities in the region of the plume generally ranging from 1.5m day^{-1} to 2.5 m day^{-1}. These observed values have previously been considered to indicate only a 'limited variance between depths (Section 1.12.1) in comparison to other aquifers' (Thornton et al, 2014).

In light of the low variance in hydraulic conductivities it is considered that the use of a concentration-based metric should provide a reasonable approximation for the fairly homogenous plume system. Nevertheless, in order to confirm the above, all major plume substrates have been weighted by the latest hydraulic conductivities (K) provided for MLS59 and MLS60 by Thornton et al (2014) and the regional hydraulic gradient 0.003–0.007 m/m westwards as approximated by Williams et al (2001), in order to obtain appropriate mass fluxes.

The trends identified within the mass flux results remained highly similar to those identified within the unweighted concentrations at both MLS59 and MLS60. An example is provided below of the mass flux calculated for pre-

pumping TPC within MLS59 (Figure 15) and MLS60 (Figure 16).

At MLS59 an upper plume fringe is observed between approximately 10 mbgl and 12 mbgl characterised by low TPC and limited mass flux. An upper plume core is present between approximately 12 mgbl and 25 mgbl characterised by TPC ranging between 1000mg/L and 2000mg/L and a mass flux of <30 mg/m^2/day. A lower plume core is present between approximately 25 mgbl and 29 mbgl characterised by TPC typically >2000mg/L and a more substantial mass flux of between 30 mg/m2/day to 65 mg/m2/day.

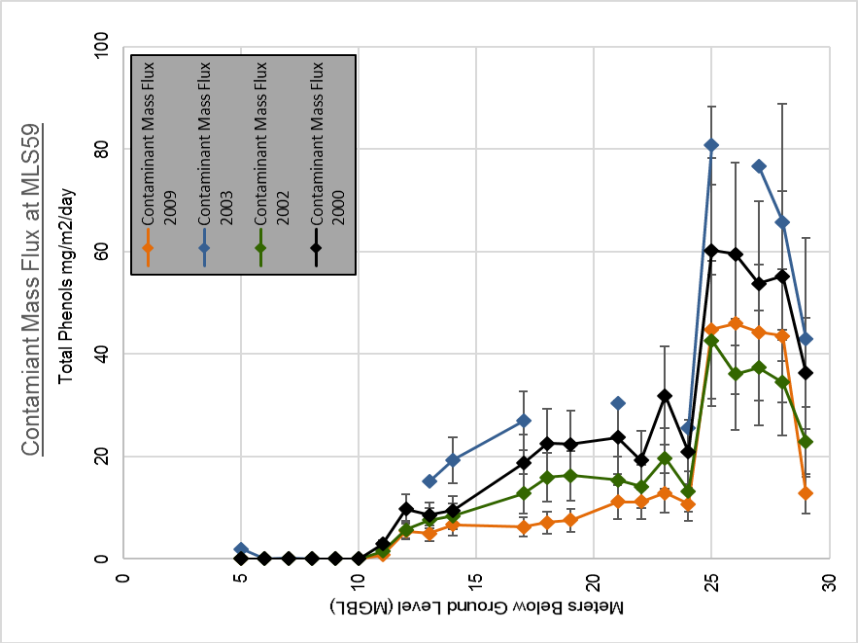

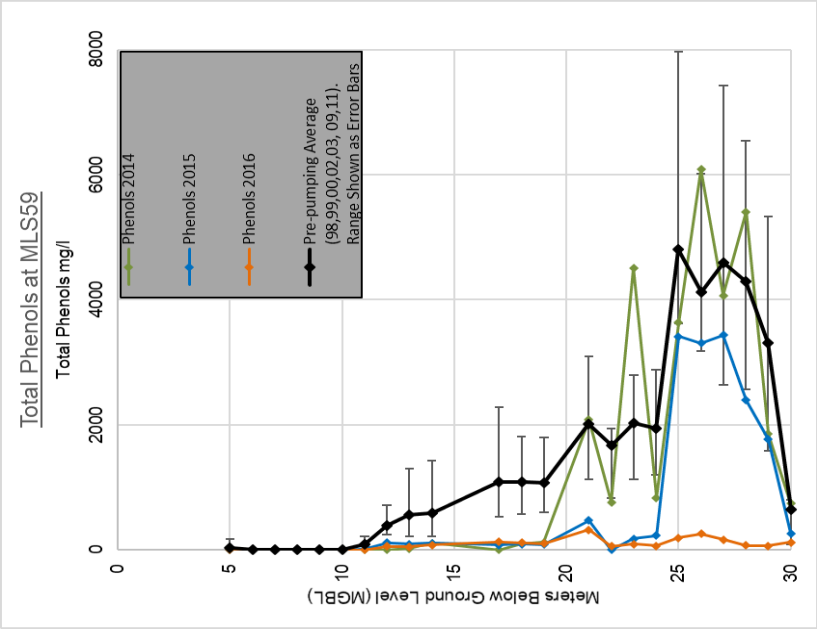

Figure 16. Mass flux (2000-2009) at MLS59 before implementation of PAT. Error bars indicate uncertainty based on approximated regional hydraulic head values (Right). In comparison to contaminant concentrations from the same periods (Left.

At MLS60 an upper plume fringe is observed between approximately 18 mbgl and 20 mbgl characterised by low TPC and limited mass flux. An upper plume core is present between approximately 21 mgbl and 27 mgbl characterised by TPC ranging between 1000mg/L and 3000mg/L and a mass flux of <30 mg/m^2/day. A middle plume core between approximately 28 mgbl and 36 mbgl characterised by TPC typically >4000mg/L and a more substantial mass flux of typically between 20 mg/m^2/day to 60 mg/m^2/day. A lower plume core between approximately 36 mgbl and 44 mgbl characterised by TPC ranging between 1000mg/L and 3000mg/L and a mass flux of <40 mg/m^2/day

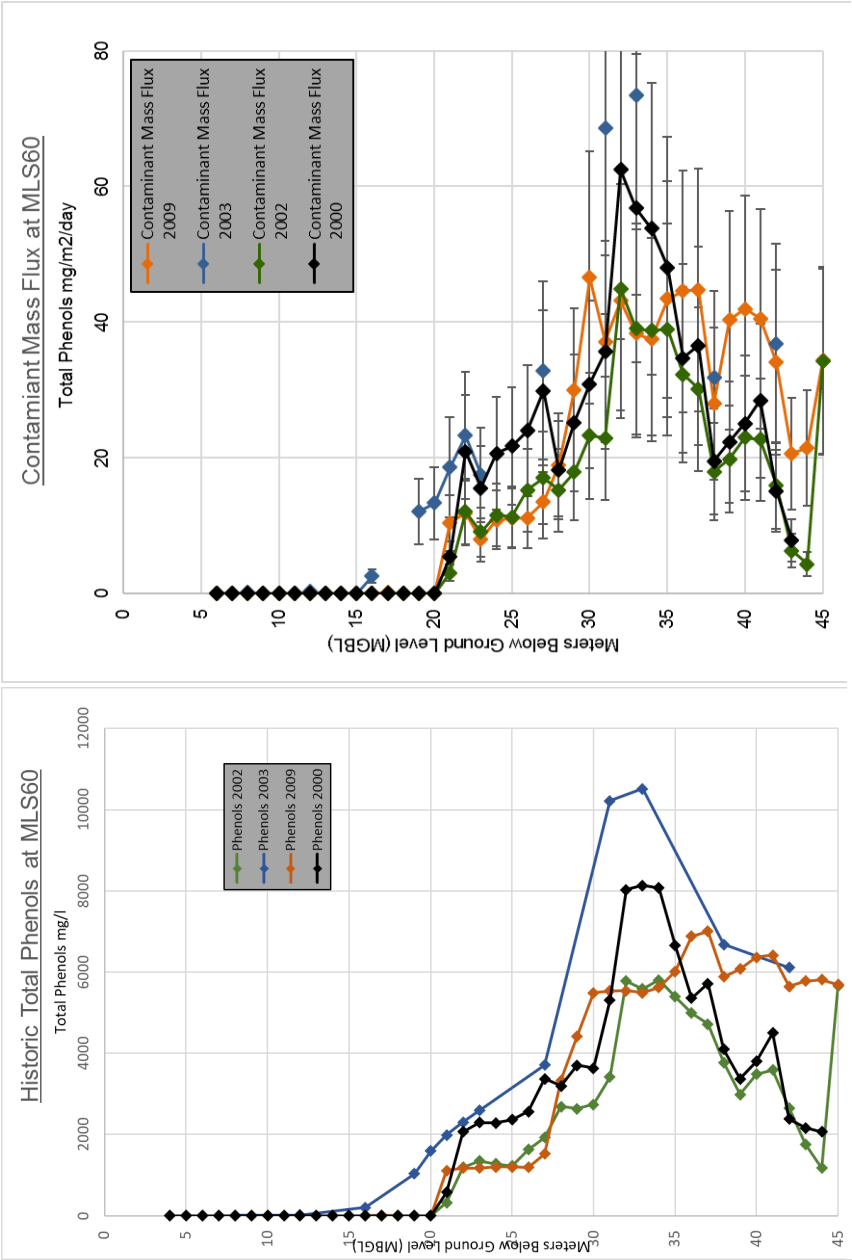

Figure 17. Mass flux (2000-2009) at MLS60 before implementation of PAT. Error bars indicate uncertainty based on approximated regional hydraulic head values (Right). In comparison to contaminant concentrations from the same periods (Left).

In light of the strong similarity in trends between the mass flux and the low variance in hydraulic conductivities it is considered that the use of a concentration-based metric should provide a reasonable approximation at the study site, which is a fairly homogenous plume system (Section 1.12.2).

Furthermore, it should be appreciated that, due to the uncertainty in the local hydraulic gradient there is a larger degree of uncertainty on mass flux estimates than on the contaminant concentrations. This uncertainty is presented on the graphs above (Figure 15. Contaminant concentrations (2000-2009) at MLS60 before implementation of PAT (Data with permission from Thornton et al, 2001 and Spence et al, 2001b).Figure 15 and Figure 15) as error bars and accounts for approximately 40% uncertainty on the mass flux.

1.13.3. Oxic Plume Fringe

Both oxic (O_2) and nitric (NO_3) contaminant reduction was found to be occurring at the plume fringe, where transverse/longitudinal dispersion act together to mix the contaminant plume with the surrounding water, creating an input of O_2 and NO_3 electron acceptors (Lerner et al, 2000; Spence et al, 2001b; Mayer et al, 2001). Nitrate concentrations have been shown to be ~50 mg/L in the plume fringe (Thornton el al, 2014)

For the study site this plume fringe was found to be between 1 m and 4 m thick, based upon several different hydro-chemical parameters (Spence et al, 2001b; Thornton et al, 2014). High cell counts and phenol degradation activity noted in this region (Lerner et al, 2000; Williams et al, 2001), further reinforces this conclusion.

However, low dispersion within the aquifer “slows the input of the energetically favourable O_2 and NO_3 oxidants” (Lerner et al, 2000). Hence these electron acceptors rapidly reduce to background levels once beyond the plume fringe, due to the coupling of this slow input and their rapid consumption within the plume fringe. Nitrate concentrations are negligible within the plume core. Dissolved oxygen is typically not presented within previous site data due to analytical interference from the contaminant

matrix but is considered likely to be restricted to the same areas of the plume as the nitrate (Thornton et al, 2014).

1.13.4. Anaerobic Plume Core

The core of the plume was found to be strongly anaerobic. Hence, anaerobic contaminant reduction processes, namely methanogenesis and BSR, were found to be the dominating in the plume core (Lerner et al, 2000).

The dominance of these processes was demonstrated by:

(1) The lack of O_2 and NO_3^- present in the plume core, indicating no potential for oxic or nitric respiration;
(2) The presence of methane throughout the plume (Lerner et al, 2000), indicating the presence of substantial methanogenesis;
(3) Analysis of SO_4 isotopic data (Lerner et al, 2000; Spence et al, 2001b), showing the presence of BSR processes in some regions of the plume; and,
(4) The presence of “partly oxidised metabolites of anaerobic digestion of phenols, found throughout the profile” (Lerner et al, 2000).

1.13.4.1. Manganese and Iron Reduction

There is some evidence of Manganese (Mn) and Iron (Fe) reduction within the anaerobic core of the plume, as indicated by the presence of Mn^{2+} and Fe^{2+} produced by these processes. However, concentrations of these products are very low with respect to the total pool of contaminants present within the plume (Lerner et al, 2000; Spence et al, 2001a).

In light of the above, whilst Mn and Fe reduction are thought to occur, the potential of these process is limited, as depletion of the respective pools of electron acceptors would occur rapidly. Thus, these processes are considered mostly insignificant within the plume (Thornton et al, 2014).

1.13.4.2. SO_4 Reduction

Sulphate (SO_4) concentrations within the plume are very high with respect to background levels; this is due to spills of H_2SO_4 which occurred at the same time as the spills of the phenolic contaminants (Lerner et al, 2000; Thornton et al, 2001). This H_2SO_4 enables bacterial sulphate reduction (BSR), which is a significant process in the pre-pumping plume.

However, BSR can be inhibited by the pollutant matrix of the phenols, and it is considered to be strongly suppressed at high levels of TPC (Spence et al, 2001b; Baker et al, 2012). This is a consequence of the high TPC supressing microbial metabolic functions, which is a well-documented effect known to occur within industrial wastewater contaminated by phenols (Goudar et al, 2000; Kumaran et al., 1997). This effect is also shown to occur when phenols are degraded via an acetate intermediary (Wang et al, 1991)

Notwithstanding the above, the inhibitory threshold has been shown to vary between studies (Goudar et al, 2000; Kumaran et al, 1997; Wang et al, 1991). The observed difference in inhibitory thresholds are believed to be due to the varying compositions of the microbial communities between studies (Thompson et al, 2005). Thus, thresholds are specific to each study site and must be ascertained by either observing the in-situ conditions or by using a representative microbial community for ex-situ studies.

In specific to the Wolverhampton site, in-situ studies indicate that the threshold for suppression of BSR at high levels of TPC occurs at around 2 g/L TPC, with BSR not being observed at TPC levels higher than this (Spence et al, 2001a; Spence et al, 2001b), see Figure 18.

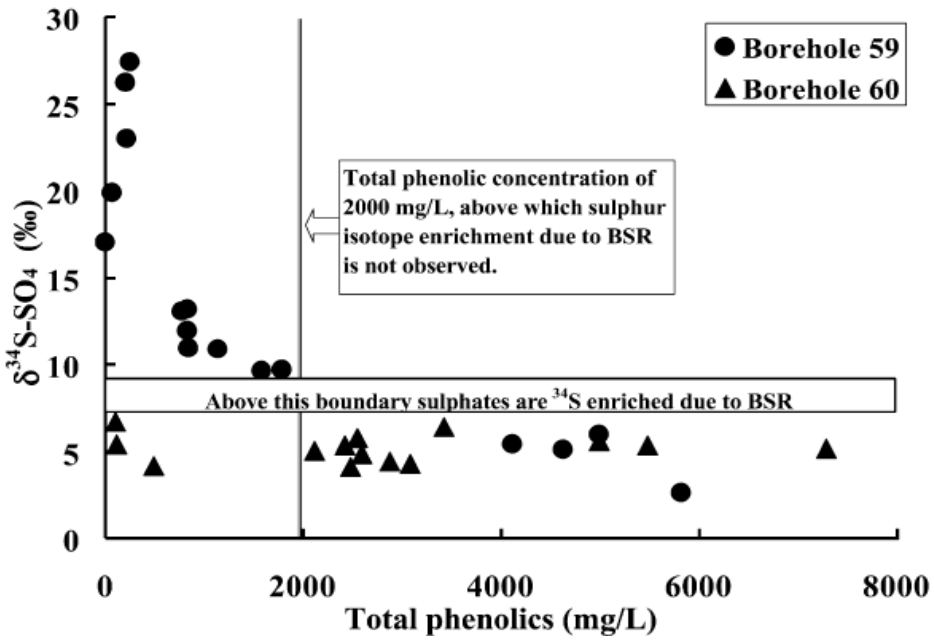

Figure 18. Plot of contaminant concentrations (total phenolics) against δ^{34}S-SO_4 (Spence et al, 2001b).

1.13.5. Total Dissolved Inorganic Carbon

Total Dissolved Inorganic Carbon (TDIC) is the total of dissolved carbon dioxide, bicarbonate and carbonate within the plume (Equation 8). TDIC concentrations within the plume increases as organic compounds (i.e. TPC) are degraded and biogenic CO_2 is added to the TDIC pool.

Equation 8

$$TDIC = CO_2 + HCO_{3-} + CO_{3^{2-}}$$

As 'vertical profiles of TDIC show no migration of CO_2 upwards' (Spence et al, 2001a), and given the hydrostatic pressure, it can be assumed that the plume is isolated from atmospheric CO_2 exchange. Furthermore, no substantial carbonate was noted in aquifer cores and carbonate is thought to be undersaturated within the aquifer water (Spence et al, 2001b).

It should be appreciated that before pumping, approximately 50mg/L of TDIC was continually present within the background water above the contaminant plume, at both MLS59 and MLS60.

This “background TDIC” can be present due to historical groundwater/atmosphere interactions and microbial activity, both of which can add CO_2 to the groundwater. In turn, this added CO_2 can form carbonic acid which can enact dissolution of naturally occurring carbonates within the aquifer. This carbonate dissolution is further contributed to by the sulphuric acid which is present within the groundwater due to historical spillages on site (Lerner et al, 2000). These interactions generate the majority of the “background” TDIC observed outside of the plume.

In light of the above, TDIC within the plume is likely to comprise a mixture of “background TDIC” and TDIC created from biogenic pathways. Due to undersaturation of carbonate within the aquifer, this TDIC is unlikely to be lost due to carbonate precipitation.

TDIC within the plume core was generally within the range of 250 mg/L to 450 mg/L, with values consistently around 500 mg/L in regions associated with the plume fringe (Thornton et al, 2001a; Thornton et al, 2001b; Spence, 2001b).

Whilst these TDIC values are increased in relation to “background TDIC” they do not distinguish between TDIC generated from carbonate dissolution and TDIC generated from the biodegradation of TPC. However, as no substantial carbonate was noted in analyses of aquifer cores from the study site (Spence., 2001), potential for dissolution of carbonate to contribute to overall TDIC pool is considered limited. Furthermore, for regions where ‘significant biodegradation of TPC is occurring, biodegradation is known to create the substantial majority of observed TDIC’ (Spence et al., 2001a). Hence, TDIC values above, and in excess of, 50 mg/L, give a good representation of total biodegradation.

Notwithstanding the above, it should be appreciated that “background” TDIC can approximated using historical and current data (such as TDIC and pH values) and subsequently factored out, this has been done for subsequent calculations which is further discussed in later chapters (Section 5.2),

1.14. Isotopic Evidence for Pre-pumping Plume Processes

1.14.1. Isotopic Effects Associated with TDIC Creation

Biogenic TDIC created within the plume due to biodegradation will have a carbon isotopic composition (δ^{13}C-TDIC) representative of its production method (section 1.11.5).

Spence et al (2001b) demonstrated that bulk pollutant TPC in general has an isotopic composition of -24 ‰ (δ^{13}C-TPC). Furthermore, it has been demonstrated that TDIC created from the oxidisation of these organic pollutants (i.e. TPC) within the plume, does not undergo significant isotopic fractionation during this process (Spence et al, 2001b). These studies were based on a limited range of contaminants from the plume (including phenol and p-cresol), however, as the contaminants chosen comprise the majority of the pollutant mass, the δ^{13}C of TDIC created due to oxidation of these contaminants can be assumed to be approximately -24 ‰.

It is considered that in the plume methanogenesis of TPC is likely undertaken by the fermentation of phenols to acetate, followed by the biodegradation of that acetate into carbon dioxide and methane (acetotrophy, Spence et al, 2001b). Phenol fermentation has no associated isotope effect and hence the carbon isotopic composition of acetate can be assumed to be the same as the bulk pollutants, -24 ‰. (δ^{13}C-Acetate).

A carbon mass model dictates that:

Equation 9

$$2 * (\delta^{13}C - TDIC) = 1 * (\delta^{13}C - CH_4) + 1 * (\delta^{13}C - Methanogenic\ TDIC)$$

This calculation (Equation 9) can be used to derive the value of methanogenic TDIC, either based upon measured δ^{13}C-CH_4 values from the plume or in line with an estimated value of δ^{13}C-CH_4 (-54 ‰, section 1.14.2). These calculations typically give enriched δ^{13}C-TDIC values.

In the case of the study site “background” δ13C-TDIC values are around -19 ‰ (Section 3.4; Thornton et al., 2014). This value can be used as baseline against which other δ13C-TDIC values can be compared.

In light of the above, c values more depleted than -19 ‰ can be considered representative of respiration, with values around -24 ‰ indicative of complete respiration dominance. However, more enriched δ^{13}C-TDIC values are indicative of a dominance of methanogenesis.

It should be appreciated that the isotopic data does not distinguish between “background TDIC” and TDIC generated from biodegradation of TPC. However, as per the above (Section 1.13.5), by approximating the quantity of “background TDIC” and understanding its δ13C-TDIC of -19 ‰, this source can be accounted for in further calculations.

The above methodology is further used in the carbon balance calculations created by Thornton et al (2014) and also the enhanced carbon balance models presented within this thesis (section 5).

1.14.2. Isotopic Effects Associated with Methanogenesis

As noted in the previous section it is considered methanogenesis within the plume likely proceeds via acetotrophy (Spence et al, 2001b), utilising acetate of a carbon isotope composition of approximately -24 ‰. (δ^{13}C-Acetate).

The enrichment factor associated with the creation of CH_4 via the degradation of acetate (acetotrophy) is generally between -25 ‰ and -35 ‰ (Whiticar, 1999), hence the δ^{13}C of CH_4 created by methanogenesis within the plume can be assumed to be the initial composition (-24 ‰) plus this enrichment factor giving a value of -54 ‰ (± 5 ‰), strongly depleted in δ^{13}C.

1.14.3. Isotopic Effects Associated with Anaerobic Methane Oxidation (AMO)

In contrast to the above, bacterial consumption of methane (Equation 10

) is associated with kinetic isotopic effect (Section 1.11.5) that leaves methane enriched in δ^{13}C-CH_4 (Whiticar et al., 1986; Whiticar, 1999). This can occur in both aerobic (MO) and anaerobic conditions (AMO).

As noted above (Section 1.14.2), methane generated within the plume could be expected to have a δ^{13}C-CH_4 value of -49 ‰ to -59 ‰. Any methane oxidation which acts on the generated methane would enrich δ^{13}C-CH_4 giving values of >-49 ‰.

Equation 10

$$CH_4 + O_2 = C\,O_2 + H^+$$

Furthermore, the methane oxidation process creates new source of CO_2, adding to the CO_2 contributed by respiration and dissolution of carbonate. (Section 1.13.5). CO_2 created via this process is strongly depleted in δ^{13}C due the initial ^{13}C within the methane pool exhibiting values of approximately -54 ‰, which then undergoes a respectively small fractionation (Whiticar et al., 1985; Whiticar, 1999).

This additional CO_2 created during methane oxidation also contributes to the TDIC pool depleting δ^{13}C-TDIC values strongly. Hence, very depleted δ^{13}C-TDIC values are indicative that some TDIC must originate from methane oxidation, with δ13C-TDIC values close to that of methane indicating that methane oxidation is the dominant process (Thornton et al., 2014).

In particular it should be noted that, in the absence of oxygen, anaerobic methane oxidation (AMO) has been observed to occur using sulphate as oxidant (Equation 11, Panganiban et al., 1979). This can result in a large decrease in CH_4 concentrations where zones of CH_4 production and sulphate reduction intersect. However, this process remains poorly understood (Whiticar et al, 1986).

Equation 11

$$CH_4 + SO_4 = CO_2 + HS_2$$

1.14.4. Isotopic Effects Associated with Bacterial Sulphate Reduction

BSR involves the reduction of sulphate leading to the production of dissolved sulphide (H_2S). Re-oxidation of this sulphide can occur leading to cycling of the sulphur pool and the negation of any potential sulphate isotope fractionation (Spence et al, 2001b). However, where organic matter is present sulphide will complex with the organic matter stabilising it and making BSR a unidirectional process (Bruchert and Pratt, 1999). Cumulative enrichment of δ^{34}S-SO_4 occurs in this scenario, due to Raleigh fractionation (section 1.11.5.1).

In light of the above, δ^{34}S-SO4 data is best viewed in comparison to source/substrate values; these source values were measured as 5.5 ‰ - 7.7 ‰ (Spence et al, 2001b; Thornton et al, 2014).

1.15. Pre-pumping Plume Models

It is generally accepted that the mixing of dissolved electron acceptors, such as oxygen and nitrate, into a plume of organic contaminates via dispersion is the key control on organic contaminant biodegradation rates (Lerner et al, 2000; Pickup et al, 2001; Tuxen et al, 2006; Zhang et al, 2009; and Thornton et al, 2014).

1.15.1. The Cirpka et al. Model

Plume models, such as that created by Cirpka el al, (1999) indicate that a large portion of microbial biodegradation in aquifers is controlled by mixing at the plume fringe.

At the plume fringe substrates (i.e. non-plume water) with an excess of electron acceptors (i.e. oxygen and nitrate) are mixed with substrates with an excess of electron donors (i.e. organic contaminants, in this case TPC), creating the necessary conditions for biodegradation and biomass creation (Figure 18).

In contrast the plume core, where electron acceptors are depleted, does not have the necessary conditions required for oxic (or sub-oxic) biodegradation. However, it should be noted that anaerobic processes such as methane can still occur, albeit these biodegradation processes tend to be an order or magnitude slower.

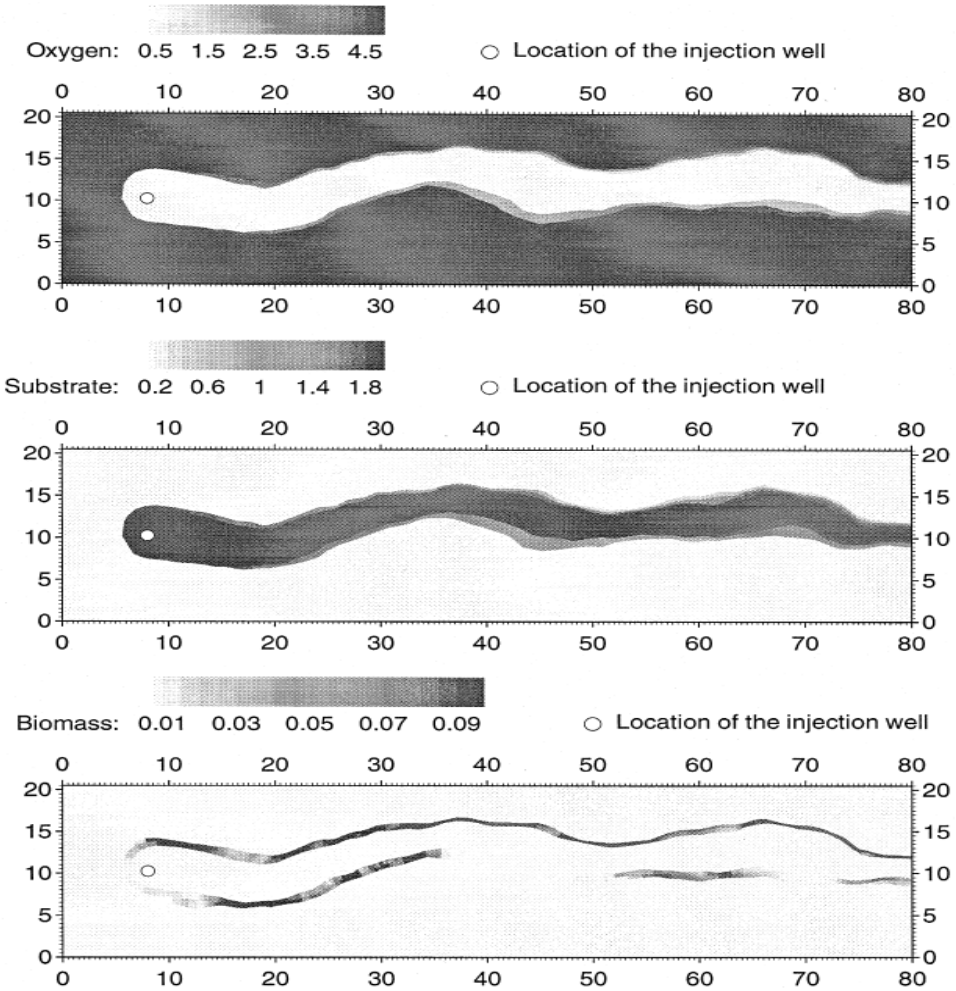

Figure 19. Cirpka et al., (1999) model showing typical organic plume development in a heterogeneous aquifer (birds eye view). High concentrations of electron acceptors (oxygen, kg^{-1}) are present outside of the plume (a), high substrate (organic contaminants, kg^{-1}) values are present inside the plume (b), with microbial biomass (kg-1, indicative of contaminant turnover) present at the at the plume fringe (c).

1.15.2. Study Site Pre-pumping Model

With regards to the study site pre-pumping data, it should be appreciated that the Cirpka et al, (1999) model has been shown to apply in general terms to the plume fringe, and with regards to the influx of oxygen and nitrate electron acceptors (Lerner et al, 2000; Thornton et al, 2001b).

However, it should be appreciated that due to the large amounts of sulphate present throughout the plume (Spence et al, 2001b; Thornton et al, 2014), the plume core does in fact have an abundance of SO_4 electron acceptors. Sulphate can be used as an electron acceptor during BSR, even within this region, so long as TPC values are below 2 g/L (section 1.13.4).

In light of the above, the conceptual pre-pumping plume model is more complex at the site than the Cirpka et al, model. However, the plume can still be broadly divided between an outer plume fringe and an inner plume core, as discussed below.

1.16. Pilot Study Site Data

The pilot study (Thornton et al, 2014), conducted in 2012 after the implementation of the PAT system, demonstrated that contaminant concentrations at MLS60 dropped rapidly after the implementation of the PAT system (Figure 20).

1.16.1. Changes in TPC Concentrations

The most pronounced effect of the PAT system during the pilot study was the significant decrease in contamination concentrations seen within the TPC dataset, during the pumped years of 2011 and 2012 (Figure 20; Thornton et al., 2014).

The pilot study found that the PAT system, which was targeted to remove water from the most contaminated zone (operating at 39 mbgl), enacted the largest reduction in TPC levels between 35 mbgl and 45 mbgl.

Moderate decreases in TPC also occurred between 27 mbgl and 35 mbgl, however, this was less pronounced than depths closer to the operating level of the PAT.

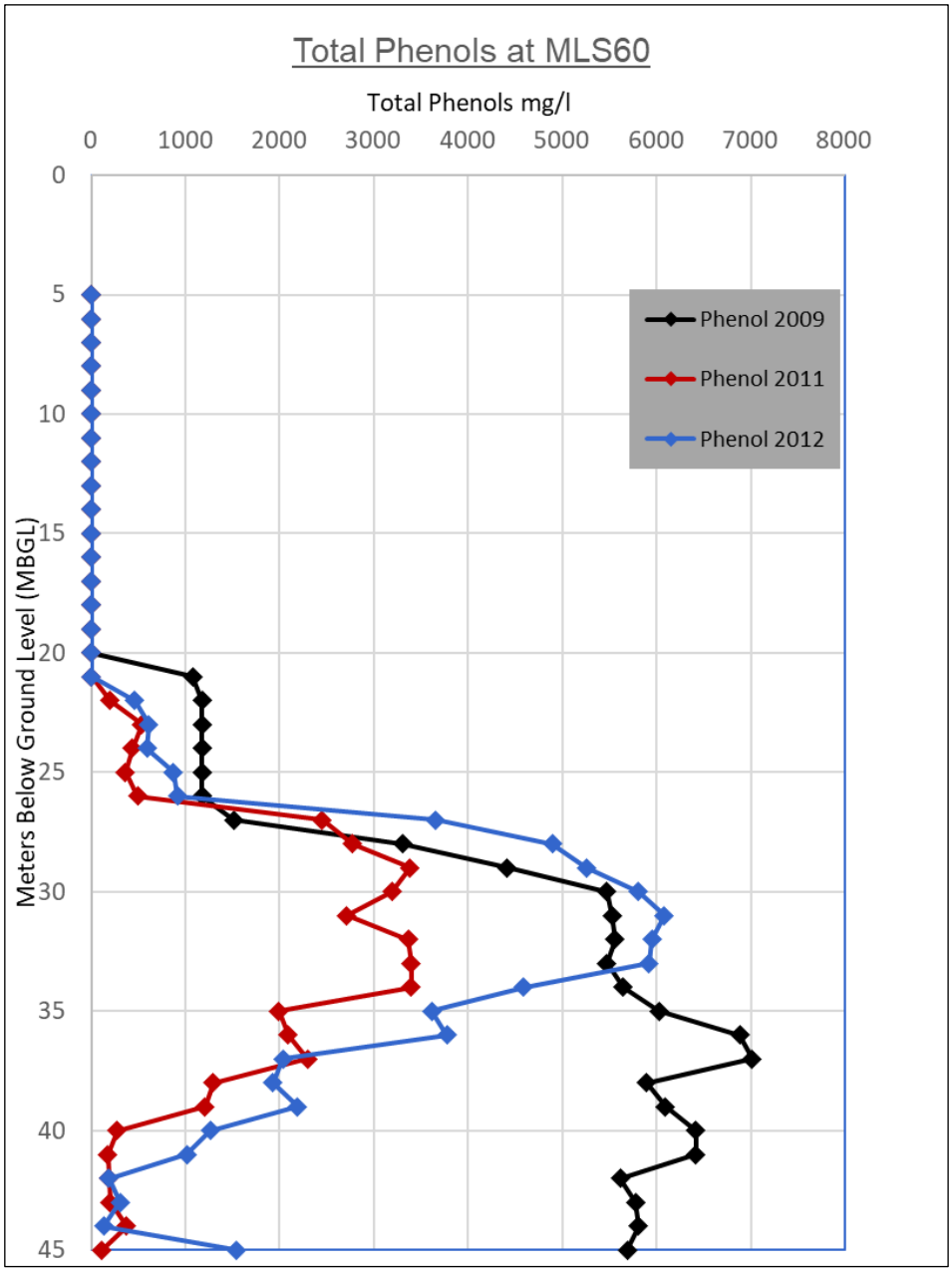

Figure 20. Plot of TPC (contamination) concentrations through time at MLS60. Including 2009, before PAT implementation and 2011/2012, after PAT implementation (Thornton et al, 2014).

1.16.2. Increases in Biodegradation Rate

Results published in Thornton et al. (2014) show a ~2 times increase in the biodegradation rate at MLS60, calculated based on an increase on the Total Dissolved Inorganic Carbon (TDIC) concentration, which increases as phenolic compounds are degraded and biogenic CO_2 is added to the TDIC pool.

An increase in the TDIC concentrations, from less than 200 mg/L to greater than 350 mg/L at specific depths which have been affected by the PAT system (Figure 21), is strongly indicative of increased biodegradation in these areas. The approximate doubling of TDIC in these areas leads to an estimated factor of 2 increase in degradation rates in these zones (Thornton et al. 2014).

‘This enhanced biodegradation is a result of decreased TPC concentrations’ (Thornton el al, 2014), which have now dropped below 2 g/L, a level that previously suppressed microbial activity (section 1.13.4), and specifically BSR (Spence et al, 2001b).

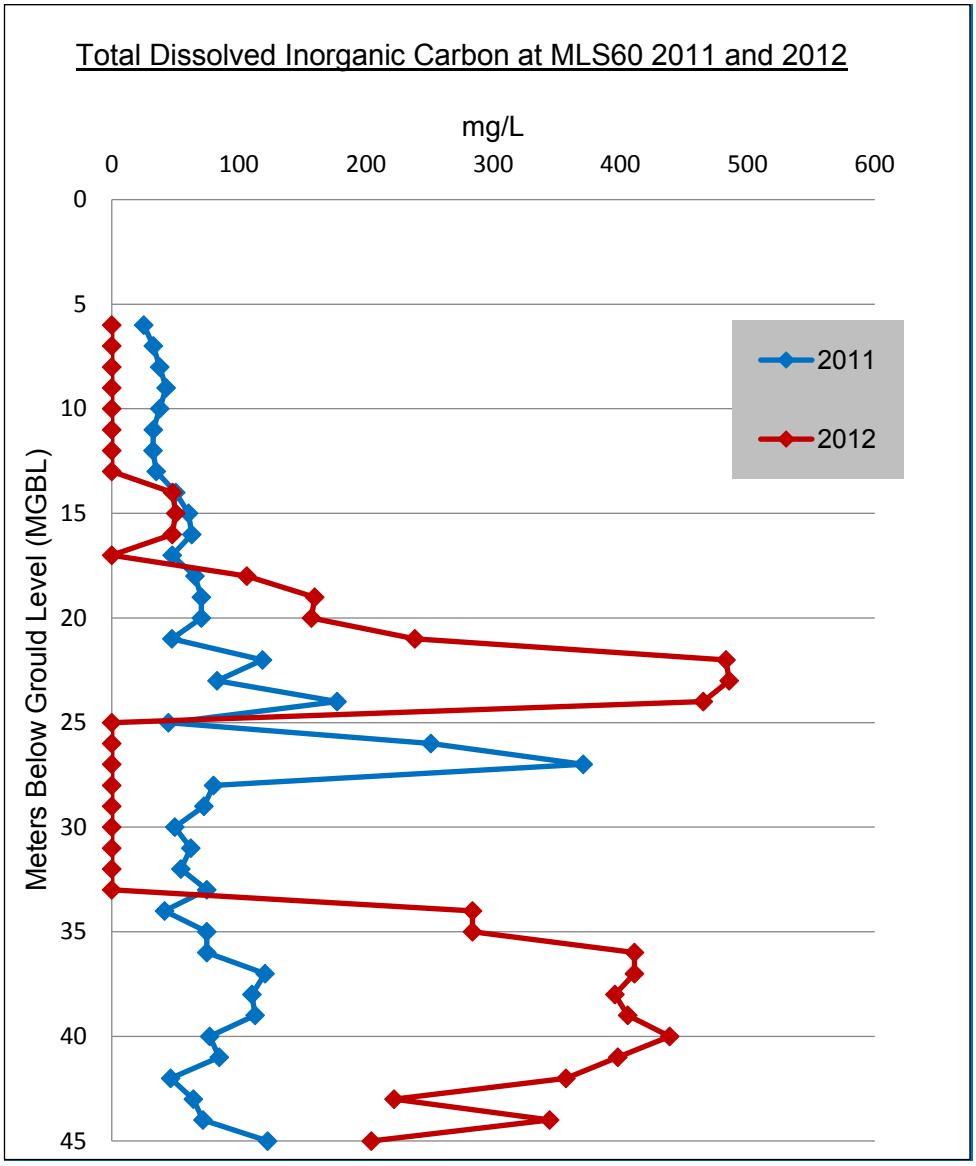

Figure 21. Plot of TDIC (mg/L) against depth (MGBL) for 2009 and 2012 for MLS60 (Thornton et al, 2014).

1.16.3. Enhanced Remediation Processes

Mass and isotope balances from the pilot survey confirmed that the additional TDIC had been created primarily by anaerobic respiration (Table 4). This increase in anaerobic respiration indicated a shift away from methanogenic dominance in the plume, which previously accounted for ~89 % of contaminant biodegradation (Thornton et al, 2014).

In light of the above, it is considered that the increases in TDIC creation and respiration processes demonstrate the ability of the PAT system to passively enhance in-situ bioremediation in the plume without further intervention (Thornton et al, 2014), meriting further study.

Contribution of respiration processes and methanogenesis to TDIC production in plume.

MLS	Depth (mbgl)	TDIC increase (mg L^{-1})	$\delta^{13}C$ of added TDIC (‰$_{V\text{-}PDB}$)	% C from methanogenesis		% C from respiration	
				Start	Added	Start	Added
59	13	200	−18.6	42	29	58	71
59	16–22	200	−18.0	29	26	71	74
59	25	200	−19.6	32	21	68	79
59	>26	200	−17.2	13	28	87	72
60	18–25	290	−20.1	44	56	25	75
60	34–42	230	−26.8[a]	89	−6[a]	11	106[a]
60	>42	85	−35.0[b]	89	[b]	11	[b]

[a] A very negative $\delta^{13}C$ value of added TDIC indicates that some respiration-derived TDIC must originate from methane oxidation.
[b] $\delta^{13}C$ value of added TDIC is close to that of methane at these depths, indicating that methane oxidation is the dominant process by which TDIC has been produced.

Table 4. Carbon balance produced by the pilot study, apportioning the increased TDIC during the 2012 sampling round (relative to 2009), between methanogenesis and respiration end members (Thornton et al., 2014).

CHAPTER 2

2. Methodologies

The methodologies utilised for gathering new field and laboratory data for this thesis are presented below. Where possible, sampling and analysis methods were maintained in line with previous sampling rounds at the site (e.g. Thornton et al, 2001; Thornton et al, 2014), in order to allow direct comparison of data. Where this was not possible, potential discrepancies are noted and discussed with the presentation of the dataset.

2.1. Field Methodologies

In order to retain consistency with previous sampling rounds, it was necessary to set up a variety of different sampling lines in the field for:

(1) groundwater hydro-chemistry;
(2) gas chemistry;
(3) groundwater isotopes; and,
(4) methane isotopes.

2.1.1. Well Purging

All sampling points were purged thoroughly through using a vacuum pump before samples were taken. This ensured that any stagnant water and fine-grained sediments caught up in the HDPE tubing were removed before a sample was taken.

For this purpose, a 2 litre (or greater) purge was conducted. At this site, a 2 litre purge has previously been shown to give consistent reading of in-field parameters such as pH, conductivity and temperature, consistent with the sampling of fresh groundwater (Thornton et al, 2001). This purge is also sufficient to remove the stagnant water filling the well packing and the HDPE line, which is always less than 2 litres.

2.1.2. Groundwater Hydro-chemistry

The first part of the hydro-chemistry sampling line (Figure 22) consisted of a peristaltic pump which took water from the borehole into a piece of in-line monitoring equipment consisting of a variety of cylinders that analysed pH, Eh, conductivity and temperature.

The sampling line was set up such that the water did not leave the HDPE tubing before entering the relevant sampling vessels, also so that the water could pass through at a constant flow rate. This allowed for an accurate measurement of groundwater parameters before the sample interacted with conditions external to the borehole.

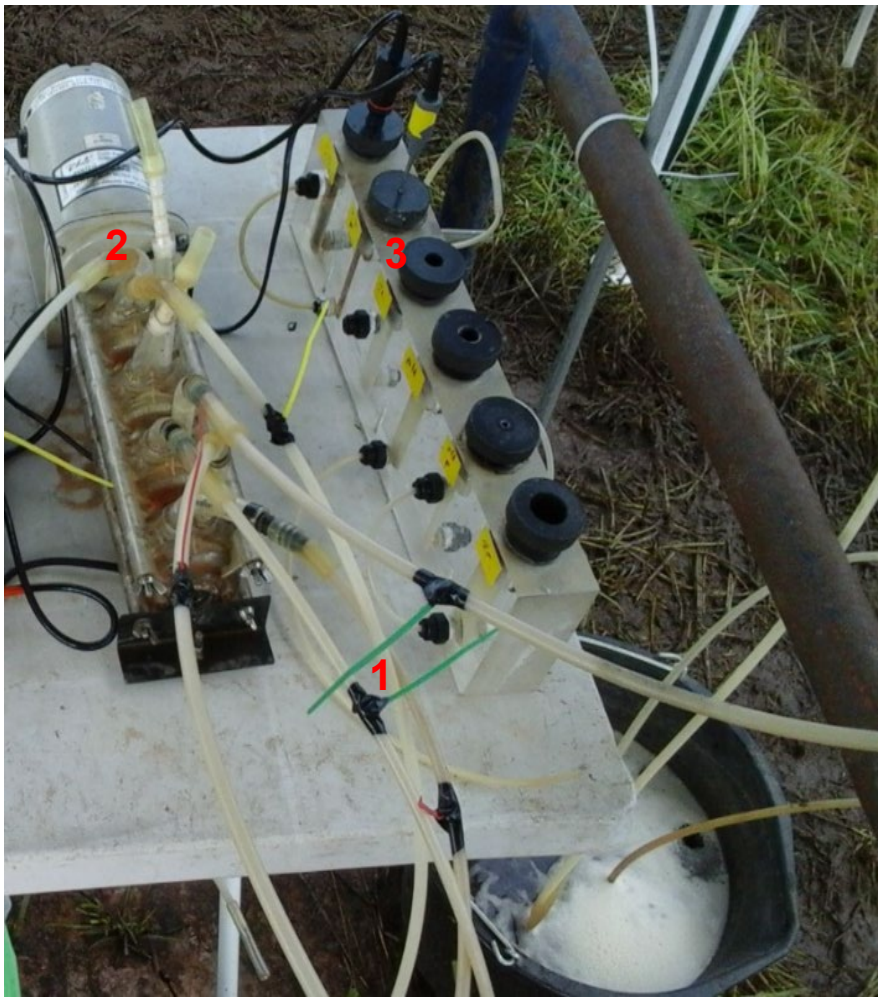

Figure 22. Groundwater hydrochemistry sampling line, showing (1) HDPE tubing coming from well, (2) Peristaltic pump and (3) In-line monitoring equipment.

Secondly, after monitoring through the in-line equipment, water samples were then filtered through a Whatman® 0.45 µm nylon filter. These samples were then stored into McCartney glass vials for the analysis of TPC, 20 ml vials for analysis of dissolved ions, and 15 ml polypropylene vials containing 5 % v/v nitric acid for metal analysis (Thornton et al, 2001).

2.1.3. Gas Chemistry

Gas chemistry samples were taken via anaerobic gas capture. This was done by bringing aquifer gasses into equilibrium with a nitrogen bubble, using Microseeps™ technology (Figure 23).

This process is a modified version of the bubble strip method first created by Chapelle et al. (1995). This method involves a vial connected to the sampling point via HDPE tubing. This bulb is then flushed with groundwater for a few minutes to eliminate air bubbles and then inverted and injected with a bubble of pure O_2 free N_2 (similarly to Chapelle et al, 1997). Pumping continues during the equilibrium phase, however the N_2 gas bubble remains at the top of the inverted vial steadily coming into equilibrium with that groundwater sample being pumped through the vial.

Samples of equilibrated gas were then taken by syringe and injected into septum sealed glass vials which were pre-filled with N_2.

Figure 23. The setup for the gas chemistry sample collection, showing (1) Microseeps™ Vial, (2) N_2 Cylinder.

2.1.4. Groundwater Isotopes

The isotope sampling line consisted of a peristaltic pump attached to the borehole well by HDPE tubing. Water was then allowed to pass through the peristaltic pump at a constant flow rate, feeding into sample collection bottles on the other side of the pump (Figure 24). Water was collected this way for in bottles for $\delta^{34}S\text{-}SO_4$ analysis and TDIC analysis.

Bottles for TDIC analysis were made of HDPE and had a volume of 0.5 L. These bottles contained 50 ml of a reagent solution, comprising of 0.5 kg/L $SrCl_2$ and 100 ml/L aqueous ammonia. The HDPE tubes were placed below the level of the reagent so that all TDIC species within the water were forced to bubble through the reagent and precipitate as $SrCO_3$ (Thornton et al, 2014).

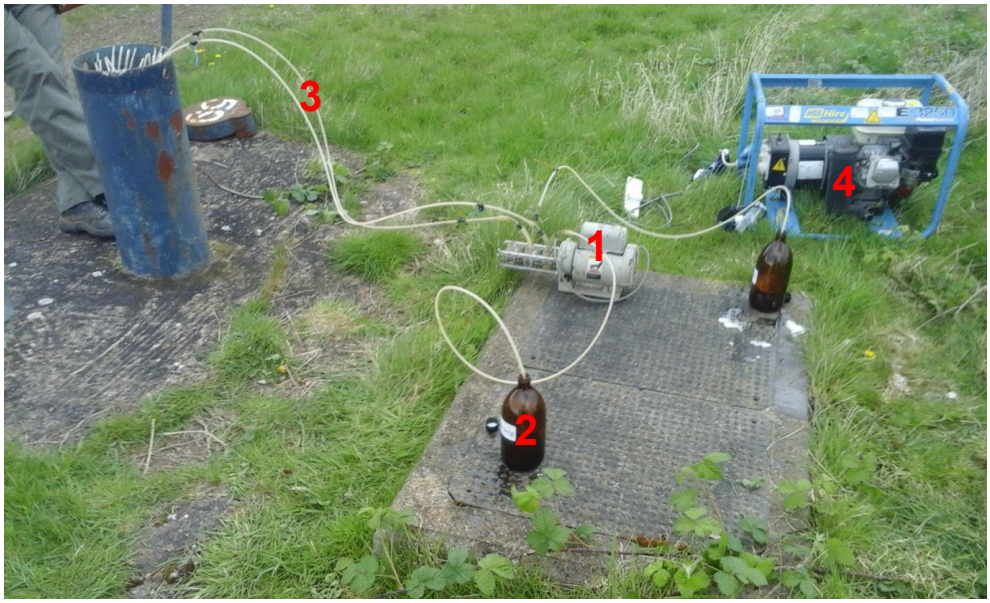

Figure 24. The setup for the δ^{34}S-SO_4 field sample collection, showing (1) Peristaltic Pump, (2) Sampling Bottles, (3) HDPE Tubing, (4) Generator. Sampling bottles were then exchanged for the correct vessels during TDIC collection.

Bottles utilised for δ^{34}S-SO_4 were made of dark brown glass and had a volume of 1 L. These bottles also contained 50 ml of a reagent solution, comprising of 130 g/L $CuCl_2$ and 150 ml/L acetic acid. Groundwater samples from the HDPE tubes were piped into the bottles which were left to simply fill. The $CuCl_2$ reagent acted to precipitate any dissolved sulphide in the water and inhibit microbial activity, whilst the acetic acid acted to prevent $CuCO_3$ formation (Thornton et al, 2014).

2.1.5. Methane Isotopes

The third sampling line consisted of a number of gas ‘blister trap bubbles’ for methane capture (Figure 24a).

After attaching the HDPE tubing from the selected sampling point to a blister trap, it was thoroughly flushed of atmospheric gas using ground water.

The blister traps were then inverted, and groundwater was run through the inverted trap. This enabled the trap to catch gasses created by the degassing of groundwater moving through the traps, including methane for

δ^{13}C-CH_4 analysis. The degassing was effective due to the pressure drop on the water as it moved to atmospheric pressure from a respectively higher pressure in the aquifer. Some groundwater was always left at the bottom of the blister trap in order to form an effective seal in combination with the glass valves (Figure 24b).

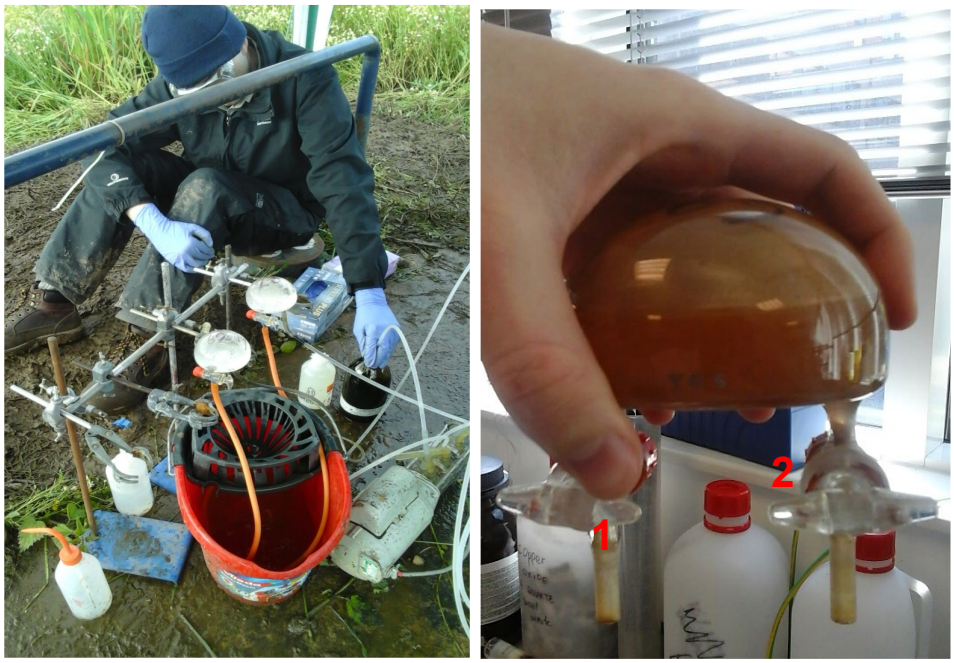

Figure 25. a) Blister trap set-up in the field and b) An inverted 'blister trap bubble' with (1) Inflow/outflow tubes (2) Valves. (Currently filled with a gas sample).

2.1.6. Sampling of Surrogate Microbes for Microcosms

In order to run microcosm studies (section 4) a representative sample of microbes needed to be collected from the aquifer at the site. To achieve this, procedures similar to those in Baker et al. (2011) were followed.

Firstly, sand of a similar geochemical makeup to the aquifer was acquired from a local Permo-Triassic sandstone mine. This sand was then autoclaved three times, in order to remove any microbes present.

Secondly, the sand was then used to fill multiple nylon mesh (200 µm) bags, with each bag containing around 100 g of sand. These bags were then suspended at the bottom of MLS59, within the standpipe, for ~6 months.

During these 6 months groundwater would flow through the stainless-steel well screen, and then the nylon mesh bags. This water would bring with it native microbes from the groundwater which would then serve to inoculate the sand with surrogate microbes. Sand packing had also been placed around the well screen previously, with the aim of keeping flow rates similar to that in the aquifer body.

Whilst retrieving the sample, care was taken to ensure that the sample remained anaerobic at all times. For this, an anaerobic glove bag was sealed to the top of the well casting and the water column, the stand-pipe and glove bag were then thoroughly flushed through with oxygen free nitrogen using a high-pressure hose (Figure 26).

The sand bags were then carefully removed from the borehole and moved through the anaerobic glove bag into and pre-prepared nitrogen filled atmospheric jar which was air-tight.

These atmospheric jars were then taken the back the laboratory and moved into fixed nitrogen chambers. At this point the sand was removed and 100 g of sand was then put into each 500 ml glass bottles sealed with septum seals. These bottles were then filled with the required phenol/reagent mix up to the 400 ml mark to create 21 separate microcosms. 50 g of sand and 20 ml of water was also taken and stored in 4 % (v/v) formaldehyde for imaging of bacteria on grains.

Figure 26. Attachment of the anaerobic gas bag.

2.2. Laboratory Methodologies

Upon returning to the lab samples were run, starting with the most volatile samples. Similar to the field methodologies, the samples were run in the same way as for previous sampling at the site (Thornton et al, 2001; Thornton et al, 2014) to allow direct comparison of data.

2.2.1. δ^{13}C-CH_4 Analysis

Gas samples from the gas blister traps were prepared for δ^{13}C-CH_4 analysis in sequence on a high vacuum purification line and then run through a VG Sira-10 mass spectrometer. Samples were then all either run or sealed in break seals by 2 weeks after the end of the sampling round to minimise gas loss and the associated isotopic fractionation. This involved the following steps:

(1) Cryogenic removal of any CO_2 from the sample;
(2) Combustion of CH_4 to CO_2 in the furnace (the C-CO_2 maintains the same isotope ratio as was previously in the C-CH_4);
(3) CO_2 was then further cryogenically purified; and,
(4) The CO_2 was then passed through the VG Sira-10 mass spectrometer.

The results recoded are δ^{13}C in ‰ relative to Vienna-PeeDee Belemnite (V-PDB). The precision of δ^{13}C-CH_4 analysis was 0.3 % (in line with Thornton et al, 2014).

2.2.2. Recovery of TDIC Data and δ^{13}C-TDIC Analysis

The $SrCO_3$ from the 500 ml TDIC bottle (section 2.1.4) was recovered by gravimetric filtration through a filter funnel. Once filtered, Samples were immediately rinsed three times with deionised water. This process was done as rapidly as possible to stop any reaction between excess Sr(aq) and atmospheric CO_2. Filters were pre-weighed before use and re-weighed after processing and drying in a 105°C oven.

TDIC concentrations were then calculated using by using the mass of $SrCO_3$ precipitated (mg) divided by the volume of sample taken (L), both of which were gravimetrically calculated. This was then corrected for purity versus a standard.

TDIC samples were then processed on a high vacuum purification line and then run through a VG Sira-10 mass spectrometer. This involved the following steps;

(1) Reaction of the $SrCO_3$ with concentrated H_3PO_4;
(2) Cryogenic purification of created CO_2 formed;
(3) Taking of sample yield for purity correction (versus standard); and,
(4) The CO_2 was then passed through the VG Sira-10 mass spectrometer, producing δ^{13}C-TDIC values.

The results recoded are δ^{13}C in ‰ relative to Vienna-PeeDee Belemnite (V-PDB). The precision of TDIC yield varies with TDIC concentration but is better than 2 % at all concentrations, the precision of δ13C-TDIC analysis was 0.1 % (in line with Thornton et al, 2014).

2.2.3. Recovery of Sulphide

$CuCl_2$ and ammonia reagents acted to precipitate any dissolved sulphide as CuS in the field (Section 2.1.4). This CuS was then filtered out of solution prior to recovery of recovery of $BaSO_4$. Due to high levels of impurities in the CuS, precipitates were run through a pyrite extraction line where reactions with HCl acid and Ag^+ produced pure Ag_2S. Sulphide concentrations in the plume could then be gravimetrically calculated.

2.2.4. Recovery of $BaSO_4$ and δ^{34}S-SO_4 Analysis

Sulphate recovery for δ^{34}S-SO_4 is achieved by precipitation as insoluble $BaSO_4$ (Spence et al, 2001b). This involved the following steps:

(1) Samples were acidified (pH 2.0 - 2.5) and heated to ~80°C on a hot plate;
(2) $BaCl_2$ solution at 100 g/L was added at 10 % of the sample volume;
(3) The $BaSO_4$ was reacted for an hour and then left to cool and coarsen;
(4) The $BaSO_4$ precipitate was then recovered by vacuum filtration; and,
(5) The filter paper was thoroughly washed with deionised water prior to drying at 50°C.

$BaSO_4$ samples were then then run through an Isoprime mass spectrometer and are reported in reported in $\delta^{34}S$ in ‰, relative to the IAEA Vienna-Cañon Diablo Troilite (V-CDT) standard. The precision of $\delta^{34}S$ analysis was 0.3 % (in line with Thornton et al, 2014).

2.2.1. Hydrochemistry Analysis

Hydrochemistry analysis were carried out by project collaborators at the University of Sheffield (Groundwater Protection and Restoration Group) in line with Thornton et al. (2014) as follows;

(1) Total phenols were analysed by high-pressure liquid chromatography, using a Perkin-Elmer Series 200 system and UV detector with a precision of ±5%.
(2) Acetate, NO_3, Mn, Fe and SO_4 were determined by ion chromatography using a Dionex 2000 system with a precision of ±3%.
(3) Methane gas was measured using a Perkin Elmer Clarus gas chromatograph with a precision of ±2%.

CHAPTER 3

3. New Field Data from the Four Ashes Site

This chapter aims to present a thorough review of the new data obtained during field surveys as part of this thesis. These field surveys were conducted in 2014, 2015 and 2016 in order to add to a time series of data for the plume gathered by previous surveys (e.g. Spence et al, 2001b; Thornton et al, 2014).

These surveys analysed a large range of chemical parameters, as discussed in the methodologies (section 2). These data will be used in later sections for comparison with historical pre-pumping data, however, this chapter will focus solely on a presentation of new data, from which key points will be highlighted and discussed in detail.

It should be noted at this point that, due to unforeseen circumstances occurring before the 2012 sampling round the PAT system was forced to cease operation at MLS59. However, despite the unforeseen nature of this cessation, data is still presented, as this provided a unique opportunity to monitor rebounding conditions in a contaminant plume after the termination of the PAT system.

Where comparing the similarity, or dissimilarity, between two datasets statistical tests were used. In general, a t-test was undertaken to determine if the averages and variances associated with two data groups indicated a significant difference. Where other tests where undertaken they are otherwise stated.

3.1. Contaminant Concentrations

TPC concentrations from the 2014, 2015 and 2016 surveys are presented below. Full statistics are presented in Appendix 1.

3.1.1. Contaminants (TPC) at MLS59

TPC concentrations at MLS59 (Figure 27), which was not being pumped during this period, generally fell within the range of historical pre-PAT levels (1998-2011) for both the 2014 and 2015 surveys. However, although there is some indication of a decrease in phenol concentrations between 10 mbgl and 20 mbgl during the 2015 sampling round.

TPC levels were generally lower towards the edge of the plume and more concentrated in the centre of the plume, similar to historical trends.

These results are indicative of a strong contamination source, which is continuing to input large amounts of contaminants into the plume and where NA is not acting to significantly attenuate the strong source input (section 1.13.1).

In general, the contaminant concentrations in MLS59 are as follows (2014 and 2015):

- Negligible concentrations ~ 5 mbgl to 11 mbgl;
- Low concentrations between ~12 mbgl and 19 mbgl;
- Moderate but variable concentrations from ~19 mbgl to 24 mbgl;
- Peak concentrations between ~24 mbgl and 29 mbgl; and,
- Low concentrations ~29 mbgl to 30 mbgl

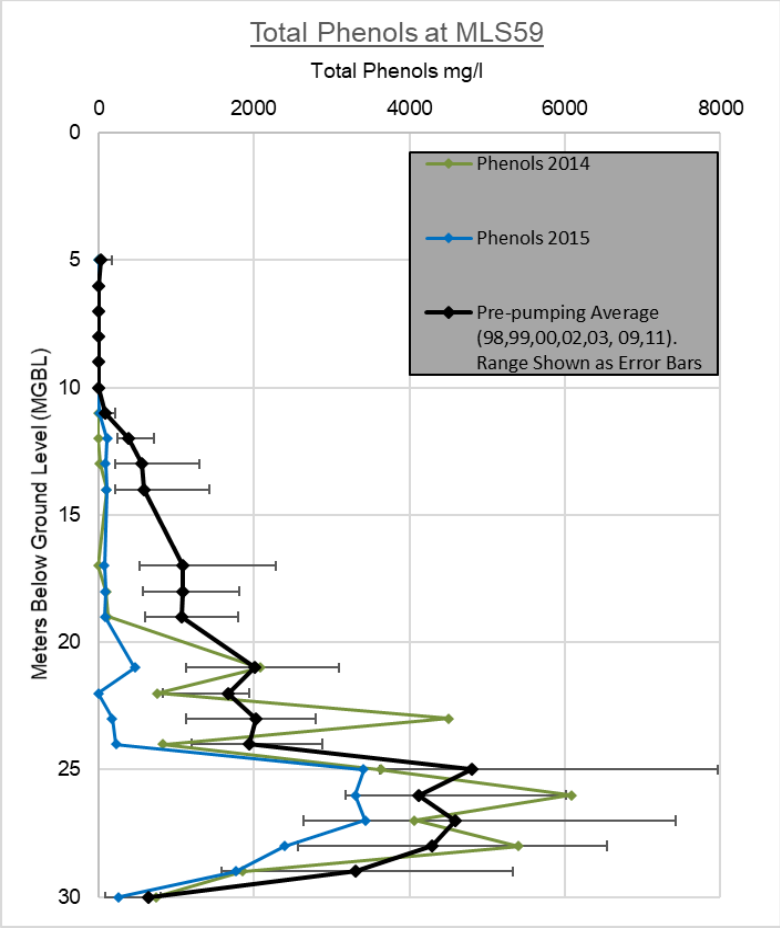

Figure 27. Contaminant concentrations at MLS59 in 2014 and 2015 in comparison to the pre-PAT average (Pre-pumping range shown as error bars).

During 2016, however, a shift in TPC levels occurred (Figure 28), with contaminant concentrations being notably different from all other surveys prior to 2015 (inclusive). There is a decrease in TPC within both the upper and lower plume in the 2016 survey, this is most marked between 25 mbgl and 29 mbgl. This has been linked with the presence of nitrate breakthrough in the lower plume, which is further discussed in later sections (section 3.2.1.1).

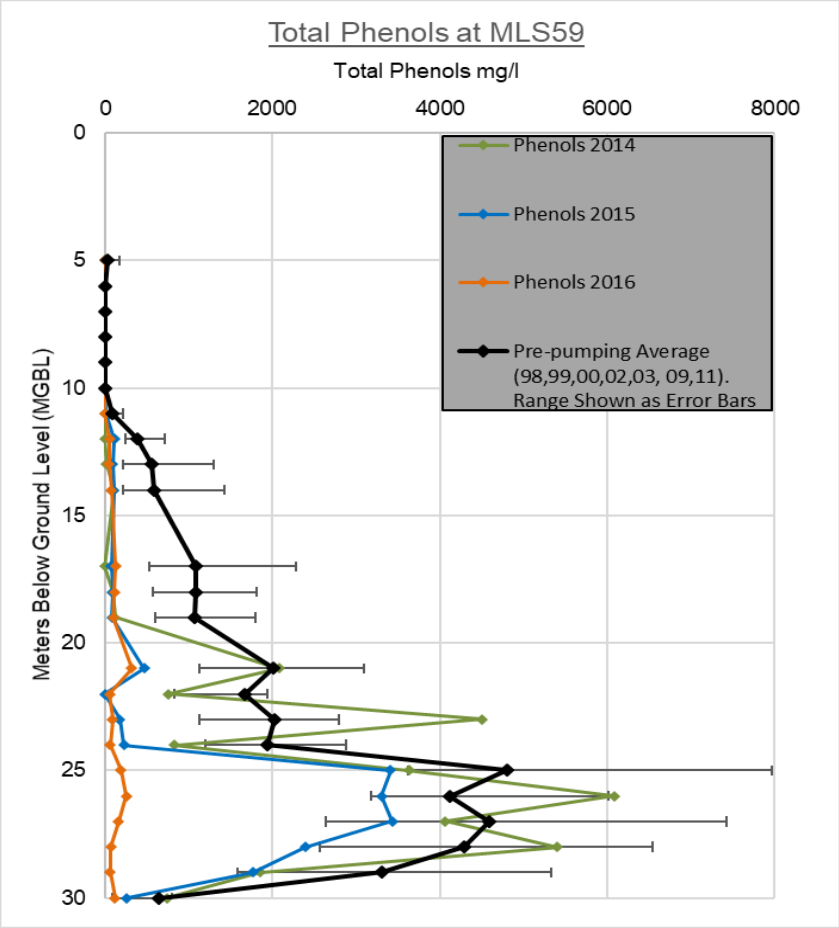

Figure 28.Contaminant concentrations at MLS59 in 2014. 2015 and 2016 in comparison to the pre-PAT average (Pre-pumping range shown as error bars).

3.1.2. Contaminants (TPC) at MLS60

TPC concentrations at MLS60 (Figure 29), which was being pumped during this period, remained heavily influenced by the PAT remediation, similarly to the 2012 pilot study (Thornton et al, 2014).

In the 2014, 2015 and 2016 surveys, TPC concentrations were lower towards the upper edge of the plume than the range of pre-PAT surveys. However, high TPC concentrations remained present in the centre of the plume, between 27 mbgl and 36 mbgl. These values typically remained within the range of pre-PAT values.

In the lower regions of the plume, between 35 mbgl and 44 mbgl, a large decrease in contaminant concentration is observed in respect to the pre-pumping range of values. This can be attributed to the direct removal of

contaminants by the action of the PAT system, which is removing contaminated water from 39 mbgl.

The decrease in contaminant concentrations at the upper edge of the plume, between 19 mbgl and 25 mbgl, may also be due to a more indirect effect of the PAT remediation. However, the decrease in this region could also be attributable to other variations such as changing contaminant input or valuations in groundwater flow.

In general, the contaminants in MLS60 follow the following pattern, since implantation of PAT:

- Low contractions between ~21 mbgl and 27 mbgl;
- Peak concentrations between ~28 mbgl and 35 mbgl;
- PAT reduced concentrations from ~36 mbgl to 44 mbgl; and,
- Low concentrations ~45 mbgl.

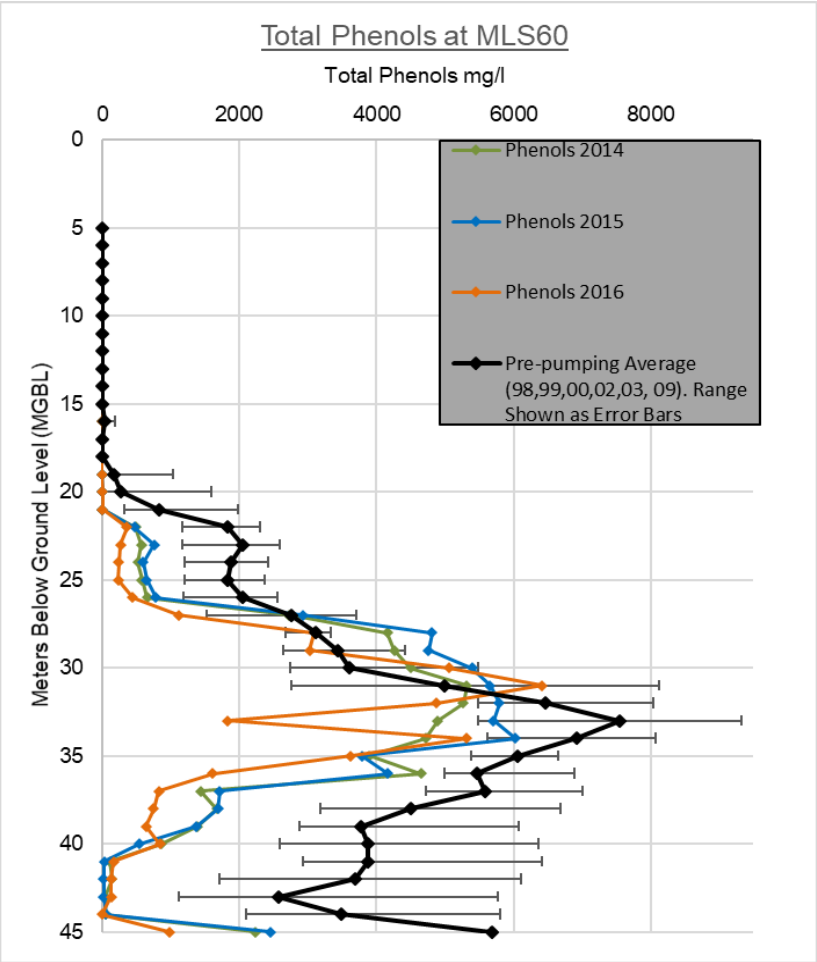

Figure 29. Contaminant concentrations at MLS60 in 2014, 2015 and 2016 in comparison to the pre-PAT average (Pre-pumping range shown as error bars).

3.2. Nitrate Concentrations

Nitrate concentrations from the 2014, 2015 and 2016 surveys are presented below. For all available data, see Appendix 1.

3.2.1. Nitrate at MLS59 (2014 and 2015)

In 2014, nitrate concentrations at MLS59 (Figure 29, not pumped), showed similar results to historical nitrate surveys at the site (Spence et al, 2001b; Thornton et al, 2014).

The nitrate data indicates that background levels of nitrate (~45 mg/L) are present outside of the plume, with low amounts of nitrate present in the plume core. Between the background water and the plume core, the upper fringe exhibits a declining nitrate edge, which is easily identifiable between 10 mbgl and 12 mbgl.

The above trends in the nitrate data can be explained due to the consumption of nearly all of the nitrate around the plume fringe (10 mbgl – 12 mbgl), similarly to historical surveys (Spence et al, 2001b). The reasons for this are outlined in the Cirpka model (section 1.15.1).

Notwithstanding the above, it should be appreciated that nitrate results for 2015 appear to fluctuate throughout the plume, however, as no associated shifts in TPC concentrations (section 3.1) or shifts in δ^{13}C-TDIC Values isotopes (section 3.4) are present, it is considered that these analyses have been affected by interference with the contaminant matrix (section 1.13.2), a effect which has previously been noted (Thornton et al, 2001). Thus, these results are not presented below but can be found within Appendix 1.

The results for 2014 showed the following:

- Background levels of nitrate from ~5 mbgl to 9 mbgl;
- Declining nitrate edge between ~10 mbgl and 12 mbgl;
- Negligible nitrate levels between ~13 mbgl and 24 mbgl; and,
- Low nitrate levels ~25 mbgl to 29 mbgl.

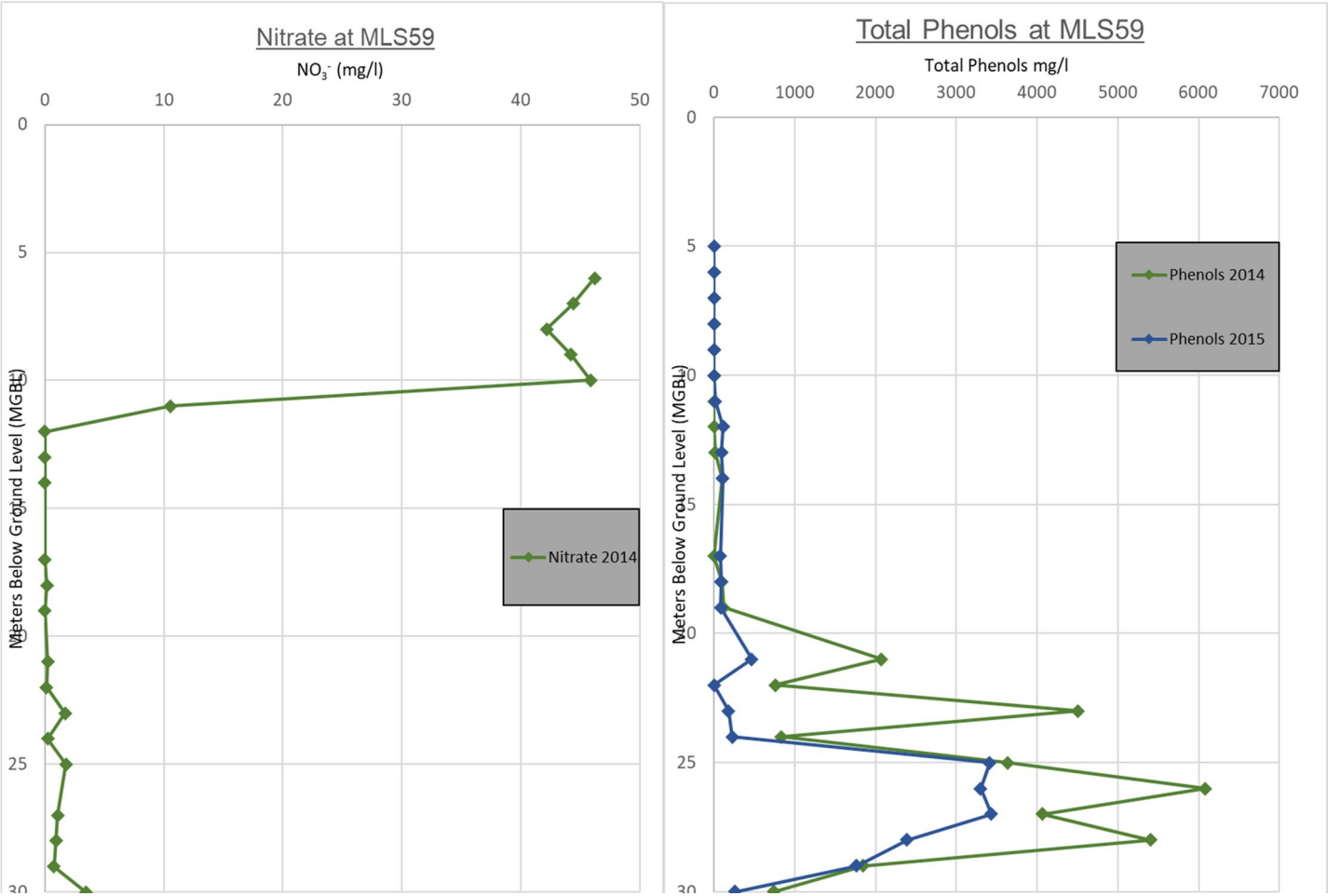

Figure 30. Nitrate concentrations at MLS59 in 2014 (left). Related to TPC 2014 and 2015 (right).

3.2.1.1. Nitrate Breakthrough at MLS59 (2016)

In 2016, the lower regions of the plume also exhibited the effects of nitrate breakthrough towards the lower plume fringe (Figure 30). Further discussion of this is provided in along with the carbon balance (section 5). The results from 2016 showed:

- Background levels of nitrate ~5 mbgl to 10 mbgl;
- Declining nitrate edge between ~10 mbgl and 13 mbgl;
- Negligible nitrate levels between ~14 mbgl and 27 mbgl; and,
- Nitrate breakthrough ~28 mbgl to 30 mbgl.

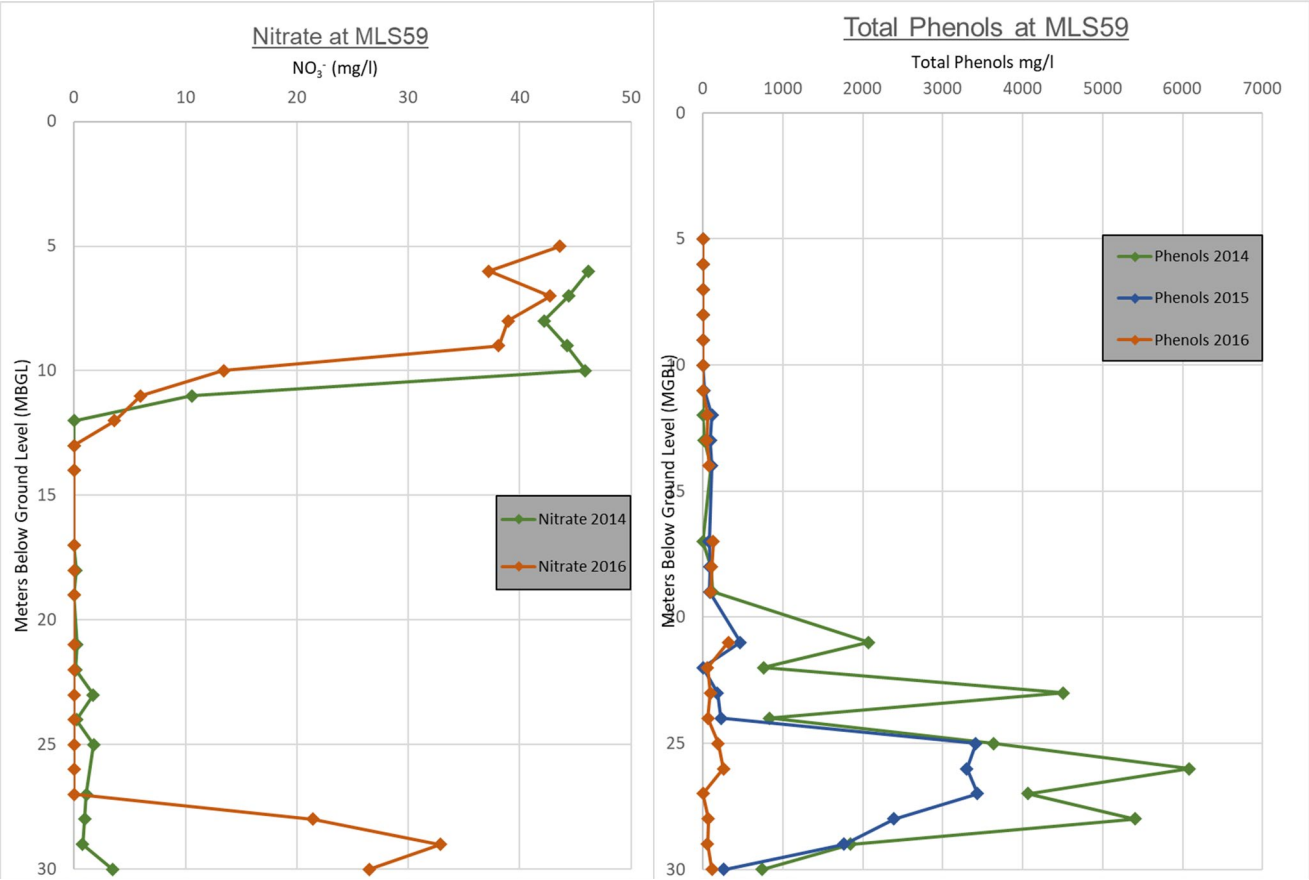

Figure 31. Nitrate concentrations at MLS59 in 2014 and 2016 (left). Related to TPC 2014, 2015 and 2016 (right).

3.2.2. Nitrate at MLS60

Nitrate concentrations at MLS60 (Figure 31, pumped), show similar results to historical surveys. This data, similar to the MLS59 data, indicates background levels of nitrate present above the plume, with low amounts of nitrate present in the plume core. Again, this is due to the consumption of nearly all nitrate around the plume fringe (section 1.13.2).

The declining nitrate edge associated with this fringe is somewhat longer and more obvious at MLS60 than MLS59, covering twice the depth. The results showed:

- Background levels of nitrate ~6 mbgl to 14 mbgl;
- A declining nitrate edge associated with nitrate reduction (section 3.2.1) from ~14 mbgl to 21 mbgl; and,
- Negligible nitrate levels between ~21 mbgl and 40 mbgl.

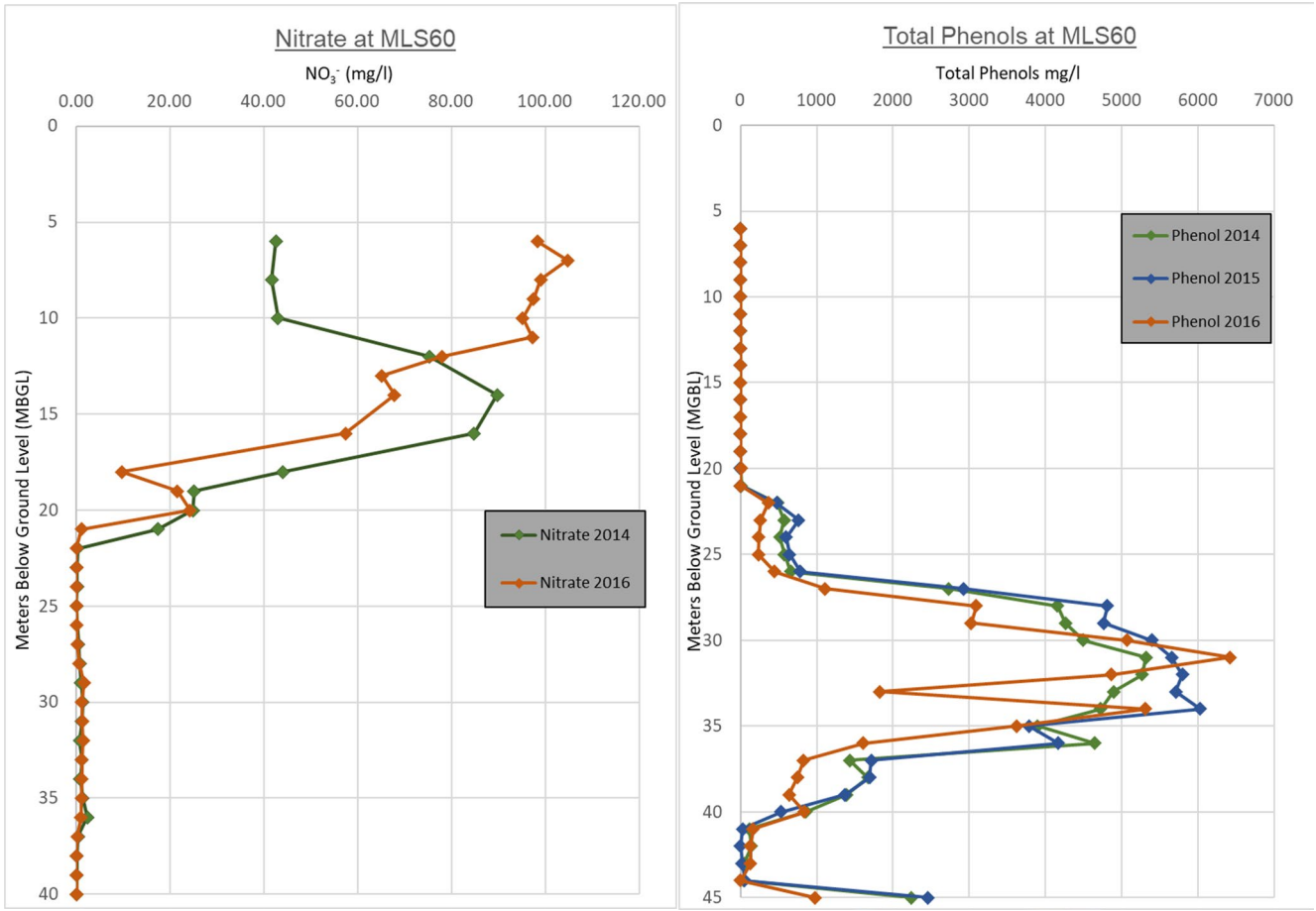

Figure 32. Nitrate concentrations at MLS60 in 2014 and 2016 (left). Related to TPC 2014, 2015 and 2016 (right).

3.3. TDIC Concentrations

Analysis of TDIC concentrations from the 2014, 2015 and 2016 surveys is presented below. Full statistics are presented in Appendix 1.

It should be appreciated that, as discussed within previous chapters (Sections 1.13.5), TDIC data does not distinguish between “background TDIC” and TDIC generated from biodegradation of TPC. However, the amount of “background TDIC” can be estimated and has been subsequently factored out for the carbon balance calculations (Section 5.2).

3.3.1. TDIC at MLS59

3.3.1.1. For 2014 and 2015

TDIC concentrations at MLS59 (Figure 32, not pumped), showed similar results to historical surveys for 2014 and 2015.

Background levels of TDIC (~50 mg/L) were present between ~5 mbgl – 10 mbgl. This corresponds well with the zone of negligible contamination (5 mbgl to 11 mbgl, Figure 32) and is indicative of non-contaminated background water. The zone between the background water and the peak contamination, between 10 mbgl and 25 mbgl, exhibits TDIC values between 240 mg/L and 330 mg/L; this is indicative of substitutional biodegradation of contaminants in this zone.

However, it is worthy of note that values between 10 mbgl and 15 mbgl are somewhat lower than the historical pre-PAT average. A decrease in contaminants between 10 mbgl and 15 mbgl was also noted (section 3.1.1), indicating the possibly of plume thinning in this region, enacted by the PAT remediation. This thinning has led to reduced TDIC creation due to the small pool of TPC available for nitrate reduction, which is a dominant process in this region (section 1.13.2).

Within the lower plume core, from 25 mbgl to 29 mbgl, TDIC values drop to ~230 mg/L, showing that biodegradation was still occurring in this zone, but

at a lesser rate than between 10 mbgl and 25 mbgl. These results are consistent with the suppression of certain forms of biodegradation (most notably BSR) in this area due to increased contaminant toxicity, as TPC is greater than 2 g/L (Spence et al, 2001a; Spence et al, 2001b; Baker et al, 2012).

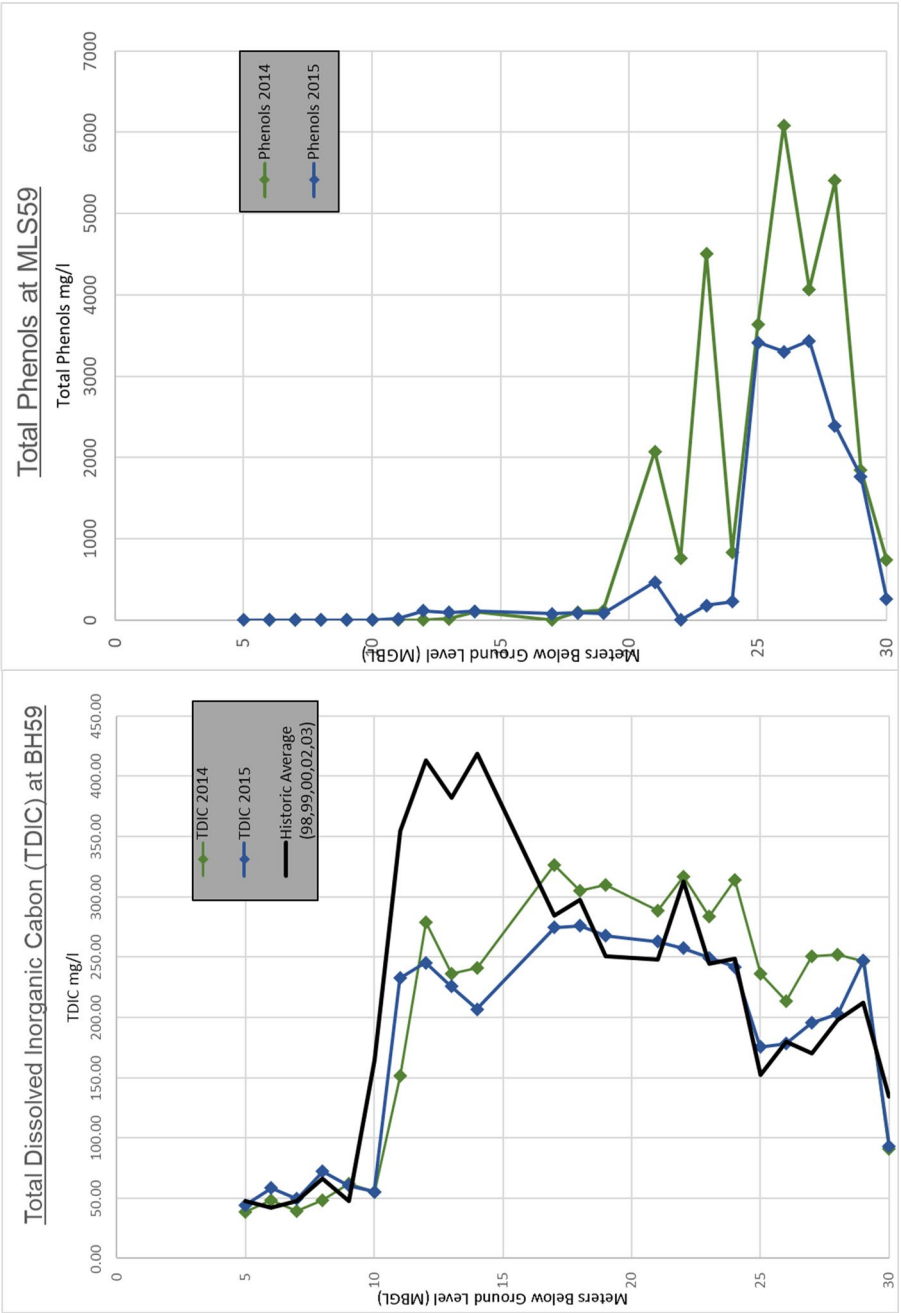

Figure 33.TDIC concentrations at MLS59 in 2014, 2015 and historical (left), in relation to TPC in2014 and 2015 (right).

3.3.1.2. For 2016

The TDIC concentrations at MLS59 (Figure 33Figure 33, not pumped) varied somewhat, due to the effect of nitrate breakthrough in 2016 (section 3.2.1.1).

For 2016, background levels of TDIC (~50 mg/L) were again present between 5 mbgl and 10 mbgl and the zone between the background water and the peak contamination; between 10 mbgl and 25 mbgl TDIC values between 240 mg/L and 330 mg/L were recorded. This showed that conditions within the upper plume fringe and the upper plume core are similar to 2014 and 2015.

However, where the lower plume core historically was (25 mbgl to 29 mbgl), TPC has decreased substantially (Figure 33) and nitrate had increased (Figure 30). These changes are paired with a drop in TDIC values, at corresponding depths.

These three datasets can be compared to outline the reasons for the nitrate breakthrough. The data demonstrates that the nitrate breakthrough is not due to the mixing of clean and contaminated water, which would result in massive amounts of biodegradation and hence high TDIC. Rather, the data displays that the TDIC concentrations in this region return to background levels (50 mg/L), which is indicative of thinning of the plume, likely affected by the action of the PAT system.

For further discussion of this and a conceptual model, please see the carbon balance discussion and conclusions (sections 5 and 6).

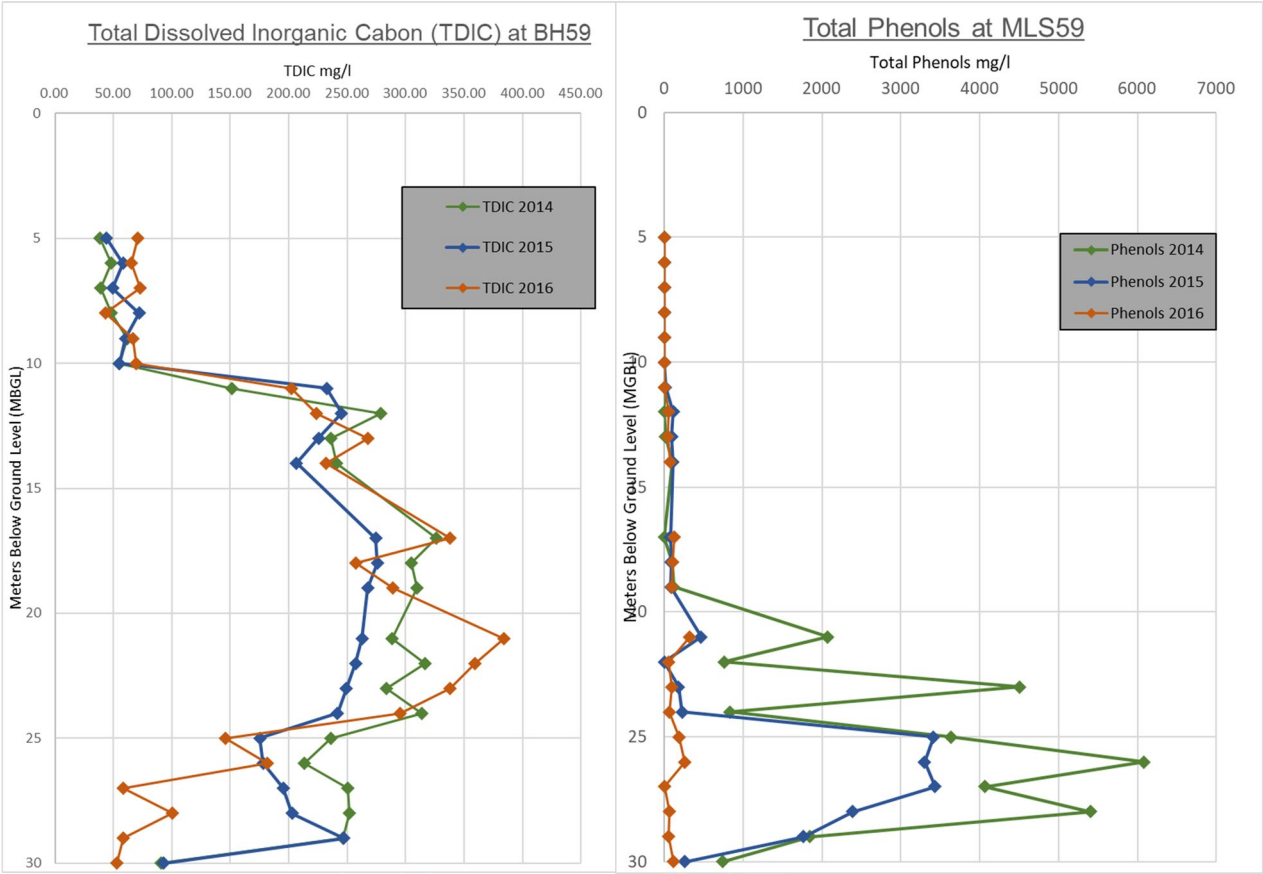

Figure 34. TDIC concentrations at MLS59 in 2014, 2015 and 2016 (left), in relation to TPC 2014, 2015 and 2016 (right).

3.3.2. TDIC at MLS60

TDIC concentrations at MLS60 (Figure 34, pumped) remained heavily influenced by the PAT remediation, in a similar way to the 2014 pilot study (Thornton et al, 2014).

Similar to MLS59, background levels of TDIC (~50 mg/L) were present between ~6 mbgl and 17 mbgl. This corresponds with negligible TPC in the same zone (Figure 29), with these data indicative of non-contaminated background water.

However, despite negligible TPC being present between 18 mbgl and 21 mbgl (Figure 29), TDIC levels of 90 mg/L – 250 mg/L are exhibited in this zone. This corresponds with the declining nitrate edge at the same depths (section 3.2.2) and is indicative of a plume fringe between 2 m and 3 m In vertical width (depending on the chemical parameter and year used for this definition). In this region, data indicate that a pool of TPC is undergoing total or near total biodegradation, due to processes dominated by nitrate reduction. However, the TDIC concentrations in this region are lower than seen elsewhere in the plume, indicating that amount of contamination undergoing complete biodegradation is limited.

High TDIC values (~500 mg/L) indicate that biodegradation is substantial in the upper part of the plume (22 mbgl to 26 mbgl). Due to the lack of available oxygen and nitrate within the plume core (Figure 31) oxic and nitric reduction are considered negligible within this region. However, TPC concentrations are below the toxic threshold of 2 g/L giving potential for BSR (Figure 29). Furthermore, data from $\delta^{34}S\text{-}SO_4$ isotopes in indicative of BSR in this region (Section 3.5.2).

However, between 28 mbgl and 34 mbgl, TDIC values fall to <175 mg/L. Again, the lack of available oxygen and nitrate indicate limited oxic and nitrate reduction within this region (Figure 31). However, an increase in TPC levels to above the 2 g/l toxic threshold (1.13.4.2) implying potential contaminant toxicity with regards to BSR (Spence et al, 2001a; Spence et al, 2001b; Baker et al, 2012). Data from $\delta^{34}S\text{-}SO_4$ isotopes are not indicative of BSR in this region (Section 3.5.2).

Below 34 mbgl, the TDIC concentrations again rise as TPC values begin to fall to below 2 g/l under the influence of the PAT system (Figure 29). Data from δ^{34}S-SO_4 isotopes are indicative of BSR in this region (Section 3.5.2) and the presence of sulphide is noted (Section 3.7.2). This region is hence exhibiting less toxic suppression than pre-PAT (Section 1.13.4), demonstrating that the PAT system acts to increase in-situ biodegradation.

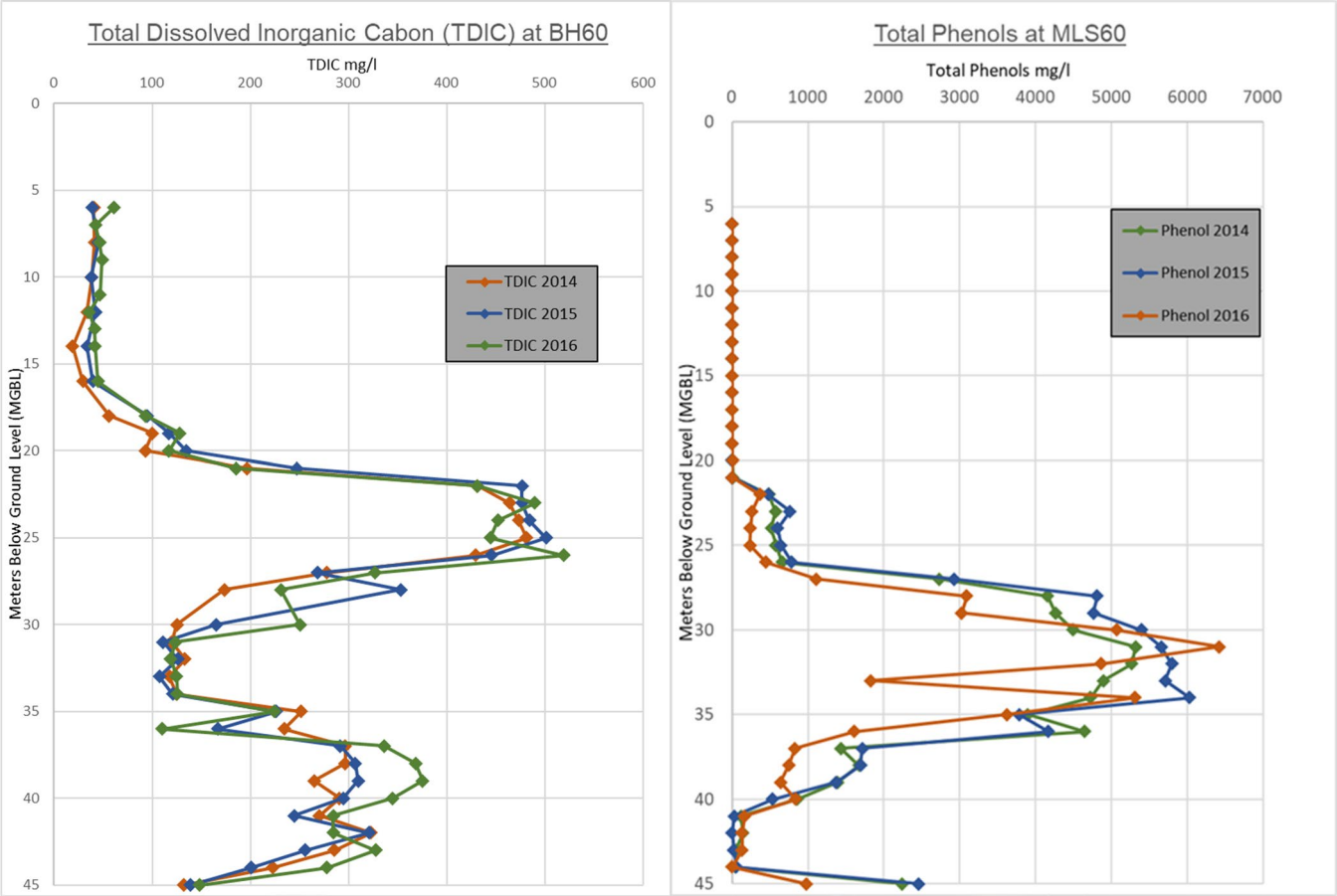

Figure 35. TDIC concentrations at MLS60 in 2014, 2015 and 2016. Related to TPC 2014, 2015 and 2016.

3.4. δ^{13}C-TDIC Values

Section 1.14.1 discusses that δ^{13}C-TDIC values are affected by respiration, methanogenesis and AMO processes. Depleted δ^{13}C-TDIC values are typical of respiration, with enriched δ^{13}C-TDIC being typical of methanogenesis.

In regions where AMO is present this causes a rapid depletion of δ^{13}C-TDIC. Hence, substantial depletion of δ^{13}C-TDIC in itself is indicative of some AMO (Section 1.14.3), with a δ^{13}C-TDIC close to that of methane indicating that methane oxidation is the dominant process (Thornton et al, 2014).

It should be appreciated that, as discussed within previous chapters (Sections 1.13.5 and 1.14.1), isotopic data does not distinguish between "background TDIC" and TDIC generated from biodegradation of TPC.

Substrate values were measured at source as -25 ‰ (Baker et al, 2012), however, δ^{13}C-TDIC is further enriched in the plume due to dissolution of naturally occurring carbonates within the aquifer (Section 1.14.1; Williams et al, 2001).

In light of the above, δ^{13}C-TDIC data is best viewed in comparison to "background TDIC" values which are understood to have a δ13C-TDIC of approximately -19 ‰ (Baker et al, 2012; Thornton et al, 2014). For further calculations, such as the carbon balance, the effects of "background TDIC" can be estimated and factored out (Section 5.2).

3.4.1. δ^{13}C -TDIC at MLS59

3.4.1.1. For 2014 and 2015

During 2014 and 2015, δ^{13}C-TDIC values at MLS59 (Figure 35, not pumped) ranged between -20 ‰ and -16 ‰. Most of the values were more enriched in δ^{13}C compared to the background values, thus indicating the predominance of methanogenesis, over respiration, in the plume.

Between 5 mbgl and 11 mbgl, δ^{13}C-TDIC was equal to that of the background water (-19 ‰), ranging between -20 ‰ and -18 ‰, indicating clean background water at these depths. However, δ^{13}C-TDIC was somewhat more enriched between 11 mbgl and 15 mbgl, ranging from -18 ‰ to -16 ‰, suggesting a dominance of methanogenesis at these depths.

Below these depths, δ^{13}C-TDIC values were somewhat less enriched, returning to values close to background water between 17 mbgl and 25 mbgl, although 2015 does appear to be a little more enriched. This is indicative of a delicate balance between respiration and methanogenesis, which can be pushed either way by slight annual fluctuations.

In the region of maximum TPC (Figure 28, 26 mbgl to 29 mbgl), δ^{13}C-TDIC values shift again, becoming slightly more enriched. This is indicative of a stronger methanogenic dominance at these depths and is probably due to suppression of BSR in this region due to high TPC concentrations (section 3.1.1).

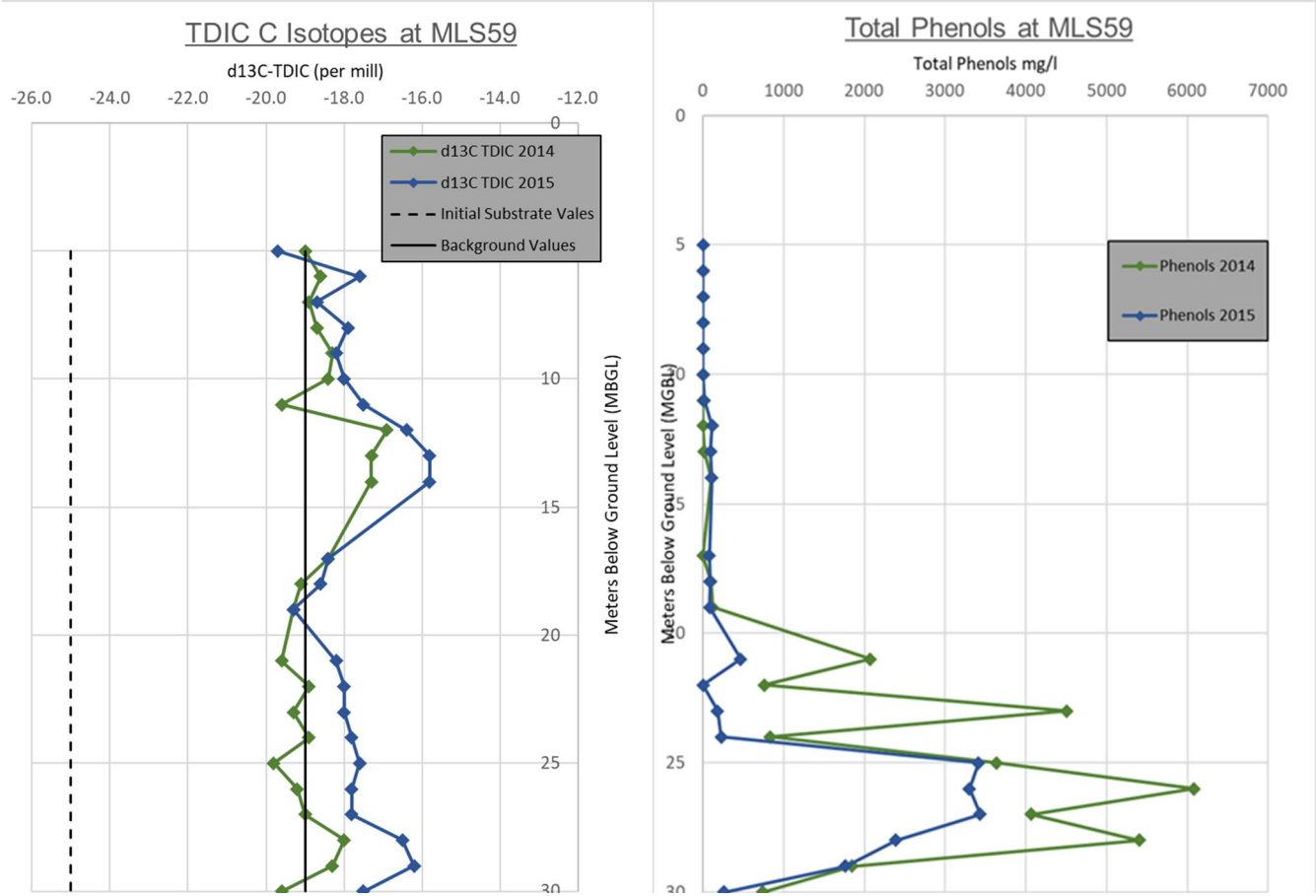

Figure 36. δ^{13}C-TDIC (left) and TPC (right) at MLS59 for 2014, 2015 and 2016.

3.4.1.2. For 2016

In 2016, δ^{13}C -TDIC values at MLS59 were again mostly enriched when compared to substrate and background values (Figure 36).

Values recorded between 5 mbgl and 7 mbgl were again similar to that of the background water. However, values recorded between 8 mbgl and 12 mbgl were more depleted, ranging between -24 ‰ and -18 ‰, showing additional respiration and/or AMO at these depths in comparison to 2014/2015.

Values at 13 mbgl and 14 mbgl showed a similar methanogenic dominance as previously seen, as did values between 18 mbgl and 25 mbgl which also showed similar trends to 2014 and 2015.

Values between 25 mbgl and 29 mbgl, however, were marginally more depleted in δ^{13}C than 2014/2015, with values returning to close to background levels (-19 ‰). This data further substantiates the values above, showing clean water in this region due to a thinning of the plume, which is a likely effect of the PAT system.

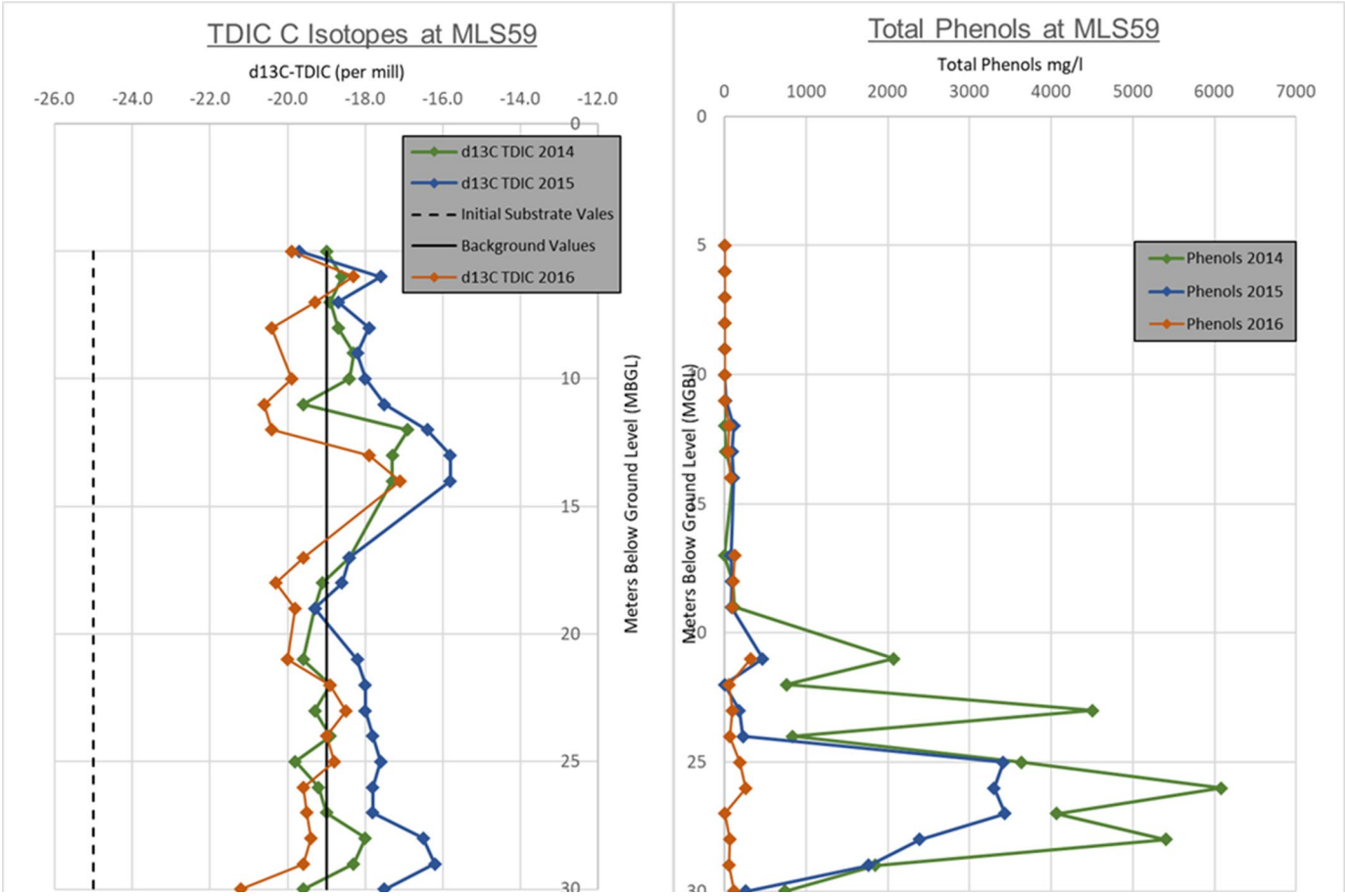

Figure 37. δ13C-TDIC (left) and TPC (right) at MLS59 for 2014, 2015 and 2016.

3.4.2. δ^{13}C-TDIC at MLS60

δ^{13}C-TDIC values at MLS60 (Figure 37, pumped) exhibited a larger range than those recorded at MLS59, ranging between -25 ‰ and -15 ‰. Values showed that some δ^{13}C was more enriched than the background values, whilst other δ^{13}C was depleted when compared with background values.

Between 5 mbgl and 12 mbgl, δ^{13}C-TDIC are more depleted than background water (-19 ‰), ranging from -22 ‰ to -20 ‰. Values between 12 mbgl and 20 mbgl were also predominantly more depleted than background values, although some 2014 and 2015 results showed some enrichment at 13 mbgl and 14 mbgl. In general, these depleted values are indicative of a dominance of respiration above the plume core where TPC levels are low.

Values at the top of the plume core (21 mbgl to 30 mbgl), are more enriched in δ^{13}C, indicating a more methanogenic dominance in this region. This is expected, as respiration processes, especially BSR, are likely to be suppressed by high TPC levels at these depths (Figure 29); this is further backed up by high methane values in this region (Figure 41).

However, values at the bottom of the plume core, between 30 mbgl and 39 mbgl, are very variable. With BSR still supressed at these depths due to high TPC, and a variable methane pool (Figure SEQ Figure * ARABIC 37), it can be concluded that the changes in δ^{13}C-TDIC at these depths is due to a shifting balance between methanogenesis and AMO. Pumping, which is occurring around 39 mbgl, is likely to have a strong effect on this delicate balance, with changes in pumping rate around the time of sampling hence effecting shifts in δ^{13}C.

Due to the action of the PAT, there is a substantially reduced contamination load between 40 mbgl and 45 mbgl, allowing BSR to be a viable process at these depths. Here, moderately depleted δ^{13}C-TDIC demonstrates that this area is dominated by respiration in comparison to historical surveys.

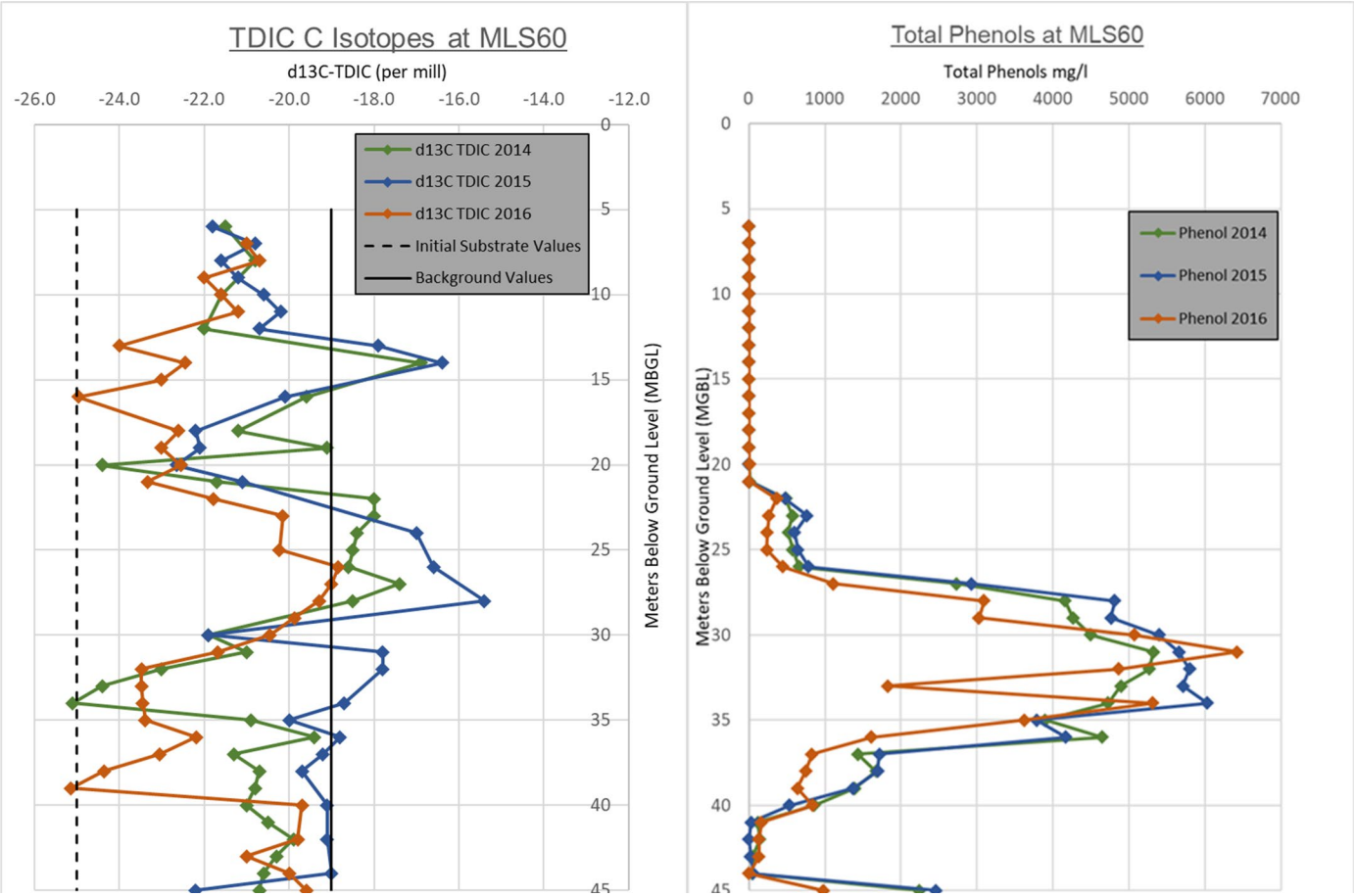

Figure 38. δ^{13}C-TDIC (left) and TPC (right) at MLS60 for 2014, 2015 and 2016.

3.5. δ^{34}S-SO_4 Values

Section 1.14.4 notes that δ^{34}S-SO_4 are affected by BSR, with BSR causing an enrichment in ^{34}S isotopes relative to the initial substrate. δ^{34}S-SO_4 data is best viewed in comparison to source/substrate values; these source values were measured as 5.5 ‰ – 7.7 ‰ (Thornton et al, 2014).

3.5.1. δ^{34}S -SO_4 at MLS59

δ^{34}S-SO_4 values at MLS59 (Figure 38, not pumped), showed similar results to historical surveys.

In 2014, 2015 and 2016, δ^{34}S-SO_4 isotope values in the non-contaminated zone between 5 mbgl and 10 mbgl were 4.0 ‰ – 5.0 ‰, which is within the range of background δ^{34}S-SO_4 measurements (4.0 ‰ – 6.0 ‰, Thornton et al, 2014). This is indicative of non-contaminated background water in this zone.

The zone between the background water and the peak contamination, from 10 mbgl to 25 mbgl (Figure 28), exhibits the highest isotopic fractionation of δ^{34}S-SO_4, with values ranging between 9.0 ‰ and 17.4 ‰. These values also have a greater isotopic fractionation than that of the H_2SO_4 waste (~7 ‰, Thornton et al, 2014) that is currently feeding the plume. This positive shift in δ^{34}S-SO_4 in the isotopic values is a strong signal that this region of the plume is subject to substantial amounts of BSR. This zone also corresponds with the zone of maximum TDIC creation (10 mbgl to 24 mbgl, Figure 33).

Within the region of peak contaminant concentrations (25 mbgl to 29 mbgl, Figure 28), δ^{34}S-SO_4 values move to 4.2 ‰ – 7.4 ‰, which is not significantly different to either background values (4.0 ‰ – 5.0 ‰) or H_2SO_4 waste values. This is consistent with the suppression of BSR at these depths due to increase contaminant toxicity (Spence et al, 2001a; Spence et al, 2001b; Baker et al, 2012), which is also highlighted by the decrease in TDIC levels (Figure 33).

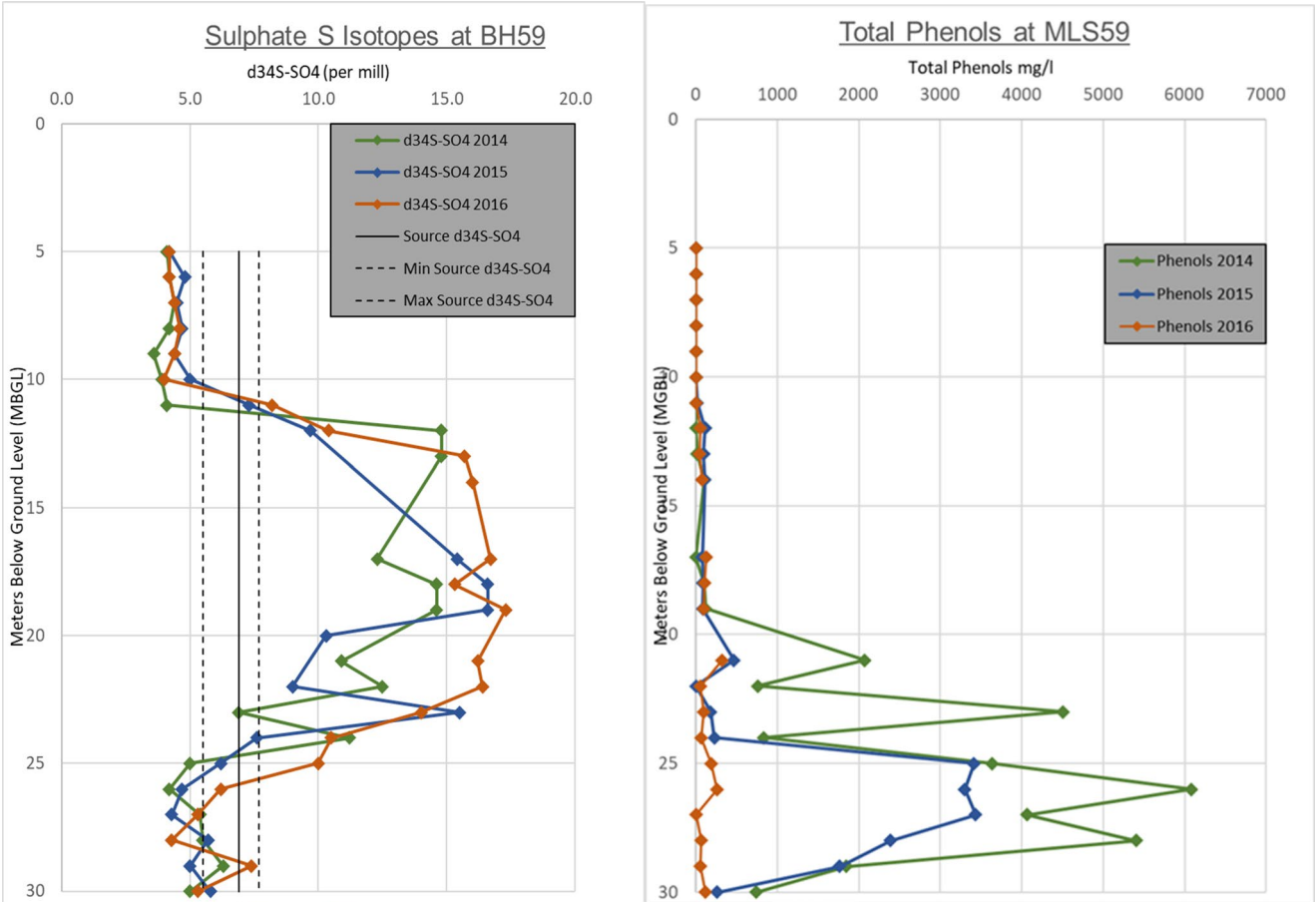

Figure 39. δ^{34}S-SO_4 TDIC concentrations at MLS59 in 2014, 2015 and 2016, in comparison to source δ^{34}S-SO_4 (left). TPC in 2014, 2015 and 2016 (right).

3.5.2. δ^{34}S-SO_4 at MLS60

Similar to the 2014 pilot study (Thornton et al, 2014), δ^{34}S-SO_4 values at MLS60 (Figure 39Figure 39, pumped), remained heavily influenced by the PAT remediation.

δ^{34}S-SO_4 isotope values in the non-contaminated zone between 6 mbgl and 11 mbgl were recorded between 5.7 ‰ - 5.8 ‰. This is within the range of background δ^{34}S-SO_4 measurements (4.0 ‰ - 6.0 ‰, Thornton et al, 2014) and is typical of non-contaminated background water in this zone.

Between 12 mbgl and 16 mbgl, δ^{34}S-SO_4 isotope values range from 2.4 - 4.0 ‰, outside of the range of background δ^{34}S-SO_4 measurements. These more negative δ^{34}S-SO_4 values cannot be explained by BSR alone, which would create a positive rather than a negative isotopic shift (section 1.14.4).

In context of the above, it is understood that a negative shift in δ^{34}S-SO_4 values can reflect the input of isotopically depleted δ^{34}S from the re-oxidation of sulphide (Massmann et al, 2003). This can occur under specific conditions where BSR is no long a unidirectional process (Section 1.14.4; Bruchert and Pratt, 1999). Based upon the sulphide observed within the plume (Section 3.7.2) and the noted action of BSR between 17 mbgl and 21 mbgl (see below), there is the potential that re-oxidation of sulphide may be occurring between 12 mbgl and 16 mbgl where the zone of BSR reduction adjoins a region were nitrate, as an oxidising agent, is present (Section 3.2.2). This may act to enact the observed shift to more negative δ^{34}S-SO_4 values.

δ^{34}S-SO_4 values ranging from 5.8 ‰ – 17.4 ‰, are observed between 17 mgbl and 25 mgbl, where contaminant concentrations remain respectively low. These values are more positive than background and H_2SO_4 waste values and are hence indicative of BSR. This shift is particularly notable between depths of 17 mbgl and 20 mgbl.

Within the region of peak contaminant concentrations (28 mbgl to 35 mbgl, Figure 29, δ^{34}S-SO_4 values shift to 5.1 ‰ - 6.7 ‰. This is close to unaltered H_2SO_4 waste values and is consistent with the suppression of BSR at these

depths due to increased contaminant toxicity (Spence et al, 2001a; Spence et al, 2001b; Baker et al, 2012). This also agrees with the decrease in TDIC levels in the same zone (Figure 34).

Between 36 mbgl and 44 mbgl, the PAT system acts to significantly reduce contaminant levels; this is paired with a positive shift in $\delta^{34}S\text{-}SO_4$ values. The shift is minor between 36 mbgl and 40 mbgl, but significant between 41 mbgl and 44 mbgl, and inversely correlates with TPC levels. $\delta^{34}S\text{-}SO_4$ values range between 4.3 ‰ and 11.5 ‰ for the 36 mbgl to 40 mbgl zone and 11.4 ‰ - 22.8 ‰ for the 40 mbgl to 44 mbgl zone. The values between 40 mbgl and 44 mbgl are significantly different from background and H_2SO_4 waste values and are strong evidence of PAT stimulated BSR in this region.

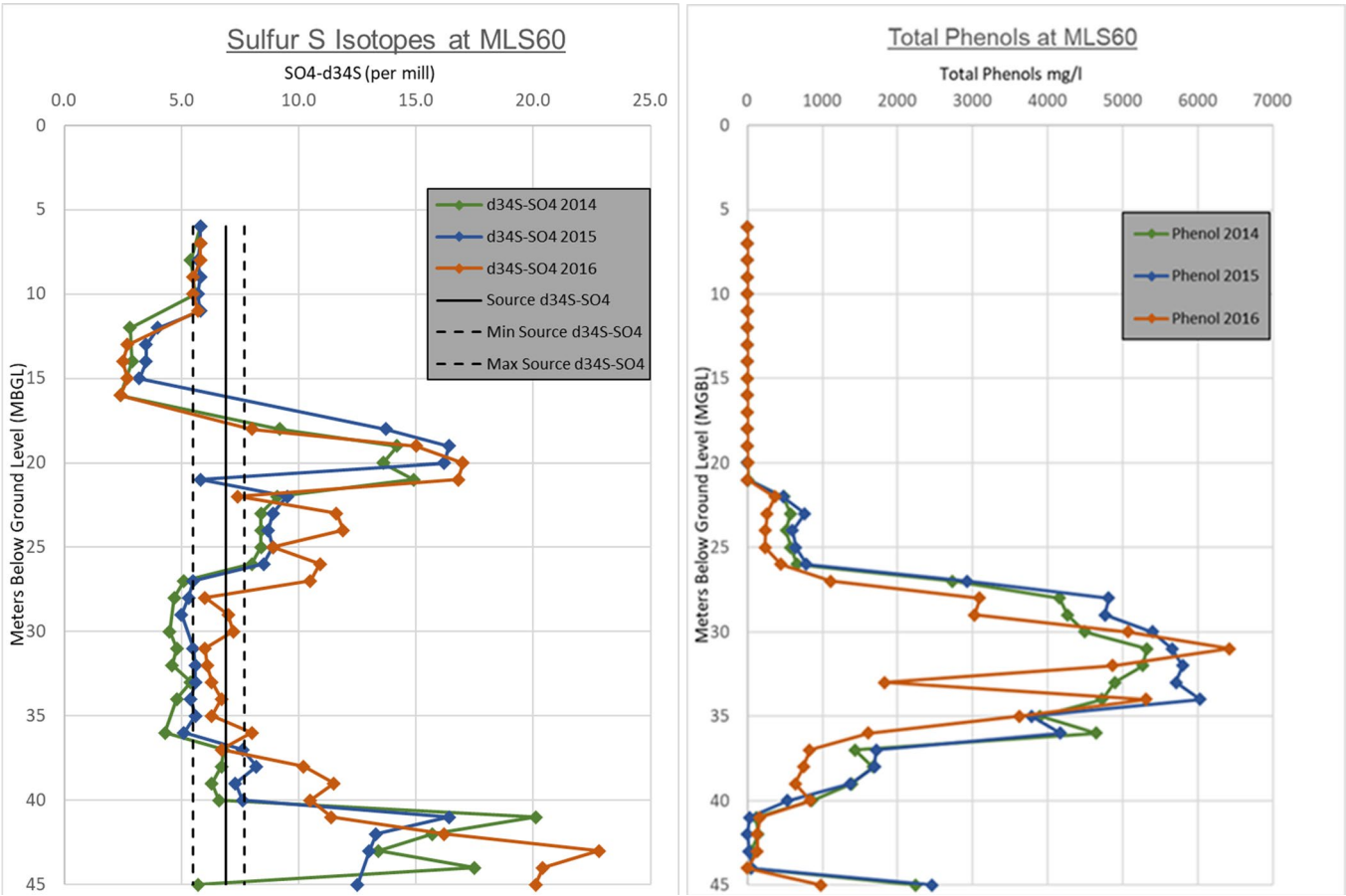

Figure 40. δ^{34}S-SO_4 concentrations at MLS60 in 2014, 2015 and 2016, in comparison to source δ^{34}S-SO_4 (left). TPC in 2014, 2015 and 2016 (right).

3.6. δ^{13}C-CH_4 Values

Section 1.14.2 discusses that the isotopic signature of CH_4 created by is representative of the methanogenic process creating it, with typical δ^{13}C-CH_4 values within the range of -54 ‰ ± 5 ‰ typical of methanogenesis (section 1.14.2; Whiticar, 1999). However, in regions where AMO is present this causes a rapid enrichment in δ^{13}C-CH_4 values.

In light of the above, δ^{13}C-CH_4 values can be compared to the range of typical methanogenesis values, with δ^{13}C-CH_4 values between -49 ‰ and -59 ‰ indicative of methanogenesis and δ^{13}C-CH_4 values more enriched than this (>-49 ‰) indicative of AMO.

3.6.1. δ^{13}C-CH_4 at MLS59

3.6.1.1. For 2014 and 2015

During 2014 and 2015, δ^{13}C-CH_4 values at MLS59 (Figure SEQ Figure * ARABIC 37, not pumped) ranged between -62 ‰ and -40 ‰ with the majority of values within the range of typical methanogenesis (section 1.14.2). This is conducive with the δ^{13}C-TDIC values during this period which indicated the dominance of methanogenesis, over respiration, in the plume (section 3.3.1.1).

Between 5 mbgl and 11 mbgl, clean background water was present (section 3.1.1), and no methane was recorded. In addition, between 11 mbgl and 15 mbgl, very low methane concentrations were recorded, consistent with the presence of a nitrate reduction zone at this depth (section 3.2.1).

Below 16 mbgl, δ^{13}C-CH_4 values are typically in the range of (or more depleted than) that expected due to methanogenesis, coupled with methane concentrations of between 5 mg/l and 20 mg/l. However, a few enriched δ^{13}C-CH_4 values are indicating a limited amount of AMO present at 24 mbgl to 25 mbgl. This evidence of AMO is also coupled with sporadic decreases of methane concentrations at associated depths.

Towards the edges of this zone of methanogenesis, an enrichment in $\delta^{13}C$-CH_4 values be seen indicating AMO, possible couples with nitrate reduction (section 3.2.1) where the zone of maximum methanogenesis interacts with the plume fringe (16 mbgl and 30 mbgl).

Notwithstanding the above, it should be appreciated that the 2014 methane concentrations are significantly lower between 10 mbgl and 22 mbgl. As this region is also associated with BSR (section 3.5.1), this may be indicative of a moving balance between these processes.

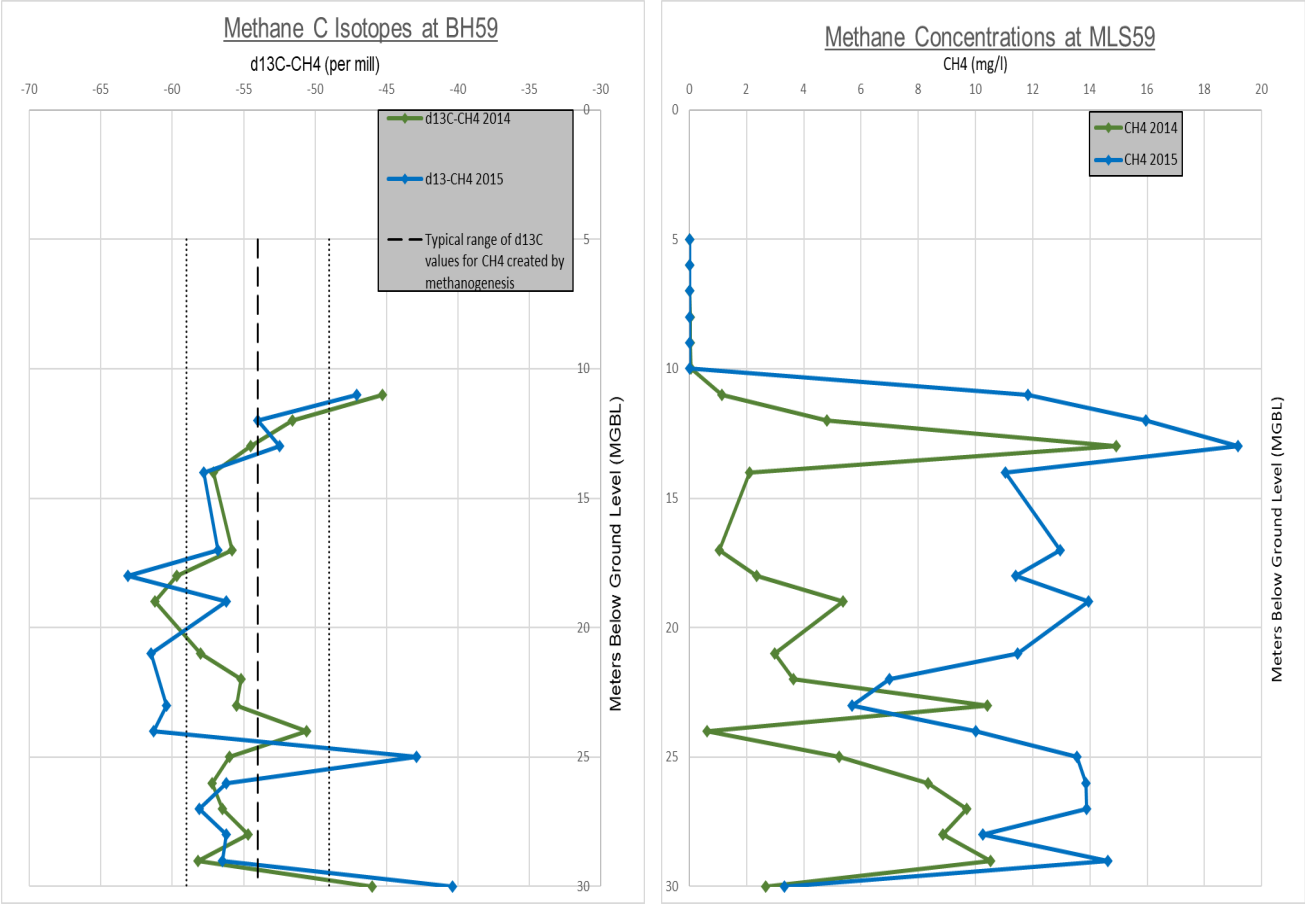

Figure SEQ Figure * ARABIC 37.δ13C-CH4 values at MLS59 in 2014 and 2015, in comparison to the typical range of δ13C-CH4 values (left). Methane concentrations at MLS59 in in 2014 and 2015 (right).

3.6.1.2. For 2014 and 2015

In 2016, $\delta^{13}C$ -CH_4 values at MLS59 (Figure 40, not pumped) were very depleted (-47 ‰ to -68 ‰) between depths of 12 mbgl and 22 mbgl indicating a methanogenic dominance in these regions consistent with 2014 and 2015 sampling rounds (section 3.6.1.1). Results at these depths are also conducive with the $\delta^{13}C$-TDIC values during this period which indicated the dominance of methanogenesis, over respiration, within this region (section 3.4.1.2).

Similarly to 2014 and 2015 and no methane was recorded in between either 5 mbgl and 11 mbgl, indicative of clean background water (Section 3.1.1) or, 11 mbgl and 15 mbgl consistent with the presence of a nitrate reduction zone (Section 3.2.1.1). In addition, the edges of this zone of methanogenesis once again exhibit an enrichment in $\delta^{13}C$-CH_4 values typical of AMO where the zone of maximum methanogenesis interacts with the plume fringe (16 mbgl, and 24 mbgl to 25 mbgl).

However, an important change to previous data is noted as no methane was recorded between depths of 26 mbgl and 30 mbgl, a region in which previous evidence may point to clean background water being present due to a potential thinning of the plume (Section 3.3.1.2). Should thinning of the plume have occurred in this region then this result would have been expected.

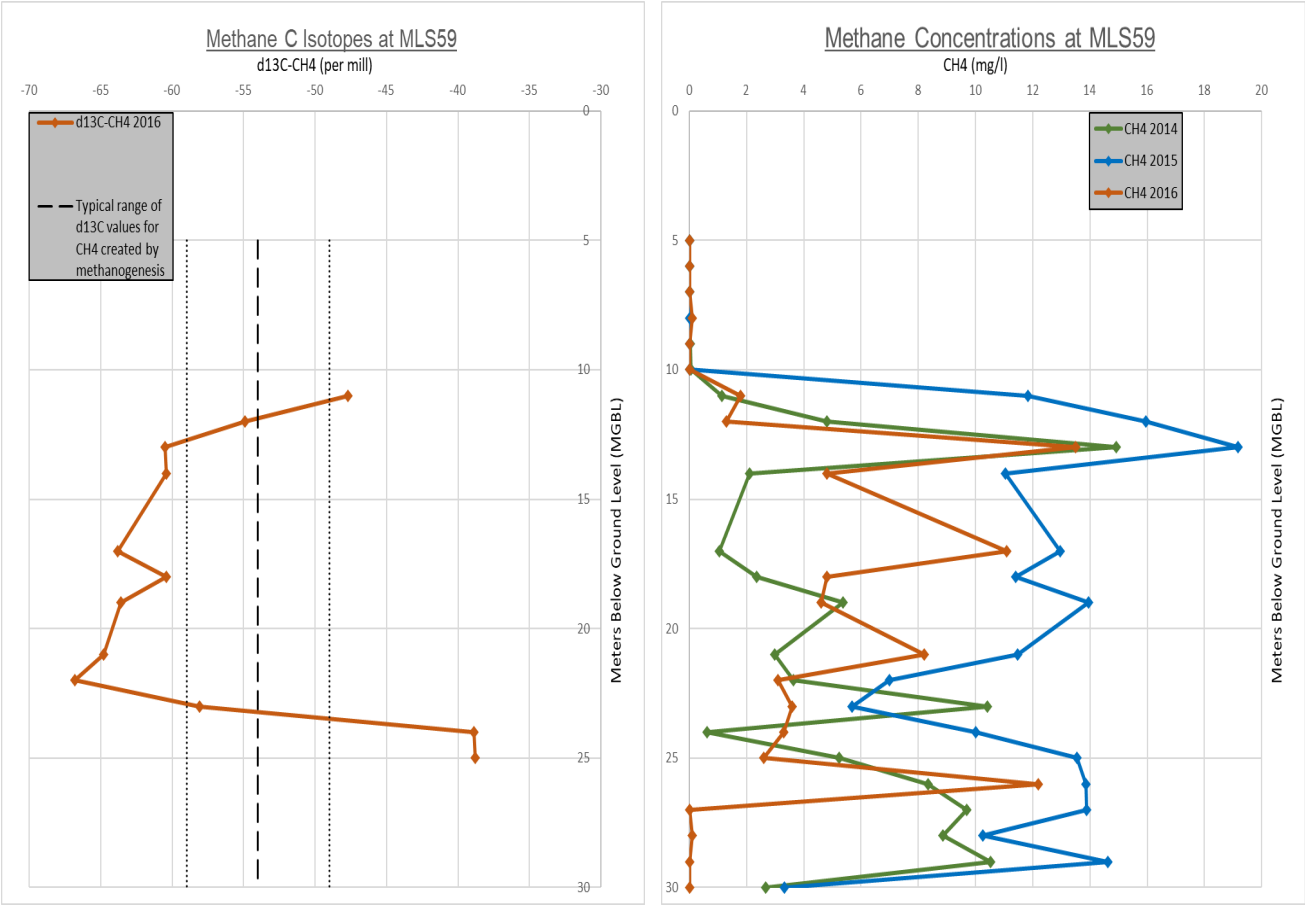

Figure 41. δ13C-CH4 values at MLS59 in 2016, in comparison to the typical range of δ13C-CH4 values (left). Methane concentrations at MLS59 in in 2014, 2015 and 2016 (right).

3.6.2. δ^{13}C-CH_4 at MLS60

δ^{13}C-CH_4 values at MLS60 (Figure 41, pumped) exhibit significantly different trends to those at MLS59 during 2014, 2015 and 2016 with δ^{13}C-CH_4 values at MLS60 ranging between -38 ‰ and -99 ‰. Methane concentrations during this time ranged between 0 mg/l and 8 mg/l.

Between 6 mbgl and 11 mbgl, clean background water was present (section 3.2.2), and no methane was recorded. In addition, between 11 mbgl and 19 mbgl, very low methane concentrations were recorded, consistent with the presence of a nitrate reduction zone at these depths (section 3.2.2).

Between 21 mbgl and 27 mbgl, δ^{13}C-CH_4 values are typically in the range of that expected due to methanogenesis, coupled with methane concentrations of around 0.1 mg/l and 2.5 mg/l, indicative of small amounts of methanogenesis within this region. This is consistent with δ^{13}C-TDIC values which are considered indicative of some methanogenesis occurring at these depths (section 3.4.2) concurrently with BSR (section 3.5.2).

Between 28 mbgl and 32 mbgl, for 2015 and 2016, an area of respectively enriched δ^{13}C-CH_4 is present indicating AMO at these depths. Methane concentrations at this depth are respectively high, between 2 mg/l and 8 mg/l indicating that methanogenesis is also occurring. As AMO exhibits a much stronger effect on δ^{13}C-CH_4 values than methanogenesis (section1.14.2), it is considered that this isotopic signature is indicative of concurring methanogenesis and AMO. It is worthy of note that this AMO zone is lower in 2016, between 35 mbgl and 38 mbgl.

Below the above zones, δ^{13}C-CH_4 values are extremely depleted (-61 ‰ to -99 ‰). Whilst, it is considered that these values are indicative of methanogenesis the large enrichment factors required to generate such values seem unfeasible. Hence it is considered that these values have been artificially altered by the PAT system which acts directly at these depths. Nonetheless, as detectable methane concentrations are present at these depths it is considered that some methanogenesis does take place in this region.

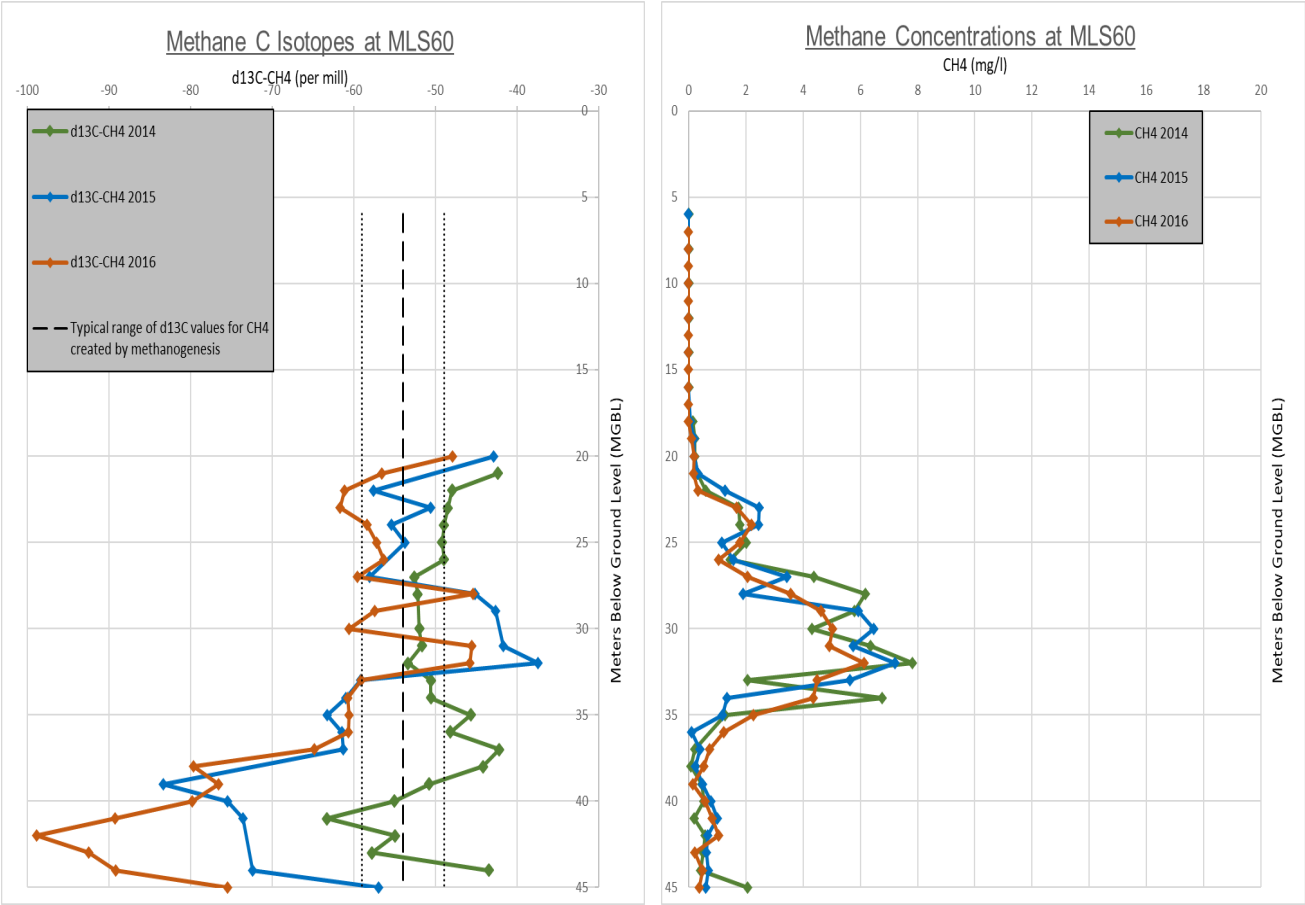

Figure 42. δ13C-CH4 values at MLS59 in 2016, in comparison to the typical range of δ13C-CH4 values (left). Methane concentrations at MLS59 in in 2014, 2015 and 2016 (right).

3.7. Sulphide Data

It should be appreciated that sulphide is considered short lived within the plume (Spence et al, 2001b), as sulphide is strongly reactive with other element within the plume such as the iron within the aquifer matrix.

Notwithstanding the above, the presence of free trace sulphide within the plume gives a strong indication of BSR activity, instantaneously at the time of sampling.

Sulphide data was highly erratic (likely due to its instantaneous nature) and unwieldy for graphical viewing hence the data is summerised in broad terms below.

3.7.1. Sulphide Data for MLS59

At MLS59, between depths of 5 mbgl and 12 mbgl no sulphide was recorded giving no indication of BSR correlating with δ^{34}S-SO_4 values (section 3.5.1) and TPC concentration (section 3.1.1) which indicate no BSR within this region.

Below this depth sulphide was overtly present between 12 mbgl and 25 mbgl, indicating strong BSR in these regions. Again, this strongly correlates with δ^{34}S-SO_4 values which indicate BSR at the same depths.

However, despite δ^{34}S-SO_4 values indicating BSR to be supressed between 25 mbgl and 30 mbgl, sulphide was detected in these regions. However, the quantities of this sulphide were significantly lower than that between 12 mbgl and 25 mbgl indicating that BSR may be functioning in a limited capacity at these depths.

Depth	Minimum Concentration (µg/l)	Average Concentration (µg/l)	Maximum Concentration (µg/l)
5 to 12 mbgl	0	0	0
12 to 18 mbgl	15	85	222
19 to 25 mbgl	16	43	146
25 to 30 mbgl	4	11	43

Table 5. Sulphide concentrations at MLS59, average for 2014, 2015 and 2016.

3.7.2. Sulphide Data for MLS60

At MLS60, between depths of 6 mbgl and 20 mbgl no sulphide was recorded giving no indication of BSR. This correlates with $\delta^{34}S\text{-}SO_4$ values (section 3.5.2) and TPC concentrations (section 3.1.2) which indicate no BSR within this region.

Between 12 mbgl and 32 mbgl, sulphide is present indicating BSR in these regions. This generally correlates with $\delta^{34}S\text{-}SO_4$ values which indicate BSR at the 19 mbgl to 27 mbgl, however it suggests that this zone may be slightly larger during some periods extending to 32 mbgl.

Despite $\delta^{34}S\text{-}SO_4$ values indicating BSR to be supressed between 32 mbgl and 37 mbgl at MLS60, sulphide was detected in these regions, However, quantities of this sulphide were significantly lower than within other regions of MLS60, indicating that BSR may be functioning in a limited capacity at these depths. This region is somewhat analogous to the lower depths of MLS59 (section 3.7.1).

Between 37 mbgl and 44 mbgl, sulphide is present indicating BSR in these regions. This correlates with $\delta^{34}S\text{-}SO_4$ values which indicate BSR at these depths.

Depth	Minimum Concentration (µg/l)	Average Concentration (µg/l)	Maximum Concentration (µg/l)
6 to 20 mbgl	0	0	0
21 to 32 mbgl	67	123	258
32 to 37 mbgl	0	24	84
37 to 44 mbgl	79	191	323

Table 6. Sulphide concentrations at MLS60, average for 2014, 2015 and 2016.

Due to the concentrations of sulphide present at MLS60 within the plume, it was possible to analyse the $\delta^{34}S$ composition of the sulphide ($\delta^{34}S$-H_2S) from a limited amount of depth locations.

By direct comparison of the $\delta^{34}S$-H_2S and $\delta^{34}S$-SO_4, it is possible to gain a reliable reading of an instantaneous enrichment (ε) for isotopes moving between the two sulphur pools. This is considered a reliable method of finding the enrichment factor (ε) for BSR as the sulphide is an instantaneous product of BSR (Spence, 2001).

Enrichment factors (ε) based this calculation ranged from -7‰ to -15‰, however it should be appreciated that these datapoints are based upon samples from depth between 37mbgl and 44 mgbl which were the only depths at which adequate amounts of sulphide were obtainable.

CHAPTER 4

4. fMicrocosm Studies of Phenol Oxidation by BSR

Previous studies, as well as the new data presented within this thesis, have demonstrated that large quantities of sulphate, typically between 30 mg/L and 80 mg/L, are present within the plume (Appendix 2). These concentrations are enough to stoichiometrically degrade large proportions of the total contaminant mass, within either a pre-pumping or active pumping scenario (sections 1.13 and 1.16).

Isotope data from the study site, both from previous studies (e.g. Spence et al, 2001b, Thornton et al, 2014) and new data presented within this thesis (section 3.5), has demonstrated that BSR is active at the site and plays a substantial role with regards to phenol oxidation. This process is particularly dominant within the plume core where levels of oxygen and nitrate are low (Spence et al, 2001b; Baker et al, 2012).

Whilst this isotope data demonstrates the substantial role of BSR at the site, determining the exact quantity of contaminant turnover by BSR has historically been hindered by large uncertainties with regards to estimating the magnitude of the enrichment factor (ε) associated with BSR within the plume (section 1.11.5).

In fact, a single estimation of BSR enrichment factor (ε, section 1.11.5) for the entire plume (such as that estimated by Spence, 2001) is unlikely to be credible, as previous studies have demonstrated that different in-situ conditions can significantly affect enrichment factors. Highly-stressed microbial communities, such as those stressed by increasing TPC toxicity, are likely to exbibit dissimilar enrichment factors to a less stressed community (Karlson et al, 2018). In addition, changes to the type of microbial consortia undertaking the BSR may also lead to dissimilar enrichment factors (Slater et al, 2001).

In order to accurately determine ε for a variety of conditions within the plume, this chapter presents data from microcosm studies which utilise microbial consortia gathered from within the plume, which are then subjected to a number of different chemical conditions. These studies serve to demonstrate that enrichment factors (ε) within the plume are likely to vary between -7‰ at high TPC concentrations, to -10‰ at low TPC concentrations.

By pairing data from these microcosms with enrichment factors (ε) from field data gathered by Spence et al. (2001) and during this study, a conceptual model relating enrichment factor to TPC concentration has been created (section 4.6). This model can then be paired with field data (section 3) to determine the quantity of contaminant turnover by BSR within the plume to a greater degree of accuracy than that of previous studies.

4.1. Experimental Background

In order to better quantify ε within the plume, the microcosm experiments were kept as similar to in-situ conditions as possible. To ensure that microbial consortia within the microcosms were in line with in-situ microbes, it was necessary to obtain microbes from the contaminant plume under anaerobic conditions. Further details on how the surrogate microbes used for this purpose were obtained from the aquifer can be found within the field methodologies section (section 2.1.6) and the microcosm methodology section (section 4.2).

As discussed above, increasing TPC toxicity is likely to substantially affect enrichment factors. Hence, in order to simulate a range of TPCs within the plume, six sets of bottle microcosms were set up (A-F). All of these microcosms were run in triplicate to allow data to be substantiated and to allow redundancy for any unforeseen circumstances.

Microcosm sets A-C were run without acetate, with a view to looking at the enrichment effects from the biodegradation of TPC:

- Set A: Low TPC, no acetate – predicted to simulate very high BSR;
- Set B: Moderate TPC, no acetate – predicted to simulate high BSR; and,
- Set C: Moderate-High TPC, no acetate – predicted to simulate moderate BSR.

Sets D-F were additionally spiked with acetate, as previous studies have demonstrated that acetate is produced and consumed readily in the plume, with the acetate having a potential role in BSR (Thornton et al, 2014):

- Set D: Low TPC, with acetate – predicted to simulate very high BSR;
- Set E: Moderate TPC, with acetate – predicted to simulate high BSR; and,
- Set F: Moderate-High TPC, with acetate – predicted to simulate moderate BSR.

Two sterile controls containing 2 g/L sodium azide, which acts to stop microbial activity, plus one sacrificial microcosm containing Iron (II) Sulphate, which acts as a visual indicator of BSR activity, were also set up as follows:

- X1 and X2: Low TPC, with acetate plus sodium azide – control 1; and,
- Y1: Low TPC, with acetate plus Iron(II) Sulphate – control 2.

It should be noted that it was not possible to conduct any microcosms at high TPC, as predicted turnover rates of sulphate within such microcosms would have been too slow to allow for significant data to be collected over an appropriate timescale. Notwithstanding this, BSR at high TPC concentrations is expected to be limited based upon field data negating the need for an accurate determination of ε under these conditions.

4.2. Experimental Methodology

4.2.1. Microcosm Setup

In order to ensure that start up conditions were as similar as possible to those in the aquifer, both groundwater and sand were gathered from MLS59 at 30 mbgl. Obtaining groundwater and sand from this depth ensured that microbial consortia within these media were representative and that sulphate reducing bacteria from the plume would be present. The sand was previously lowered to this depth and inoculated for 8 months prior to removal. Both the groundwater and sand were collected and transported back to the laboratory anaerobically. For more details please see the fieldwork methodologies (section 2.1.6).

Once the samples of groundwater and inoculated sand had been returned to the laboratory, they were moved into anaerobic chambers. Subsequently, groundwater samples were mixed for homogenisation and 50 ml was set aside for initial analyses.

The inoculated sand was then evenly distributed between 250 ml bottles, putting around 50 g of wet sand (~40 ml) in each bottle. These bottles had been previously washed using hydrochloric acid and then sterilised three times using an autoclave. The inoculated sand was then topped up with non-inoculated sand, previously sterilised three times using the autoclave, to ensure that around 50 ml of sand was present in each bottle.

Concentration analysis on the original groundwater indicated an initial TPC concentration of around 0.2 g/L. The original water was then separated into three different inoculum mixtures, with a mixture of phenols added where required, ensuring that this mix was as close as reasonably practicable to in situ conditions:

1) Low TPC – Original groundwater (0.2 g/L TPC);
2) Medium-Low TPC – Original groundwater + 0.4 g/L phenolic mix (Total 0.6 g/L TPC); and,
3) Medium TPC – Original groundwater + 1.6 g/L phenolic mix (Total 1.8 g/L TPC).

The bottles previously filled with 50 ml sand were then filled with the required phenol inoculum to the 200 ml mark and sealed with septum seal which would allow later sampling with syringe. These bottles were left to acclimatise for 10 days before they were spiked with the required additional substances. These additional substances were sodium sulphate (for sets A-X), sodium acetate (for D-Y), sodium azide (X only). These compounds were added to the bottles in the correct proportions to make sulphate and acetate concentrations up the desired levels (see Table 7).

For ease of reference, final microcosm conditions are detailed below;

<table>
<tr><th colspan="3">Bottle Numbers</th><th>TPC Concentrations (g/L)</th><th>Sodium Sulphate</th><th>Sodium Acetate</th><th>Sodium Azide</th><th>Iron (II) Sulphate</th></tr>
<tr><td>A1</td><td>A2</td><td>A3</td><td>0.2 (Initial)</td><td rowspan="7">Yes (to 2.8 g/L SO_4)</td><td rowspan="3">No</td><td rowspan="6">No</td><td rowspan="7">No</td></tr>
<tr><td>B1</td><td>B2</td><td>B3</td><td>0.6</td></tr>
<tr><td>C1</td><td>C2</td><td>C3</td><td>1.8</td></tr>
<tr><td>D1</td><td>D2</td><td>D3</td><td>0.2 (Initial)</td><td rowspan="6">Yes</td></tr>
<tr><td>E1</td><td>E2</td><td>E3</td><td>0.6</td></tr>
<tr><td>F1</td><td>F2</td><td>F3</td><td>1.8</td></tr>
<tr><td colspan="2">X1</td><td>X2</td><td>0.2 (Initial)</td><td>Yes</td></tr>
<tr><td colspan="3">Y1</td><td>0.2 (Initial)</td><td>No</td><td>No</td><td>Yes (to 2.8 g/L SO_4)</td></tr>
</table>

Table 7. Microcosm conditions after spiking.

4.2.2. Sampling Regime

In order to ensure that the derivation of enrichment factors (ε) be statistically viable, approximately 20 samples were taken from each microcosm throughout the sampling period.

In an ideal scenario, samples would be taken with a high sampling frequency during periods of rapid activity and lower frequency during periods of slow activity, as this would allow for the most accurate derivation

of ε. Hence, as activity within the microcosms was expected to decrease over time due to depletion of TPC, sampling was initially taken at a high frequency, with sampling frequency reduced over time. This was made possible by using results from TPC analysis to better inform sampling rates.

Notwithstanding the above an exception was made for Set B1, where after approximately 40 days, a rapid decrease in phenols and unexpected variations in other chemical parameters led to the conclusion that the septum on this sample was ruptured. Nonetheless, sets B2 and B3 were still viable. B1 is not considered further in this section, however, results for this microcosm can be found within Appendix 2.

4.2.3. Analysis Parameters

Several parameters were chosen for analysis during the microcosm studies, including contaminants, electron acceptors and acetate.

Where comparing the similarity, or dissimilarity, between parameters t-tests were undertaken to determine if the averages and variances indicated a significant difference.

4.2.3.1. Contaminants (TPC and p-cresol)

Total phenolic compounds (TPC) and p-cresol were analysed using a high-pressure liquid chromatography (Perkin-Elmer Series 200 system with UV detector), utilising the technique derived by Spence (2001). Appropriate calibration standards were used with a detection limit of 1mg/L^{-1}. Instrument precision was initially estimated to be ±5 %, with overall technique precision based upon control microcosm data estimated at ±6 % (section 4.5.1).

Whilst both TPC and p-cresol provide an indication of contaminant concentrations within microcosms, it should be appreciated that each parameter has different advantages and disadvantages. TPC values provide a more complete picture of total contaminant than p-cresol values. However, the total TPC pool is large and somewhat slow to biodegrade which can, at times, present issues regarding data analysis and trend definition.

P-cresol is a significant constituent within the TPC pool (section 1.12.3; 10 % – 15 % of TPC), is known to be one of the least recalcitrant compounds within phenolic mixtures (Bossert and Young, 1986). Studies by Spence et al. (2001b) at the study site indicate that p-cresol is one of the first contaminants to biodegrade within the plume system and can contribute a large proportion (>40 %) of the total biodegraded mass in many instances. Thus, it was considered that p-cresol could provide better trend definition than TPC within microcosm studies (as per Spence et al, 2001b).

Notwithstanding the above, it is recognised that whilst p-cresol can be indicative of TPC biodegradation, it is not directly comparable to the entire TPC pool. Hence, with regards to the final derivation of ε, TPC data is used preferentially over p-cresol data. Notwithstanding this, comparatively scaled ε values (not presented) for the TPC and p-cresol datasets were generally within error.

4.2.3.2. Ions (Sulphate, Nitrate and Acetate)

Major ions, including NO_3 and SO_4 electron acceptors, and acetate were analysed by ion chromatography (Dionex 2000). Appropriate calibration standards were used with a detection limit of 1 mg/L^{-1}. Instrument precision was ±3 %. Again, this technique was in similar accord to that in described by Thornton et al, (2001a) and Spence et al, (2001b).

It should be appreciated that analyses of O_2 within the system were subject to interference with the contaminant matrix and hence, ceased after the third sampling round; these results are not presented. This was not unexpected and has been observed during previous studies (e.g. Thornton et al, 2014, section 3.2). Notwithstanding this, any ingress of O_2 within the microcosms would likely be coupled with increased NO_3, data for which is presented below (section 4.5.4).

4.2.3.3. Sulphate (δ^{34}S-SO_4) Isotopes

Sulphate isotopes were analysed by precipitation and recovery of $BaSO_4$, followed by analysis of δ^{34}S-SO_4 using an Isoprime mass spectrometer,

using the same procedure as those used for the field measurements (section 2.2.4).

4.3. Limitations

Whilst microcosm conditions were kept as similar as possible to those in-situ, some limitations with this data analysis are acknowledged.

Firstly, it was necessary for sulphate concentrations to deviate from in-situ conditions for the purposes of the experiment. Sulphate within the microcosms was required to be around 2.8 g/L, much higher than values in-situ (section 3.5). There were two main requirements which necessitated this increase in concentration:

1) In order to provide enough sulphate to biodegrade the entire pool of TPC, if required; and,
2) In order that the sufficient amounts for analysis could be obtained without removing excess water from the microcosms (water levels in the microcosms were required to be >50 % of the maximum at all times).

Secondly, it should be appreciated that whilst conditions within the microcosm bottles were kept as similar as possible to in-situ conditions at all times, it is impossible to avoid the intrinsic effects due to differences between moving groundwater in a flowing aquifer and a sedentary bottle setting, this is termed the “bottle effect”.

In addition to the limitations mentioned above, due to practical limitations, samples could not be taken from the microcosm daily, nor analysed instantly. However, samples were preserved during the time between sampling and analysis (e.g. within a 0.2 % v/v sodium azide or 4 % v/v Formaldehyde solution). However, the impact of this is anticipated to be limited with respect to the calculation of the enrichment factor ε, which is time integrated over long periods using linear regression and is thus not heavily reliant on sampling frequency.

Notwithstanding the above limitations, a comparison between ε values from the microcosm results, 2014 - 2016 sulphide data and analyses conducted

by Spence et al, (2001b), indicates that data from the microcosms is largely consistent with that of in-situ conditions.

4.4. Modelling with the Rayleigh Equation

Within a closed system, such as the microcosms described above, fractionation of sulphate isotopes due to BSR has been shown to obey Rayleigh fractionation (Equation 1, section 1.11.5), with a characteristic enrichment factor ε (Equation 12; Rees, 1973). However, this is subject to negligible sulphide re-oxidation within that system.

Equation 12

$$\delta^{34}SO_4(t) = \delta^{34}SO_4(o) + \varepsilon\, Ln\big(SO_4(t)/SO_4(o)\big)$$

Where:

$\delta^{34}SO_4(t)$ = $\delta^{34}SO_4$ at time t;

$\delta^{34}SO_4(o)$ = original $\delta^{34}SO_4$;

ε = Enrichment Factor;

$SO_4(t)$ = Concentration of SO_4 at time t; and,

$SO_4(o)$ = Original concentration of SO_4.

By rearranging this equation, it is possible to produce an equation that can be used for the derivation of ε (Equation 13), given the correct data.

Equation 13

$$\varepsilon = \frac{\delta^{34}SO_4(t) - \delta^{34}SO_4(o)}{Ln\big(SO_4(t)/SO_4(o)\big)}$$

Frequent analysis of SO_4 concentrations and $\delta^{34}SO_4$ values throughout the duration of the experiment was undertaken during the microcosm studies (section 4.2.3). Hence, data gathered from the microcosms can provide values for $\delta^{34}SO_4(t)$, $\delta^{34}SO_4(o)$, $SO_4(t)$ and $SO_4(o)$, allowing an enrichment factor (ε) for sulphate to be calculated (Equation 13).

The Rayleigh equation can also be presented in graphical form by plotting $\delta^{34}SO_4$ against $Ln(SO_4)$. This graph will have a gradient of ε (Figure 53; section 4.6).

4.5. Microcosm Results

4.5.1. Sterile Microcosms (Set X)

In the sterile controlled microcosms (Set X), no significant p-cresol or TPC loss was observed (Figure 42), indicating that the sodium azide was sufficient to halt any microbial activity. However, it is worth noting that TPC and p-cresol amounts between the start and the end of the microcosms did vary, albeit only marginally. This variance is likely due to uncertainties and errors within the sampling and analysis techniques.

For the sterile microcosms, >90 % of samples varied between 94 % and 106 % of the starting values throughout the 120 days. This uncertainly is larger than the associated uncertainties in analysis (Section 2.2.1). Hence, for the purposes of discussion, data precision is considered to be ±6 %, in the lack of further relevant information. Thus, any TPC and p-cresol values falling within 6 % of each other cannot be considered statistically different.

It should be noted that a small number of outlying data points were present, both within the sterile microcosm and others presented within this section. It is considered that these samples may have been affected by either (a) interference between the contaminant matrix and the sampling equipment or (b) sample degradation between the point of sampling and the time of analysis (this could be due to a number of factors, including unforeseen chemical reactions).

Notwithstanding the above, it is considered that there is no feasible pathway for the generation of phenol contaminants within the microcosms. Thus, it is not considered feasible for values of TPC and/or p-cresol to increase significantly above initial concentrations (>200 % of original concentration) or to increase significantly between two subsequent sampling points (>1 g/L increase). Therefore, results fitting these criteria have been considered erroneous and have been excluded from graphical and statistical calculations.

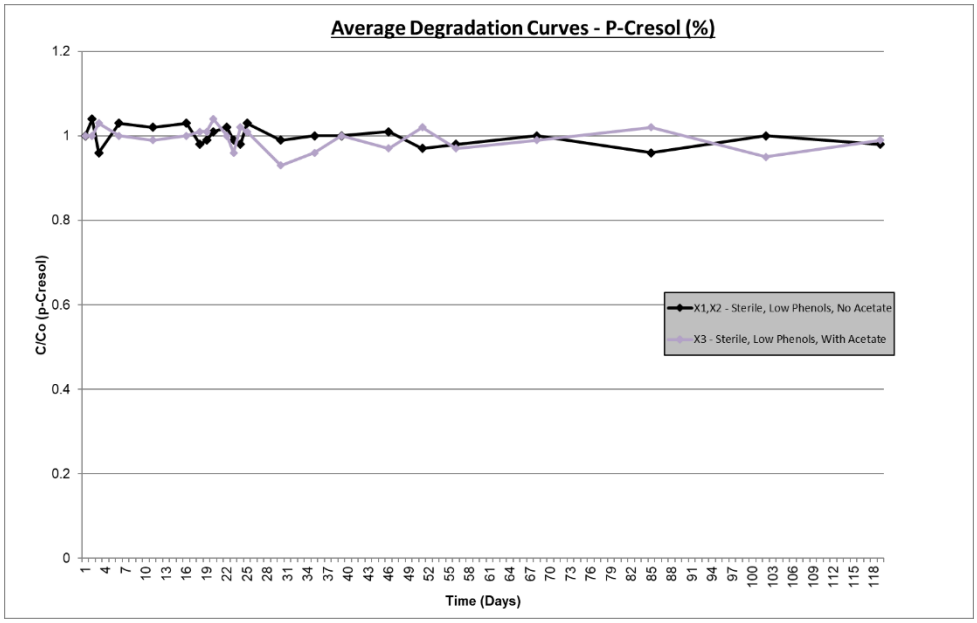

Figure 43. P-cresol concentrations for the sterile microcosms; showing Percentage (%) of P-cresol remaining against time.

4.5.2. Active Microcosms (Sets A to F)

4.5.2.1. TPC and P-Cresol Concentrations

All active microcosms displayed very low shifts in p-cresol and TPC concentrations between initial set up and the time of spiking with sodium sulphate (10 days). During this period, nearly all samples indicated a negligible change (< 6 %) in contamination values, with the remaining samples being within ± 8 % of the initial TPC concentrations.

Post-spiking, biodegradation rates remained negligible for a period of 7 - 12 days, bringing total lag phase up to 17 - 22 days (Table 8). Subsequently, all active microcosms observed rapid decrease in p-cresol values, coupled with an associated decline in TPC (Table 8). Whilst TPC continued to decline throughout the sampling period, p-cresol amounts reached a stable minimum in all microcosms after 10 to 12 weeks.

The total loss of p-cresols during the sampling period was 82 % - 94 % for microcosms not spiked with acetate (Sets A-C). However, this was an order of magnitude lower, 8 % - 14 %, for the microcosms which were spiked with acetate (Sets D-F). TPC losses followed a similar trend, ranging from 19 % - 28 % in sets A-C but between 1 % - 6 % in sets D-F.

Biodegradation of p-cresol, as one of the least recalcitrant constituents within the TPC pool (Spence, 2001), accounts for between 70 % and 85 % of the total TPC biodegradation. Consequently, the remaining 15 % to 30 % of biodegradation during the monitored period is due to biodegradation of other, potentially more recalcitrant, components within the TPC pool.

Triplicate sets displayed broadly similar results, with losses of p-cresol and TPC varying by less than 10 % between triplicate samples.

			Chemical Environment		**Time Parameters**		**Chemical Parameters**	
Microcosm Numbers			**Phenols (g/L)**	**Acetate**	**Total Lag Phase (Days[1])**	**Minimum Stable p-cresol (Days[1])**	**P-cresol loss (%)**	**Total Phenols loss (%)**
A1	**A2**	**A3**	0.2	No	17-19	At 67-84	86-94	20-28
	B2	**B3**	0.6		17	At 67-84	88-92	20-28
C1	**C2**	**C3**	1.8		18-21	At 84-96	82-88	19-26
D1	**D2**	**D3**	0.2	Yes	18	At 67-84	9-14	2-5
E1	**E2**	**E3**	0.6		18	At 67-84	8-12	1-6
F1	**F2**	**F3**	1.8		18-22	At 84	8-12	2-6

Table 8. P-Cresol and Phenol loss statistics for active microcosms (Sets A to F).

[1] Dates are approximate to closest sampling point

Degradation curves for p-cresol and TPC are presented in Figure 43 and Figure 44.

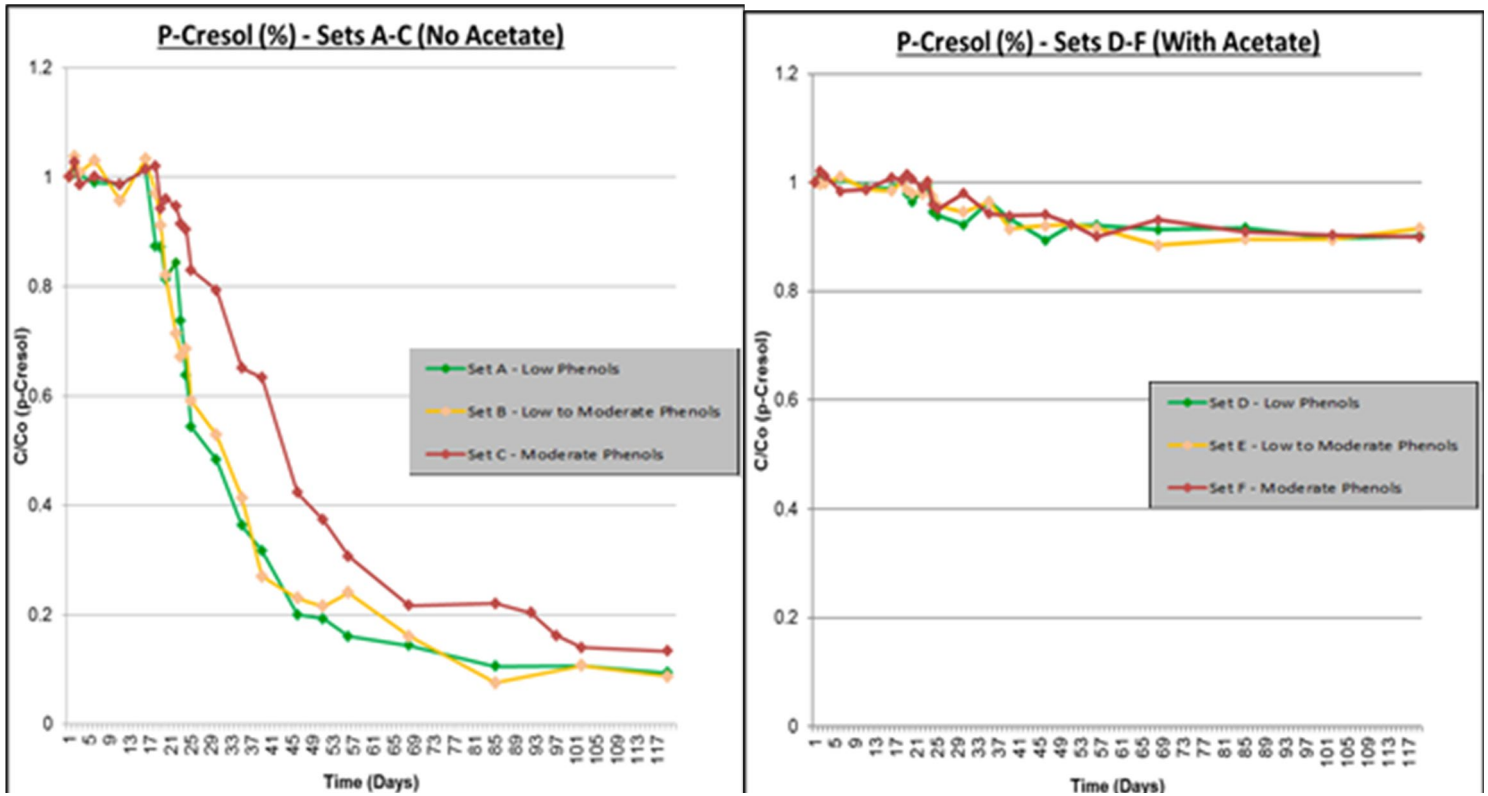

Figure 44. P-cresol concentrations for the active microcosms; showing percentage (%) of p-cresol remaining against time.

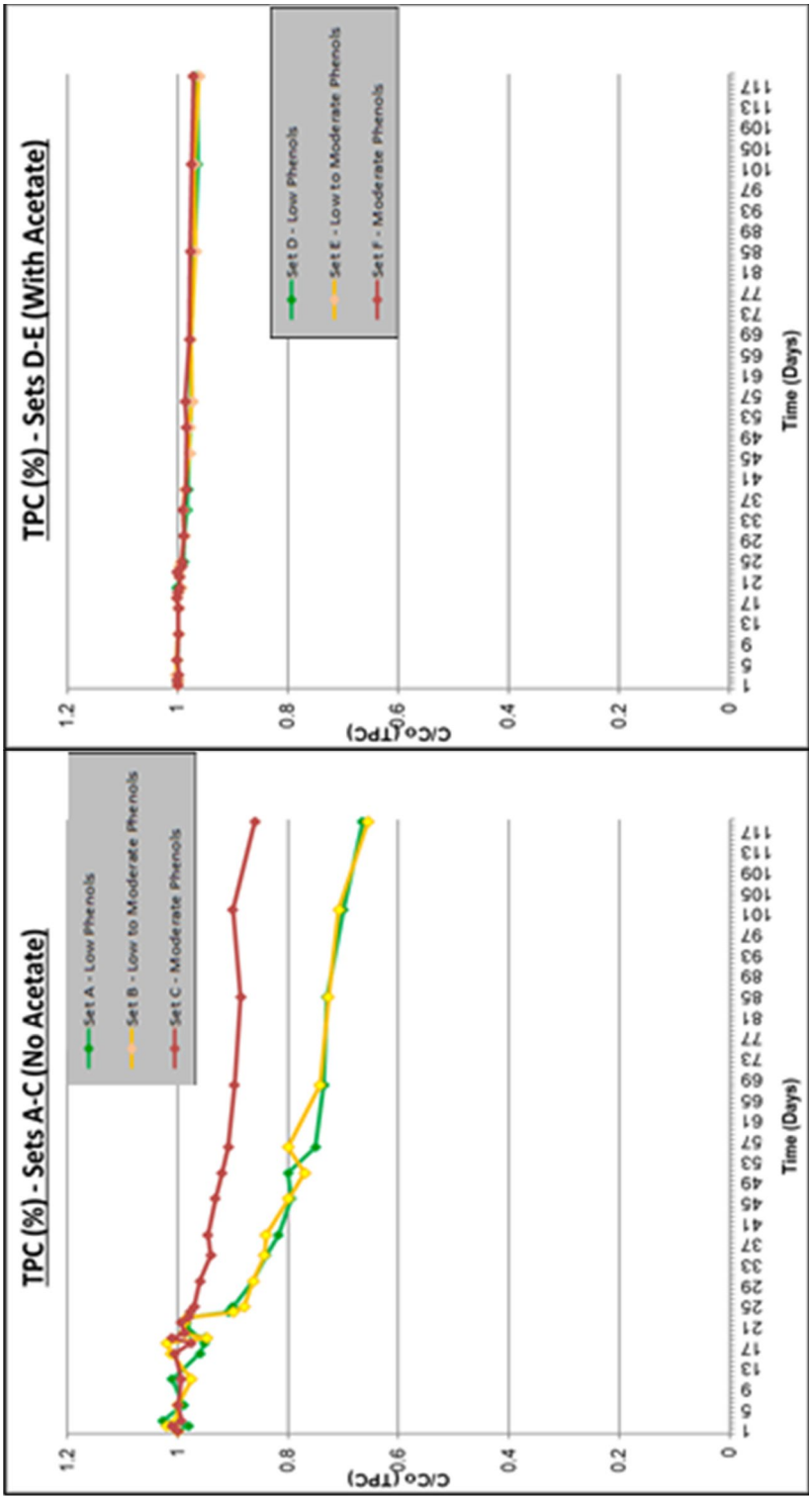

Figure 45. TPC concentrations for the active microcosms; showing percentage (%) of TPC remaining against time.

Within sets A-C, three different phases can be identified during the run-time:

1) P-cresol concentrations and TPC concentrations are initially stable (lag phase);
2) P-cresol concentrations exhibit a rapid decrease, whilst TPC concentrations decrease steadily; and,
3) P-cresol concentrations stabilise, whilst TPC concentrations continue to decrease steadily.

Decreases in TPC and p-cresol appear to be more substantial within sets A and B (low and low-medium TPC respective) than within set C (medium TPC) throughout the sampling period. This difference is in line with lower TPC biodegradation, likely associated with a (marginally) higher degree of toxic inhibition within set C, which had the highest TPC values (1.8 g/L).

With regards to sets D-F, a similar initial lag phase can be identified. Concentrations in p-cresol and TPC concentrations after this lag phase show a steady decline, however the rate of decrease is significantly lower than observed for sets A-C.

4.5.2.2. Acetate Concentrations

As indicated above (section 4.2), acetate was added to microcosm sets D-F, as previous in-situ data suggests that acetate may be generated within the plume (potentially by fermentation) and then rapidly consumed by reduction processes, such as BSR (e.g. Spence, 2001). Thus, it is considered that acetate may interact strongly with BSR at the site (Thornton et al, 2014).

The addition of acetate to microcosms D-F, whilst maintaining concurrent sets A-C without acetate, allowed for a comparison to be made. Thus, it was possible to assess if:

1) Acetate was preferentially consumed by microbial activity over TPC; and,
2) Enrichment factors (ε) varied due to the presence of acetate.

The results of sets D-F indicated that acetate concentrations decreased rapidly after the initial lag phase (18-28 days, Figure 45). In comparison to TPC, acetate was consumed more rapidly by an order of magnitude, whilst it was consumed more rapidly than p-cresol by a factor of ~5. It is, therefore, considered that acetate is utilised preferentially to TPC and p-cresol by microbes within Sets D-F, reinforcing previous in-situ data (Spence et al, 2001b).

Enrichment factors in the acetate (and other) microcosms are discussed within section 4.6.

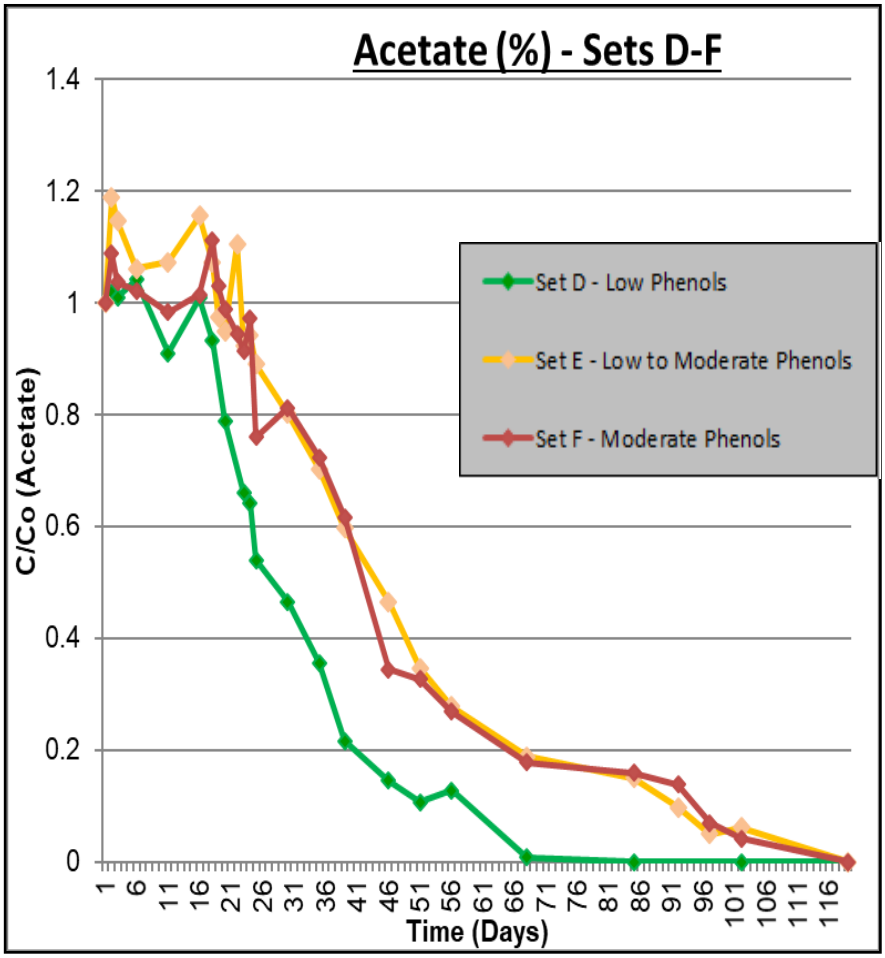

Figure 46. Acetate concentrations for the active microcosms; showing percentage (%) of acetate remaining against time.

4.5.3. Sulphate Concentrations

Sulphate concentration values for microcosms A-F are presented below (Figure 46). Similar to TPC and acetate, sulphate concentrations in all microcosms exhibited an initial lag phase lasting between 18 to 22 days.

After this initial lag period, sulphate concentrations began to decrease steadily, however, there were differences between sets. Amongst these differences, a significant change in sulphate values can be seen when comparing moderate phenol sets (C and F) to the moderate-low and low phenol sets (A, B, D and E).

Decreases in sulphate concentrations were slightly larger within microcosms containing acetate (sets D-F) than within those which did not contain acetate (sets A-C). By the end of the sampling period, the decreases in respective sulphate concentrations were around 10 % greater within the acetate-containing microcosms.

Concentrations of sulphate within the microcosms are large (2.8 g/L). Thus, it is considered unlikely that any reactions between sulphate and sand within the microcosms would act to reduce sulphate concentrations by a significant percentage. Moreover, no significant evidence of sulphate (or sulphide) interaction with in-situ minerals has been found by previous studies (Spence, 2001).

In light of the above, it is considered safe to assume that the majority of lost sulphate is used for BSR. Total loss of sulphate can be stoichiometrically balanced with total contaminant loss (TPC + acetate) using the relevant equations (section 1.9). This method indicates that biodegradation reactions are using sulphate, i.e. BSR could account for 86 % - 118 % of TPC biodegradation (see Appendix 2).

It is understood that, as a practical impossibility, biodegradation reactions utilising sulphate (i.e. BSR) cannot account for contaminant loss that has not occurred (i.e. 100 %). Therefore, BSR reactions can only account for 100 % of TPC biodegradation as a maximum. It is considered that the presence of values greater than 100 % are due to a number of assumptions within this methodology. Nevertheless, these values give a strong indication that the majority of contaminant biodegradation within the microcosms is due to BSR.

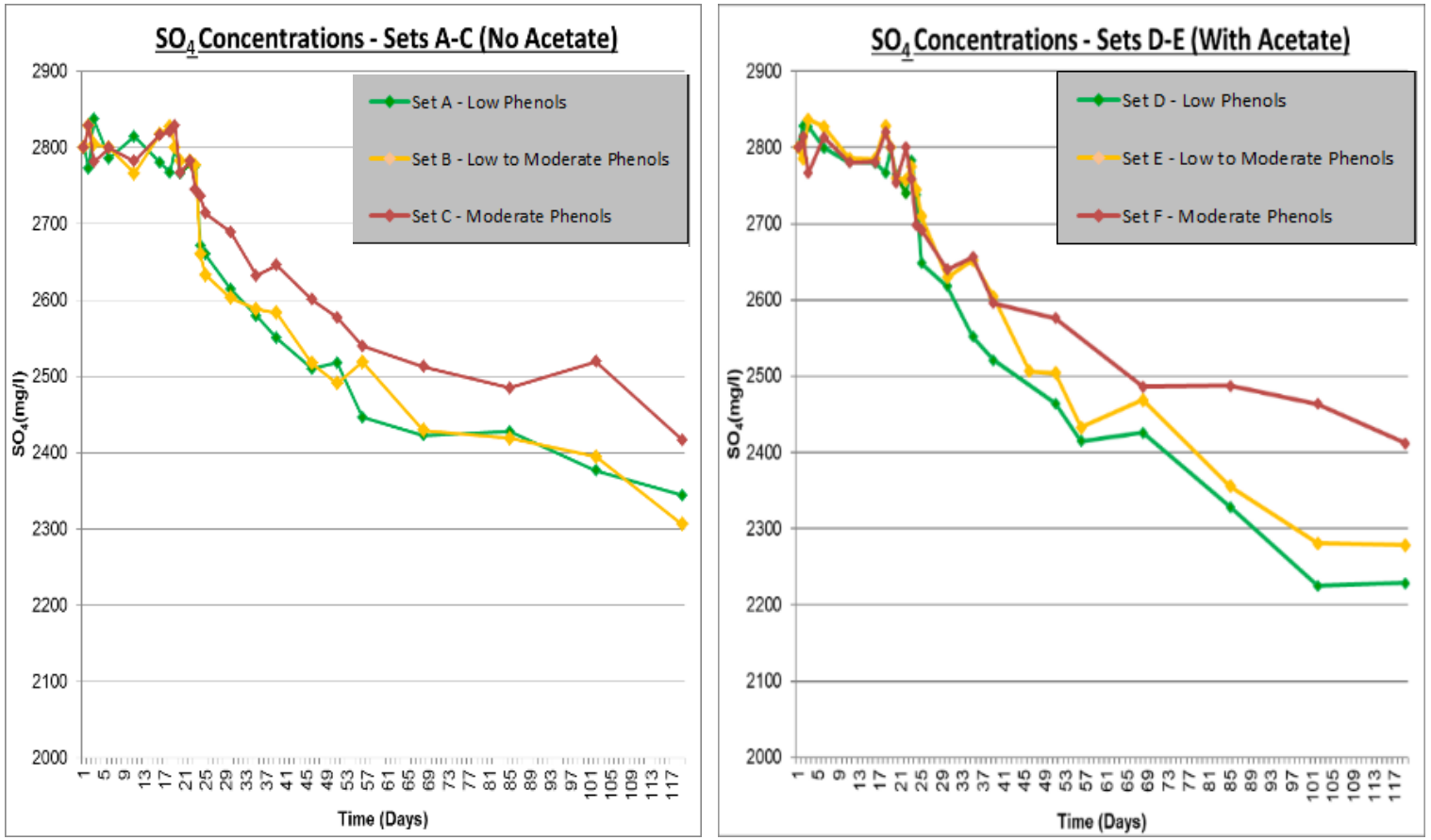

Figure 47. SO_4 Concentrations against time.

4.5.4. Nitrate Concentrations

For completeness, nitrate concentrations were monitored within the microcosms. Nitrate was found to be below detection levels in nearly all samples (Appendix 2).

With regards to the small number of samples where nitrate was found (see Appendix 2), the amounts of nitrate present were in small quantities (comparative to TPC concentrations) of generally less than <1 mg/L. Furthermore, the pattern of these samples was sporadic, with no overall trend apparent.

In light of the above, it is considered unlikely that these quantities of nitrate will have contributed significantly to contaminant turnover within the microcosms, and as such are not anticipated to significantly affect biodegradation pathways.

The only exception to this was microcosm B1, which saw a massive increase in nitrate up to 21 mg/L after around 40 days. This nitrate continued to increase before this microcosm was eventually discarded, due to both this information and other evidence to support a ruptured septum.

4.5.5. $\delta^{34}SO_4$ Values (Sets A-C, Without Acetate)

$\delta^{34}SO_4$ isotope values for sets A-C are presented below (Figure 47 and Figure 48). $\delta^{34}SO_4$ isotopes starting values, for these sets, ranged between 5.0 ‰ and 6.4 ‰, with values remaining relatively unchanged (<1 ‰ variance) in readings during the first 20 days (lag phase). Following this phase, $\delta^{34}SO_4$ concentrations showed a general enrichment in all set A-C microcosms.

With regards to sets A and B, $\delta^{34}SO_4$ values increased from ~5 ‰ to ~8 ‰ during the 190-day observation period (Figure 47). A marginally smaller shift was present in set C which increased from around ~5 ‰ to ~7.5 ‰ in the same period (Figure 48).

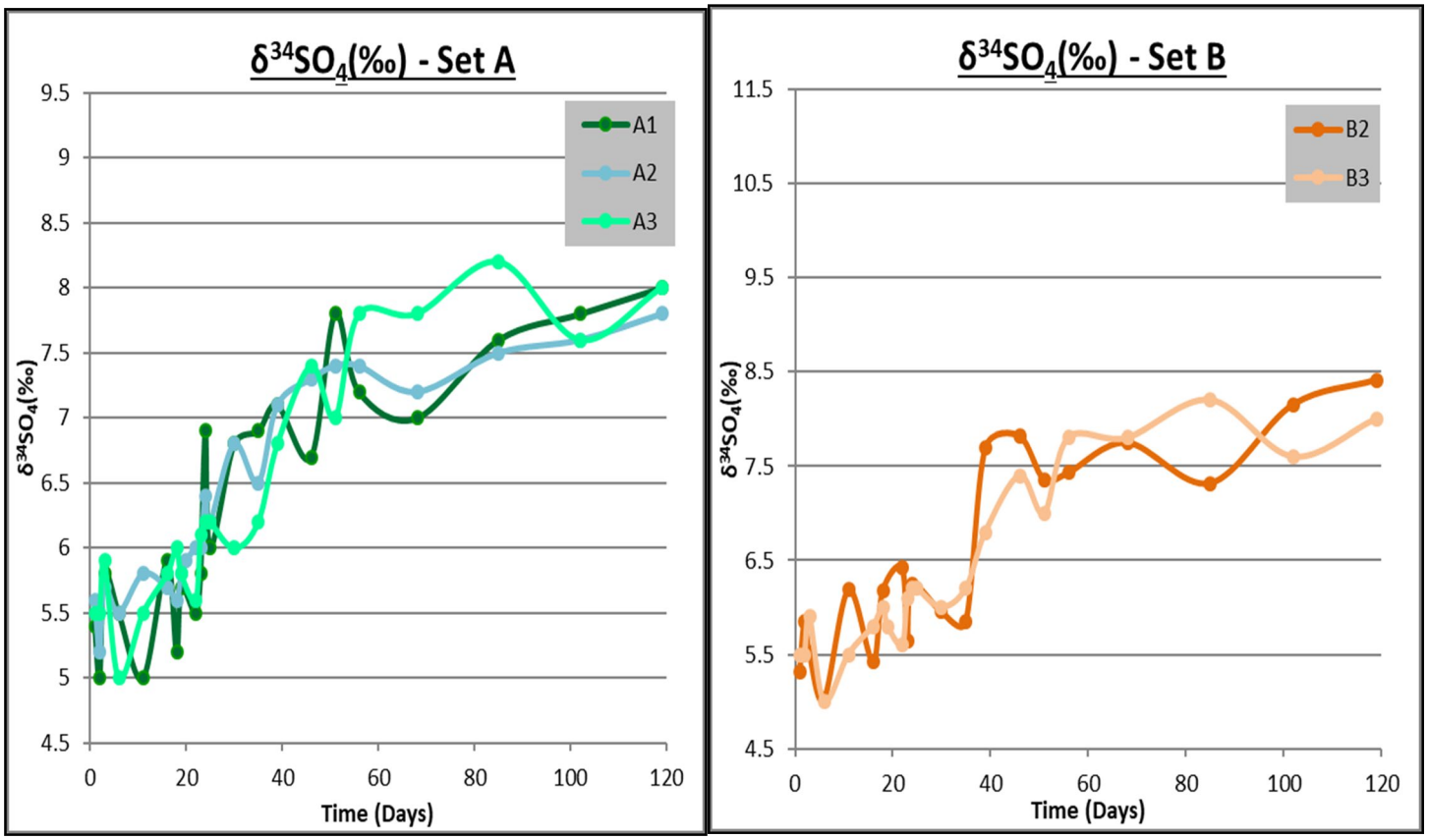

Figure 48. $\delta^{34}SO_4$ isotope values for sets A and B.

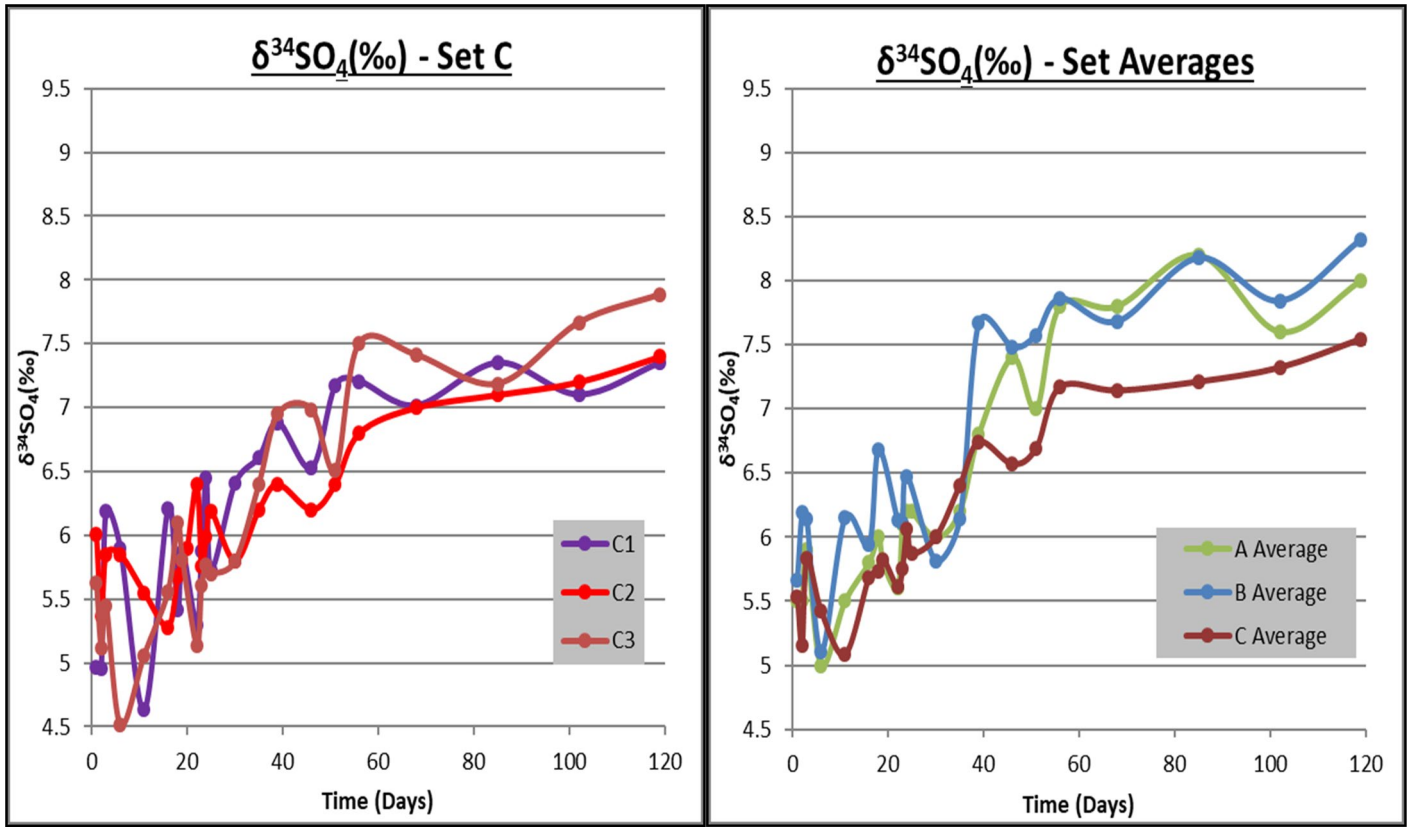

Figure 49. $\delta^{34}SO^{4}$ isotope values. Set C and Set A-C Averages.

4.5.6. $\delta^{34}SO_4$ Values (Sets D-F, Without Acetate)

$\delta^{34}SO_4$ isotope values for sets D-F are presented below (Figure 49 and Figure 50). For these sets, starting values of $\delta^{34}SO_4$ isotopes ranged between 4.7 ‰ and 6.3 ‰. Similar to sets A-C, $\delta^{34}SO_4$ isotope values in these microcosms remained relatively unchanged in readings, during the first 20 days.

$\delta^{34}SO_4$ concentrations after this period showed a positive trend in all microcosms from sets D-F. In each of these sets, $\delta^{34}SO_4$ values increased from ~5 ‰ to ~8 ‰ during the 190-day observation period.

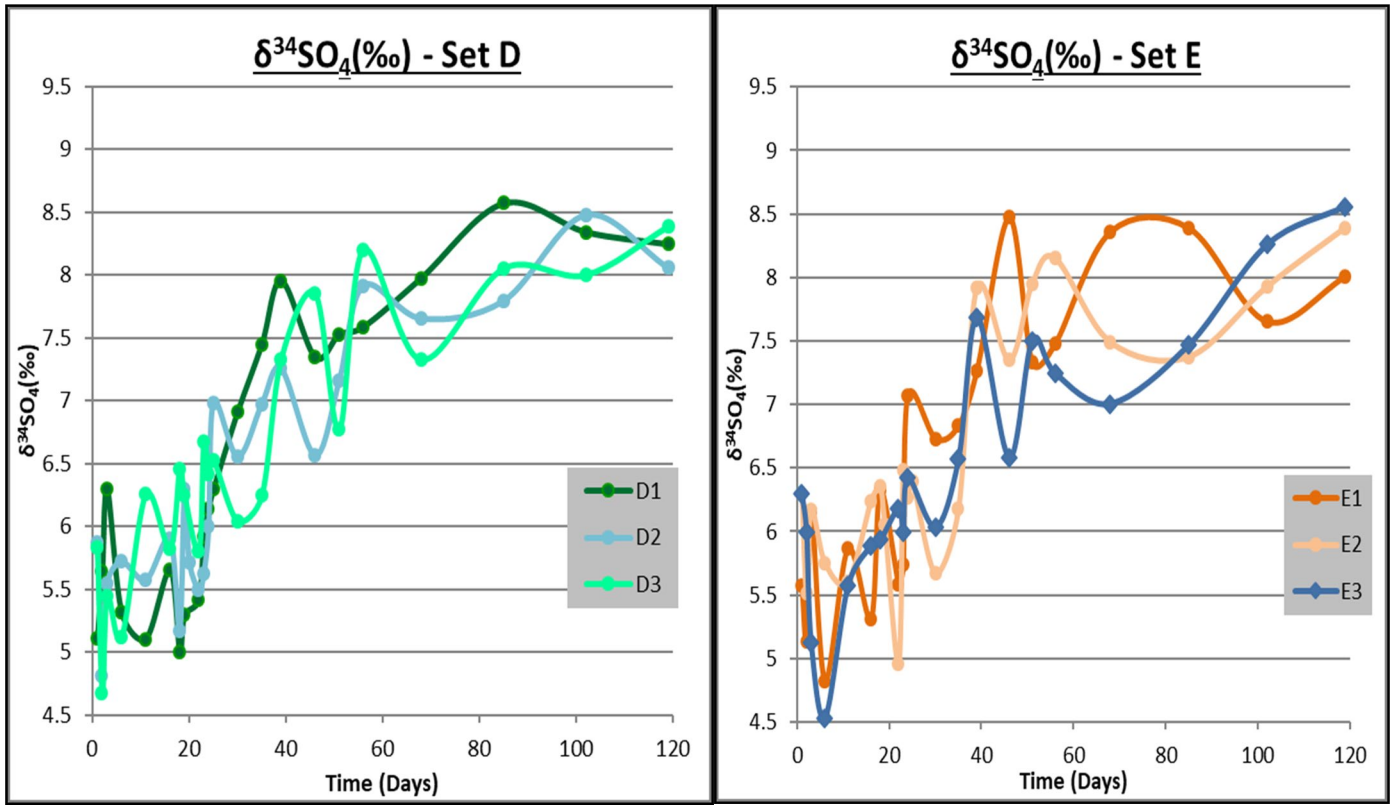

Figure 50. $\delta^{34}SO_4$ isotope values for sets D and E.

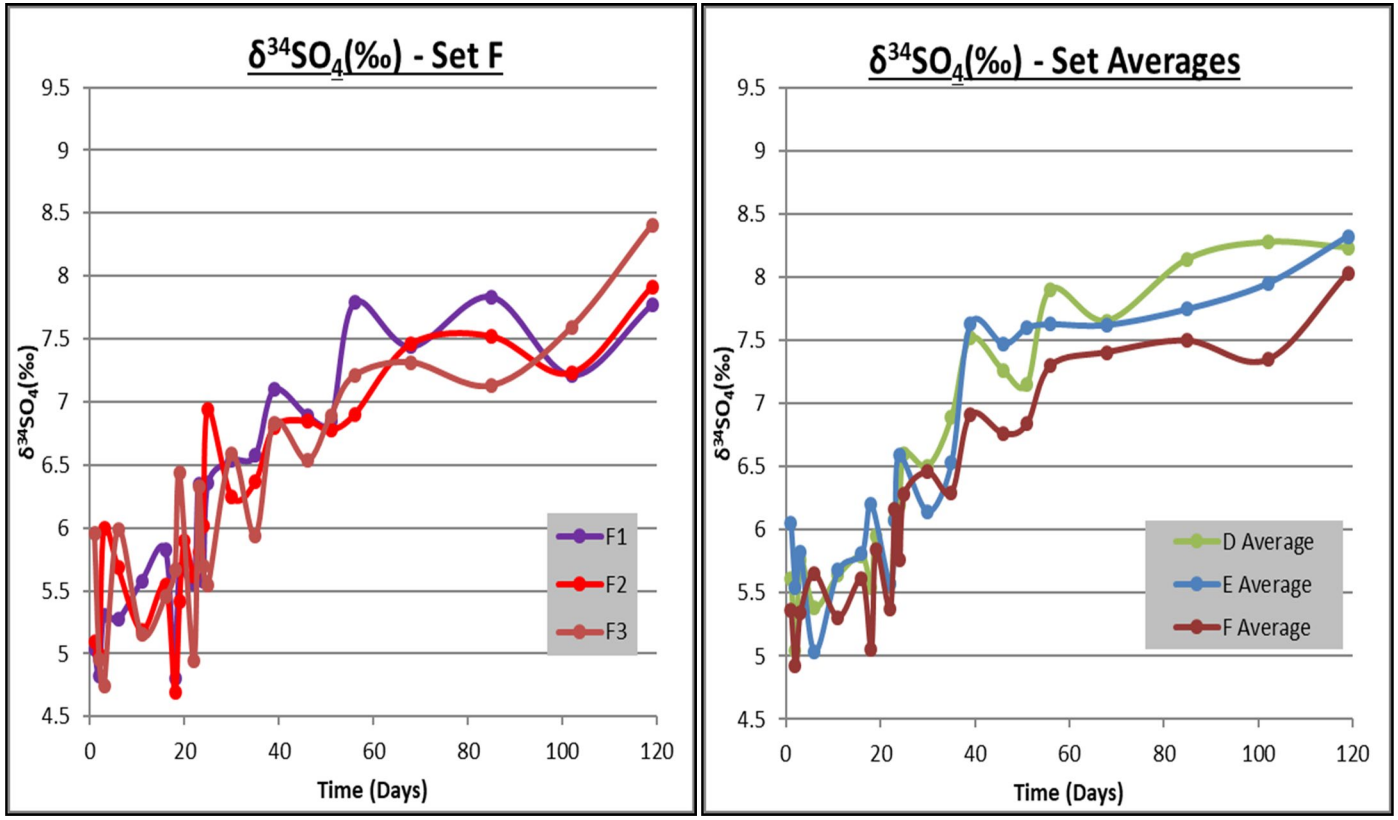

Figure 51. $\delta^{34}SO_4$ isotope values. Set F and Set D-F Averages

4.6. Calculation of the Enrichment Factor (ε)

Enrichment factors were calculated utilising $\delta^{34}SO_4$ and SO_4 values from the microcosm data. These data were plotted in the graphical form $\delta^{34}SO_4$ vs $Ln(SO_4)$. This graph is derived from the Rayleigh equation and with a gradient of ε. For further discussion of the Rayleigh equation see sections 1.11.5.1 and 4.4.

One example of such a plot (Set A) is displayed in Figure 51. Overall enrichment factors and correlation strengths from these analyses are presented in Table 7. A full set of ε value calculations is included within Appendix 4.

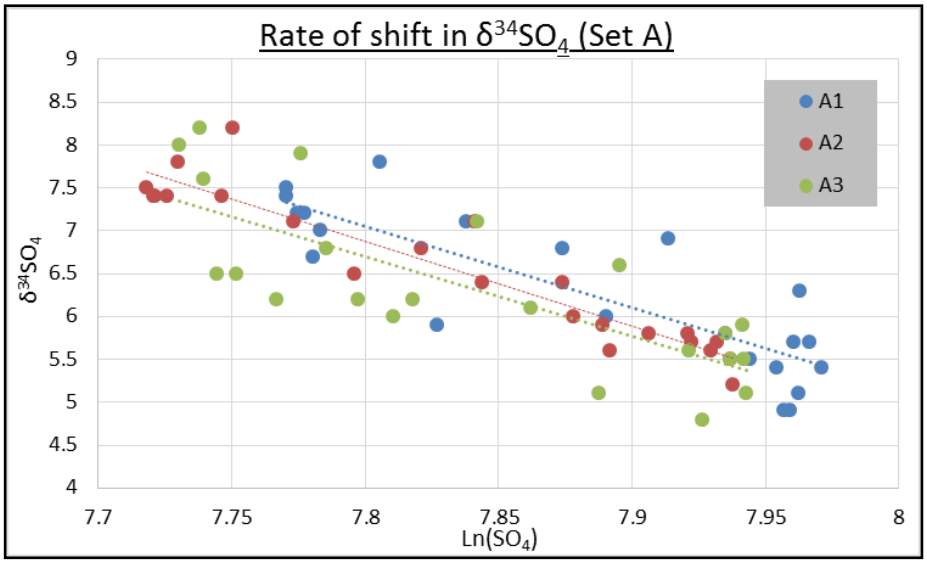

Figure 52. An example of a $\delta^{34}SO_4$ vs $Ln(SO_4)$ plot, displaying trend lines with the gradient ε.

					Enrichment factor (ε)		Correlation	
Microcosm Numbers			**Phenols (g/L)**	**Acetate**	**Range**	**Average**	**Average r^2**	**Standard Deviation**
A1	**A2**	**A3**	Low	No	-9.0 to -11.1	-9.8	0.68	0.8
	B2	**B3**	Low-Medium		-9.8 to -10.4	-10.2	0.59	0.2
C1	**C2**	**C3**	Medium		-8.0 to -8.9	-8.4	0.78	0.3
D1	**D2**	**D3**	Low	Yes	-9.4 to -9.9	-9.6	0.64	0.2
E1	**E2**	**E3**	Low-Medium		-9.1 to -9.9	-9.4	0.72	0.3
F1	**F2**	**F3**	Medium		-7.6 to -8.6	-8.0	0.62	0.4

Table 9. Enrichment factors and correlation strengths for all active microcosm sets (A-F).

4.6.1. Similarities and Significant Differences Between Microcosm Sets

T-tests and Wilcoxon tests, of enrichment factor values indicate no significant difference between sets A, B, D and E, and no significant difference between sets C and F. However, there is a significant difference when comparing sets A and B against set C, and when comparing sets D and E against set F.

These statistical analyses can be compiled into a similarity matrix (Table 10), based on correlations between microcosm sets.

	A	B	C	D	E	F
A						
B						
C						.
D						
E						
F						

	Similar
	Not Similar

Table 10. Similarity matrix for enrichment factors within all active microcosm sets (t-test only).

Using this t-test matrix, it is possible to group the microcosms into two similar sets:

(1) those with low and low-medium phenols – sets A, B, D, E; and,
(2) those with medium phenols – sets C and F.

4.6.2. Similarities Between Acetate and Non-acetate Microcosm Sets

The above analysis indicates no significant differences between the acetate and non-acetate microcosms of similar phenol concentrations. Enrichment factors (ε) do not vary significantly due to the presence of acetate, despite acetate being used preferentially over TPC or p-cresol when present (section 4.5.2.2).

In light of the above, it considered that the biodegradation substrate is exerting little influence on enrichment factors (ε). Hence any shifts in ε values are likely due to differences between TPC concentrations within the microcosms, as this was the only other experimental variable.

4.6.3. Comparison of TPC and ε Values

Hence, given that TPC concentration is likely the major factor affecting ε values within the microcosms, appropriate ε values for a given TPC concentration could feasibly be assigned.

By extrapolating values from the microcosm studies, it is possible to derive the appropriate ε values at any given TPC concentration. This extrapolation can be presented graphically (Figure 53), including likely upper and lower bounds.

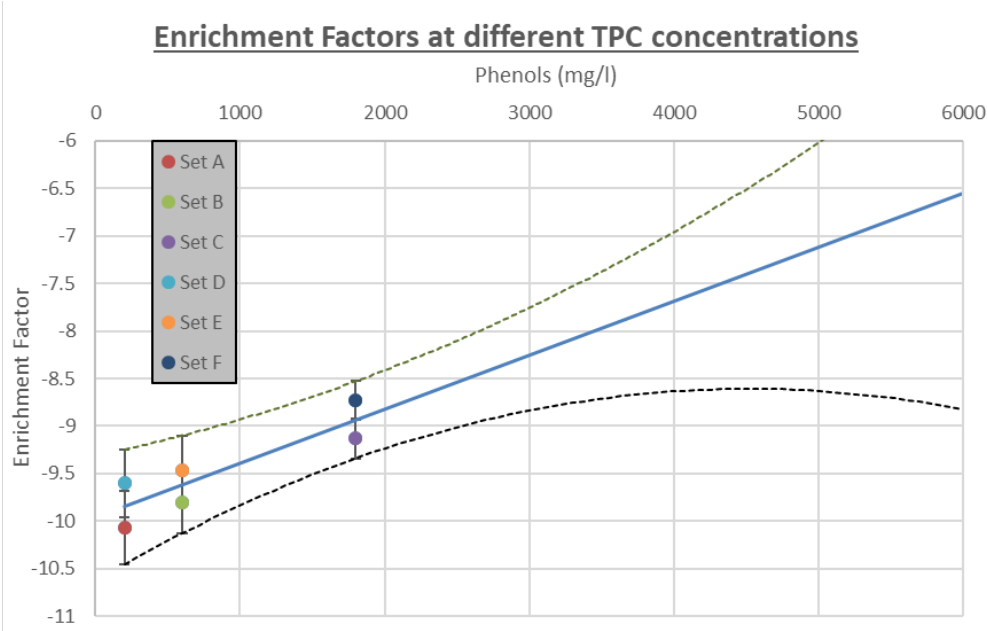

Figure 53. A plot of enrichment factor (ε) against TPC concentrations, between 0 mg/L and 6000 mg/L. Statistical extrapolation (linear extrapolation of averages – solid line), likely upper and lower bounds (polynomial extrapolation of max/min values – dashed lines).

As noted in section 4.1, it was not feasible to conduct any microcosms at TPC levels over 1.6 g/L, as runtimes of these microcosms would have been too long for any significant data to be collected over an appropriate timescale. Furthermore, concentrations of TPC less the 0.2 g/L would have likely been subject to the opposite effect with degradation proving too fast for an accurate assessment of the enrichment factor.

In light of the above, it was necessary to extrapolate the results from the obtained data range, 0.2g/L TPC to 1.6g/L TPC, to estimate the likely ε values for the full range of contaminant concentrations observed within the plume. This extrapolation is based upon the assumption that the response of the microbial community stays the same (i.e. the average stress increases linearly with increased contamination).

Notwithstanding the above, extrapolation of ε values is expected to be generally accurate where close to the range of tested TPC concentrations (i.e. between 0 g/L and 2 g/L). Whilst uncertainties are expected to increase away from the range of measured values, BSR is only expected to occur in regions of the plume where TPC concentrations are between 0 g/L and 2 g/L, as data from both this study (Section 3.5) and previous studies (Thornton et al., 2013) indicates that BSR is strongly inhibited at concentrations over 2 g/L. Thus, the need for an accurate determination of ε in regions of high TPC is negated.

Furthermore, as no BSR occurs above 2 g/L TPC, should the linear relationship between ε and TPC break down at high TPC concentrations the overall conclusions would not be significantly affected.

4.6.4. Suitability of Range of ε Values

The analyses above, indicate that a range of ε values from ~10‰ at low TPC to around ~7‰ at regions of high TPC, but independent of the presence of acetate. This provides evidence that microbial communities stressed by contaminant toxicity within the plume (Spence et al, 2001a; Spence et al, 2001b; Baker et al, 2012) are indeed exhibiting dissimilar enrichment factors to the less stressed community. In general, the more stressed microbes tend to fractionate isotopes respectively less, a phenomenon which has been well observed within a number of previous studies (Karlson et al, 2018).

In light of the limitations on the microcosm analyses (section 4.3) this data is best viewed in light of additional in-situ data. It is possible to compare values of ε against $\delta^{34}SO_4$ values derived from in-situ sulphide results which represent instantaneous ε values at one given point in time.

Sulphide results gathered both during this study and during previous studies (Spence, 2001), are not subject to some of the errors noted in section 4.3 (most notably the bottle effect). These results indicate a range of ε values between -7‰ and -15‰, (Section 3.7; Spence., 2001) largely in line with the range of the microcosm results.

CHAPTER 5

5. Enhanced Carbon Balance

5.1. Spatial Distribution of Dominant Pathways

The data gathered during this thesis, as well as previous studies both related to this site (Spence et al, 2001b, Thornton et al, 2001a, Baker et al, 2012) and in the wider area (Harrison et al, 2001, Pickup et al, 2001; Rizoulis et al, 2012; Wu et al, 2006) have demonstrated that the significance of different biodegradation pathways varies widely within contaminant plumes.

Numerous hydrological and chemical factors have been documented to affect the dominance of these biodegradation pathways. However, data from the study site specifically serves to outline that, that plume biochemistry still follows the Cirpka et al (1999, section 1.15.1), with the exception of zones of TPC >2 g/L which acts to 'sterilise' respiration processes. This is true both in non-pumped conditions (Spence et al, 2001b, Thornton et al, 2001a, Baker et al, 2012) and during pumping (section 3, Thornton et al, 2014).

5.2. A Carbon Balance for Semi-quantitative Analysis

In order to provide a semi-quantitative analysis of the spatial distribution of biodegradation pathways, a mass and isotope carbon balance can be utilised (Hunkeler et al, 1999a). Such a carbon balance serves to apportion total carbon turnover to different biodegradation pathways allowing for a more robust interpretation of data.

Thornton et al, (2014) created one such model for the plume, utilising TDIC values (a proxy for total carbon turnover), and δ^{13}C-TDIC values which are indicative of the TDIC source (section 1.16.3).

Using this approach, the sources of carbon turnover can be estimated by apportioning the carbon to two end members: respiration CO_2 and

methanogenic CO_2, which are assigned different $\delta^{13}C$ compositions from field data (section 3).

A discussed within previous chapters (Sections 1.13.5 and 1.14.1), it should be appreciated that the isotopic data does not distinguish between "background TDIC" and TDIC generated from biodegradation of TPC. However, as per the above, the quantity of "background TDIC" can be estimated, in light of observed values outside of the plume and known pH values. Furthermore, "background TDIC" is understood to have a δ13C-TDIC of approximately -19 ‰ (Baker et al, 2012; Thornton et al, 2014). In light of this, "background TDIC" can be factored out before undertaking further calculations as below.

5.2.1. Apportioning Carbon Turnover Between Respiration and Methanogenesis

$\delta^{13}C$ compositions for respiration CO_2, can be assumed based upon the fact that complete respiration of TPC would lead to TDIC with a $\delta^{13}C$ equal to the that of the initial organic contaminants, −26 ‰ (Thornton et al, 2014).

In light of the above, the $\delta^{13}C$ of CO_2 created through methanogenesis, can be calculated from $\delta^{13}C$-CH_4 values measured in the respective plume samples (section 3.4.1), employing the below equations (Equation 14; Equation 15):

Equation 14

$$2 * \delta^{13}C[Initial\ organic\ contaminants] = \delta^{13}C[Methane] + \delta^{13}C[Methanogenic\ CO_2]$$

Equation 15

$$\delta^{13}C[Methanogenic\ CO_2] = 2 * \delta^{13}C[Initial\ organic\ contaminants] - \delta^{13}C[Methane]$$

After assignment of these two end member values, these values along with measured $\delta^{13}C$-TDIC values can be used to apportion TDIC values to the two respective end members, TDIC[Meth] and TDIC[Resp] (Equation 16).

Equation 16

$$100\,\% * \delta^{13}C[TDIC] = (\%\,TDIC[Resp] * -26\,‰ + \%\,TDIC[Meth] * \delta^{13}C[Methanogenic\ CO_2])$$

5.3. Creating the Enhanced Carbon Balance

Whilst the calculation above serves as semi-quantitative method to proportion carbon turnover between respiration TDIC[Resp] and methanogenic TDIC[Meth] processes, this analysis offers no subdivision within the respiration pool to outline the contributions of different sub-processes (i.e. BSR, nitrate and oxic reduction are all grouped as respiration).

However, by utilising additional data from this thesis in the form of fractionation factors for BSR (at different TPC concentrations, section 4.6), total carbon turnover by BSR be calculated by an alternative method, as described below.

5.3.1. Utilising Fractionation Factors

An assessment of total BSR can be conducted by calculating total sulphate loss, within a given sample, and stoichiometrically apportioning this to TDIC creation, TDIC[BSR], using the relevant biodegradation equation (Equation 17).

Equation 17

$$5 * C_6H_5OH + 14 * SO_4 = 30 * CO_2 + H_2O + 14 * H_2S$$

The action of the biodegradation pathway (Equation 17) is reinforced by the observation of hydrogen sulphide within the plume (section 3.5).

Total sulphate loss can be calculated by the difference between initial sulphate concentrations and current sulphate concentrations. As the current sulphate, within a given sample, is measured (section 3.5), it is therefore only necessary to calculate the original sulphate. This can be done using the Rayleigh equation (Equation 3).

Equation 18

$$\varepsilon = \frac{\delta^{34}SO_4(t) - \delta^{34}SO_4(o)}{Ln\left(SO_4(t)/SO_4(o)\right)}$$

Where:

$\delta^{34}SO_4(t)$ is the $\delta^{34}SO_4$ at time t;

$\delta^{34}SO_4(o)$ is the original $\delta^{34}SO_4$;

$SO_4(t)$ is the SO_4 at time t; and,

$SO_4(o)$ is the original SO_4.

A value for the original sulphate concentration ($SO_4(o)$) can then be derived by imputing values into the equation for:

(1) fractionation factor, based upon the values derived during the microcosm studies (section 4.6);
(2) $\delta^{34}SO_4(t)$ and $SO_4(t)$ values from respective plume profile samples; and,
(3) a value for $\delta^{34}SO_4(o)$ based upon values of 6 ‰ - 7 ‰ from samples taken by Thornton et al, (2014).

5.3.2. Apportioning Respiration TDIC between BSR and Non-BSR Processes

Based on the calculation above, total carbon turnover due to BSR can now be individually calculated separate of TDIC[Resp] (calculated in section 5.2.1). Hence, by utilising the techniques above to calculated both TDIC[Resp] and TDIC[BSR] for any given sample or plume region, TDIC created by respiration but not BSR, TDIC[Non-BSR Resp] can be calculated (Equation 19).

Equation 19

$$TDIC[Non - BSR\ Resp] = TDIC[Resp] - TDIC[BSR]$$

5.3.1. Advantages of the Enhanced Carbon Balance

The techniques outlined above serve to enhance the original Thornton et al, 2014 carbon balance model for the plume, allowing the data generated within this thesis to be subjected to improved modelling techniques.

In addition, due to the nature of the new isotopic enrichment data (ε, section 4.6) , which is calculated at different TPC concentrations, it is considered that these fractionation factors are applicable to previous data sets provided that data are corrected the relevant TPC concentration at the time of sampling. Thus, the above improved model can then be used to analyse all historical data for the plume, in order to better outline shifts in the dominant biodegradation processes, and particularly BSR throughout the plume's history.

The main advantages of the enhanced model are as follows:

(1) Greater subdivision of processes – TDIC[Resp] is now separated into TDIC[BSR] and TDIC[Non-BSR]; and,
(2) Improved model confidence – Two different techniques are now used to reinforce each other within the new carbon balance.

5.4. Assumptions and Limitations

There are several assumptions involved in utilising such a carbon model including:

- The initial isotope ratio of the organic contaminants was assumed to be −26 ‰, as measured by Spence et al (2001b);
- Methanogenically derived TDIC was assumed to be created by acetoclasis from acetate which has a δ^{13}C of −26 ‰ (section 1.14.1); and,
- AMO is negligible at the depths analysed, contributing a low amount of the total carbon pool and therefore not affecting δ^{13}C-TDIC ratios.

Uncertainties within the data that is utilised in these calculations, namely TDIC, δ^{13}C-TDIC and δ^{34}S-SO_4 values (section 3), as well BSR fractionation factors (section 4.6), are also associated with calculation outputs. More details on these uncertainties can be found in the chapters from which this data is derived.

It should also be appreciated that the water sampled from the MLS samplers has a long-term complex history. As such the carbon balance represents a "cumulative signature" of the conditions which a parcel of water has passed through rather than just a snapshot in time.

5.5. Grouping of Carbon Balance Data

The full results of the carbon balance calculations are presented in Appendix 3. Summarised results are shown below, with respect to the different regions of the plume which are as outlined in section 3.

MLS59:

- 10 mbgl to 12 mbgl – Zone A, Upper Plume Fringe;
- 13 mbgl to 24 mbgl – Zone B, Upper Plume Core; and,
- 25 mbgl to 29 mbgl – Zone C, Lower Plume Core,

MLS60:

- 18 mbgl to 20 mbgl – Zone D, Upper Plume Fringe;
- 21 mbgl to 27 mbgl – Zone E, Upper Plume Core;
- 28 mbgl to 36 mbgl – Zone F, Middle Plume Core; and,
- 37 mbgl to 45 mbgl – Zone G, Lower Plume Core (Pre-Pumping) or Pumping Influenced Zone (During Pumping).

5.6. Carbon Balance Results – Process Proportions

5.6.1. MLS59 Results – Pre-pumping

An averaged carbon balance for the years of pre-pumping, between 1999 to 2010, at MLS59 was created in order to outline the proportions of different processes within the plume, during this period.

During this period, Zone A, 10 mbgl to 12 mbgl, displays a low amount of methanogenesis, which contributes an average of 14 % to the total TDIC pool. Contributions of BSR, within this region are also low, contributing ~5 % of the total TDIC pool. This is strongly indicative of a region of the plume dominated by respiration processes using energetically favourable electron acceptors such as oxygen and nitrate, derived from interaction with uncontaminated groundwater at the edge of the plume (~81 % of the total TDIC pool).

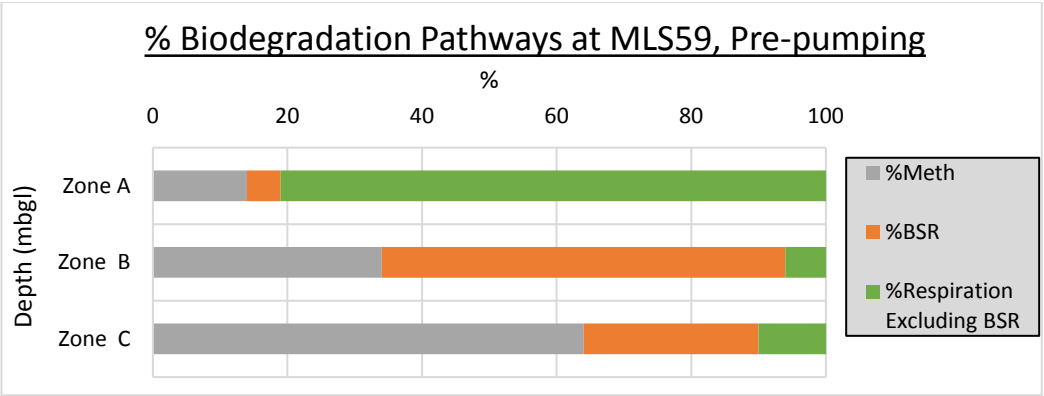

Figure 54. Average carbon balance for MLS59 before 2011 when pumping started.

Pre-pumping data for Zone B, 13 mbgl to 25 mbgl, indicated that there is a predominance of respiration, over methanogenesis, during this period. Respiration contributes an average of 66 % to the total TDIC pool in this region (Figure 54). There is some yearly variability within pre-pumping data for this region, with the total contribution from respiration ranging from 58 % to 85 %. Within the pool of respiration related TDIC, the majority of this is related to BSR, which contributes an average of 60 % of the total TDIC pool, 90 % of the total respiration in this region. However, it is worthy of note that some methanogenesis does still occur concurrently with BSR within Zone B, contributing an average of 34 % of the total TDIC pool.

Proportions of methanogenesis are much higher within Zone C, the lower plume core, than within the upper plume core. In this region, the proportion of methanogenesis climbs to an average of 64 %. Yearly variability for Zone C is high with contributions from methanogenesis reduced, to as low as 35 % TDIC contribution, in a limited number of sampling rounds.

It should be noted that the data above is averaged between a number of pre-pumping years. As such, it should be appreciated that the proportions of respective processes do vary from year to year. However, the range of values typically fall within +/- 15% of the average, with the exception of 2003 which exhibits increased proportions of methanogenesis within Zone B and Zone C. This increase in methanogenesis in 2003, is also coupled with higher TPC values throughout the plume, particularly in respect to the upper plume core.

Indeed, additional analysis of the variability within Zone B and Zone C indicates that sampling rounds exhibiting higher methanogenesis, are often coupled with higher TPC concentrations, considered to be due to either changes in source characteristics through time or variations in the groundwater flow field (Section 1.13.1). The carbon balance shows BSR to be highly variable at these depths, ranging from 5 % (in 2003) up to 50 %.

The above indicates that suppression of BSR due to contaminant toxicity from high levels of TPC (Thornton el al, 2014) may be a significant factor within Zone B and Zone C.
Bearing in mind the 2 g/L threshold proposed by Spence et al (2001b, section 1.13), the following can be considered as a conceptual model for the region surrounding MLS59 during the pre-pumping period:

(1) An upper plume fringe dominated by respiration due to an influx of oxygen and nitrate electron acceptors;
(2) An upper plume core dominated by BSR where TPC concentrations (1 g/L to 2 g/L, section 1.13) are not consistently high enough to supress this process, but also where some methanogenesis concurrently occurs; and,
(3) A lower plume core where BSR is more supressed and methanogenesis dominates due to high TPC concentrations (3 g/L to 8 g/L, section 1.13).

5.6.2. MLS59 Results – During Pumping

MLS59 was pumped for almost two years during 2011 and early 2012, before this ceased due to unforeseen circumstances. An averaged carbon balance for these two years has been created.

During this period, Zone A, 10 mbgl to 12 mbgl, still exhibits broadly similar conditions to pre-pumping, displaying a low amount of methanogenesis (22 %), with a dominance of non-BSR respiration processes which contribute 77% of the total TDIC pool. Within this region contributions of BSR are also low, ~% of the total TDIC pool.

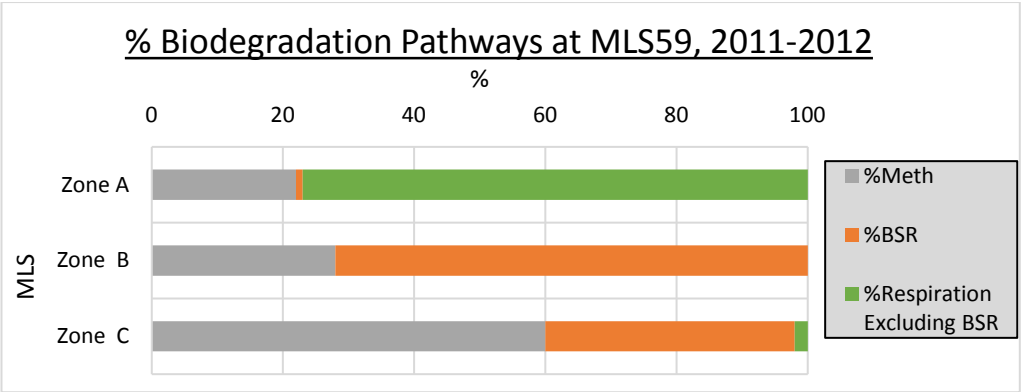

Figure 55. Average carbon balance for MLS59 for 2011 and 2012.

Zone B, the upper plume core, exhibits an increase in respiration from pre-pumped values, with respiration contributing an average of 72 % to the total TDIC pool during this period (Figure 55). Calculations of BSR for this region (section 5.3) established that around 80 % of the pool of total TDIC is created related to respiratory BSR (Appendix 3). However, this result requires further interpretation as this result establishes that BSR is greater than total respiration, making the results incompatible. It is noted that calculations of BSR and respiration are each subject to uncertainties of ~6% (based upon microcosm study uncertainties, Section 4.5.1) hence total respiration could feasibly be as high as 77 % with BSR feasibly being as low as 75 %. Hence, a conceivable solution is that in fact that the entire pool of respiration at these depths is between 75 % and 77 % with this entirely contributed by BSR.

However, it also worthy of note that the TPC concentration in Zone B is balanced at around 2 g/L during this period. Hence, changes in source term or, fluctuation in groundwater flow (Section 1.13.1) may be affecting the balance of this region significantly by elevating or decreasing concentrations above or below the 2 g/L threshold.

As with the pre-pumped data, it is worthy of note the some methanogenesis does occur concurrently with BSR within Zone B, albeit in somewhat reduced proportions, contributing 28 % to the TDIC pool; a value significantly less (~7 % less) than pre-pumping.

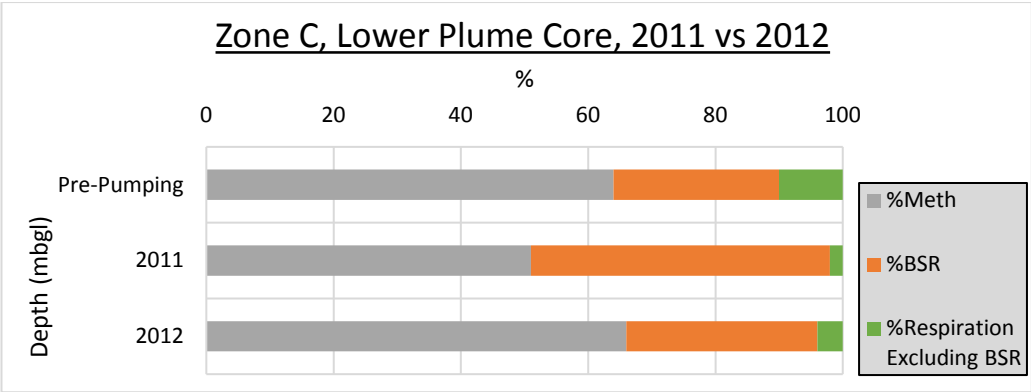

Figure 56. Carbon balance for the lower plume core at MLS59.

During this period, average values for Zone C exhibit similar trends to pre-pumping values, with methanogenesis contributing 60 % of the TDIC pool, as opposed to 64 % pre-pumping. However, there is a notable difference between 2011 and 2012 values within Zone C (Figure 56). For this region, 2011 data exhibits a substantial change from pre-pumped values with the proportion of respiration increasing by ~12 % and BSR itself increasing by ~20 %. In contrast, the proportions of processes in 2012 are much similar to pre-pumping values.

In light of the above and based on the fact that pumping at MLS59 ceased in late 2012 due to unforeseen circumstances causing excess pump stress on the in-situ pump, it is considered that pumping during the 2012 sampling round may also have been somewhat affected by these conditions. Hence it is concluded that the 2011 data may be more representative of the plume conditions during the period of optimal pumping rate and pump functionality.

The following can be considered as a conceptual model for MLS59 during the pumped period:

(1) An upper plume fringe dominated by oxygen and nitrate respiration similarly to pre-pumping (section 5.6.1);
(2) An upper plume core which is subject to a small increase in BSR, due to marginal decreases in TPC concentrations reducing toxicity (Spence et al, 2001b); and,
(3) A lower plume core where BSR exhibits a greater contribution than pre-pumping, but methanogenesis still plays a key role. This is due

to TPC reduced to at or around the 2 g/L threshold, dipping below the toxic threshold (Spence et al, 2001b) at certain points.

5.6.3. MLS59 Results – Post-pumping

5.6.3.1. MLS59 2014 and 2015

Datasets for 2014 and 2015 have been averaged to show plume conditions after cessation of pumping at MLS59 in late 2012.

During this period, Zone A, the upper plume fringe, continued to exhibit a dominance of non-BSR respiration, which contributed 83 % of the total TDIC pool.

However, within Zone B, respiration, and in particular BSR, values begin to fall in comparison to pumped values. BSR falls from 72 % pre-pumping to 68 % in 2014 and then 60 % in 2015; this may be linked with the recovery of contaminant concentrations which begin to return to values circa those pre-pumping by 2014 (typically 1 g/L to 3 g/L, section 1.13.1), which are close to the toxic threshold (Spence et al, 2001b), acting to supress BSR at the depths.

Zone C, the lower plume core exhibits highly variable conditions in 2014, with TPC in this region varying widely. Due to this, conclusions from the carbon balance for this region are limited; with the main points noted being:

(1) Conditions are in significant flux; and,
(2) Methanogenesis increases within some areas of the plume.

Notwithstanding the above, Zone C data from the 2015 sampling round exhibits more stable behaviour, with proportions of methanogenesis and respiration in the plume core returning to levels similar to pre-pumping. During 2015, methanogenesis contributes around 66 % to total TDIC, similar to the 64 % pre-pumping.

However, it is worthy of note that BSR is indicated to have contributed approximately 40 % of the total TDIC within in zone C, despite high TPC levels within this region (>2 g/L). This may be due to the time integrated

nature of the mass balance results which still represent the historical record of BSR, as water in which BSR had previously been stimulated by the action of PAT now migrates, from upgradient, past the sampling location (Section 5.4). Similarly, the large amounts of BSR seen within Zone B could also be linked to this effect.

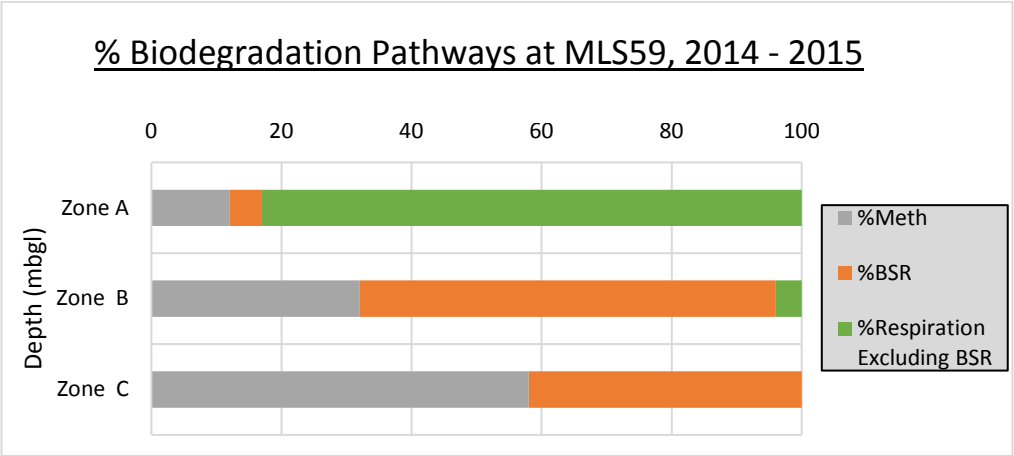

Figure 57. Carbon Balance for MLS59 in 2014 and 2015.

The following can be considered as a conceptual model for MLS59 during the post-pumping period:

(1) conditions have returned to those similar to pre-pumping by 2015;
(2) an upper plume fringe dominated by respiration similarly to pre-pumping (section 1.13);
(3) an upper plume core still dominated by BSR but to a lesser degree than during pumping linked to increased inhibition due to recovering TPC values; and,
(4) a lower plume where BSR and methanogenesis are both occurring, however, methanogenesis is dominant as TPC values are high (typically 3 g/L to 6 g/L, section 3.1.1).

5.6.3.2. MLS59 2016

During 2016, nitrate breakthrough (or plume 'constriction') was noted to have occurred within MLS59 (section 3.2.1.1), significantly affecting TPC concentrations within the plume (section 3.1.1); hence, this year has been analysed separately.

Within Zone A increased proportions of respiration are seen at the upper plume fringe (10 mbgl to 13 mbgl), during this period. This increase in respiration cannot be accounted for by an increase in BSR, reflecting that this additional respiration is likely to be present due to an increase in respiration process utilising other electron acceptors which have now become available in this region such as nitrate and oxygen.

A similar argument can be made for depths between 13 mbgl to 25 mbgl and 25 mbgl to 29 mbgl, which are also affected by this nitrate breakthrough, seeing a ~40 % and ~65 % increase in non-BSR respiration values respectively (Figure 58).

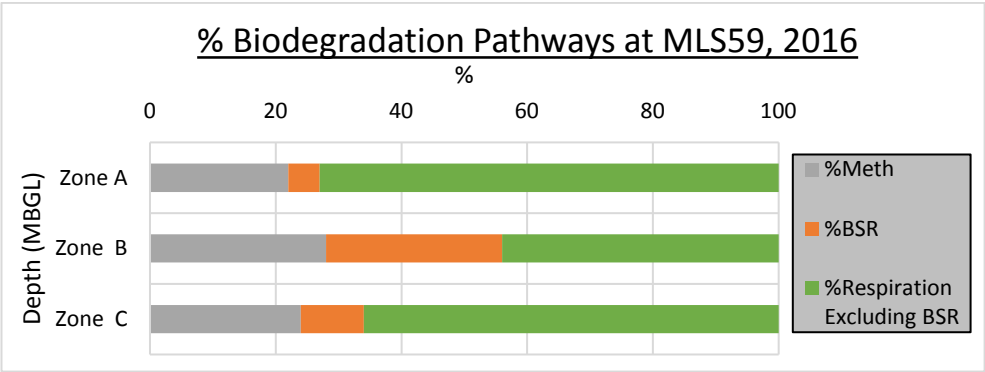

Figure 58. Carbon Balance for MLS59 in 2016.

5.6.4. MLS60 Results – Pre-pumping

An averaged carbon balance has also been created for the years of pre-pumping at MLS60, from 1999 to 2010 (Figure 59).

During this period, Zone D, the upper plume fringe, exhibits a large proportion of non-BSR respiration, likely due to respiration process utilising the nitrate and oxygen electron acceptors available at these depths.

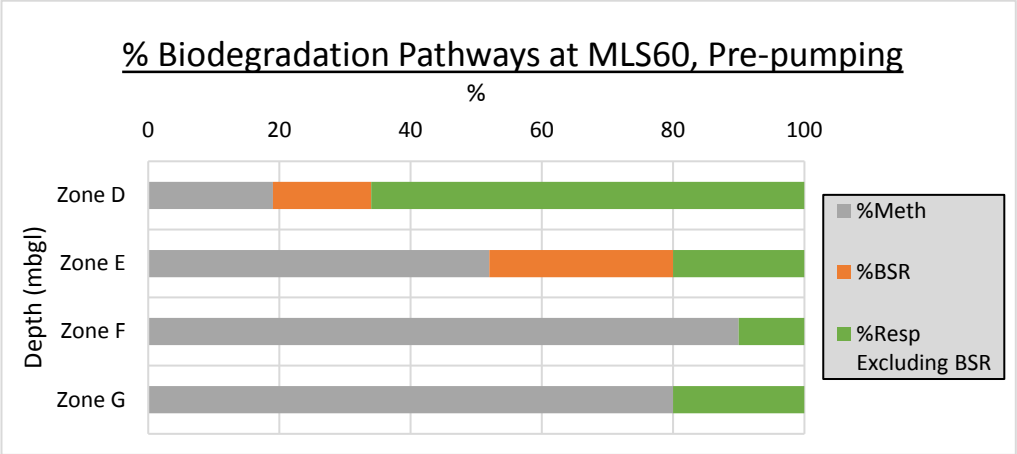

Figure 59. Average carbon balance for MLS60 before 2011 when pumping started.

All other regions of the plume, Zones E-G, have a dominance of methanogenesis over respiration. In Zone E, the upper plume core exhibits an average of 52 % methanogenesis. Some BSR does occur concurrently with methanogenesis within this region; indicating that contaminant toxicity in this region (1 g/L to 2 g/L, section 1.13.1) is not enough to completely suppress BSR. However, it is worth of note that proportions BSR do vary from year to year within this region, potentially due to changes in source term or variations in groundwater flow (Section 1.13.1) elevating this region to either above or below the 2 g/L toxic threshold for BSR (Spence et al, 2001b).

In contrast to the above, Zones F and G, display a much higher proportion of methanogenesis, 90 % in Zone F and 80 % in Zone G. BSR is completely absent at these depths; strongly indicating suppression of this process by contaminant toxicity in these regions of high TPC (Typical 3 g/L to 8 g/L, section 1.13.1).

As with MLS59, it should be noted that the data above is averaged between a number of pre-pumping years. However, yearly variability at MLS60 is more limited in comparison to MLS59, particularly in regard to zones F and G, with methanogenesis strongly dominant in all years. The range of values typically fall within +/- 12% of the average.

The following can be considered as a conceptual model for MLS60 during the pre-pumping period:

(1) an upper plume fringe dominated by respiration due to an excess of oxygen and nitrate electron acceptors;
(2) an upper plume core where BSR and methanogenesis concurrently occur, due to TPC values which vary between above and below the toxic threshold (2 g/L, Spence et al, 2001b); and,
(3) a middle and lower plume core where methanogenesis dominates, and where BSR is completely supressed due to high TPC concentrations.

5.6.5. MLS60 Results – During Pumping

5.6.5.1. 2011 and 2012

Pumping started at MLS60 in 2011 and is ongoing. Data from 2011 and 2012 data have been grouped to show initial changes in process dominance due to this pumping (Figure 60).

Pumping has served to reduce contaminant levels at MLS60, with these decreases in TPC concentration are especially notable in the lower plume (Zone G) between 36 mbgl and 45 mbgl, moving from an average of 5 g/L pre-pumping (section 1.13.1) to generally less than 0.2 g/L during pumping (section 3.1.2; Thornton et al, 2014). In addition, decreases in TPC also occur in the upper plume (Zone E, 22 mbgl to 36 mbgl), from an average of ~2 g/L pre-pumping (section 1.13.1) to ~0.7 g/L during the pumped period (section 3.1.2; Thornton et al, 2014). Although the magnitude of this decrease varies somewhat between years.

During this period Zone D, the upper plume fringe, 18 mbgl to 22 mbgl, was not significantly different from pre-pumping values. Non-BSR respiration was still dominant and in similar proportions, 62 % compared to 63 % pre-pumping.

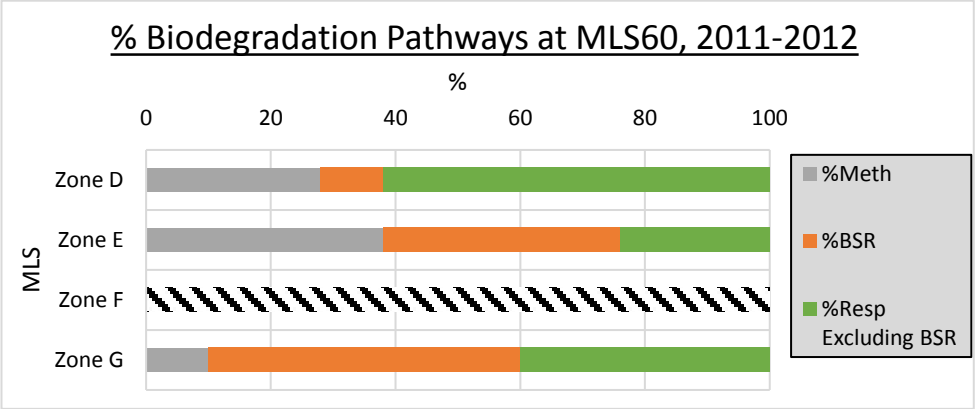

Figure 60. Average carbon balance for MLS60 for 2011 and 2012.

Notwithstanding the above, the proportion of methanogenesis is seen to significantly decrease within the Zones E and G, with respiration becoming significantly more dominant.

This change is particularly notable within Zone G where 90 % of the total carbon pool is now contributed by respiration as opposed to 20 % pre-pumping. Within the increase of respiration at these depths, BSR and non-BSR related respiration are both noted to increase. However, within Zone E increases in respiration is almost entirely coupled to increases in BSR.

Completion of the carbon balance was not possible for Zone F, as calculations for this area were unable to accurately quantify the relevant proportions of respiration and methanogenesis. This has been apparent in previous carbon balances (e.g. Thornton et al, 2014) in areas where AMO is present, as this process cannot be modelled within the carbon balance calculations, yet it causes a rapid depletion of δ^{13}C-TDIC, which leads to negative values of δ^{13}C-TDIC, making calculations invalid (section 1.14.1).

Hence, whist it is not possible to calculate process proportions within Zone F, the significant depletion of δ^{13}C-TDIC in this region in itself is indicative of some AMO, with a δ^{13}C-TDIC values close to that of methane at some depths indicating that methane oxidation is the dominant process (Thornton et al, 2014). However, it should be noted that yearly variability in this region of the plume is very high, with δ^{13}C-TDIC and δ^{13}C-CH_4 values (section 3.4.2), indicating that methanogenesis is also present in this region,

balanced with the AMO. In light of this, processes in this region are likely to comprise a delicate balance between methanogenesis and AMO could explaining the initial discrepancy.

The following can be considered as a conceptual model for MLS60 during the 2011 to 2012 pumping period:

(1) an upper plume fringe dominated by respiration due to an excess of oxygen and nitrate electron acceptors;
(2) an upper plume core where BSR increases respective to pre-pumping conditions due to decreased (average 0.7 g/L), but variable (ranging from 0.5 g/L to 1.6 g/L), TPC concentrations;
(3) a middle plume core where AMO and Methanogenesis occur; and,
(4) a lower plume core where respiration, including large amounts of BSR occurs, as TPC concentrations are not high enough to supress BSR (<0.2 g/L).

5.6.5.2. 2014, 2015 and 2016

With pumping continuing at MLS60 through to 2016, further datasets from 2014, 2015 and 2016 have been analysed to reinforce and expand on 2011 and 2012 data (Figure 61).

Again, for this period, values for Zone D, were not significantly different from pre-pumping values with non-BSR respiration was still dominant albeit in slightly higher proportions, 75 % compared to 68 % pre-pumping.

Analysis of data from Zone F indicated that this region continued to be affected by large amounts of AMO during this period, as indicated by significantly depleted δ^{13}C-TDIC values (sections 1.13.5 and 3.4.2).

Zones E and G exhibit proportions of total respiration and methanogenesis that are not significantly different from those in the 2011/2012 data. However, the proportion of BSR increases, particularly within Zone G, rising to 68 % compared to 50 % in 2011/2012. Several reasons can be attributed to this shift including: (1) stabilisation of conditions within this region has allowed a stable community of sulphate reducers to form, or (2) other electron acceptors such as Mn which were initially present in small

quantities in this region of the plume have now been used up leaving sulphate as the most energetically favourable electron acceptor.

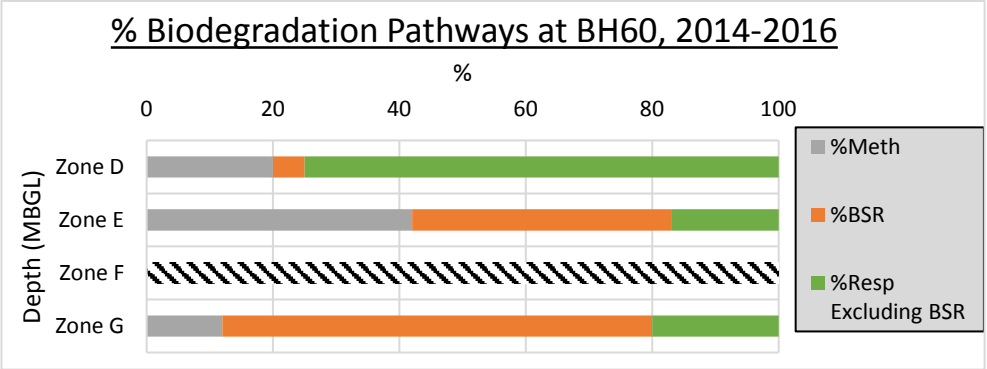

Figure 61. Average carbon balance for MLS60 between 2014 and 2016.

In light of the above, the conceptual model for this period can be considered similar to that of 2011/2012, however with a greater proportion of BSR within Zone G.

5.7. Carbon Balance Results – Changes in Turnover

Whilst the above analysis serves to outline the proportions of different biodegradation process within the plume, it should be appreciated that TDIC yields (as a proxy of total carbon turnover) are not consistent throughout the plume.

In order to quantify the raw TDIC yields (g/L) by process, TDIC values at any given depth can be multiplied by the relevant process proportion, from the calculations above (section 5.2.1). This will give an estimated TDIC yield (g/L) for each process.

These yields can then be depth integrated across the plume depth profiles in order to give an estimated plume turnover per process (g/L) at MLS59 and MLS60. However, it must be appreciated that as these results are based upon sampling positions at MLS59 and MLS60 only, their applicability the wider plume will require further discussion.

5.7.1. MLS59 – TDIC Turnover by Process

With regards to TDIC turnover at MLS59, it should be appreciated that total TDIC was typically in the range of 200 mg/L to 300 mg/L during the pre-pumping period, with values at the higher end of this range typically present within the upper plume (section 1.13.5). In contrast, during the years of pumping TDIC values were up to ~400 mg/L (Thornton et al, 2014; section 3.3.1), an increase of approximately 150 mg/L.

These TDIC values have been assigned to different processes based upon the turnover proportions previously calculated (sections 5.2.1 and 5.3.2) and the data is presented below (Figure 62).

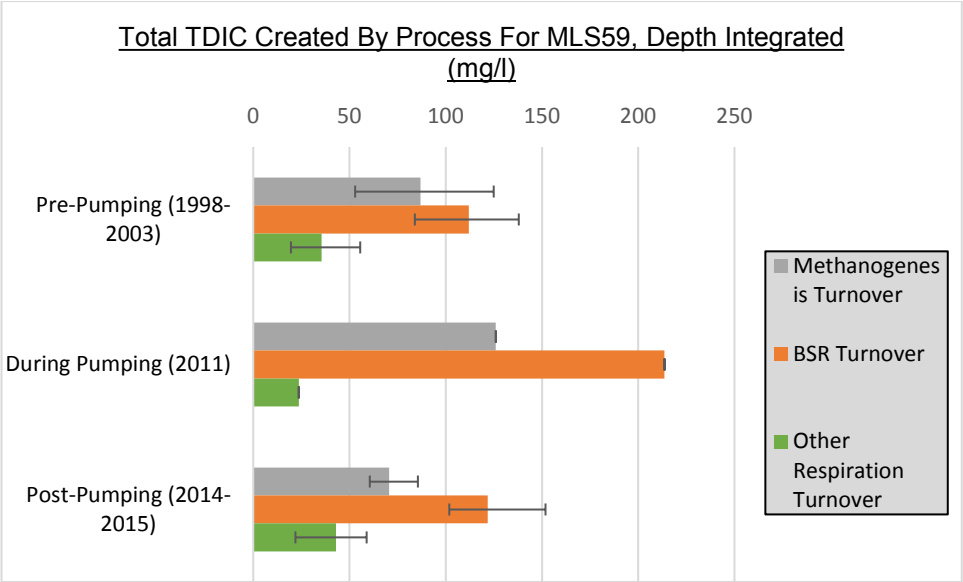

Figure 62. TDIC Created by process for MLS59, depth integrated (Yearly range indicated as error bars.

This data shows that methanogenesis and BSR appear to be generating significant amounts of TDIC, throughout all sampling rounds. Non-BSR respiration contributes to the TDIC pool in a more limited capacity.

With regards to respective changes between the pre-pumped, during pumping and post-pumped data; methanogenesis and BSR are seen to increase substantially upon the upstart of pumping. In order to better assess the shifts in TDIC creation enacted by different pumping conditions

it is possible to replot the above data utilising TDIC totals from the pre-pumping years as the zero-reference point (Figure 63).

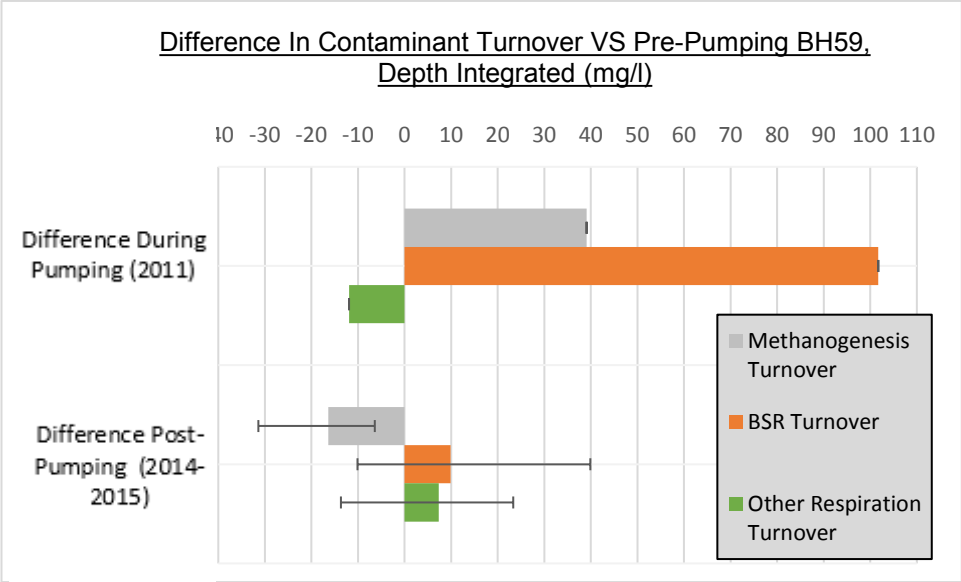

Figure 63. TDIC Created by process for MLS59, in relation to pre-pumping values (zero). Yearly range indicated as error bars.

Of the approximately 150 mg/L increase in TDIC values at MLS59, enacted due to pumping (section 3.3.1), BSR accounts for the vast majority of this increase, 102 mg/L, with methanogenesis contributing a 39 mg/L increase, respectively.

In addition, non-BSR respiration appears to decrease to a limited extent during this period. The reason for this decrease is uncertain, however it may be linked to variations in source term or groundwater flow (Section 1.13.1) affecting quantities of TPC within the plume fringe where the majority of other respiration is occurring.

Post-pumping turnover rated appear to return to those comparable to pre-pumping, with TDIC turnovers, for respective processes within 10 mg/L of pre-pumping values.

5.7.2. MLS60 – TDIC Turnover by Process

With regards to TDIC turnover at MLS60, it should be appreciated that total TDIC was typically in the range of 150 mg/L to 250 mg/L during the pre-

pumping period, with values at the higher end of this range typically present within the upper plume (section 1.13.5). In contrast, during the years of pumping TDIC values were typically between 200 mg/L and 350 mg/L throughout the plume (section 3.3.2).

These TDIC values have been assigned to different processes based upon the turnover proportions previously calculated (sections 5.2.1 and 5.3.2) and the data is presented below (Figure 64 and Figure 65).

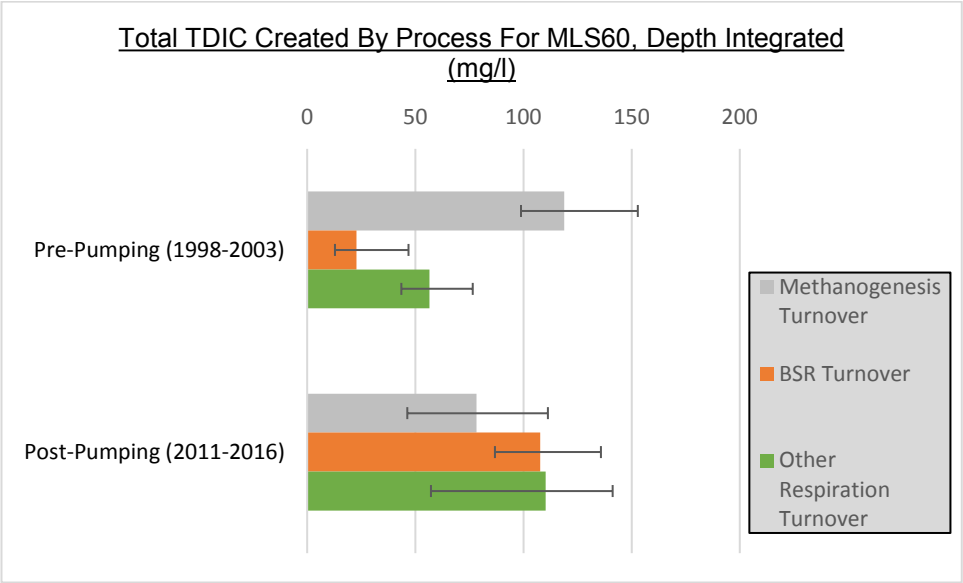

Figure 64. TDIC Created by process for MLS60, depth integrated. Yearly range indicated as error bars.

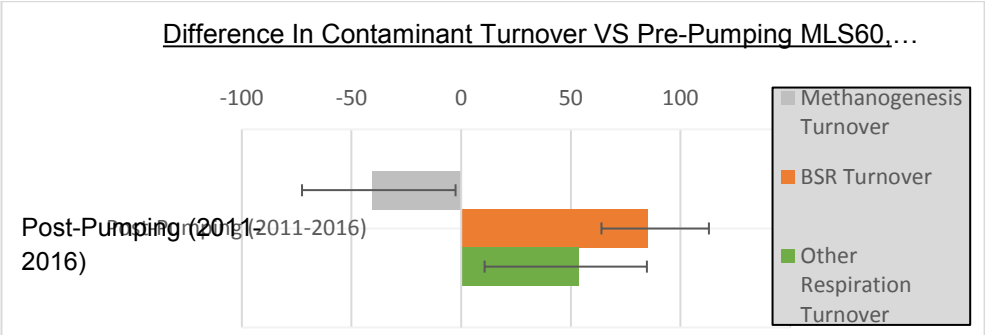

Figure 65. TDIC Created by process for MLS60, in relation to pre-pumping values (zero). Yearly range indicated as error bars.

This data shows that methanogenesis generates significant amounts of TDIC (119 mg/L) pre-pumping, with BSR and other respiration being of less importance, 23 mg/L and 57 mg/L respectively.

However, after the initiation of PAT at the site, both BSR and other respiration see massive increases, of 53 mg/L and 84 mg/L respectively, with methanogenesis turnover decreasing by 41 mg/L. The increases in BSR are likely linked to decreases in contaminant concentrations reducing plume toxicity, with increases in other respiration likely linked to additional mixing of nitrate and oxygen electron acceptors into the plume by the action of PAT.

5.8. Carbon Balance Results – Implications

Whist it should be appreciated that differences are present between the MLS59 and MLS60 sampling points, and between separate sampling rounds, the data above serves to outline an overall conceptual plume model , which is outlined below and is presented in diagramatic form in section 6.2. Furthermore this data can be reinforced by direct evidence from the field sampling rounds.

The following conceptual model is outlined, for pre-pumping scenarios;

Model Constraint	**Evidence**	**Comments**
Typical concentrations of TDIC are between 200 mg/L and 300 mg/L. Contaminant turnovers tend to be towards the lower end of this range in the inner plume core and towards the upper end of this range in plume fringe regions.	TDIC concentrations (section 3.3).	

Model Constraint	Evidence	Comments
A plume fringe (typically 2 m to 3 m), is present which is dominated by (non-BSR) respiration. This is likely to comprise oxic and nitrate respiration. BSR and methanogenesis are outcompeted in these regions by these more energetically favourable processes (section 1.9).	An abundance of nitrate electron acceptors in this region (section 3.2). δ^{34}S-SO_4 values comparable to background mineral acid values (section 3.5). Low methane concentrations (section 1.13) Respective carbon balances for plume fringe areas exhibit lower proportions of methanogenesis (<20 %) and BSR (<15 %).	Oxygen and nitrate are likely mixed into the plume from non-contaminated water outside the plume, via the action of diffusion and dispersion (section 1.6).
In outer core regions of the plume, where TPC concentrations are not consistently above 2 g/L, BSR occurs. However, the occurrence of BSR within these regions occurs concurrently with methanogenesis.	Enriched δ^{34}S-SO_4 values in comparison to background mineral acid values (section 3.5) Methane concentrations still exhibit δ^{34}C-CH_4 values indicative of some methanogenesis within these regions (Section 1.13). Respective carbon balances for outer plume core regions exhibit contaminant turnover due to both BSR (30 % to 60 %) and methanogenesis (30 % to 60 %).	TPC concentrations below 2 g/L are not considered high enough to supress BSR significantly (Spence et al, 2001b).

Model Constraint	Evidence	Comments
	However, little other respiration is present.	
In inner core regions of the plume (Typically >2 g/L TPC), methanogensis is dominant.	Methane concentrations exhibit δ^{34}C-CH_4 values indicative of large amounts of methanogenesis within these regions (section 1.13). Respective carbon balances for inner plume core regions indicate that methanogenesis is responsible for between 60 % and 80 % of TDIC creation pre-pumping (sections 5.6 and 5.7). but little other respiration (<20 %).	TPC concentrations above 2 g/L are considered high enough to supress BSR significantly (Spence et al, 2001b).

The follwing conceptual model is outlined, for regions of the plume affected by pumping;

Model Constraint	Evidence	Comments
Concentrations of TDIC are between 200 mg/L and 300 mg/L within the inner plume core. However, concentrations of TDIC are higher at depths close to the operation of the PAT system, where TPC concentrations have been significantly reduced (TDIC typically >300 mg/L).	TDIC concentrations (section 3.3).	The action of the PAT system may stimulate increased mixing of water rich in oxygen and nitrate into the plume from outside, allowing increased degradation around the plume fringe (sections 1.6 and 3.2.1.1).

Model Constraint	Evidence	Comments
TPC concentrations near to the plume fringe are also enhanced (Typically >400 mg/L).		
A plume fringe (typically 2 m to 3 m), is present which is dominated by (non-BSR) respiration turnover, which is likely oxic and nitrate respiration. BSR and methanogenesis are mainly outcompeted in these regions by these more energetically favourable processes (section 1.10).	An abundance of oxygen and nitrate electron acceptors in this region (section 3.2). Respective carbon balances for plume fringe areas exhibit lower proportions of methanogenesis (<30 %) and BSR (<10 %).	Oxygen and nitrate are likely mixed into the plume from non-contaminated water outside the plume, via the action of diffusion and dispersion (section 1.6).
In regions of the plume, where TPC concentrations are reduced to below 2 g/L, BSR is stimulated. The occurrence of BSR within these regions occurs concurrently with methanogenesis. However, the proportions of methanogenesis in these regions is significantly lower than during pre-pumping.	Enriched $\delta^{34}S$-SO_4 values in comparison to background mineral acid values and pre-pumping values (section 3.5). Methane concentrations still exhibit a $\delta^{34}C$-CH_4 indicative of some methanogenesis within these regions (section 3.6). Respective carbon balances for outer plume these regions indicate around 10 %, typically	TPC concentrations below 2 g/L are not considered high enough to supress BSR significantly (Spence et al, 2001b).

Model Constraint	Evidence	Comments
	lower than pre-pumping values of around 20 %.	
With reference to MLS60, it is possible for an inner core with regions of high TPC (>2 g/L) to persist in the plume during PAT. Methanogensis and AMO can both be active in these regions.	TPC values (section 3.1). Severely fluctuating δ^{34}C-CH_4 values, are indicative of large amounts of a delicate balance between methanogenesis and AMO within these regions (section 3.6.2).	TPC concentrations around 2 g/L are considered high enough to supress BSR significantly (Spence et al, 2001b). It is considered that AMO may be stimulated in these regions due to significant amounts of methane in these regions (section 3.6.2), creating favourable conditions for methane oxidisers to compete with or outcompete other biodegradation processes.
Plume 'constriction' can occur due to the afffect of the PAT system.	Decreased TPC concentrations, nitrate and TDIC concentrations around the plume fringes in 2016 (section 3). An increase of non-BSR related respiration within the above datasets.	

The follwing conceptual model is outlined, for the post-pumping scenario;

Model Constraint	Evidence	Comments

In-situ conditions become comparable to pre-pumping conditions. This occurs within a timescale of 2 to 3 years.	Respective carbon balances for the plume indicate that degradation pathways eventually return to those comparable to pre-pumping (section 5.6.3). Concentrations of many chemical parameters (e.g. TPC) have returned to pre-pumping values 2 years after the cessation of pumping. By 3 years after pumping in-situ chemistry is almost indistinguishable from pre-pumping (section 3).	

CHAPTER 6

6. Discussion and Conclusions

6.1. Discussion

6.1.1. Historical Plume Condition

Despite some yearly variance, previous studies provide a time-series of data which serve to outline that a plume of phenolic contaminants (TPC) is present at Four Ashes site, diving at a shallow angle (~5°; Spence et al, 2001a) into the upper layers of the unconfined Sherwood Sandstone aquifer below the site (sections 1.12 and 1.13).

Datasets gathered before the start of targeted PAT (section 1.13; Spence et al, 2001a; Thornton et al, 2014), demonstrate that during this period TPC concentrations within the plume are graded from lower concentrations at the plume fringe to higher concentrations within the plume core. Data from both MLS59 and MLS60, indicate that this grading within the plume can be utilised to broadly divide the plume into three different regions in relation to TPC concentrations (section 1.13). These regions are generally defined as (1) the plume fringe (TPC 2 mg/L – 50 mg/L), (2) the outer plume core (TPC 50 mg/L – 2000 mg/L) and (3) the inner plume core (TPC >2000 mg/L).

At the plume fringe, where the outer edges of the plume are mixing with external aquifer groundwater, which is free of phenolic contaminants, via dilution and dispersion (section 1.6), oxygen and nitrate are seen to be present in significant quantities (section 1.13.2). The presence of these electron acceptors strongly implies that aerobic and nitric reduction have a significant potential to contribute to contaminant turnover in this region. These processes are the most energetically favourable process for microbial contaminant biodegradation (Zehnder, 1988; Londry and Fedorak, 1991; Pickup et al, 2001), and as such outcompete the competition from other processes in this region (section 1.10).

In contrast to the plume fringe, both the inner and outer plume core exhibits negligible concentrations oxygen and nitrate, which are generally below detection limits. In addition to this, iron concentrations within the plume core are considered too low to indicate a contribution of iron reduction to contaminant turnover (section 1.13.4) and no such activity has been noted within previous studies of the plume (Spence et al, 2001a, Spence et al, 2001b).

The lack of viable, more-energetically favourable, biodegradation processes within the plume core acts to make BSR the most energetically favourable process which can be considered as viable within this region (Spence et al, 2001a). However, despite this, previous studies have demonstrated that the BSR is not always dominant within the plume core. Instead the function of sulphate reducing microbial communities within the plume core are dramatically influenced by TPC concentrations (Pickup et al, 2001; Spence et al, 2001a; Baker et al, 2012).

Within the outer plume core, where TPC concentrations are below 2 g/L, microbial activity is dominated by BSR as expected. However, for the inner plume core, which has significantly higher concentrations of TPC generally higher that 2 g/L, BSR is noted to be comparatively limited, with methanogenesis left as the only viable process in this region (Spence et al, 2001b). The mechanism responsible for this suppression of BSR at regions of high TPC is unconfirmed however it is consistent with toxic inhibition of BSR due to phenols known antimicrobial properties (section 1.13; Thornton et al, 2014).

Overall these data indicate that the pre-pumped plume generally conforms to the Cirpka et al. (1999) model, exhibiting an active plume fringe with mostly inactive plume core. However, where the Cirpka et al. (1999) model indicates a lack of externally supplied electron acceptors as the mechanism for the mostly inactive plume core, the mechanism at the Wolverhampton site is actually due to toxic inhibition of respiration processes within the plume core as significant concentrations of sulphate are present as part of the contaminant load.

6.1.2. Plume Condition During the Pilot Study (Thornton et al, 2014)

Remediation of the Four Ashes site by targeted PAT intervention started in late 2009. After this time, conditions within the Four Ashes plume are seen to shift significantly (section 1.16; Thornton et al, 2014). Data from 2012 demonstrate that TPC concentrations decrease within the plume under direct action from the PAT system, with the largest decreases (>5 g/L reduction) present at or close to the water extraction depths of the PAT system.

These changes in TPC concentrations are strongly coupled with significant increases in in-situ contaminant turnover at the site, with an approximate doubling of TDIC concentration (indicative of biodegradation, section 1.13.5) recorded in the initial 2012 dataset (Thornton et al, 2014). This increase in contaminant turnover was particularly notable at depths close to the action of the PAT system where the TPC concentrations were the most significantly reduced; in these regions TDIC concentrations increase by up to 3.5 times their original value.

In addition, alterations in the relative proportions of respiration and methanogenesis were noted in the post-PAT system. In particular, shifts away from methanogenesis towards respiration were noted to be present within regions of decreased TPC (Thornton et al, 2014).

6.1.3. Plume Conditions 2014 to 2016

Additional data gathered in 2014, 2015 and 2016 has been presented within this thesis (section 3), adding to previous time-series of data for the Four Ashes site. Where possible field data were collected using techniques similar to previous studies (section 2) in order to allow data to be directly compared.

This new time-series data continues to describe similar changes in plume hydrochemistry and biodegradation pathways to those seen, during pumping, in the Thornton et al (2014) pilot study, which reinforces and adds

further credence to the conclusions of that study (sections 1.13 and 6.1.3.1).
Due to the termination of pumping at MLS59, this 2014 to 2016 data also captures rebounding conditions after this cessation of PAT at MLS59 in 2011 (sections 5.6.3 and 6.1.3.2).

6.1.3.1. Step Change in Conditions During PAT Operation

In contrast to MLS59 where the cessation of PAT occurred in 2011, the action of PAT is continual at MLS60. In this region of the plume, pilot study data indicated a significant decrease in contaminant concentrations in relation to those pre-pumping (Thornton et al, 2014), due to the action of the PAT system. This decrease in contaminant concentrations was noted to persist throughout the 2014 to 2016 datasets, with TPC values close to those in the pilot study, albeit with a limited amount of yearly variation which is likely attributable to source term variability or changing groundwater flow (Section 1.13.1; Section 3.1.2).

These decreases in contaminant concentrations are most notable within the plume core where the PAT system is deliberately targeted. This is particularly true at MLS60, where contaminant values drop from ~5500 mg/L pre-pumping to ~2000 mg/L during pumping (section 3.1.2). However, the action of the PAT system appears to effect general decreases in contaminant concentrations, in pumped regions of the plume, during all years.

TDIC concentrations, in pumped MLS60 region of the plume, continued to show extremely similar values to those from Thornton et al (2014), indicating consistent amounts of contaminant turnover in this region during the 2012 to 2016 pumped period (section 3.3.2). Furthermore, TDIC during this period continued to be strongly defined by region and correlated with TPC concentrations, indicating that toxic inhibition of anaerobic processes at high TPC played the key role during this period (Spence et al, 2001b).

As such, substantial decreases in contaminant concentrations can be seen in the plume core in relation to pre-PAT conditions, coupled with increases

in contaminant turnover. Hence, it is therefore apparent that enhanced in-situ biodegradation can be seen within this region.

Furthermore, as contaminant concentrations and biodegradation rates between 2012 and 2016 are largely equivalent, it can be inferred that the that action of the PAT system is actually affecting a 'step change' on in-situ biogeochemical conditions, as opposed to a transient effect. It is considered that should the action of the PAT system remain consistent then this "step change" would likely persist until final plume collapse; holding contaminant concentrations at a reduced level and effecting enhanced in-situ biodegradation.

6.1.3.2. Rebounding Conditions Post PAT Operation

Pilot study data indicated that, for MLS59, a significant decrease in contaminant concentrations was affected during the period of PAT operation (Thornton et al, 2014). This decrease was particularly notable within the plume core where TPC concentrations reduced from values of ~4500 mg/L to ~1500 mg/L (section 1.16). However, data for the 2012 to 2015 period indicates rebounding contaminant levels after the cessation of PAT (section 3.1.1).

This recovery is consistent with known plume mechanics, as the volume of water in which contaminant concentrations had been previously reduced by PAT action migrates downgradient away from the MLS59, being replaced with unaffected contaminated water migrating from upgradient.

The recovery of TPC at MLS59 during this period was also coupled with a return of other hydro-chemical parameters to pre-pumping levels. Notably, sulphate concentrations and isotopic indications of BSR ($\delta^{34}S\text{-}SO_4$; section 3.5.1), are again similar to pre-pumping values, consistent with the mechanism described above.

Contaminant turnover during this period is still substantial within the upper plume core where contaminant concentrations fall below the toxic threshold for BSR (2 g/L; Spence et al, 2001a). However, a significant decrease in contaminant turnover is apparent within the lower plume core during the

2014 to 2015 period, where TDIC with values were seen to reduce from ~300 mg/L during pumping (2011) to ~150 mg/L post pumping (2014-2015; section 3.3). This decrease in contaminant turnover, coupled with the increases in contaminant concentrations during the same period, is consistent with the return of toxic suppression of BSR in this region as contaminant values recover to pre-pumping values above 2 g/L (section 3.1.1; Spence et al, 2001a).

The carbon balance during this period offers credence to the above, indicating a fall in the amount of contaminant turnover due to respiration, and particularly BSR, within the plume during this period (section 5.6.3). In addition, proportions of methanogenesis are seen to increase.

It is also worthy of note that some slight changes were observed within the upper plume core, which exhibits slightly lower values of contaminant turnover, during the 2014 to 2015 period. This may be indicative of early plume 'constriction' (section 6.1.3.3). However, in general TDIC levels are consistent with rates of contaminant turnover returning those similar pre-pumping, throughout most of the plume.

In light of the above, contaminant levels and other hydro-chemical parameters have remained consistently similar to those pre-pumping throughout the 2014 and 2015 sampling round (section 1.13). This signifies of the return of pre-pumping conditions and it is considered that this is indicative of a 'reversal of the initial step change'.

6.1.3.3. Plume 'Constriction'

As discussed above, decreased TDIC values were noted at MLS59 within the upper plume fringe during the 2015 sampling round (section 3.3.1), coupled with a slight increase in nitrate concentration (section 3.2.1). These changes become more apparent during the 2016 sampling round with nitrate values spiking throughout the plume and TDIC values falling significantly within the upper and lower plume fringes.

In addition to the above, contaminant concentrations at MLS59 drop below ~1500 mg/L throughout the plume core during 2016 with nitrate values

spiking infrequently (section 3.2.1). As contaminant turnover is also reduced during this period, it is considered unlikely that decreases in contaminant concentrations during this period are due to increased biodegradation. Water in these regions now appears to have strikingly similar characteristics to background water, adding credence plume 'constriction' within this region as an explanation.

A mechanism for such a plume 'constriction' does exist, namely as an effect of the changes in hydraulic conditions enacted by the PAT extracting water.

This 'constriction' could take place in a number of forms, one of which could including the 'upconing' of the water from depths below the base of the plume. This could be enacted by continuing the PAT operation at MLS60 which extracts water at significant depth (39m bgl), which may induce mixing of the plume and the breakdown of its stratification towards its base.

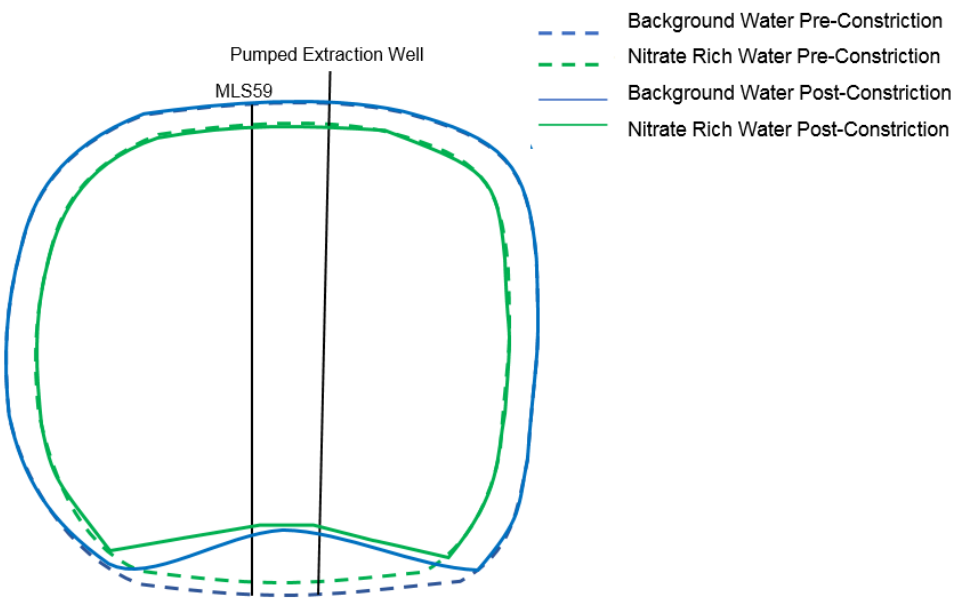

Figure 66. Front view of the plume at MLS59, showing an exaggerated conceptual model of an 'upconing' effect (not to scale).

It should be appreciated that the vertical distance from the edge of the plume to the pumping well is anticipated to be significantly shorter <10m than the lateral distance to the edge of the plume >30m, as determined by a 1 mg/L threshold (Thornton et al, 2014). In light of this it is considered

that vertical mixing of the plume is likely to be more significant than lateral mixing from greater distances.

It should be appreciated that the concentrations of TPC extracted by the well and the well pumping rate were not available to this study. However, it is known that the pumping well has been designed such that the capture zone of the well exceeds the edge of the plume, as defined by a 1 mg/L phenol contour (Aspinwall and Co. 1992). In light of this; the overall capture zone of the extraction well is >30m in width and lateral mixing still remains possible, albeit to a likely lesser extent than vertical mixing. Should specific data on the extraction well be made available, then this data could be utilised in order to undertake a more specific analysis which would aid with further interpretation of this data.

Notwithstanding the above, there remains the opportunity for a 'fingering' effect whereby media, such as nitrate, has been shown to intrude deeper into the plume in layers of higher hydraulic conductivities (Figure 67; Nicolaides et al, 2015). Hydraulic conductivities were previously measured in-situ at the plume and found typically fall between 1.5m day^{-1} and 2.5 m day^{-1} in the region of the plume (Thornton et al, 2014).

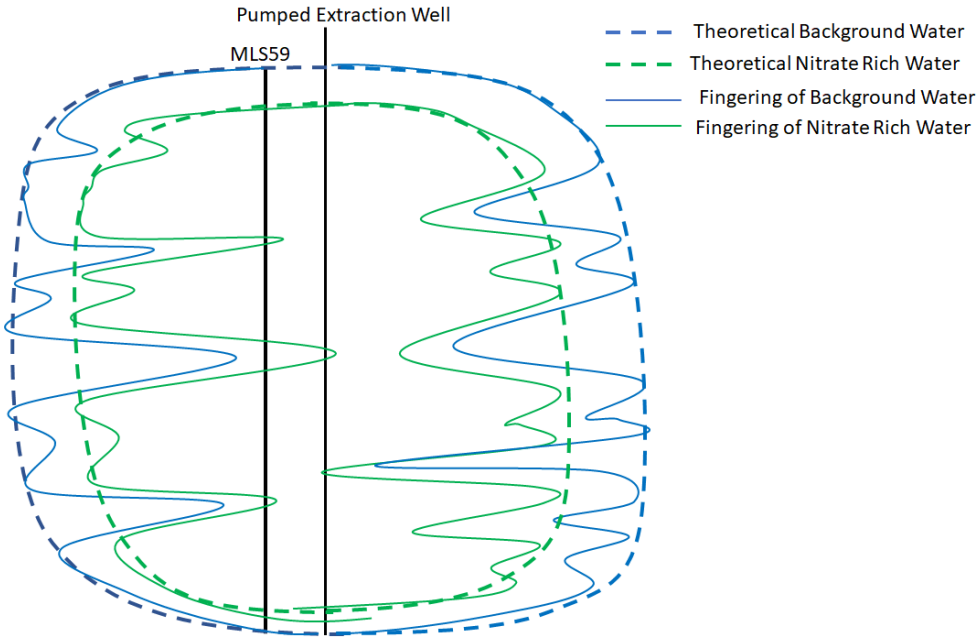

Figure 67. Front view of the plume at MLS59, showing an exaggerated conceptual model of the 'fingering' effect (not to scale).

Unfortunately, similar effects may also be seen due to a temporary decrease in contaminant source term or natural variations in the groundwater flow field (section 1.13.1), which may cause fluctuations in plume width or reductions in TPC at the plume fringe allowing nitrate to persist. Furthermore, such an effect was not seen at MSL60. In light of this, in order fully confirm the nature of these data, and/or the occurrence of plume constriction, further work would be required.

6.1.4. Shifting Biodegradation Mechanisms During PAT

Previous studies both related to this site and in related areas (Spence et al, 2001b, Baker et al, 2012, Harrison et al, 2001, Pickup et al, 2001) have demonstrated that the significance of different biodegradation pathways varies widely based upon relative in situ hydrological and chemical conditions.

Numerous hydrological and chemical factors have been noted to affect the dominance of biodegradation pathways, however data from the study site serves to outline that, amongst these factors, contaminant concentration is thought to exert the largest influence (Spence et al, 2001b, Thornton et al, 2001a, Baker et al, 2012, Thornton et al, 2014).

Carbon balance models (section 5), created for the plume by utilising the TDIC values, stable isotope and fractionation factor values gathered both during this research and from previous studies, show that biodegradation pathways at the Four Ashes site are drastically affected by the operation of the PAT system. These changes are particularly noticeable in the plume core where in-situ conditions are most strongly affected by the action of the PAT system.

6.1.4.1. Increases in Proportions of Respiration and BSR at MLS60

At MLS60, significant increases in respiration proportions were noted throughout the plume during the previous 2011 and 2012 sampling rounds (Thornton et al, 2014). From 2014 to 2016, proportions of respiration remain very similar to those in 2011 and 2012, with proportions of

respiration varying only marginally, <10 % difference, between 2011 and 2016 (section 5.6.5).

In particular, the largest increases in respiration are seen between 36 mbgl and 45 mbgl, where TPC concentrations have been most reduced, close to the operation depth of the PAT system. These increases in respiration are coupled with large increases in BSR, which on average accounts for approximately 75 % in the total increase in respiration (section 5.6.5). Notwithstanding the above, proportions of BSR do increase steadily during the period. Whilst the precise reason for this increase in BSR is unknown, it is consistent with a developing of a community of sulphate reducers within this region of the plume, which increasing outcompetes non-BSR reducers over time.

6.1.4.2. Concurrent AMO and BSR at MLS60

Both Methanogenesis and AMO are observed to occur concurrently with BSR at MLS60 (sections 3.6.2 and 5.6.5). Other studies have also noted similar concurrent utilisation of anaerobic electron acceptors and methanogenesis, even where methanogenesis is energetically unfavourable (Chapelle, 2001; Lee et al, 2008).

In particular, methanogenesis is still a significant process between 22 mbgl and 36 mbgl at MLS60 due to contaminant concentrations remaining over 2 g/L, however this process is also noted to a limited extent in most regions of the plume.

In contrast to the above, AMO appears to be limited entirely to the ‘border zone’ between the depths of maximum BSR (37 mbgl - 45 mbgl; section 3.5.2) and significant methanogenesis (22 mbgl - 25 mbgl; 3.6.2). In this region values of TPC are close to the 2 g/L threshold and somewhat variable, offering plausibility to the idea of cohabiting methanogens and sulphate reducers. It is reasoned that within this ‘border zone’ conditions are likely to facilitate methane production (via methanogenesis) with BSR reduction not completely supressed. Thus, with the presence of methane and sulphate reducing bacteria, this creates the potential for anaerobic oxidation of methane by sulphate reduction (Caldwell et al, 2008) within this

region. Unfortunately, data gathered within this thesis does not allow for quantification of this process.

6.1.5. Optimal Positioning of the PAT System

Pumping on site is currently being undertaken at a location which approximately bisects the plume laterally (Figure 12. Plan view of the plume, not to scale. Adapted from Baker et al (2012).; ~5 m offset from MLS60) and is targeted to the zone of highest contamination, 39 mbgl (Section 1.12.2). Pumping rates are not known for the current period but have historically been within the range of 0.3 m^3h^{-1} to 2.6 m^3h^{-1}.

When solely considering the PAT system in terms of ex-situ treatment, targeting the zone of highest contamination is likely to prove mechanically efficient by enabling the extraction of the largest amount of contamination for the least pumping. Furthermore, by positioning the extraction in a location which bisects the plume laterally a hydraulic containment zone which captures extents of the plume efficiently can be achieved (Section 1.4.3). Pumping rates have also been historically determined for the purpose of hydraulic containment (Section 1.12.2).

However, when considering the complex interactions that the PAT is enacting on the in-situ biodegradation, it is possible that an alternative well placement depth may prove more efficient. Different placement depths could lead to significant variations in vertical or lateral mixing; hence it may be possible to achieve further enhancement of in-situ biodegradation via this method.

Conceptually, should the extraction point be higher, increased mixing within the upper plume core could occur potentially reducing contaminant concentrations to below the 2 g/L threshold in this location (Section 3.1) and thus stimulating BSR (Section 1.13.4.2).

Should the extraction point be lower, it could be expected that the main zone of influence would fall below the lower plume core, allowing contaminant concentrations to recover to over 2 g/L in this area (Section 6.1.3.2). Thus, high contaminant toxicity would again be present reducing the potential for BSR (Section 1.13.4.2).

In terms of cost effectiveness, it should be appreciated that by moving the well away from the current positioning, in order to further enhance in-situ biodegradation, the mechanical effectiveness of the ex-situ treatment would be reduced. However, depending on the nature of a revised positioning, the increase in in-situ biodegradation and associated reduction in the amount of TPC required to be treated ex-situ may be sufficient to offset the respective loss in efficiency with regards to the mechanical effectiveness of the ex-situ treatment.

As part of further work, it would be highly beneficial to obtain extraction well data and information with regards to the cost of ex-situ TPC treatment. Accurate records of TPC concentrations within extracted water and pumping rates could be used in conjunction with data from this study to model different potential positionings for the extraction well, allowing further design of a ‘smart’ PAT system.

6.2. Revised Plume Model

Sampling rounds during pumped year have indicated that TDIC increased by an average by ~150 % within the plume during the years of active PAT (section 3.3). However, this increase in TDIC, and hence contaminant turnover, is not split evenly throughout the plume but instead strongly coupled with areas of where TPC has been decreased significantly by the action of the PAT system (section 3.1).

In particular, areas where TPC concentrations have been decreased to below 2 g/L threshold for BSR exhibit the largest changes in contaminant turnover (section 3.3). In contrast, areas where TPC experienced minimal changes due to the action of PAT intervention exhibited contaminant turnover levels more consistent with those seen during the pre-pumping period.

Analysis of the pumped years from both MLS59 and MLS60, indicates that total increases in contaminant turnover are around 250 mg/L - 300 mg/L within zones where TPC concentrations have been reduced to significantly below the 2 g/L threshold. This however can rise to above 400 mg/L at certain depths. In contrast, smaller increases of TDIC around 150 mg/L are

observed is areas where TPC has been decreased by the action of the PAT system but has not crossed below the 2 g/L threshold.

Stochiometric analysis, shows that plume water within PAT affected zones, where TPC <2 g/L, has been subject to intrinsic biodegradation of 40 mg/L - 50 mg/L during its lifetime (up 70 mg/L in some regions). In contrast a similar calculation shows that zones where TPC remained >2 g/L, even after the effects of PAT has been subject to lower amounts of biodegradation typically within the range of 20 mg/L – 30 mg/L during its lifetime.

Based on the above and previous data presented within this thesis (Section 3; Section 5), it is proposed that a conceptual model for biodegradation within the plume could utilise the following facts:

(1) A plume fringe in which nitrate reduction is dominant persists in the upper and lower regions of the plume. This fringe is typically 2m in vertical width, however the action of the PAT system appears to have increased this width of the upper plume fringe to approximately 4m at MLS60. Total biodegradation of TPC can be assumed to have occurred at the plume fringes;
(2) Water in zones of the plume where TPC has been reduced to below 2 g/L by the actions of PAT could be assumed to have undergone around 45 mg/L phenol of total biodegradation during its lifetime; and,
(3) Water in zones of the plume where TPC remains greater than 2 g/L could be assumed to have undergone around 25 mg/L Phenol of total biodegradation during its lifetime.

A conceptual plume model is presented as Figure 68, below. This conceptual model advances on that in previous studies exhibiting a nitrate reducing plume fringe similar to the Cirpka et al, (1999) model (Section 1.15.1) and utilising previous data and the toxic thresholds (Spence et al, 2001b) in light of the specific areas affected by the action of the PAT system (Section 3; Section 5).

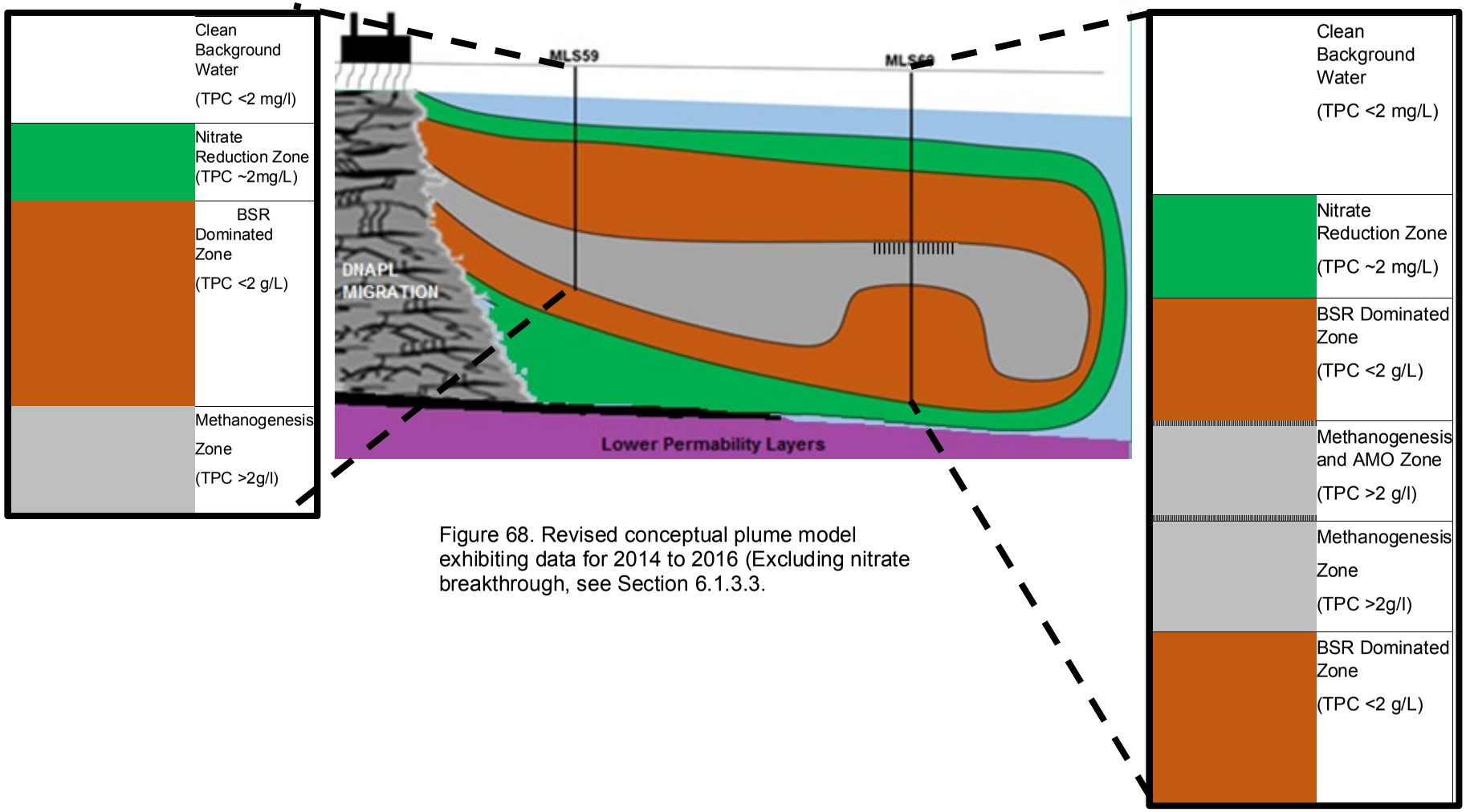

Figure 68. Revised conceptual plume model exhibiting data for 2014 to 2016 (Excluding nitrate breakthrough, see Section 6.1.3.3.

6.3. Conclusions

This thesis has presented a several new geochemical and isotopic datasets, both from samples taken in-situ at the Wolverhampton site (section 3) and from lab-based data which utilises media from the Wolverhampton site (section 4).

These results and the subsequent carbon balance analysis (section 5) and discussion (section 6) have served to highlight the following:

(1) The changes in plume geochemistry due to the PAT system, observed during the pilot study (Thornton et al, 2014) are not short-lived and are considered indicative of 'step change'. As such these new conditions are likely to persist so long as the PAT system continues to act;

(2) During pumping, there is a sustained increase in contaminant turnover for in regions in which the PAT has reduced the TPC concentrations, based on TDIC datasets;

(3) The mechanism responsible for the increase in contaminant turnover, within PAT affected regions, is BSR, based upon the carbon balance model. Data, including TPC values and $\delta^{34}S\text{-}SO_4$ isotope values, strongly indicate that the cause behind the increase of BSR is a reduction in plume toxicity; and,

(4) Indications of additional nitrate are present at MLS59, in later years. Data, including TPC and TDIC concentrations, indicate that this may be due to either plume constriction or a reduction in contaminant source term.

The evidence presented articulates that the action of the PAT system at the Wolverhampton site is sufficient to produce significant perturbations within the plume hydrochemistry. These perturbations allow additional mixing an enact altered contaminant loadings, reducing loadings to levels that favour the increased natural in-situ biodegradation at the site.

In turn, this increased in-situ biodegradation acts to increase the rate at which plume remediation progresses and lowers the amount of contaminated water which is required to be treated ex-situ. Thus, the

overall remediation costs are reduced and the carbon footprint of the treatment is lowered.

These findings have significance beyond the study site scenario and may be applicable to other contaminant plumes of similar hydrochemistry, similar PAT action or where contaminants are present that exhibit toxicity to microbes. Furthermore, the strength of the datasets provided add additional credibility to the use of stable isotopes and carbon balance techniques as a long term monitoring tool for contaminant plumes.

6.4. Recommendations for Further Work

Whilst this thesis has further defined the mechanisms of biodegradation within the plume at the Wolverhampton site, further study with regards to the site is merited in the following areas:

(1) Better constraint of the plume lifetime within PAT scenario. In order to achieve this, the data from this thesis could be fed into a reactive transport model. This model could be designed to look at:
    a. Plume lifetime with regards to either complete removal of the phenolic contaminants (although the feasibility of this should be assessed); and/or,
    b. Plume lifetime with regards to partial removal of phenolic contaminants such that the remaining contaminants are reduced to below the toxic threshold and have adequate time to biodegrade before reaching a given receptor;

(2) Better constraint of the lateral extent of the PAT affected zone. This could include further boreholes upstream of MLS60 in order to monitor the lateral extent of contaminant reductions. Any further data could then be fed back into the reactive transport model;

(3) Applicability of the new plume model to other contaminant plumes. This model may have applicability where:
    a. An excess of electron acceptors is present within the plume core, although not due to an influx from external uncontaminated water; and/or,
    b. With contaminants which may exhibit a similar toxic threshold; and,

(4) Further analysis of the nitrate ingress at MLS59. This could include additional time-series data, including nitrate and TPC concentrations, in order to better define the rate and extent of plume constriction and establish if any subsequent plume thinning may occur.

(5) Further design of the ‘smart’ PAT system. This could include obtaining well data with regards TPC concentrations in the extracted water and pumping rates. These data could then be used in conjunction with data from this study to model different potential positionings for the extraction well, in view of determining optimal positioning.

.

References

Aggarwal, P.K. and Hinchee, R.E. 1991. Monitoring in situ biodegradation of hydrocarbons using stable carbon isotopes. *Environmental Science and Technology*. **25**(6), pp.1178-1180.

Ajoku, G.A.O. and Oduola, M.K. 2013. Kinetic model of pH effect on bioremediation of crude petroleum contaminated soil. 1. model development. *American Journal of Chemical Engineering.* **1**(1), pp.6-10.

Anneser, B., Einsiedl, F., Meckenstock, R.U., Richters, L., Wisotzky, F. and Griebler, C. 2008. High-resolution monitoring of biogeochemical gradients in a tar oil-contaminated aquifer. *Applied Geochemistry*. **23**(6), pp.1715-1730.

Appelo, C. and Postma, D. 2005. *Geochemistry, Groundwater and Pollution*. 2nd Edition. Rotterdam: Balkema.

Aspinwall and Co. 1992. *Site Investigation at Synthetic Chemicals Limited, Four Ashes: Phase 6*. Unpublished.

Baker, K.M., Bottrell, S.H., Thornton, S.F., Peel, K.E. and Spence, M.J. 2012. Effect of contaminant concentration on *in situ* bacterial sulfate reduction and methanogenesis in phenol-contaminated groundwater. *Applied Geochemistry*. **27**(10), pp.2010-2018.

Bear, J., Cheng, A.H.D. 2010. *Modeling Groundwater Flow and Contaminant Transport*. Unknown: Springer-Science.

Bedient, P.B. and Rifai, H.S. 1992. Ground water contaminant modeling for bioremediation: A review. *Journal of Hazardous Materials*. **32**(2-3), pp.225-243.

Brüchert, V. and Pratt, L.M. 1999. Stable Sulfur Isotopic Evidence for Historical Changes of Sulfur Cycling in Estuarine Sediments from Northern Florida. *Aquatic Geochemistry*. **5**(3), pp.249-268.

Baker G. 1977. Anaerobic digestion of aromatic compounds in the presence of nitrate. *FEMS Microbiology Letters*. **1**, pp.103-108.

Bottrell S.H., Hayes P.J., Bannon M. and Williams G.M. 1995. Bacterial sulfate reduction and pyrite formation in a polluted sand aquifer. *Geomicrobiology Journal*. **13**(2), pp.75-90.

Buttle, J.M. 1994. Isotope hydrograph separations and rapid delivery of pre-event water from drainage basins. *Progress in Physical Geography*. **18**(1), pp.16-41.

Canfield, D.E. 1993. Organic Matter Oxidation in Marine Sediments. In: Wollast R., Mackenzie F.T. and Chou L. eds. *Interactions of C, N, P and S Biogeochemical Cycles and Global Change. NATO ASI Series (Series 1: Global Environmental Change), vol 4.* Berlin: Springer, pp.333-363.

Canfield, D.E. and Des Marais, D.J. 1993. 1. Biogeochemical cycles of carbon, sulfur, and free oxygen in a microbial mat. *Geochimica et Cosmochimica Acta*. **57**(16), pp.3971-3984.

Carey, M. A., Finnamore, J. R., Morrey, M. J. and Marsland, P. A. 2000. *R&D Publication 95: Guidance on the Assessment and Monitoring of Natural Attenuation of Contaminants in Groundwater*. [Online]. Almondsbury: Environment Agency. [Accessed 20 05 2015]. Available from: https://www.claire.co.uk/component/phocadownload/category/27-wall-documents%3Fdownload%3D569:guidance-on-the-assessment-and-monitoring-of-natural-attentuation-of-contaminants-in-groundwater+&cd=1&hl=en&ct=clnk&gl=uk.

Chapelle, F.H., McMahon, P.B., Dubrovsky, N.M., Fujii, R.F., Oaksford, E.T. and Vroblesky, D.A. 1995. Deducing the Distribution of Terminal Electron-Accepting Processes in Hydrologically Diverse Groundwater Systems. *Water Resources Research*. **31**(2), pp.359-371.

Chapelle, F.H., Vroblesky, D.A., Woodward, J.C. and Lovley, D.R. 1997. Practical Considerations for Measuring Hydrogen Concentrations in Groundwater. *Environmental Science and Technology*. **31**(10), pp.2873-2877.

Chapelle, F. 2001. *Ground-water Microbiology and Geochemistry*. New York: John Wiley & Sons.

Chapelle, F.H., Bradley, P.M., Thomas, M.A. and McMahon, P.B. 2009. Distinguishing Iron-Reducing from Sulfate-Reducing Conditions. *Groundwater*. **47**(2), pp.300-305.

Cherry, J.A. 1984. Contaminant Migration in Groundwater: Processes and problems. In: Wilson J. Ed. *Proceedings of the 2nd National Groundwater Conference – The Fate of Toxics in Surface and Groundwater.* Philadelphia, Academy of Natural Sciences. pp. 72.

Cherry, J.A., Gillham, R.W. and Barker, J.F. 1984. Contaminants in groundwater: Chemical processes. In: Bredehoeft. J.D. Ed. *Groundwater contamination*. Washington, D.C.: National Academy Press. pp. 46-64.

Christensen, T.H, Bjerg, P.L., Banwart, S.A., Jakobsen, R. Heron, G. and Albrechtsen, H.J. 2000. Characterization of redox conditions in groundwater contaminant plumes. *Journal of Contaminant Hydrology*. **45,** pp.165–241.

CL:AIRE. 2002. *CL:AIRE Technical Bulletin Number 2: Multilevel Sampling Systems*. [Online]. London: CL:AIRE. [Accessed 02 02 2015]. Available from: https://www.claire.co.uk/component/phocadownload/category/17-technical-bulletins.

Cohen, R.M., Mercer, J.W., Greenwald, R.M. and Beljin, M.S. 1997. *Design guidelines for conventional pump-and-treat systems*. [Online]. Washington DC: United States Environmental Protection Agency. [Accessed 18 07 2019]. Available from: https://www.lm.doe.gov/cercla/documents/Weldon Spring_docs/Groundwater/GW-900-901-1.05.pdf.

Cribbin, L.B., Winstanley, H.F., Mitchell, S.L., Fowler, A.C. and Sander, G.C. 2014. Reaction front formation in contaminant plumes. *Journal of contaminant hydrology*. **171**, pp.12-21.

Chu, M., Kitanidis, P.K. and McCarty, P.L. 2005. Modeling microbial reactions at the plume fringe subject to transverse mixing in porous media: When can the rates of microbial reaction be assumed to be instantaneous?. *Water resources research*. **41**(6), pp.1-15.

Cirpka, O.A., Frind, E.O. and Helmig, R. 1999. Numerical simulation of biodegradation controlled by transverse mixing. *Journal of Contaminant Hydrology*. **40**(2), pp.159-182.

Chambers, L.A. and Trudinger, P.A. 1979. Microbiological fractionation of stable sulfur isotopes: A review and critique. *Geomicrobiology Journal*. **1**, pp.249-293.

Craig, H. 1957. Isotopic standards for carbon and oxygen and correction factors for mass-spectrometric analysis of carbon dioxide. *Geochimica et Cosmochimica Acta*. **12**, pp.133-149.

Department for Environment, Food and Rural Affairs (DEFRA). *SP1001: Contaminated Land Remediation*. [Online]. UK: DEFRA. [Accessed 12 09 2016]. Available from: http://sciencesearch.defra.gov.uk/Default.aspx?Menu=Menu&Module=More&Location=None&Completed=0&ProjectID=16184.

Dohare, D., Deshpande, S. and Kotiya, A. 2014. Analysis of groundwater quality parameters: A review. *Research Journal of Engineering Sciences*. **3**(5), pp.26-31.

Environment Agency. 2001. *Guidance on monitoring of landfill: Leachate, Groundwater and Surface Water. R&D Report HOCO_232*. [Online]. Bristol: Environment Agency. [Accessed 23 11 2016]. Available at: https://www.sepa.org.uk/media/28992/guidance-on-monitoring-of-landfill-leachate-groundwater-and-surface-water.pdf.

Environment Agency. 2005. *Indicators for Land Contamination*. [Online]. Bristol: Environment Agency. [Accessed 22 11 2016]. Available at: https://assets.publishing.service.gov.uk/government/uploads/system/uploads/attachment_data/file/290711/scho0805bjmd-e-e.pdf.

Environment Agency. 2006. *Science Report SC020093: Guidance on the design and installation of groundwater quality monitoring points*. [Online]. Bristol: Environment Agency. [Accessed 23 11 2016]. Available at: https://assets.publishing.service.gov.uk/government/uploads/system/uploads/attachment_data/file/290727/scho0106bkct-e-e.pdf.

Environment Agency. 2016. *Dealing with contaminated land in England*. [Online]. Bristol: Environment Agency. [Accessed 05 01 2016]. Available at: https://assets.publishing.service.gov.uk/government/uploads/system/uploads/attachment_data/file/513158/State_of_contaminated_land_report.pdf.

Environmental Protection Act 1990 c. 43. Controller of HMSO:UK.

European Commission. 2013. *Science for Environment Policy In-depth Report: Soil Contamination: Impacts on Human Health*. [Online]. [Accessed 25 07 2016]. Available at: http://ec.europa.eu/science-environment-policy.

Foght, J., 2008. Anaerobic Biodegradation of Aromatic Hydrocarbons: Pathways and Prospects. *Journal of Molecular Microbiology and Biotechnology*. **15**(2-3), pp.93-120.

Fowler, A.C., Winstanley, H.F., McGuinness, M.J. and Cribbin, L.B. 2014. Oscillations in soil bacterial redox reactions. *Journal of theoretical biology*. **342**, pp.33-38.

Gorde, S.P. and Jadhav, M.V. 2013. Assessment of Water Quality Parameters: A Review. *Journal of Engineering Research and Applications*. **3**(6), pp.2029-2035.

Guo, L., Santschi, P.H. and Warnken, K.W. 1995. Dynamics of dissolved organic carbon (DOC) in oceanic environments. *Limnology and Oceanography*. **40**, pp.1392-1403.

Harrison, I., Williams, G.M., Higgo, J.J.W., Leader, R.U., Kim, A.W. and Noy, D.J. 2001. Microcosm studies of microbial degradation in a coal tar distillate plume. *Journal of contaminant hydrology*. **53**(3-4), pp.319-340.

Huber, S. and Prokop, A. 2012. *Progress in the management of contaminated sites*. Luxembourg: Publications Office of the European Union.

Hunkeler, D., Höhener, P., Bernasconi, S. and Zeyer, J. 1999a. Engineered in situ bioremediation of a petroleum hydrocarbon-contaminated aquifer: assessment of mineralization based on alkalinity, inorganic carbon and stable carbon isotope balances. *Journal of Contaminant Hydrogeology*. **37**, pp.201–223.

Hunkeler, D., Aravena, R. and Butler, B.J. 1999b. Monitoring Microbial Dechlorination of Tetrachloroethene (PCE) in Groundwater Using Compound-Specific Stable Carbon Isotope Ratios: Microcosm and Field Studies. *Environmental Science and Technology*. **33**(16), pp.2733-2738.

Hoefs, J. 2018. *Stable Isotope Geochemistry*. 8th Edition. Switzerland: Springer International Publishing.

Hoffman, F. 1993. Groundwater remediation using “smart pump and treat”. *Groundwater*. **31**(1), pp.98-106.

Kaplan, I. R. 1975. Stable Isotopes as a Guide to Biogeochemical Processes. *Proceedings of the Royal Society of London: Series B, Biological Sciences*. London: Royal Society. **189**(1095), pp.183–211.

Kendall, C. and Caldwell E.A. 1998. Chapter 2 - Fundamentals of Isotope Geochemistry. In: Kendall, C. and McDonnell, J.J. eds. *Isotope Tracers in Catchment Hydrology*. Unspecified: Elsevier, pp.51-86.

Kumari, R.K. and Mohan, P.M. 2018. Review on Dissolved Organic Carbon and Particulate Organic Carbon in Marine Environment. *Indonesian Journal of Marine Sciences*. **23**(1), pp.25-36.

Lerner, D.N., Thornton, S.F., Spence, M.J., Banwart, S.A., Bottrell, S.H., Higgo, J.J., Mallinson, H.E., Pickup, R.W. and Williams, G.M. 2000. Ineffective natural attenuation of degradable organic compounds in a phenol-contaminated aquifer. *Groundwater*. **38**(6), pp.922-928.

Lerner, D.N. Kueper, B.H. Wealthall, G.P. Smith, J.W.N. and Leharne, S.A. 2003. *An illustrated handbook of DNAPL transport and fate in the subsurface*. [Online]. Bristol: Environment Agency. [Accessed 20 08 2018]. Available from: http:// eprints.whiterose.ac.uk/90412/1/DNAPL%20 handbook%20final.pdf.

Logue, J.B., Findlay, S.E. and Comte, J. 2015. Microbial responses to environmental changes. *Frontiers in microbiology*. **6**, p.1364.

Logue, J.B., Stedmon, C.A., Kellerman, A.M., Nielsen, N.J., Andersson, A.F., Laudon, H., Lindström, E.S. and Kritzberg, E.S. 2016. Experimental insights into the importance of aquatic bacterial community composition to

the degradation of dissolved organic matter. *The ISME Journal*. **10**(3), p.533.

Massmann, G., Tichomirowa., M., Merz, C. and Pekdeger, A. 2003. Sulfide oxidation and sulfate reduction in a shallow groundwater system (Oderbruch Aquifer, Germany). *Journal of Hydrology*. **278**(1–4), pp.231-243.

Mayer, K.U., Benner, S.G., Frind, E.O., Thornton, S.F. and Lerner, D.N. 2001. Reactive transport modeling of processes controlling the distribution and natural attenuation of phenolic compounds in a deep sandstone aquifer. *Journal of Contaminant Hydrology*. **53**(3-4), pp.341-368.

McDonnell, J.J. and Kendall, C. 1992. Isotope tracers in hydrology. *Eos Transactions American Geophysical Union*. **73**(24), pp.260-261.

McMahon, A., Heathcote, J., Carey, M. and Erskine, A., 2001. Guide to good practice for the development of conceptual models and the selection and application of mathematical models of contaminant transport processes in the subsurface. National Groundwater & Contaminated Land Centre. Environment Agency. UK. Report NC/99/38, 2.

McMahon, P.B. and Chapelle, F.H. 2008. Redox processes and water quality of selected principal aquifer systems. *Groundwater*. **46**(2), pp.259-271.

McMillan, L.A., Rivett, M.O., Wealthall, G.P., Zeeb, P. and Dumble, P., 2018. Monitoring well utility in a heterogeneous DNAPL source zone area: Insights from proximal multilevel sampler wells and sampling capture-zone modelling. *Journal of contaminant hydrology*, **210**(1), pp.15-30.

Mercer, J.W., Skip, D.C. and Griffin, D. 1990. *Basics of pump-and-treat ground-water remediation technology*. [Online]. Robert S. Kerr Environmental Research Laboratory: US Environmental Protection Agency. [Accessed 25 02 2016]. Available from: https://nepis.epa.gov/Exe/ZyPURL.cgi?Dockey=30001IV1.txt.

Meckenstock, R.U., Elsner, M., Griebler, C., Lueders, T., Stumpp, C., Aamand, J., Agathos, S.N., Albrechtsen, H.J., Bastiaens, L., Bjerg, P.L. and Boon, N. 2015. Biodegradation: updating the concepts of control for

microbial cleanup in contaminated aquifers. *Environmental Science and Technology*. **49**(12), pp.7073–7081.

Morris, B.L. 2005. Hydrogeological notes for the Sheffield district. British Geological Survey. [Online]. Unpublished: British Geological Survey. [Accessed: 22/07/2019]. Available from: http://nora.nerc.ac.uk/id/eprint/11049/

Nicolaides, C., Jha B., CuetoFelgueroso L. and Juanes, R. 2015. Impact of viscous fingering and permeability heterogeneity on fluid mixing in porous media. *Water Resources Research*. **51**(4), pp.2634–2647.

Nielsen, D. and Nielsen, G. 2007. *The Essential Handbook of Ground-Water Sampling*. Boca Raton: CRC Press.

Newton, R. and Bottrell, S. 2007. Stable isotopes of carbon and sulphur as indicators of environmental change: past and present. *Journal of The Geological Society*. **164**, pp.91-708.

National House-Building Council and Environment Agency. 2008. *R&D Publication 66: Guidance for the Safe Development of Housing on Land Affected by Contamination*. [Online]. Bristol: Environment Agency. [Accessed 30 08 2018]. Available from: http://www.nhbc.co.uk/NHBCPublications/LiteratureLibrary/Technical/filedownload,33595,en.pdf.

Nyer, E.K., Palmer, P.L., Carman, E.P., Boettcher, G., Bedessem, J.M., Lenzo, F., Crossman, T.L., Rorech, G.J. and Kidd, D.F. 2001. *In-situ Treatment Technology*. [Online]. Boca Raton: Taylor & Francis Group. [Accessed 25 06 2017]. Available from: https://www.taylorfrancis.com/books/9781566705288.

Pickup, R.W., Rhodes, G., Alamillo, M.L., Mallinson, H.E.H., Thornton, S.F. and Lerner, D.N. 2001. Microbiological analysis of multi-level borehole samples from a contaminated groundwater system. *Journal of Contaminant Hydrology*. **53**(3-4), pp.269-284.

Puls, R.W. and Barcelona, M.J., 1996. *Low-flow (minimal drawdown) ground-water sampling procedures*. Michigan: US Environmental Protection Agency.

Rayleigh, S.R.S. 1896. Theoretical considerations respecting the separation of gases by diffusion and similar processes. *The London, Edinburgh, and Dublin Philosophical Magazine and Journal of Science*, **42**(259), pp.493-498.

Rees, H.C., Oswald, S.E., Banwart, S.A., Pickup, R.W. and Lerner, D.N. 2007. Biodegradation processes in a laboratory-scale groundwater contaminant plume assessed by fluorescence imaging and microbial analysis. *Applied and environmental microbiology*. **73**(12), pp.3865-3876.

Rivett, M.O., Petts, J., Butler, B. and Martin, I. 2002. Remediation of contaminated land and groundwater: experience in England and Wales. *Journal of Environmental Management*. **65**(3), pp.251-268.

Rivett, M.O., Chapman, S.W., Allen-King, R.M., Feenstra, S. and Cherry, J.A. 2006. Pump-and-treat remediation of chlorinated solvent contamination at a controlled field-experiment site. *Environmental science and technology*. **40**(21), pp.6770-6781.

Rivett, M.O. Tomlinson, D.W., Thornton, S.F., Thomas, A.O., Leharne, S.A. and Wealthall, G.P. 2014. *An Illustrated Handbook of LNAPL Transport and Fate in the Subsurface*. [Online]. London: CL:AIRE. [Accessed 10 02 2018]. Available from: www.claire.co.uk/LNAPL.

Rizoulis, A., Elliott, D.R., Rolfe, S.A., Thornton, S.F., Banwart, S.A., Pickup, R.W. and Scholes, J.D., 2013. Diversity of planktonic and attached bacterial communities in a phenol-contaminated sandstone aquifer. *Microbial Ecology*. **66**(1), pp.84-95.

Schulze-Makuch, D. 2009. Advection, dispersion, sorption, degredation, attenuation. In: Silveira, L. and Usunoff, E.J. eds. *Groundwater – Volume 2*. Paris: EOLS, pp.55-69.

Spence M.J. 2001. *Isotopic Fractionation as a Diagnostic Tool for In-situ Biodegradation.* Ph.D. thesis, University of Leeds.

Spence, M.J., Bottrell, S.H., Higgo, J.J.W, Harrison, I. and Fallick, A.E. 2001a. Denitrification and phenol degradation in a contaminated aquifer. *Journal of Contaminant Hydrology*. **53**(3–4), pp.305-318.

Spence, M.J., Bottrell, S.H., Thornton, S.F. and Lerner, D.N. 2001b. Isotopic modelling of the significance of bacterial sulphate reduction for phenol attenuation in a contaminated aquifer. *Journal of Contaminant Hydrology*. **53**(3–4), pp.285-304.

Summersgill, I.M. 2014. Remediation and redevelopment of derelict land in the UK-lessons learnt over three decades; Challenges remaining. In: Bouazza, A., Yuen, S.T.S. and Brown, B. eds. *7th International Congress on Environmental Geotechnics: iceg2014*. Barton: ACT, pp.206-218.

Syms, P. 2010. *Land, Development and Design*. 2nd Edition. Chichester: Blackwell Publishing Limited.

Thornton, S.F., Quigley, S., Spence, M.J., Banwart, S.A., Bottrell, S. and Lerner, D.N. 2001a. Processes controlling the distribution and natural attenuation of dissolved phenolic compounds in a deep sandstone aquifer. *Journal of Contaminant Hydrology*. **53**(3-4), pp.233-267.

Thornton, S.F., Lerner D.N. and Banwart S.A. 2001b. Assessing the natural attenuation of organic contaminants in aquifers using plume-scale electron and carbon balances: model development and analysis of uncertainty and parameter sensitivity. *Journal of Contaminant Hydrogeology*. **53**(3-4), pp.199-232.

Thornton, S.F., Baker, K.M., Bottrell, S.H., Rolfe, S.A., McNamee, P., Forrest, F., Duffield, P., Wilson, R.D., Fairburn, A.W. and Cieslak, L.A. 2014. Enhancement of in situ biodegradation of organic compounds in groundwater by targeted pump and treat intervention. *Applied Geochemistry*. **48**, pp.28-40.

Tuxen, N., Albrechtsen, H.J. and Bjerg, P.L. 2006. Identification of a reactive degradation zone at a landfill leachate plume fringe using high resolution sampling and incubation techniques. *Journal of Contaminant Hydrology*. **85**(3-4), pp.179-194.

US EPA. 1996. *Pump and Treat Ground Water Remediation A Guide for Decision Makers and Practitioners*. [Online]. [Accessed 25 05 2016 YYYY]. Available from: https://nepis.epa.gov/Exe/ZyPURL.cgi?Dockey= 30004PC8.txt.

US EPA. 2008. *Systematic Approach for Evaluation of Capture Zones at Pump and Treat Systems*: *Final Project Report*. [Online]. [Accessed 25 05 2016]. Available from: https://nepis.epa.gov/Exe/ZyPURL.cgi?Dockey=60000MYO.txt.

Van Breukelen, B.M. and Griffioen, J. 2004. Biogeochemical processes at the fringe of a landfill leachate pollution plume: potential for dissolved organic carbon, Fe(II), Mn(II), NH_4, and CH_4 oxidation. *Journal of Contaminant Hydrology*. **73**(1-4), pp.181-205.

Valentin L., Nousiainen, A. and Mikkonen, A. 2013. Introduction to Organic Contaminants in Soil: Concepts and Risks. In: Vicent, T., Caminal, G., Eljarrat, E. and Barceló, D. eds. *Emerging Organic Contaminants in Sludges: Analysis, Fate and Biological Treatment*. Berlin Heidelberg: Springer-Verlag, pp.1-29.

Vidali, M., 2001. Bioremediation. an overview. *Pure and Applied Chemistry*. **73**(7), pp.1163-1172.

Williams, G.M., Pickup, R.W., Thornton, S.F., Lerner, D.N., Mallinson, H.E.H., Moore, Y. and White, C. 2001. Biogeochemical characterisation of a coal tar distillate plume. *Journal of Contaminant Hydrogeology*. **53**(3-4), pp.175-197.

Whiticar, M.J. 1999. Carbon and hydrogen isotope systematics of bacterial formation and oxidisation of methane. *Chemical Geology*. **161**(1), pp.291-314.

Whiticar, M. J. and Faber, E. 1985. Methane oxidation in marine and limnic sediments and water columns. *Proceedings of the 12th International Meeting on Organic Geochemistry*. In: D. Leythauser and J. Rullkotter. Eds. *Advances in Organic Geochemistry.* Federal Republic of Germany, Jülich, p. 20.

Whiticar, M.J., Faber, E. and Schoell, M. 1986. Biogenic methane formation in marine and freshwater environments: CO_2 reduction *vs.* acetate fermentation - Isotope evidence. *Geochimica et Cosmochimica Acta*. **50**(5), pp.693-709.

Wu, Y., Lerner, D.N., Banwart, S.A., Thornton, S.F. and Pickup, R.W. 2006. Persistence of fermentative process to phenolic toxicity in groundwater. *Journal of Environmental Quality*. **35**(6), pp.2021-2025.

Zhang, X., Huang, G.H., Lin, Q. and Yu, H. 2009. Petroleum-contaminated groundwater remediation systems design: A data envelopment analysis based approach. *Expert Systems with Applications*. **36**(3), pp.5666-5672.

Appendix 1 – Field Data

MLS59 – 2014

Data Analysed by Sheffield GRPG	
Data Analysed at University of Leeds	

Depth (mbgl)	Total phenols (mg/L)	TDIC (mg/L)	O2 (dissolved - mg/L)	NO3- (mg/L)	Mn (mg/L)	Fe (mg/L)	SO4 (mg/L)	S2- (mg/L)	Acetate (mg/L)	CH4 (aq), mg/L	TDIC-d13C (per mill)	SO4-d34S (per mill)	CH4-d13C (per mill)
5	#N/A	38.7	#N/A	#N/A	#N/A	#N/A	#N/A	0.0	#N/A	0.0	-19.0	4.1	#N/A
6	0.0	48.3	8.1	46.2	0.0	0.2	20.9	0.0	0.0	0.0	-18.6	4.2	#N/A
7	0.0	39.2	7.8	44.4	0.0	5.0	20.0	0.0	0.0	0.0	-18.9	4.4	#N/A
8	0.0	48.1	7.3	42.2	0.0	0.2	22.6	0.0	0.0	0.0	-18.7	4.2	#N/A
9	0.0	61.7	6.8	44.2	0.0	0.2	20.7	0.0	0.0	0.0	-18.3	3.6	#N/A
10	0.0	55.0	5.4	45.9	0.1	0.2	20.7	0.0	0.0	0.1	-18.4	3.9	#N/A
11	1.8	151.2	0.0	10.6	0.5	1.1	9.8	0.0	12.5	1.1	-19.6	4.1	-45.3
12	0.0	278.8	0.0	0.0	1.5	4.3	7.6	89.2	80.8	4.8	-16.9	14.8	-51.6
13	19.9	236.1	0.0	0.0	2.0	4.6	2.3	14.5	65.2	14.9	-17.3	14.8	-54.5
14	103.2	241.0	0.0	0.0	2.0	4.5	1.0	48.2	9.6	2.1	-17.3	#N/A	-57.1
15	#N/A	#N/A	#N/A	#N/A	#N/A	#N/A	#N/A	#N/A	#N/A	0.0	#N/A	#N/A	#N/A
16	#N/A	#N/A	#N/A	#N/A	#N/A	#N/A	#N/A	#N/A	#N/A	0.0	#N/A	#N/A	#N/A
17	0.0	326.5	0.0	0.0	6.5	18.8	17.0	209.8	42.0	1.0	-18.4	12.3	-55.8
18	99.9	305.2	4.5	0.2	14.4	31.0	38.7	50.6	23.2	2.3	-19.1	14.6	-59.7
19	118.7	309.4	0.0	0.0	12.3	32.6	32.2	16.9	31.1	5.4	-19.3	14.6	-61.2
20	#N/A	#N/A	#N/A	#N/A	#N/A	#N/A	#N/A	#N/A	#N/A	0.0	#N/A	#N/A	#N/A
21	2075.4	288.6	0.0	0.3	11.8	29.6	80.7	26.5	44.1	3.0	-19.6	10.9	-58.0
22	759.4	316.8	0.0	0.1	11.5	25.6	25.9	33.8	35.2	3.6	-18.9	12.5	-55.2
23	4509.5	283.5	0.0	1.7	11.4	32.0	59.8	24.1	47.3	10.4	-19.3	6.9	-55.5
24	834.3	314.0	0.0	0.2	8.5	27.0	21.7	139.9	35.0	0.6	-18.9	11.2	-50.6
25	3632.9	236.2	0.6	1.8	10.4	33.4	62.3	33.8	47.0	5.2	-19.8	5.0	-56.0
26	6082.8	213.5	0.0	3.0	7.6	25.0	87.8	19.3	42.5	8.4	-19.2	4.2	-57.2
27	4067.7	250.2	0.0	1.1	6.9	25.4	58.8	0.0	38.6	9.7	-19.0	5.4	-56.5
28	5406.0	251.6	0.0	0.9	6.7	24.7	74.4	4.8	39.1	8.9	-18.0	5.5	-54.7
29	1847.1	246.1	0.0	0.8	6.2	22.7	28.8	0.0	37.2	10.5	-18.3	6.3	-58.2
30	741.3	91.2	0.0	3.4	2.0	8.0	22.5	43.4	13.3	2.7	-19.6	5.0	-46.0

MLS59 – 2015

Depth (mbgl)	Total phenols (mg/L)	TDIC (mg/L)	O2 (dissolved - mg/L)	NO3- (mg/L)	Mn (mg/L)	Fe (mg/L)	SO4 (mg/L)	S2- (mg/L)	Acetate (mg/L)	CH4 (aq), mg/L	TDIC-d13C (per mill)	SO4-d34S (per mill)	CH4-d13C (per mill)
5	0.0	44.2	5.9	43.3	0.0	0.0	21.6	0.0	0.0	#DIV/0!	-19.0	4.1	#N/A
6	0.0	58.2	6.1	47.6	0.0	0.0	23.2	0.0	0.0	0.0	-18.6	4.2	#N/A
7	0.0	49.3	6.1	43.1	0.0	0.0	21.9	0.0	0.0	0.0	-18.9	4.4	#N/A
8	0.0	71.9	5.5	45.3	0.0	0.0	23.4	0.0	0.0	0.0	-18.7	4.2	#N/A
9	0.0	60.5	5.4	44.5	0.0	0.0	22.3	0.0	0.0	0.0	-18.3	3.6	#N/A
10	0.0	55.2	4.9	41.4	0.0	0.1	20.9	0.0	0.0	0.0	c	3.9	#N/A
11	15.8	232.4	0.9	16.2	0.2	0.4	12.7	0.0	0.0	11.8	-19.6	4.1	-47.1
12	112.4	245.3	0.0	14.7	1.0	3.1	16.1	93.9	10.7	16.0	-16.9	14.8	-54.0
13	92.9	225.7	0.0	12.1	1.5	2.8	14.0	16.0	9.0	19.2	-1.3	14.8	-52.5
14	107.6	206.8	0.0	1.6	1.7	4.7	10.3	50.4	9.8	11.0	-17.3	#N/A	-57.8
15	#N/A		#N/A	#N/A	#N/A	#N/A	#N/A	#N/A	#N/A	0.0	#N/A	#N/A	#N/A
16	#N/A		#N/A	#N/A	#N/A	#N/A	#N/A	#N/A	#N/A	0.0	#N/A	#N/A	#N/A
17	79.1	274.4	0.0	12.3	6.9	28.7	25.9	222.2	4.4	13.0	-18.4	12.3	-56.8
18	89.5	275.9	0.0	0.0	9.6	38.8	37.0	52.7	1.2	11.4	-19.1	14.6	-63.1
19	82.8	267.7	0.0	8.9	7.8	32.3	27.1	16.0	4.2	13.9	-19.3	14.6	-56.2
20	#N/A		#N/A	#N/A	#N/A	#N/A	#N/A	#N/A	#N/A	0.0	#N/A	#N/A	#N/A
21	469.3	262.7	0.0	11.6	24.9	5.9	36.0	27.5	5.4	11.5	-19.6	10.9	-61.5
22	0.0	257.1	0.0	0.0	18.2	4.3	6.0	36.7	0.8	7.0	-18.9	12.5	#N/A
23	179.0	249.3	0.0	0.8	19.1	4.3	22.1	25.2	5.2	5.7	-19.3	6.9	-60.4
24	228.8	241.7	0.0	1.1	21.9	4.2	21.1	18.3	5.0	10.0	-18.9	11.2	-61.3
25	3411.3	175.2	0.0	0.9	20.0	4.6	38.1	36.7	4.8	13.6	-19.8	5.0	-42.9
26	3299.9	178.2	0.0	14.9	20.4	4.9	48.9	146.6	6.0	13.9	-19.2	4.2	-56.2
27	3432.8	195.4	0.0	11.8	15.9	4.4	46.8	0.0	5.6	13.9	-19.0	5.4	-58.1
28	2392.6	202.9	0.0	12.1	14.5	4.3	34.0	4.6	5.5	10.3	-18.0	5.5	-56.2
29	1764.6	247.3	3.3	10.8	14.4	4.5	24.3	0.0	5.9	14.6	-18.3	6.3	-56.5
30	262.2	92.7	2.6	14.1	0.3	0.2	11.0	41.2	0.9	3.3	-19.6	5.0	-40.4

MLS59 – 2016

Depth (mbgl)	Total phenols (mg/L)	TDIC (mg/L)	O2 (dissolved - mg/L)	NO3- (mg/L)	Mn (mg/L)	Fe (mg/L)	SO4 (mg/L)	S2- (mg/L)	Acetate (mg/L)	CH4 (aq), mg/L	TDIC-d13C (per mill)	SO4-d34S (per mill)	CH4-d13C (per mill)
5	0.0	71.1	-	43.6	1.3	0.2	20.7	0.0	0.0	0.0	-19.9	4.2	#N/A
6	0.0	65.4	-	37.2	6.1	0.2	19.1	0.0	0.0	0.0	-18.3	4.2	#N/A
7	0.0	73.2	-	42.7	0.8	0.2	19.0	0.0	0.0	0.0	-19.3	4.4	#N/A
8	0.0	43.3	-	39.0	2.2	0.2	19.5	0.0	0.0	0.1	-20.4	4.6	#N/A
9	0.0	66.8	-	38.1	2.7	0.2	18.6	0.0	0.0	0.0	#N/A	4.4	#N/A
10	0.0	69.7	-	13.4	9.2	0.2	19.5	0.0	0.0	0.0	-19.9	4.0	#N/A
11	0.0	202.2	-	6.0	56.6	0.4	6.2	0.2	0.0	1.8	-20.6	8.2	-47.7
12	56.6	223.4	-	3.6	1088.4	2.6	7.3	0.6	13.0	1.3	-20.4	10.4	-54.9
13	46.0	267.4	-	0.0	1255.1	1.6	6.6	0.1	0.0	13.5	-17.9	15.7	-60.5
14	77.0	332.4	-	0.0	1575.0	3.4	0.8	0.3	3.6	4.8	-17.1	16.0	-60.4
15	#N/A	#N/A	-	#N/A	#N/A	#N/A	#N/A	#N/A	#N/A	#DIV/0!	#N/A	#N/A	#N/A
16	#N/A	#N/A	-	#N/A	#N/A	#N/A	#N/A	#N/A	#N/A	#DIV/0!	#N/A	#N/A	#N/A
17	129.5	337.6	-	0.0	4249.0	16.3	32.5	1.9	3.2	11.1	-19.6	16.7	-63.8
18	109.9	257.4	-	0.0	7990.4	33.0	34.0	1.6	6.7	4.8	-20.3	15.3	-60.4
19	99.6	288.9	-	0.0	7000.7	25.3	23.1	0.6	4.1	4.6	-19.8	17.3	-63.6
20	#N/A	#N/A	-	#N/A	#N/A	#N/A	#N/A	#N/A	#N/A	#DIV/0!	#N/A	#N/A	#N/A
21	321.0	383.9	-	0.0	424899.2	13.2	42.3	0.8	8.4	8.2	-20.0	16.2	-64.8
22	57.9	359.3	-	0.0	1960.7	6.9	1.7	0.9	4.7	3.1	-18.9	16.4	-66.8
23	92.4	338.0	-	0.0	1910.4	8.3	1.3	0.5	6.7	3.6	-18.5	14.0	-58.1
24	63.1	295.6	-	0.0	1626.5	9.2	0.3	0.4	1.2	3.3	-19.0	10.5	-38.9
25	189.6	145.9	-	0.0	2395.5	19.1	1.8	0.2	4.2	2.6	-18.8	10.0	-38.8
26	255.8	181.5	-	0.0	2335.7	20.9	4.5	0.7	5.1	12.2	-19.6	6.2	-60.5
27	#N/A	58.4	-	0.0	1601.6	5.4	46.4	0.6	0.0	0.0	-19.5	5.3	-58.8
28	68.8	100.7	-	21.5	200.8	0.2	42.0	0.0	0.0	0.1	-19.4	4.3	-55.3
29	59.8	58.8	-	32.9	254.9	0.3	18.6	0.0	0.0	0.0	-19.6	7.4	-44.4
30	116.1	53.1	-	26.5	4.9	0.2	22.2	0.2	0.0	0.0	-21.2	5.3	-49.3

MLS60 – 2014

Depth (mbgl)	Total phenols (mg/L)	TDIC (mg/L)	O2 (dissolved - mg/L)	NO3- (mg/L)	Mn (mg/L)	Fe (mg/L)	SO4 (mg/L)	S2- (mg/L)	Acetate (mg/L)	CH4 (aq), mg/L	TDIC-d13C (per mill)	SO4-d34S (per mill)	CH4-d13C (per mill)
6	0.00	40.49	6.20	42.51	0.02	0.22	10.42	0.00	0.13	0.02	-21.50	5.80	#N/A
7	#N/A	#N/A	#N/A	#N/A	#N/A	#N/A	#N/A	#N/A	#N/A	#N/A	#N/A	#N/A	#N/A
8	0.00	41.45	5.10	41.63	0.00	0.18	11.69	0.00	0.00	0.02	-20.80	5.40	#N/A
9	#N/A	#N/A	#N/A	#N/A	#N/A	#N/A	#N/A	#N/A	#N/A	#N/A	#N/A	#N/A	#N/A
10	0.00	38.16	4.90	42.96	0.01	0.17	11.43	0.00	0.10	0.01	-21.60	5.60	#N/A
11	#N/A	#N/A	#N/A	#N/A	#N/A	#N/A	#N/A	#N/A	#N/A	#N/A	#N/A	#N/A	#N/A
12	0.00	33.91	1.60	75.26	0.10	0.23	27.61	0.00	0.00	0.01	-22.00	2.80	#N/A
13	#N/A	#N/A	#N/A	#N/A	#N/A	#N/A	#N/A	#N/A	#N/A	#N/A	#N/A	#N/A	#N/A
14	0.00	18.87	1.50	89.72	0.23	0.09	43.12	0.00	0.00	0.01	-16.90	2.90	#N/A
15	#N/A	#N/A	#N/A	#N/A	#N/A	#N/A	#N/A	#N/A	#N/A	#N/A	#N/A	#N/A	#N/A
16	0.00	29.32	0.60	84.82	0.21	0.13	44.92	0.00	0.00	0.01	-19.60	2.40	#N/A
17	#N/A	#N/A	#N/A	#N/A	#N/A	#N/A	#N/A	#N/A	#N/A	#N/A	#N/A	#N/A	#N/A
18	0.00	56.23	0.00	44.07	1.56	0.23	50.87	0.00	0.00	0.14	-21.20	9.20	#N/A
19	0.00	100.36	0.00	25.16	2.32	0.36	57.15	0.00	0.00	0.22	-19.10	14.20	#N/A
20	0.00	92.92	0.00	24.84	2.29	0.27	59.21	0.00	0.00	0.22	-24.40	13.60	#N/A
21	9.97	196.23	0.00	17.31	9.15	25.52	71.59	142.30	2.97	0.30	-21.70	14.90	-42.40
22	486.36	431.11	2.20	0.27	21.68	36.18	185.02	156.80	47.30	0.60	-18.00	9.10	-48.00
23	573.25	463.68	0.00	0.09	25.31	31.90	210.32	91.60	50.22	1.75	-18.00	8.40	-48.50
24	519.73	473.11	0.00	0.18	23.33	30.92	223.83	#N/A	45.20	1.79	-18.40	8.40	-49.00
25	579.42	481.02	0.00	0.00	23.47	33.34	207.00	123.00	50.25	2.02	-18.50	8.40	-49.20
26	659.39	429.08	0.80		25.17	32.52		67.50		1.44	-18.60	8.00	-49.00
27	2730.27	277.44	0.00	0.51	46.50	46.64	359.46	246.00	161.00	4.38	-17.40	5.10	-52.60
28	4158.86	173.56	0.00	0.78	33.28	42.96	270.39	98.90	109.07	6.18	-18.50	4.70	-52.20
29	4261.55	#N/A	0.50	0.98	31.56	33.98	249.25	#N/A	93.95	5.80	#N/A	#N/A	#N/A
30	4496.82	125.09	2.00	1.35	24.04	11.23	209.80	118.20	83.00	4.31	-21.90	4.50	-52.00
31	5317.27	119.77	0.00	1.14	20.00	6.02	181.54	144.70	68.55	6.35	-21.00	4.80	-51.70
32	5266.14	133.28	0.00	0.78	19.13	6.02	177.17	19.30	69.37	7.82	-23.00	4.60	-53.40
33	4892.39	117.38	3.50	1.15	19.70	4.91	179.02	79.60	68.82	2.05	-24.40	5.40	-50.60
34	4721.23	124.76	0.00	0.82	19.07	4.96	183.79	0.00	66.17	6.76	-25.10	4.80	-50.60
35	3896.93	251.82	0.40	1.38	13.77	6.38	141.33	0.00	27.97	1.27	-20.90	#N/A	-45.70
36	4649.93	234.45	0.50	2.36	13.39	4.43	193.22	0.00	23.05	#N/A	-19.40	4.30	-48.20
37	1431.74	296.78	1.70	0.34	9.04	7.18	54.30	38.60	26.00	0.22	-21.30	6.80	-42.20
38	1671.17	296.58	1.90	0.15	10.85	8.79	56.07	127.80	10.13	0.08	-20.70	6.70	-44.20
39	1396.14	264.87	0.50	0.07	8.01	4.95	48.12	154.40	15.72	0.46	-20.80	6.30	-50.80
40	857.59	290.55	0.00	0.00	8.10	20.69	26.06	209.80	26.97	0.54	-21.00	6.60	-55.10
41	117.23	270.41	3.80	0.09	5.06	46.32	5.07	79.60	43.22	0.19	-20.50	20.10	-63.30
42	142.99	323.04	0.80	0.16	5.59	52.76	2.29	200.20	120.46	0.57	-19.90	15.70	-55.00
43	50.20	285.49	0.00	1.93	5.05	47.85	3.38	209.80	44.79	0.52	-20.30	13.40	-57.80
44	47.68	222.41	0.00	0.23	4.63	33.48	15.37	306.30	7.83	0.42	-20.60	17.50	-43.50
45	2238.66	132.12	0.00	13.40	10.12	4.15	100.13	9.60	25.96	2.07	-20.70	5.70	#N/A

MLS60 – 2015

Depth (mbgl)	Total phenols (mg/L)	TDIC (mg/L)	O2 (dissolved - mg/L)	NO3- (mg/L)	Mn (mg/L)	Fe (mg/L)	SO4 (mg/L)	S2- (mg/L)	Acetate (mg/L)	CH4 (aq), mg/L	TDIC-d13C (per mill)	SO4-d34S (per mill)	CH4-d13C (per mill)
6	0.00	38.88	5.80	76.97	0.32	0.10	17.03	0.00	0.00	0.00	-21.80	5.80	#N/A
7	0.00	40.61	#N/A	81.57	0.01	0.00	17.54	0.00	0.00	#N/A	-20.80	5.80	#N/A
8	0.00	45.30	5.50	74.56	0.00	0.04	15.29	0.00	0.00	0.00	-21.60	5.70	#N/A
9	0.00	43.79	#N/A	77.91		0.00	15.53	0.00	0.00	#N/A	-21.20	5.80	#N/A
10	0.00	38.08	4.60	81.31	0.00	0.00	16.10	0.00	0.00	0.00	-20.60	5.70	#N/A
11	0.00	43.71	#N/A	70.16	0.00	0.00	15.13	0.00	0.00	#N/A	-20.20	5.80	#N/A
12	0.00	42.01	1.20	81.22	0.07	0.00	22.28	0.00	0.00	0.00	-20.70	4.00	#N/A
13	0.00	37.93	#N/A	71.31	0.09	0.00	15.01	0.00	0.00	#N/A	-17.90	3.50	#N/A
14	0.00	33.72	0.60	90.94	0.12	0.00	41.16	0.00	0.00	0.00	-16.40	3.50	#N/A
15	#N/A	#N/A	#N/A	#N/A	#N/A	#N/A	#N/A	#N/A	#N/A	#N/A	#N/A	#N/A	#N/A
16	0.00	39.85	0.20	91.32	0.15	0.00	44.33	0.00	0.00	0.00	-20.10	3.20	#N/A
17	#N/A	#N/A	#N/A	#N/A	#N/A	#N/A	#N/A	#N/A	#N/A	#N/A	#N/A	#N/A	#N/A
18	0.00	95.11	0.40	55.14	0.97	0.00	45.20	0.00	0.00	0.07	-22.20	13.70	#N/A
19	0.00	117.12	0.10	31.75	1.71	0.00	53.40	0.00	0.00	0.20	-22.10	16.40	#N/A
20	0.66	134.51	0.00	35.47	1.62	0.00	51.41	0.00	0.00	0.19	-22.65	16.20	-42.90
21	0.64	247.25	0.00	11.94	7.38	31.17	58.40	151.22	0.00	0.34	-21.10	5.80	#N/A
22	226.17	476.66	0.80	0.70	18.48	44.72	186.08	164.96	5.79	1.28	#N/A	9.50	-57.60
23	331.15	476.65	0.00	0.27	21.69	29.89	236.87	96.23	7.98	2.48	#N/A	8.90	-50.60
24	287.71	484.04	0.00	0.71	22.64	33.61	220.87	#N/A	7.53	2.44	-17.00	8.70	-55.40
25	303.04	500.93	0.00	0.71	21.54	33.60	212.79	128.31	7.48	1.16	#N/A	8.90	-53.80
26	346.31	445.82	0.00	4.11	20.80	26.90	245.69	71.03	8.69	1.57	-16.60	8.50	#N/A
27	1420.00	268.30	0.00	5.97	38.16	44.56	338.69	258.90	18.10	3.44	#N/A	5.50	-58.10
28	2143.11	352.98	0.00	4.84	28.55	43.26	268.00	105.39	12.75	1.91	-15.40	5.30	-45.20
29	2286.21		0.00	7.53	23.91	24.42	248.68	#N/A	0.00	5.92	#N/A	5.00	-42.70
30	2675.83	165.41	0.00	6.80	16.04	7.16	200.40	123.72	0.00	6.46	-21.90	#N/A	#N/A
31	2791.25	111.24	1.10	6.11	14.14	4.08	175.49	153.51	0.00	5.75	-17.80	5.50	-41.70
32	2885.82	125.82	0.00	4.90	13.25	3.72	184.24	20.62	0.00	7.22	-17.80	5.60	-37.50
33	2845.44	107.48	0.90	2.24	14.86	3.75	176.84	82.48	0.00	5.63	#N/A	5.60	-59.20
34	2966.29	120.92	0.40	4.08	14.69	2.92	180.59	0.00	0.00	1.33	-18.70	5.40	-61.00
35	1715.54	226.44	0.20	8.43	9.69	12.51	135.74	0.00	0.00	1.19	-20.00	5.60	-63.30
36	1841.37	166.73	1.80	1.08	9.14	10.85	146.74	0.00	0.00	0.11	-18.80	5.10	-61.50
37	787.97	291.37	0.90	1.09	6.41	7.98	54.56	41.24	0.00	0.40	-19.20	7.60	-61.30
38	770.89	306.80	0.20	10.61	8.06	12.62	57.40	132.89	0.00	0.24	-19.70	8.20	#N/A
39	634.73	309.57	0.00	10.14	5.69	17.22	37.78	162.67	0.00	0.50	#N/A	7.30	-83.40
40	228.72	294.49	0.80	8.51	4.89	47.82	17.61	222.24	0.00	0.78	-19.10	7.60	-75.50
41	5.70	244.58	0.50	1.00	4.06	44.18	0.65	114.56	0.00	1.00	#N/A	16.40	-73.60
42	0.00	320.75	1.40	0.00	3.80	38.48	0.02	210.79	0.00	0.66	-19.10	13.30	#N/A
43	3.26	256.03	0.80	1.01	3.47	32.57	0.57	222.24	0.00	0.62	#N/A	13.00	#N/A
44	19.74	200.44	0.20	0.69	3.68	20.62	12.56	323.06	0.00	0.70	-19.00	#N/A	-72.40
45	1206.61	138.52	3.60	15.08	7.01	3.53	92.66	9.16	0.00	0.61	-22.20	12.50	-57.0

MLS60 – 2016

Depth (mbgl)	Total phenols (mg/L)	TDIC (mg/L)	O2 (dissolved - mg/L)	NO3- (mg/L)	Mn (mg/L)	Fe (mg/L)	SO4 (mg/L)	S2- (mg/L)	Acetate (mg/L)	CH4 (aq), mg/L	TDIC-d13C (per mill)	SO4-d34S (per mill)	CH4-d13C (per mill)
6	0.00	60.79	-	98.39	0.00	0.17	17.67	0.00	0.00	#N/A	-21.00	5.80	#N/A
7	0.00	42.29	-	104.73	0.00	0.17	16.65	0.00	0.00	0.000601	-20.70	5.80	#N/A
8	0.00	46.59	-	98.96	0.00	0.16	17.28	0.00	0.00	#DIV/0!	-22.00	5.50	#N/A
9	0.00	48.96	-	97.51	0.01	0.22	17.59	0.00	0.00	0.000313	-21.60	5.50	#N/A
10	1.90	#N/A	-	95.13	0.00	0.14	17.68	0.21	0.00	#DIV/0!	-21.20	5.70	#N/A
11	2.20	46.68	-	97.23	0.00	0.14	16.79	#N/A	0.00	0.000421	#N/A	#N/A	#N/A
12	2.17	35.94	-	78.03	0.12	0.06	31.87	0.10	0.00	#DIV/0!	-24.00	2.70	#N/A
13	0.00	41.34	-	65.16	0.10	0.06	37.20	0.10	0.00	0.000906	-22.45	2.50	#N/A
14	0.00	41.59	-	67.87	0.12	0.05	44.36	0.24	0.00	#DIV/0!	-23.00	2.70	#N/A
15	#N/A	#N/A	#N/A	#N/A	#N/A	#N/A	#N/A	#N/A	#N/A	0.000252	#N/A	#N/A	#N/A
16	0.00	44.57	-	57.39	0.14	0.04	43.78	#N/A	0.00	#DIV/0!	#N/A	#N/A	#N/A
17	#N/A	#N/A	#N/A	#N/A	#N/A	#N/A	#N/A	#N/A	#N/A	0.001299	#N/A	#N/A	#N/A
18	0.00	93.50	-	9.63	0.94	0.08	51.24	0.03	0.00	#DIV/0!	-23.00	15.00	#N/A
19	0.00	128.23	-	21.55	0.01	0.17	51.73	0.07	0.00	0.108087	-22.55	17.00	-47.90
20	5.60	117.10	-	24.20	0.62	0.16	53.98	0.10	0.00	0.194427	-23.34	16.80	-56.60
21	2.94	185.33	-	1.09	6.51	25.32	65.81	0.72	0.02	0.174004	-21.79	7.40	-61.20
22	365.03	431.35	-	0.00	4.70	43.14	194.08	1.28	8.66	0.32257	-20.15	11.60	-61.70
23	264.85	489.63	-	0.00	18.67	36.80	210.59	1.48	3.01	1.671922	#N/A	11.90	-58.40
24	241.69	452.00	-	0.00	20.61	30.92	238.47	#N/A	11.55	2.197024	-20.23	8.90	-57.20
25	236.26	444.26	-	0.00	17.73	33.36	214.48	0.45	10.87	1.787353	-18.84	10.90	-56.40
26	448.65	518.79	-	0.11	19.27	38.14	244.42	0.85	12.68	1.049886	-19.00	10.50	-59.60
27	1113.96	327.26	-	0.16	0.12	56.77	369.20	1.50	5.27	2.069487	-19.29	6.00	-45.40
28	3090.51	230.95	-	0.68	0.12	50.32	270.07	1.52	13.57	3.563795	-19.88	7.00	-57.50
29	3025.75	#N/A	-	1.66	0.12	35.99	268.97	0.35	18.68	4.631577	-20.45	7.20	-60.60
30	5066.04	250.47	-	1.19	19.06	12.27	231.17	0.22	15.01	5.019285	-21.68	6.00	-45.60
31	6419.18	123.37	-	1.25	15.01	6.40	184.22	0.32	15.10	4.907448	-23.48	6.10	-45.80
32	4867.58	118.95	-	1.49	15.90	6.39	182.77	0.23	14.33	6.142531	-23.48	6.30	-59.10
33	1830.48	124.90	-	1.15	15.26	5.61	182.94	0.50	12.36	4.493066	-23.45	6.70	-60.80
34	5312.49	125.44	-	1.19	15.05	5.72	190.58	0.38	14.35	4.359585	-23.39	6.30	-60.60
35	3623.60	224.83	-	1.11	13.44	9.34	172.35	0.84	7.07	2.266613	-22.19	8.00	-60.70
36	1611.64	110.26	-	1.01	10.32	10.50	143.02	0.61	6.60	1.234907	-23.04	6.70	-64.90
37	825.83	335.96	-	0.23	7.88	16.92	54.50	0.60	6.61	0.737207	-24.36	10.20	-79.70
38	746.67	368.33	-	0.00	10.72	14.09	56.20	1.38	2.01	0.536027	-25.14	11.50	-76.60
39	637.20	375.25	-	0.00	7.28	12.16	48.01	1.65	6.86	0.144457	-19.70	10.50	-79.80
40	841.92	344.71	-	0.11	5.05	44.01	18.72	0.87	13.00	0.573073	#N/A	11.40	-89.30
41	165.26	284.49	-	0.16	3.94	41.43	6.29	1.30	16.29	0.82801	-19.80	16.20	-98.90
42	132.38	284.36	-	0.00	3.88	35.66	4.33	1.53	13.42	1.040396	-21.00	22.80	-92.50
43	132.37	327.35	-	0.00	4.06	38.41	7.70	1.41	4.20	0.218646	-20.00	20.40	-89.20
44	0.00	278.19	-	0.00	4.03	22.79	12.89	0.64	0.72	0.480829	-19.60	20.10	-75.50
45	975.23	148.53	-	19.56	7.29	3.73	85.50	0.00	8.25	0.38018	-22.40	12.50	-53.2

Appendix 2 – Microcosm Data

	Total Phenolic Compounds (mg/l)						P-Cresols (mg/l)						Acetate (mg/l)		
Time (Days)	Set A (Average)	Set B (Average)	Set C (Average)	Set D (Average)	Set E (Average)	Set F (Average)	Set A (Average)	Set B (Average)	Set C (Average)	Set D (Average)	Set E (Average)	Set F (Average)	D (Average)	E (Average)	F (Average)
0	0.22	0.60	0.81	0.24	0.60	0.80	0.05	0.11	0.16	0.05	0.11	0.15	0.24	0.62	0.83
1	0.21	0.62	0.83	0.24	0.60	0.80	0.05	0.11	0.16	0.05	0.11	0.15	0.25	0.74	0.91
2	0.22	0.60	0.80	0.24	0.60	0.80	0.05	0.11	0.15	0.05	0.11	0.15	0.25	0.72	0.86
5	0.22	0.60	0.81	0.24	0.60	0.80	0.05	0.11	0.15	0.05	0.11	0.14	0.25	0.66	0.85
10	0.22	0.59	0.80	0.24	0.60	0.80	0.05	0.11	0.15	0.05	0.11	0.15	0.22	0.67	0.82
15	0.21	0.61	0.82	0.24	0.60	0.80	0.05	0.11	0.15	0.05	0.11	0.14	0.25	0.72	0.85
17	0.21	0.62	0.77	0.24	0.60	0.81	0.05	0.12	0.17	0.05	0.11	0.15	0.23	0.67	0.93
18	0.21	0.57	0.83	0.24	0.60	0.80	0.04	0.11	0.15	0.05	0.10	0.15	#N/A	0.61	0.86
19	0.21	0.60	0.80	0.24	0.60	0.80	0.04	0.11	0.15	0.04	0.11	0.15	0.19	0.59	0.82
21	0.21	0.60	0.80	0.24	0.60	0.80	0.05	0.10	0.14	0.05	0.10	0.15	#N/A	0.69	0.79
22	0.21	0.59	0.78	0.24	0.60	0.80	0.04	0.10	0.14	0.05	0.10	0.15	0.16	0.58	0.76
23	0.20	0.54	0.78	0.24	0.60	0.80	0.04	0.10	0.14	0.05	0.10	0.15	0.16	0.59	0.81
24	0.20	0.53	0.77	0.23	0.60	0.80	0.04	0.08	0.11	0.05	0.10	0.15	0.13	0.56	0.63
29	0.19	0.52	0.75	0.23	0.60	0.80	0.03	0.09	0.12	0.05	0.11	0.15	0.11	0.50	0.68
34	0.18	0.51	0.72	0.23	0.60	0.80	0.03	0.08	0.11	0.05	0.10	0.15	0.09	0.44	0.60
38	0.18	0.51	0.72	0.23	0.59	0.79	0.03	0.07	0.09	0.05	0.11	0.15	0.05	0.37	0.51
45	0.17	0.48	0.70	#N/A	0.59	#N/A	0.02	0.04	0.06	0.05	0.11	0.15	0.04	0.29	0.29
50	0.17	0.46	0.68	0.23	0.59	0.79	0.02	0.04	0.05	0.05	0.11	0.15	0.03	0.22	0.27
55	0.16	0.48	0.67	0.23	0.59	0.79	0.01	0.03	0.05	0.04	0.10	0.15	0.03	0.17	0.22
67	0.16	0.45	0.65	0.23	0.59	0.79	0.01	0.03	0.04	0.05	0.11	0.16	0.00	0.12	0.15
84	0.16	0.44	0.63	0.23	0.58	0.79	0.01	0.03	0.04	0.04	0.11	0.14	BDL	0.09	0.13
101	0.15	0.43	0.65	0.23	0.58	0.78	0.01	0.02	0.02	0.05	0.10	0.14	BDL	0.04	0.03
118	0.14	0.39	0.72	0.23	0.58	0.78	0.01	0.02	0.02	0.05	0.11	0.15	BDL	BDL	BDL

	Sulphate (mg/l)						d34S-SO4 (per mill)					
Time (Days)	Set A (Average)	Set B (Average)	Set C (Average)	Set D (Average)	Set E (Average)	Set F (Average)	Set A (Average)	Set B (Average)	Set C (Average)	Set D (Average)	Set E (Average)	Set F (Average)
0	2800.00	2800.00	2800.00	2800.00	2800.00	2800.00	5.50	5.20	5.69	5.61	6.05	5.36
1	2771.33	2828.87	2828.50	2828.71	2785.84	2814.44	5.23	5.30	6.51	5.05	5.55	4.92
2	2837.96	2804.03	2781.48	2828.99	2838.03	2764.67	5.80	5.80	7.30	5.77	5.82	5.35
5	2785.42	2799.32	2799.31	2799.32	2827.76	2814.37	5.33	#N/A	5.55	5.39	5.04	5.65
10	2814.01	2764.84	2781.56	2781.68	2785.53	2780.34	5.43	5.60	7.57	5.65	5.68	5.31
15	2780.00	2816.24	2816.77	2780.00	2785.47	2781.66	5.80	6.00	5.48	5.80	5.81	5.61
17	2767.00	2827.12	2820.00	2767.00	2828.48	2820.00	5.60	6.15	6.04	5.55	6.20	5.05
18	2800.00	2800.00	2827.24	2800.00	2800.00	2800.00	5.77	6.30	6.73	5.95	#N/A	5.84
19	2766.00	2782.05	2768.14	2766.00	2760.00	2754.16	#N/A	5.95	6.88	#N/A	#N/A	#N/A
21	2777.42	2781.92	2782.17	2745.99	2757.48	2800.00	5.70	6.60	7.86	5.58	5.58	5.37
22	2774.81	2776.26	2744.92	2788.44	2775.82	2758.78	5.97	6.70	6.05	6.08	6.07	6.16
23	2667.90	2657.29	2736.03	2743.75	2741.79	2690.87	6.50	7.00	4.72	6.19	6.59	5.76
24	2660.56	2634.86	2717.97	2650.72	2711.25	2685.71	6.13	7.25	6.24	6.60	#N/A	6.28
29	2605.31	2606.46	2684.81	2629.65	2633.93	2647.00	6.53	8.00	7.45	6.50	6.14	6.46
34	2581.15	2573.50	2625.95	2556.29	2649.90	2659.99	6.20	8.00	9.51	6.89	6.53	6.29
38	2542.59	2582.38	2648.31	2539.81	2602.92	2589.06	7.00	7.55	9.64	7.51	7.63	6.91
45	2506.38	2517.17	2610.11	#N/A	2517.61	#N/A	7.53	8.30	14.64	7.26	7.47	6.76
50	2521.82	2467.54	2567.38	2484.92	2494.24	2575.89	7.10	8.40	13.73	7.15	7.60	6.84
55	2463.83	2522.80	2536.19	2474.58	2435.27	#N/A	7.47	8.80	14.97	7.90	7.62	7.30
67	2428.44	2450.36	2520.06	2464.75	2477.30	2492.11	7.60	#N/A	16.67	7.65	7.62	7.40
84	2430.13	2410.16	2479.20	2390.92	2343.96	2490.72	7.80	9.75	20.14	8.14	7.74	7.49
101	#N/A	2367.61	2379.75	2520.42	2287.68	2281.00	2437.23	10.55	23.36	8.27	7.95	7.34
118	#N/A	2331.00	2318.69	2396.24	2307.58	2280.40	2414.86	11.90	24.21	8.23	8.32	8.03

Appendix 3 – Carbon Balance Data

Carbon Balance - MLS59 2014							
	TDIC-d13C (per mill)	SO4-d34S (per mill)	CH4-d13C (per mill)	d13C Methanogenic CO2 (per mill)	%[RESP]	%[METH]	%[BSR]
Zone A	-18.4	5.0	#N/A	#N/A	84	16	7
	-19.6	7.3	-45.3	6.7			
	-16.9	9.7	-51.6	6.4			
Zone B	-17.3	#N/A	-54.5	2.5	78	22	68
	-17.3	#N/A	-57.1	5.1			
	#N/A	#N/A	#N/A	#N/A			
	#N/A	#N/A	#N/A	#N/A			
	-18.4	15.4	-55.8	3.8			
	-19.1	16.6	-59.7	7.7			
	-19.3	16.6	-61.2	8.2			
	#N/A	10.3	#N/A	#N/A			
	-19.6	#N/A	-58.0	-6.0			
	-18.9	9.0	-55.2	-3.0			
	-19.3	15.5	-55.5	-3.0			
	-18.9	7.6	-50.6	-1.4			
	-19.8	6.2	-56.0	-4.0			
Zone C	-19.2	4.7	-57.2	-5.2	38	62	38
	-19.0	4.3	-56.5	-14.5			
	-18.0	5.7	-54.7	-12.7			
	-18.3	5.0	-58.2	-6.2			

Carbon Balance - MLS59 2015							
	TDIC-d13C (per mill)	SO4-d34S (per mill)	CH4-d13C (per mill)	d13C Methanogenic CO2 (per mill)	%[RESP]	%[METH]	%[BSR]
Zone A	-18.4	3.9	#N/A	#N/A	92	8	3
	-19.6	4.1	-47.1	4.9			
	-16.9	14.8	-54.0	2.0			
Zone B	-1.3	14.8	-52.5	0.5	58	42	60
	-17.3	#N/A	-57.8	5.8			
	#N/A	#N/A	#N/A	#N/A			
	#N/A	#N/A	#N/A	#N/A			
	-18.4	12.3	-56.8	4.8			
	-19.1	14.6	-63.1	11.1			
	-19.3	14.6	-56.2	4.2			
	#N/A	#N/A	#N/A	#N/A			
	-19.6	10.9	-61.5	9.5			
	-18.9	12.5	#N/A	#N/A			
	-19.3	6.9	-60.4	-8.4			
	-18.9	11.2	-61.3	-9.3			
	-19.8	5.0	-42.9	-9.1			
Zone C	-19.2	4.2	-56.2	-14.2	46	54	46
	-19.0	5.4	-58.1	-16.1			
	-18.0	5.5	-56.2	-4.2			
	-18.3	6.3	-56.5	-4.5			

Carbon Balance - MLS59 2016							
	TDIC-d13C (per mill)	SO4-d34S (per mill)	CH4-d13C (per mill)	d13C Methanogenic CO2 (per mill)	%[RESP]	%[METH]	%[BSR]
Zone A	-19.9	4.0	#N/A	#N/A	78	22	5
	-20.6	8.2	-47.7	-4.3			
	-20.4	10.4	-54.9	2.9			
Zone B	-17.9	15.7	-60.5	8.5	72	28	28
	-17.1	16.0	-60.4	8.4			
	#N/A	#N/A	#N/A	#N/A			
	#N/A	#N/A	#N/A	#N/A			
	-19.6	16.7	-63.8	11.8			
	-20.3	15.3	-60.4	8.4			
	-19.8	17.3	-63.6	11.6			
	#N/A	#N/A	#N/A	#N/A			
	-20.0	16.2	-64.8	12.8			
	-18.9	16.4	-66.8	14.8			
	-18.5	14.0	-58.1	6.1			
	-19.0	10.5	-38.9	-13.1			
	-18.8	10.0	-38.8	-13.2			
Zone C	-19.6	6.2	-60.5	8.5	76	24	18
	-19.5	5.3	-58.8	6.8			
	-19.4	4.3	-55.3	3.3			
	-19.6	7.4	-44.4	-7.6			

Carbon Balance - MLS60 2014							
	TDIC-d13C (per mill)	SO4-d34S (per mill)	CH4-d13C (per mill)	d13C Methanogenic CO2 (per mill)	%[RESP]	%[METH]	%[BSR]
Zone D	-21.2	9.2	#N/A	#N/A	73	26	6
	-19.1	14.2	#N/A	#N/A			
	-24.4	13.6	#N/A	#N/A			
	-21.7	14.9	-42.4	-9.6			
Zone E	-18.0	9.1	-48.0	-4.0	56	43	40
	-18.0	8.4	-48.5	-3.5			
	-18.4	8.4	-49.0	-3.0			
	-18.5	8.4	-49.2	-2.8			
	-18.6	8.0	-49.0	-3.0			
Zone F	-17.4	5.1	-52.6	0.6	#N/A	#N/A	#N/A
	-18.5	4.7	-52.2	0.2			
	#N/A	#N/A	#N/A	#N/A			
	-21.9	4.5	-52.0	0.0			
	-21.0	4.8	-51.7	-0.3			
	-23.0	4.6	-53.4	1.4			
	-24.4	5.4	-50.6	-1.4			
	-25.1	4.8	-50.6	-1.4			
	-20.9	#N/A	-45.7	-6.3			
	-19.4	4.3	-48.2	-3.8			
Zone G	-21.3	6.8	-42.2	-9.8	77	22	60
	-20.7	6.7	-44.2	-7.8			
	-20.8	6.3	-50.8	-1.2			
	-21.0	6.6	-55.1	3.1			
	-20.5	20.1	-63.3	11.3			
	-19.9	15.7	-55.0	3.0			
	-20.3	13.4	-57.8	5.8			
	-20.6	17.5	-43.5	-8.5			
	-20.7	5.7	#N/A	#N/A			

Carbon Balance - MLS60 2015							
	TDIC-d13C (per mill)	SO4-d34S (per mill)	CH4-d13C (per mill)	d13C Methanogenic CO2 (per mill)	%[RESP]	%[METH]	%[BSR]
Zone D	-22.2	13.7	#N/A	#N/A	80	19	0
	-22.1	16.4	#N/A	#N/A			
	-22.7	16.2	-42.9	-9.1			
	-21.1	5.8	#N/A	#N/A			
Zone E	#N/A	9.5	-57.6	5.6	59	40	41
	#N/A	8.9	-50.6	-1.4			
	-17.0	8.7	-55.4	3.4			
	#N/A	8.9	-53.8	1.8			
	-16.6	8.5	#N/A	#N/A			
Zone F	#N/A	5.5	-58.1	6.1	#N/A	#N/A	#N/A
	-15.4	5.3	-45.2	-6.8			
	#N/A	5.0	-42.7	-9.3			
	-21.9	#N/A	#N/A	#N/A			
	-17.8	5.5	-41.7	-10.3			
	-17.8	5.6	-37.5	-14.5			
	#N/A	5.6	-59.2	7.2			
	-18.7	5.4	-61.0	9.0			
	-20.0	5.6	-63.3	11.3			
	-18.8	5.1	-61.5	9.5			
Zone G	-19.2	7.6	-61.3	9.3	84	15	67
	-19.7	8.2	#N/A	#N/A			
	#N/A	7.3	-83.4	31.4			
	-19.1	7.6	-75.5	23.5			
	#N/A	16.4	-73.6	21.6			
	-19.1	13.3	#N/A	#N/A			
	#N/A	13.0	#N/A	#N/A			
	-19.0	#N/A	-72.4	20.4			
	-22.2	12.5	-57.0	5.0			

Carbon Balance - MLS60 2016							
	TDIC-d13C (per mill)	SO4-d34S (per mill)	CH4-d13C (per mill)	d13C Methanogenic CO2 (per mill)	%[RESP]	%[METH]	%[BSR]
Zone D	-23.0	15.0	#N/A	#N/A	87	12	9
	-22.6	17.0	-47.9	-4.1			
	-23.3	16.8	-56.6	4.6			
	-21.8	7.4	-61.2	9.2			
Zone E	-20.2	11.6	-61.7	9.7	60	39	43
	#N/A	11.9	-58.4	6.4			
	-20.2	8.9	-57.2	5.2			
	-18.8	10.9	-56.4	4.4			
	-19.0	10.5	-59.6	7.6			
Zone F	-19.3	6.0	-45.4	-6.6	#N/A	#N/A	#N/A
	-19.9	7.0	-57.5	5.5			
	-20.5	7.2	-60.6	8.6			
	-21.7	6.0	-45.6	-6.4			
	-23.5	6.1	-45.8	-6.2			
	-23.5	6.3	-59.1	7.1			
	-23.5	6.7	-60.8	8.8			
	-23.4	6.3	-60.6	8.6			
	-22.2	8.0	-60.7	8.7			
	-23.0	6.7	-64.9	12.9			
Zone G	-24.4	10.2	-79.7	27.7	91	8	75
	-25.1	11.5	-76.6	24.6			
	-19.7	10.5	-79.8	27.8			
	#N/A	11.4	-89.3	37.3			
	-19.8	16.2	-98.9	46.9			
	-21.0	22.8	-92.5	40.5			
	-20.0	20.4	-89.2	37.2			
	-19.6	20.1	-75.5	23.5			
	-22.4	12.5	-53.2	1.2			